ENGINEERING FUNCTIONAL INTERFACES FOR BIOSENSING, MINIMIZATION OF PROTEIN ADSORPTION, AND STRUCTURAL SELF-HEALING

ENGINEERING FUNCTIONAL INTERFACES FOR BIOSENSING, MINIMIZATION OF PROTEIN ADSORPTION, AND STRUCTURAL SELF-HEALING

A Thesis

Submitted to the School of Graduate Studies

in Partial Fulfillment of the Requirements

for the Degree

Doctor of Philosophy

McMaster University

DOCTOR OF PHILOSOPHY (2016) McMaster University

(Chemical Engineering) Hamilton, Ontario

TITLE: Engineering Functional Interfaces for Biosensing, Minimization of Protein Adsorption, and Structural Self-Healing

AUTHOR: Xudong Deng

B.Eng. (Zhejiang University)

M.Eng. (Zhejiang University)

SUPERVISORS: Professor Carlos D. M. Filipe

Professor Todd R. Hoare

NUMBER OF PAGES: viii, 121

Abstract

This thesis describes strategies on how to efficiently modify biological interfaces either effectively to reduce nonspecific protein binding in various contexts or to encourage specific interfacial interactions following exposure to a ligand or following the disruption of a biomaterial. Nonspecific protein adsorption at interfaces is a significant issue in the development of robust biosensors and implantable biomaterials, and modifying surfaces to achieve this goal is currently a complicated and relative inefficient process. On the other hand, current protein immobilization methods, including physical and covalent attachment, can interfere with specific binding sites, thus reducing the efficiency of bio-recognition events and resulting in a loss of specific binding potential that, for example, significantly compromises biosensor performance. In addition to the protein binding, dynamic interfacial interactions are sometimes desirable to allow for rapid and reversible responses to external stimuli when particular applications are targeted. In this thesis, I report on new approaches for efficient protein passivation and immobilization as well as a new type of self-healing hydrogel that can serve as platforms for the development of functional biosensors and biomaterials.

In the first part of the thesis, a simple, scalable procedure to passivate paper against non-specific protein adsorption is introduced. This method is based on a simple sequential dipping protocol inspired by the polyelectrolyte layer-by-layer approach, but instead using covalently reactive hydrazide and aldehyde-functionalized poly(oligoethylene glycol) oligomers (both of which can be easily synthesized via one or two-step chemistries). This sequential dipping method creates a thin hydrogel layer around the cellulose fibers within the paper network without affecting the fiber morphology or macropore network of the paper that effectively lowered non-specific adsorption of a broad range of proteins to the paper by at least one order of magnitude. This method was subsequently applied in the fabrication of paper-based microfluidic sensors that enable protein transport in lateral flow assays as well as paper-based enzyme-linked immunosorbent assays (ELISAs) that exhibit both lower limits of detection and higher dynamic ranges relative to papers blocked with the conventional blocking agents. The simplicity of this surface modification method has great potential to be applied in various paper-based biosensors or for coating other porous media (e.g. membranes) to counteract biofouling.

The next part of this thesis was dedicated to developing a simple, mixing-based protocol for conjugating hyaluronic acid (HA) on the surface of a contact lens, again using hydrazone chemistry to perform the coupling. This simple conjugation method, based on a two-step preparation technique consisting of laccase/TEMPO-mediated oxidation of the surface of poly(2-hydroxyethyl methacrylate) (PHEMA)-based contact lenses followed by covalent grafting of hydrazide-functionalized HA via simple immersion, can be achieved under ambient conditions without the need for any external crosslinkers or energy. The resulting lenses were significantly more wettable,

more water-retentive, and less prone to protein adsorption than the native lenses, all of which are key factors in improving the comfort and functionality of the lens for a patient. These characteristics were achieved without causing any significant changes in terms of the transparency, refractive index, or key mechanical properties of the lens.

The third part of this thesis describes a new approach for performing highly sensitive immunosorbent assays by combining the adsorption capacity of graphene oxide with the high sensitivity of the quartz crystal microbalance (QCM). Specifically, by functionalizing graphene oxide with biotin and subsequently complexing with avidin, the irreversible adsorption of graphene oxide to the surface of a gold QCM biosensor is used as a linking layer for functionalizing a QCM sensor with antibodies. Given the broad availability of multiple types of biotinylated capture antibodies, such an interface provides a flexible substrate for performing a variety of immunoassays of interest. Furthermore, the whole immunoassay process takes less than 5 hours, faster than (or at least comparable with) other approaches that are practically and chemically more complex. As a proof-of-concept, rabbit IgG at concentrations ranging from 0.1 ng/mL to 10 μg/mL (six orders of magnitude) could be quantitatively detected with high sensitivity and selectivity.

Finally, I developed a new method to prepare fast self-healing hydrogels from hyaluronic acid and poly(vinyl alcohol), exploiting the dynamic crosslinking of boronate esters at both neutral and acidic pH. The hydrogel underwent fast (<1 minute) and effective self-healing in both macroscopic cleave/heal tests and microscopic rheological shear tests, providing a hydrogel scaffold with dynamic crosslinking capability over a broad pH range relevant to physiological applications.

Overall, these fabrication techniques can be widely used for the simple and scalable preparation of stable, functional and unique biological interfaces for both therapeutic and diagnostic applications.

Acknowledgements

First of all, I would like to express my deep appreciation for my supervisors, Dr. Carlos D.M. Filipe and Dr. Todd R. Hoare, for their kind guidance, generous advice and constant support throughout my PhD projects. In the year 2012, Dr. Filipe opened a door for me to come to McMaster, giving me the chance to face the world-leading research projects and to meet the world-top scientists here, and later Dr. Hoare greatly expanded my horizon in the area of polymer chemistry and chemical engineering. Their keen interest and continuous passion in research give me great encouragement in realizing new ideas and developing new technologies during my journey of PhD program here in McMaster. I am truly grateful for the opportunities I got in both Filipe lab and Hoare lab.

I would also like to thank my advisory committee members, Dr. Robert H. Pelton, Dr. Michael A. Brook and Dr. Emily D. Cranston for their instruction, suggestions and discussions. Each time I gained quite a lot from the committee meetings, which gave both great improvement and important corrections of my work. I would also like to acknowledge Dr. John D. Brennan and Dr. Heather Sheardown for their very insightful thoughts and guidance in different aspects of my work.

All the current and previous group members from Dr. Filipe, Dr. Hoare and Dr. Pelton's labs are acknowledged for their generous help, support and encouragement. For here I just name a few of them: Dr. Zhuyuan Zhang, Dr. Yaqin Xu, Dr. Sana Jahanshahi-Anbuhi, Mr. Vincent Leung, Ms. Robin Ng, Mr. Kevin Pennings and especially my research assistant Ms. Mengsu Chen, all from Filipe lab; Dr. Niels Smeets, Dr. Lukas Sadowski, Dr. Daryl Sivakumaran, Dr. Mathew Patenaude, Ms. Maryam Badv, Ms. Fei Xu, Ms. Rabia Mateen, Ms. Emilia Bakaic, Mr. Scott Campbell, Mr. Trevor Gilbert, Ms. Madeline Simpson, Ms. Sahar Mokhtari, and Mr. Ivan Urosev from Hoare lab; Dr. Songtao Yang, Dr. Zhen Hu, Dr. Emil Gustafsson, Dr. Jingyun Wang, Dr. Zuohe Wang, Dr. Roozbeh Mafi, Mr. Qiang Fu, Ms. Xiaofei Dong, Ms. Carla Abarca, Mr. Dong Yang, Ms. Yuanhua Li, and Mr. Lunquan Yu from Pelton lab. Without them, I cannot imagine what I can get only by working alone. The valuable trainings and discussions, as well as teamwork support from all of them are greatly appreciated. Dr. Clémence Sicard, Dr. Qiang Zhang, Dr. Meng Liu, Dr. M Monsur Ali, Ms. Carmen Carrasquilla, Mr. Michael Wolfe from the joint lab of Dr. John D.Brennan and Dr. Yingfu Li, and Dr. Jianfeng Zhang, Ms. Banafsheh Rastegari, Ms. Myrto Korogiannaki from Sheardown lab, are appreciated for their helping in the biochemical experiments.

I would like to thank our lab manager Mr. Doug Keller and all McMaster Chemical Engineering office staffs and technical staffs for their administrative assistant and technical support. NSERC is acknowledged here for research funding support through CREATE Biointerfaces training program.

Last but not least, I want to express my very special thanks to my parents, my family members, and my wife Linwan Wei. Their endless and unreserved support, constant and unconditional encouragement makes my PhD study much impressive and meaningful. Especially, Linwan gives me love, care, and support, which is always my greatest treasure in my life.

Table of Contents

Abbreviations

5-FITC	5-fluorescence isothiocyanate
5-FTSC	fluorescein-5-thiosemicarbazide
ADH	adipic acid dihydrazide
AFM	atomic force microscope
ATR-FTIR	attenuated total reflection-Fourier transform infrared spectroscopy
ATRP	atom transfer radical polymerization
DIW	deionized water
BSA	bovine serum albumin
CLSM	confocal laser scanning microscopy
ECM	extracellular matrix
EDC	N'-ethyl-N-(3-dimethylaminopropyl)-carbodiimide
EGDMA	ethylene glycol dimethacrylate
ELISA	enzyme-linked immunosorbent assay
FTIR	Fourier-transform infrared spectroscopy
HA	hyaluronic acid
HEMA	2-hydroxyethyl methacrylate
HSA	human serum albumin
IgG	immunoglobulin G
LbL	layer-by-layer
LCST	lower critical solution temperature
LOD	limit of detection
$M(EO)_2MA$	di(ethylene glycol) methyl ether methacrylate
MPC	2-methacryloyloxyethyl phosphorylcholine
M_W	molecular weight

NHS	N-hydroxysuccinimide
NMR	nuclear magnetic resonance
OEG	oligo(ethylene glycol)
PAA	polyacrylic acid
PBS	phosphate-buffered saline
PEG	poly(ethylene glycol)
PEGDA	poly(ethylene glycol) diacrylate
PEGMA	poly(ethylene glycol) methacrylate
PEO	poly(ethylene oxide)
pCBMA	poly(carboxybetaine methacrylate)
PDI	polydispersity index
PG	polyglycerol
PHEMA	poly(2-hydroxyethylmethacrylate)
PLL	poly(L-lysine)
pMPC	poly(methacryloyloxyethyl phosphorylcholine
POEGMA	poly(oligoethylene glycol methyl ether methacrylate)
PPO	poly(propylene oxide)
pSBMA	poly(sulfobetaine methacrylate)
PVA	poly(vinyl alcohol)
QCM-D	quartz crystal microbalance with dissipation monitoring
RGD	arginine-glycine-asparate
SAM	self-assembled monolayer
SEC	size-exclusion chromatography
SEM	scanning electron microscopy
SI-ATRP	surface-initiated atom transfer radical polymerization

SPR	surface plasmon resonance
TEMPO	(2,2,6,6-tetramethylpiperidin-1-yl)oxidanyl
UV	ultraviolet
XPS	X-ray photoelectron spectroscopy

Chapter 1 Introduction

1.1 Literature review

1.1.1 Protein interactions with biomaterials

When the surface of an implanted biomaterial (synthetic or natural) comes into contact with a biological fluid, such as blood, a cascade of interdependent events takes place and several signals are generated.[1] Protein adsorption onto the surface is considered the most important factor in the interaction between the biological fluid and the biomaterial. Many factors affect the extent of protein adsorption, including electrostatic interactions, water-mediated hydrophobic and hydration forces (Figure 1.1).[2-5]

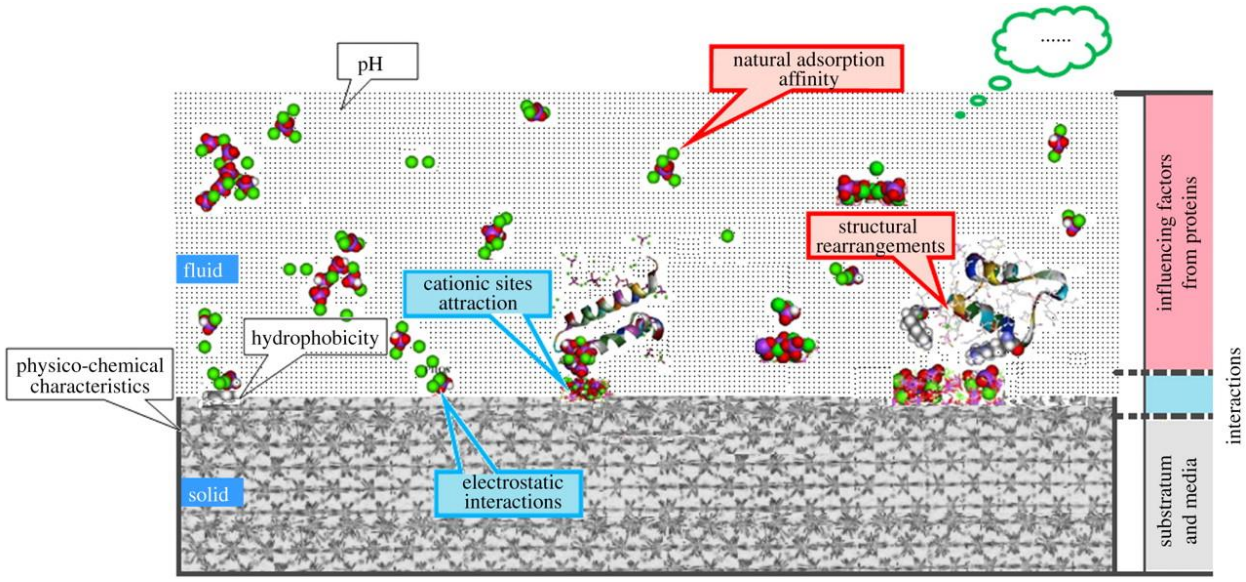

Figure 1.1 Schematic of the major factors affecting protein adsorption. (Figure reproduced from Ref.[5])

Nonspecific protein adsorption is a dynamic process that occurs very quickly, typically only seconds after the fluid meets the surface of the material, which generates an adsorbed layer,[6] and triggers a cascade of biological events.[7-8] For *in vivo* implants, this adsorbed layer activates an irrevocable host defense mechanism, which is known as the foreign body reaction, which finally results in the production of a fibrous avascular capsule that isolates the material from its surroundings. This prevents further physical, chemical or physiological interaction with its surroundings.[6] In the case of *in vivo* implants, protein fouling not only reduces the efficacy of devices, but also results in thrombosis and other negative side effects.[9] Negative effects of protein

fouling also take place in *in vitro* applications, since the adsorbed layer may clog the pores or inhibit specific binding of molecules to these devices.[10-11] For example, nonspecific adsorption of proteins significantly reduces the sensitivity of *in vitro* diagnostic assays, especially in the case of immunological assays.[12] In addition, proteins in the adsorbed layer undergo a slow denaturation process (Figure 1.2), which typically induces immunological responses *in vivo* or leading to failure in terms of specific sensing.[13]

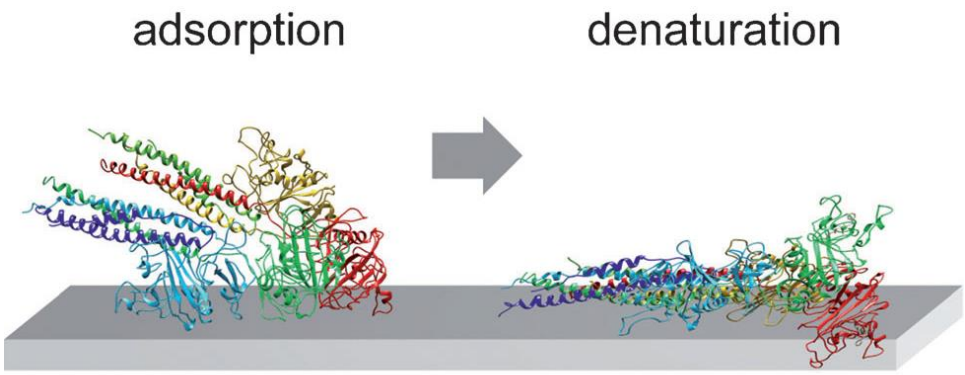

Figure 1.2. Dynamic adsorption and denaturation of proteins on a bare surface. (Figure reproduced from Ref.[8])

The reduction of nonspecific protein adsorption plays a key role in improving the compatibility and efficiency of biomaterials. The primary approach used is through chemical modification of the surface through polymer coatings (Figure 1.3). Such coating provide a 'stealth' effect,[14] which is attributed to the high level of hydration of the hydrophilic polymer backbones, steric repulsion, and reduction of the surface energy of the biomaterial.[6, 15-16] Among these factors, hydration forces have been suggested as the key in determining whether a surface will promote or reduce protein adsorption.[17] Following this rule, various types of polymer coatings were designed as the protein-resistant layer to cover a 'bioinert' material. These coatings include polypeptides,[18] poly(ethylene glycol),[19] polyglycerol,[20] polysaccharides,[21] polyoxazoline,[22] poly(propylene sulfoxide),[23] poly(phosphoester),[14] polyvinylpyrrolidone[24] and zwitttterionic polymers such as phosphorylcholine and sulfobetaine or carboxybetaine polymers.[25-27] These coated surfaces resist non-specific binding of proteins, and are widely used in implants and devices *in vivo* such as catheters, prosthetic devices, contact lenses, drug delivery vehicles, as well as in immunoassays such as enzyme-linked immunosorbent assay (ELISA) and patterned cell culture materials for *in vitro* applications.[12, 28]

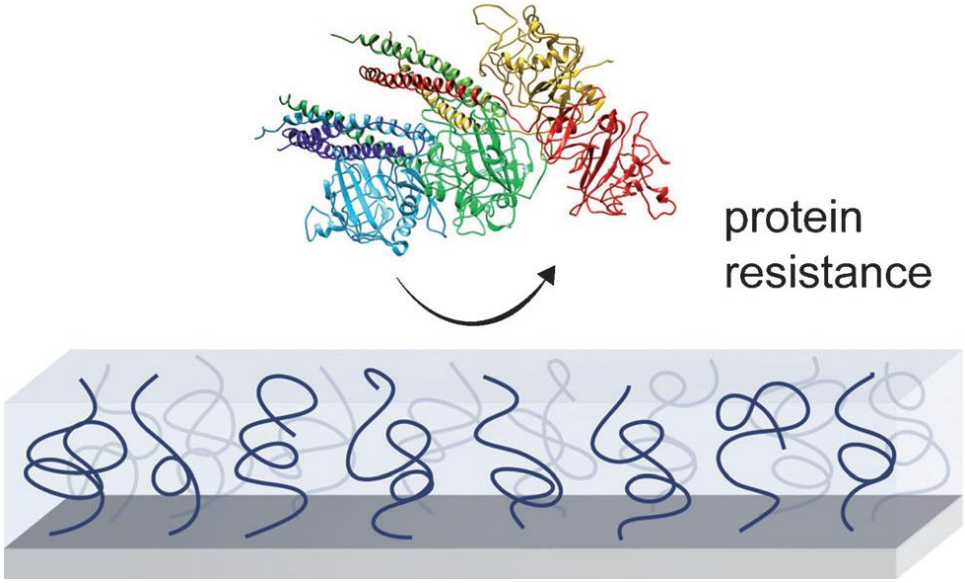

Figure 1.3 Protein resistance is imparted by polymer-coated surface. (Figure reproduced from Ref.[8])

In the other extreme, techniques have been created with the intention to promote specific protein adsorption, as to impart biological function to the material, thereby generating a bioactive surface.[27, 29] Immobilization of certain proteins enables both localization and retention of the required functions at the bio/material interface, such as providing appropriate signals that direct certain biological activities, or increasing the efficacy of biological signaling at the interface.[6] For instance, integrin, a dimeric receptor composed of α- and β-subunits that span the cell membrane, is responsible for mediating binding and interactions between cells and structural proteins of the extracellular matrix (ECM). [30-31] In turn, the cells are able to recognize and bind to the bioactive regions of the biomaterial, which are immobilized with structural proteins of the ECM, providing mechanical stability to the cytoskeleton as well as initiating cytoplasmic signaling cascades.[32-34]

In summary, understanding and controlling protein adsorption on biomaterial surfaces is essential to preparing either bioinert or bioactive surfaces. These two techniques can be combined to prepare functional bioactive surfaces, improving the efficacy of biomaterials (Figure 1.4). The following sections in this Introduction chapter will further discuss the methods, especially focusing on surface coating, that are used for preventing nonspecific protein binding as well as promoting specific protein immobilization in details.

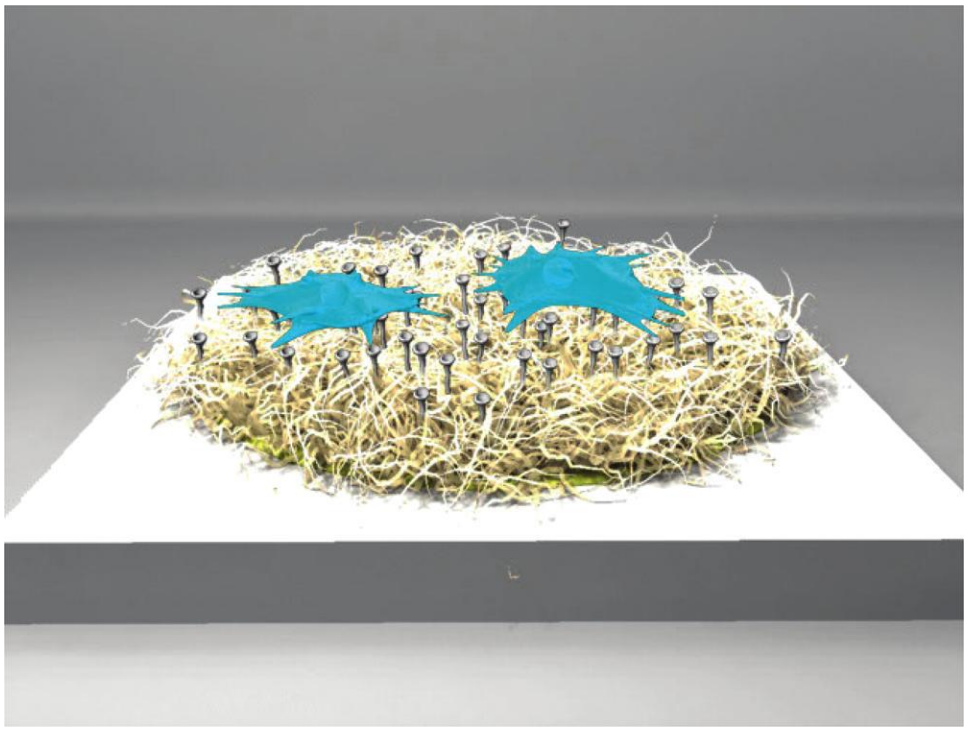

Figure 1.4 Combined approach whereby nonspecific protein adhesion is prevented with an antifouling layer (off-white) allowing only the selected bioactive signaling motifs (dark gray) to be displayed on the surface for interacting with target (in this case the cell in blue). (Figure reproduced from Ref.[6])

1.1.2 Polymer coatings for protein passivation

Preparation strategies of the polymer coating layer on biomaterial surfaces include but are not limited to: self-assembled monolayer (SAM),[19] non-covalent physisorption,[35] covalent chemisorption,[36] spin coating,[37] surface gelation,[38-39] and layer-by-layer (LbL) assembly[40].

1.1.2.1 Monolayer Coatings

Self-assembled monolayer (SAM) is considered a very effective method to prepare polymer coatings on various types of biomaterial surfaces with high chain density and high surface coverage. The first SAM designed for protein resistance was achieved by Whitesides and co-workers.[19] In that work, the ω-functionalized alkanethiolate SAM terminated with hexa(ethelene glycol) coated on gold through thiol chemistry efficiently reduced protein adsorption. Following that work, several other types of oligo- or poly(ethylene glycol) (OEG or PEG) have been investigated on gold and other metal surfaces.[41] The chemical structure of OEG and PEG which possesses both internal and terminal hydrophilicity favors the formation of hydration layer in the interior and covering the surface of the SAM is shown in Figure 1.5.

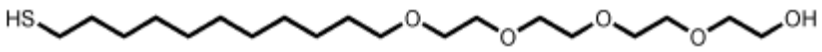

Figure 1.5 Molecular structure of the OEG-terminated alkanethiol molecule for SAM formation on gold. (Figure reproduced from Ref.[42])

The mechanism of why PEG and OEG chains lead to protein repulsion has been extensively discussed. The physical and chemical nature of the ethylene glycol itself is an important part of the explanation. Andrade and de Gennes attributed this to the conformational flexibility of the PEG chain, based on the ideas derived from colloid stabilization.[43] Grunze et al. proposed that the interaction of water with the OEG SAM as being the determinant factor, while the steric stabilization provided by the terminal OEG chains was deemed not as important.[41, 44-46] Chen et al summarized that the nonfouling abilities are correlated to the hydration layer near the polymer surface based on their observations, since the bonded water layer served as a physical and energetic barrier to prevent protein adsorption.[47-49] Chain flexibility was also believed to be an important factor in protein repulsion especially when using long-chain polymers, due to the steric repulsion induced by an unfavorable decrease in entropy.[43, 50] The combination of surface hydration and chain flexibility (i.e. steric repulsion) work together to achieve the nonfouling ability for SAM, hydrophilic polymer chains and zwitterionic polymer chains (Figure 1.6).[47] The interactions between proteins and two typical antifouling polymers of PEG and poly(sulfobetaine methacrylate) (pSBMA) in aqueous solution were examined using fluorescence spectroscopy, atomic force microscopy and nuclear magnetic resonance.[51] The results from this research clearly demonstrated the existence of weak hydrophobic interactions between PEG and proteins, while there were no detectable interactions between pSBMA and proteins. The elimination of protein interaction with pSBMA could be due to an enhanced surface hydration of zwitterionic groups in pSBMA.

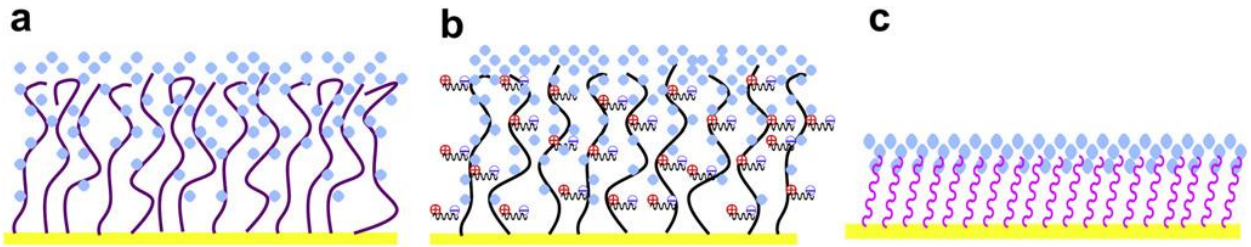

Figure 1.6 Illustration of chain hydration and chain flexibility of (a) hydrophilic polymers, (b) zwitterionic polymers, and (c) SAMs, which contribute to surface resistance to nonspecific protein adsorption in different ways. For a and b, both chain hydration and chain flexibility play a role in protein resistance, while for c, surface hydration plays the key role. (Figure reproduced from Ref.[47])

Whitesides proposed that the displaying of kosmotropes-molecules in SAMs stabilizes the native structure of proteins and is the main reason for protein resistance- without needing to consider the nature of polymer chain (Figure 1.7).[28] In his theory, a system is composed of a protein, water, and the molecule displayed on the surface (solute). When the concentration of the molecule is lower in the "local domain" than in the "bulk domain", the protein is considered to be preferentially hydrated, which means the molecule is well excluded from the protein surface and leads to good protein repellency.

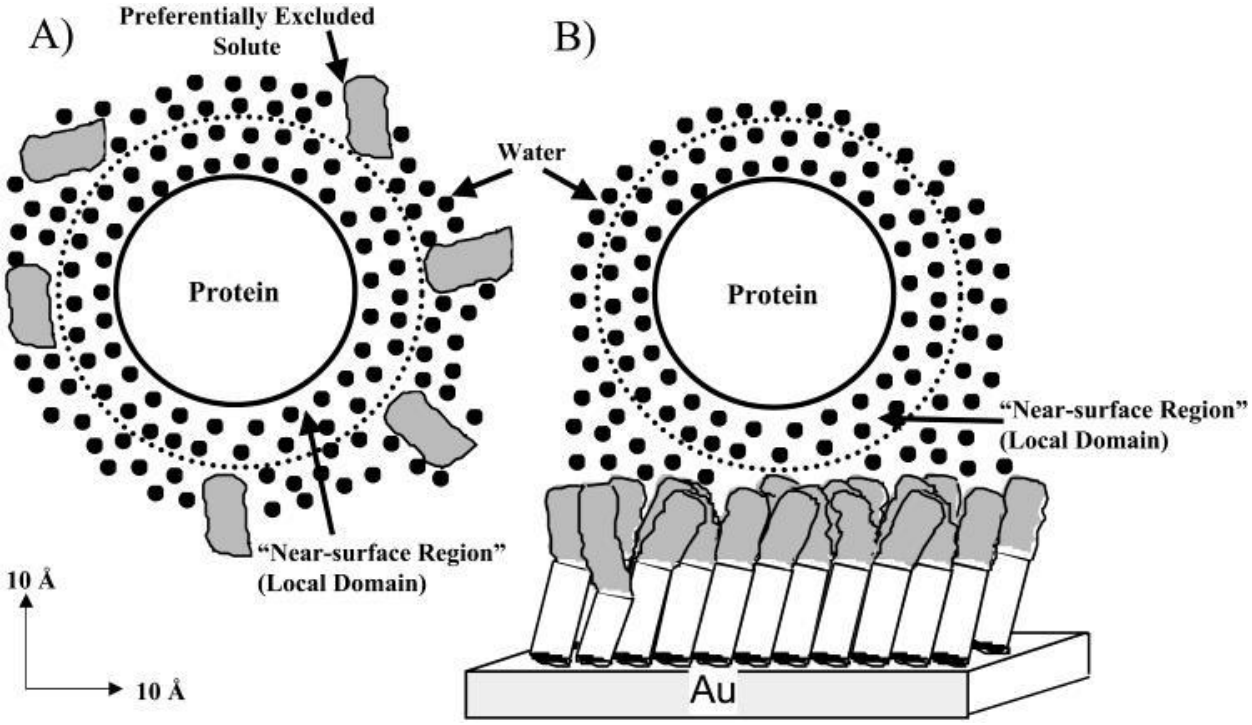

Figure 1.7 (A) Schematic illustration of a solute that is completely excluded from the surface of the protein (the local domain) and (B) schematic illustration of a protein that does not adsorb onto a surface. The surface is completely excluded from the surface of the protein (the local domain) and there are no surface-protein contacts. (Figure reproduced from Ref.[28])

Due to the good performance of PEG and OEG chains in repelling proteins from surfaces, various types of OEG and PEG derivatives have been developed to improve the protein resistance properties, and the method for the assembly of these new polymers was no longer confined solely to a SAM route. For instance, a amphiphilic block copolymer of PEG-PPO [poly(propylene oxide)] could be physically adsorbed onto hydrophobic surfaces in an aqueous solution, and reduce the protein adsorption low levels.[52] Poly(L-lysine)-b-poly(ethylene glycol) (PLL-PEG) block copolymers have the ability to adhere to a surface through charge effects (PLL possesses positive

charge) forming PEG barriers that repel proteins.[53-54] However, these physically adsorbed polymer layers are not stable enough and can easily detach when the physiochemical conditions change (e.g. the pH and the ionic strength of the solution). Therefore, chemical linking through covalent bond forming to immobilize the polymer chains was developed for practical applications.

In addition to the thiol chemistry mentioned above, silanes (on silicon oxide),[36] catechols (on metal and metal oxide),[55] and phosphates (on metal oxide)[56] have been used to chemically tether polymer chains onto certain types of surfaces. One example comes from a widely applied material-independent coating using mussel-inspired polydopamine, the most commonly used catechol. This method requires a simple one-step dip-coating to form a protein-resistant polydopamine layer through Michael addition or a Schiff base reaction.[38, 57-59] For other types of surfaces which do not contain active functional groups, pretreatment, including plasma, ozone, electron beam, UV irradiation and special chemical reagents, is required to activate the surface and generate active groups for further polymer tethering.[60] With the assistance from functional groups, polymer side chains can be easily conjugated onto the surface.

Both the chemical structure and the 3D architecture of the polymer chains or the topology of the polymer coating layers are highly important to efficiently cover the surface of the substrate and prevent protein adsorption. The special architecture influences both the steric effect as well as the anchoring sites of proteins. Typical structures of the designed protein-resistant polymer chains are summarized in Figure 1.8.

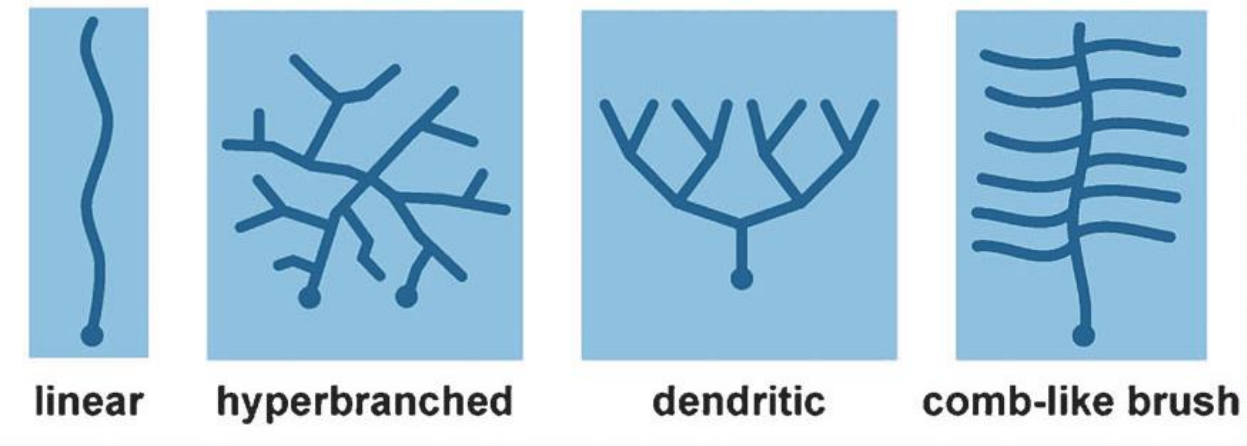

Figure 1.8 Schematic of typical functional tail chains with linear, hyperbranched, dendritic, and comb-like brush architectures of protein-resistant polymers. (Figure reproduced from Ref.[8])

Through the use chemical linkers, hyperbranched and dendritic polymers can be immobilized on the surface of biomaterials, which could cover larger surface areas as compared to using linear molecules of equal molecular weight.[61] These type of tree-like structures have particular advantages in coating rough surfaces.[20] For example, polyglycerol (PG) dendrons showed similar or better protein resistance and higher stability as compared to PEG monolayer coatings.[62] This type of technology, which chemically crosslinks the functional group on the surface to the end-functional group on the polymer chain, is referred to as "grafting to" technique, while performing the polymerization process *in situ* and from the surface of the material is referred to as a "grafting from" technique.[63]

"Grafting from" methods have been extensively reported for achieving protein-resistant polymer coatings. Chilkoti and co-workers did surface-initiated atom transfer radical polymerization (SI-ATRP) of oligo(ethylene glycol) methyl methacrylate (OEGMA) starting from a chemically tethered SAM of initiator ω-mercaptoundecyl bromoisobutyrate, and formed comb-like structured polymers (Figure 1.9).[64-65] In another approach, the ATRP initiator [2.2]paracyclophane-4-methyl 2-bromoisobutyrate was first deposited onto the surface through chemical vapor deposition, and then a subsequent poly[oligo(ethylene glycol) methyl methacrylate] (POEGMA) was polymerized to generate protein-resistant coatings.[66] These types of high-density comb-like polymer brushes composed of POEGMA and copolymers with poly(poly(ethylene glycol) methacrylate) (poly(PEGMA)) could drastically reduce protein adsorption on surfaces.[12, 67-68] Comb-shaped super hyper-branched dendritic glycerol acrylate and glycerol monomethacrylate brushes also provide an ideal environment to repel protein adsorption from human blood plasma.[69]

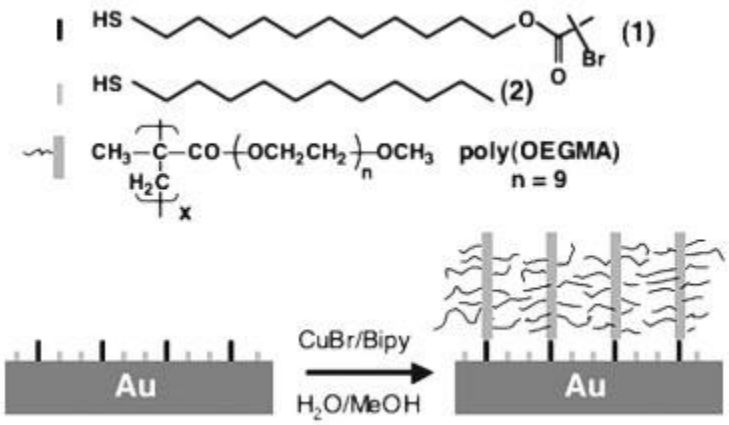

Figure 1.9. Schematic of SI-ATRP of OEGMA from a mixed SAM of an initiator-functionalized alkanethiol (1) and a diluent alkanethiol (2) on gold. (Figure reproduced from Ref.[64])

POEGMA, a non-linear PEG, is a new versatile building-block for the preparation of smart bio-relevant materials (Figure 1.10). It is non-toxic, non-immunogenic, cytocompatible and protein-repellent. A more specific property of POEGMA is that the copolymerization of different OEGMA

monomers of different lengths allows for precise control over the lower critical solution temperature (LCST) of the polymer.[70] This makes the surface coating hydrophilic at high temperatures yet remain strongly protein-repellent.[71-74] With the help of "grafting from" strategies, POEGMA polymer brushes have been prepared through SI-ATRP for creating anti-protein fouling properties on gold, silicon, titanium, stainless steel and plastic surfaces [72, 75-79]. These anti-fouling surfaces show promise in applications such as bio-arrays, biosensors and implants.[12, 80-81] Furthermore, the active chain ends (terminal alkyl halides) were preserved in the SI-ATRP process, offering an opportunity for further surface functionalization.[82-83]

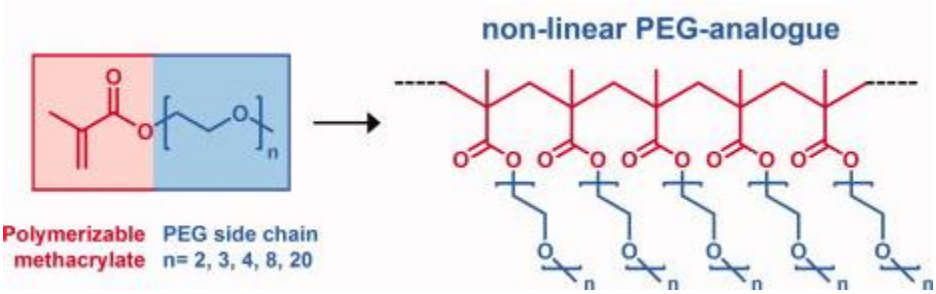

Figure 1.10 Molecular structure of non-linear PEG analogues constructed with OEGMA monomer. (Figure reproduced from Ref.[70])

Another big group of polymer candidates for protein-resistant coating of materials are zwitterionic molecules.[25, 84] They also have strong binding ability to water, and possess no net charge as a whole. Since all proteins have randomly distributed positive and negative charges on their surface, they can easily adhere to either positively or negatively charged surfaces.[85] Zwitterionic polymers are a nanoscale homogenous mixture of balanced charged groups (Figure 1.11), which is believed to be the key of their nonfouling properties. In the recent years, zwitterionic polymers including poly(2-methacryloyloxyethyl phosphorylcholine) (pMPC),[86] pSBMA,[87] poly(carboxybetaine methacrylate) (pCBMA)[79] and mixed charged polymers[88] were synthesized *in situ* using "grafting from" technique. The first three polymers can be categorized into polybetaines that carry a positive charge and a negative charge on the same monomer unit, while the last one is polyampholytes carries 1:1 positive and negative charge on different monomer units. It has been shown that pSBMA and pCBMA coatings have comparable or even better performance in protein resistance than POEGMA.[88] However, zwitterionic polymers still have two limitations for their application: 1) they are sensitive to pH and ionic strength; 2) the synthesis of the monomer is complicated.[25]

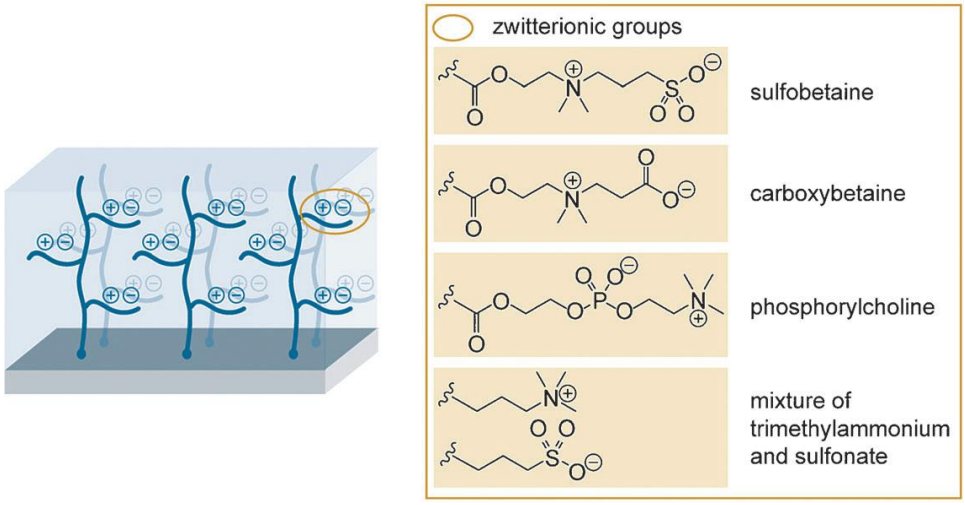

Figure 1.11 Molecular structures of several zwitterionic molecules used in protein-resistant coatings. (Figure reproduced from Ref.[8])

Carbohydrates, namely polysaccharides or oligosaccharides, are hydrophilic, non-charged natural polymers which also have been employed to prevent undesired nonspecific adsorption of proteins,[21, 89] mimicking the highly hydrated state on biological cell membranes. Oligosaccharide-terminated SAM showed good resistance to protein fouling.[90] Oxidized dextran coated surfaces have also been shown to reduce protein adsorption.[91] Hyaluronic acid (HA) films directly immobilized to various types of solid substrates, repelled protein and remained stable to a larger extent than other polysaccharides.[92] In addition, surfaces made through the chemical grafting of HA onto gold substrate have also shown excellent antifouling performance against protein adsorption,[93] however, few cases have been reported to coat HA onto the surface of soft substrates such as hydrogels. Synthesized block copolymer containing polysaccharides, such as poly (L-lysine)-graft-dextran, were also used to protect charged surface like metal oxide from protein fouling. [94] Polymer brushes of N-substitute acrylamide containing different carbohydrates were able to reduce protein fouling from single protein solutions.[95]

1.1.2.2 Multilayer and Hydrogel Coatings

All of the above mentioned monolayer coatings are simple and highly effective methods to modify surfaces and minimize protein adsorption onto surfaces. This coating technology, is however limited to certain types of substrates, due to their chemical and physical nature, which might require harsh pretreatment before coating. Monolayer coating is also limited by low polymer density and relatively thin coating,[96] and are often fragile to thermal and oxidation degradation, making the long term stability of coating challenging.[94, 97] Multilayer technologies, including surface gelation,[38-39] layer-by-layer assembly[40] accompanied with chemical or physical crosslinking,[98] were developed to allow using various types of substrates. The goals of these

technologies are also to simplify the process, make the pretreatment steps as mild as possible and to prolong the life scale of the coating. Multilayer polymer coating often leads to thick coats- it is desirable to have precise control not only on the thickness of the coat but also on the morphology of the coating, while achieving high surface coverage (Figure 1.12).

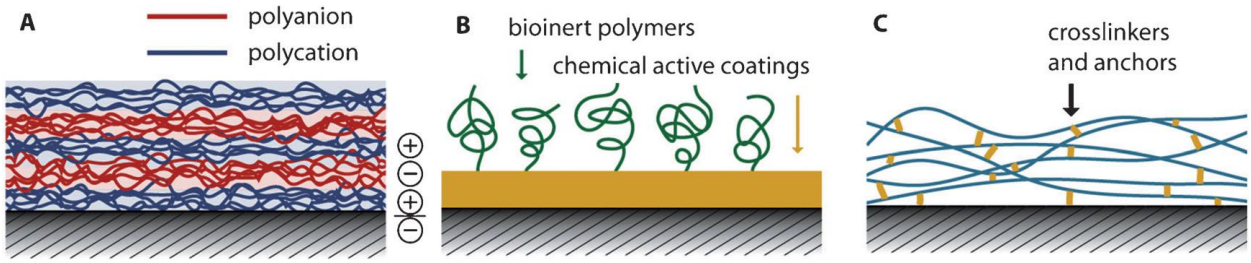

Figure 1.12 Schematic of various coating techniques: a) layer-by-layer (LbL) assembled coating, b) a bioinert coating tethered onto a chemically active layer, c) a homogeneous multilayer coating with cross-linking. (Figure reproduced from Ref.[8])

PEG derivatives are still preferable as the first choice in preparing multilayer protein-resistant coatings. For example, a thick and stable surface coating, based on the aggregation of an amphiphilic four-armed PEG-dopamine polymer gelated into particles, can lower the protein adsorption on metal oxide surfaces.[38] Layer-by-layer (LbL) assembly of polyelectrolytes often generates charged multilayers, which do not meet the requirements needed to attain protein repulsion. Specially designed copolymers composed of poly(l-lysine)-poly(ethylene glycol) (PLL-PEG) can solve part of this charge problem, since it has at one end a positively charged PLL block sticking to the negatively charged surface, whereas the other end contains non-charged PEG exposed away from the surface. A typical example is a negatively charged surface first coated LbL with poly(allylamine hydrochloride) (PAH, polycationic) and poly(styrene sulfonate) (PSS, polyanionic), and lastly coated with a final layer of PLL-PEG, which effectively resisted protein adsorption.[40]

Multi-branched polymers are widely employed in generating cross-linked multilayers. For example, a mixture of epoxy- and amino-functionalized star-PEGs, can undergo self-crosslinking on the surface of substrates to form a chemically homogeneous protein-resistant coating.[98] A combination of LbL and crosslinking techniques was used by anchoring dendritic polyglycerol (dPG) using dopamine on a metal oxide surface, followed with stacking free catechols and dPG LbL, resulting in excellent protein resistance (reduced more than 70% of adsorption) and long-term stability.[99] In summary, these multilayer coating approaches can be done under mild conditions, since the immobilization of polymers was related to weak interactions such as

hydrogen bonding, electrostatic interactions, hydrophobic interaction, Van der Waals force, and self-driven crosslinking, which expands the choices of substrates and simplifies the coating steps.

In the conventional approach to an antifouling surface via grafting of polymer brushes, the degradation and detachment of grafted polymer chains would expose the underlying layer, leading to a loss of the antifouling effect. A special type of multi-layer protein repellent polymer coating is the self-healing surface coating on a 3D porous material generated from polymeric chains grafted both to the surface of the 3D network and inside the host network material.[100] In this case, the pH-responsive poly(2-vinylpyridine) (P2VP) films with the 3D grafting of poly(ethylene oxide) (PEO) in physiological conditions (pH 7.4 and 37 °C) show a 4-fold increase in longevity of antifouling behavior than the material with the surface grafted polymer. If a fraction of the grafted polymers is damaged, the proposed material with 3D polymer grafting retains its antifouling property due to the spontaneous (driven by an emerging gradient in a chemical potential) replacement of damaged chains with segments of the chains stored inside the film in proximity to the interface (Figure 1.13).

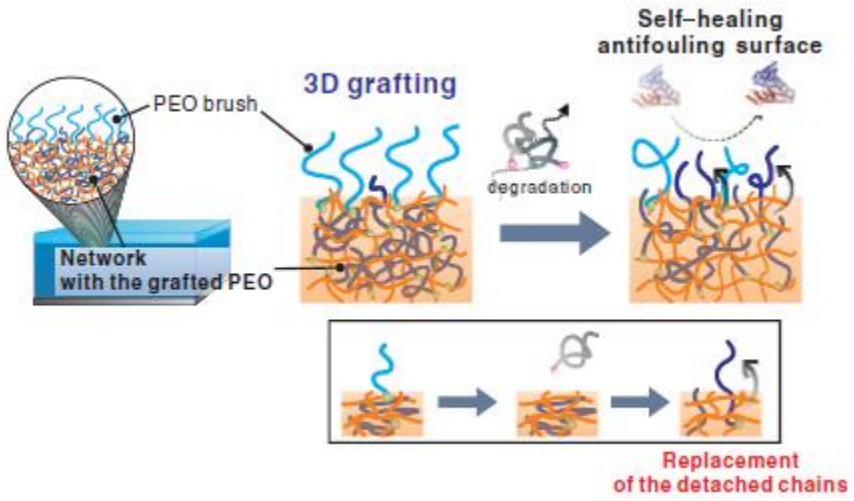

Figure 1.13 Schematic illustration of the 3D polymer grafting of PEO on the surface and inside of a P2VP network film. The self-healing aspect of the antifouling property is due to the rearrangement of internally grafted polymers to the interface (marked as dark blue chains). (Figure reproduced from Ref.[100])

Hydrogels are polymer networks extensively swollen with water that exhibit no flow in the steady-state. They sometimes are found as colloidal gels in which water is the dispersion medium.[101] They can be good candidates for various applications ranging from biomedical to daily chemical, such as drug delivery systems, biosensors, and superabsorbent polymer in diapers.[102-103] Hydrogels are less prone to protein adsorption relative to most biomaterials due to their hydrophilic and highly hydrated nature. Therefore, hydrogels prepared with aforementioned hydrophilic polymers are used for their protein-resistant properties. PEG based hydrogel is still the gold standard for

minimizing protein adsorption,[104] while other hydrogels prepared by POEGMA,[105] poly(vinyl alcohol),[106] dextran,[107] zwitterionic polymers,[108] polyoxazoline,[109] and also perform well in terms of protein repellency.

Copolymerization with hydrophilic monomers is another way to build in the protein resistant properties into hydrogels. For example, PHEMA-based hydrogels engineered with 0.5 mol% PEGMA and MPC in the range of 5–10 mol% lead to up to 64% less protein adsorption as compared to PHEMA, when incubated with the common extracellular matrix proteins including fibronectin, collagen or laminin.[110] Hydrogels prepared by copolymerizing carboxybetaines monomers with 2-hydroxyethyl methacrylate (HEMA) significantly reduced protein adsorption from blood plasma.[111]

Protein resistant hydrogels are applied in coating cell culture plates to facilitate or control the adhesion and growth of certain types of cells. For example, polyampholyte hydrogels prepared with equimolar quantities of positively charged [2-(acryloyloxy)ethyl] trimethylammonium chloride (TMA) and negatively charged 2-carboxyethyl acrylate (CAA) monomers were resistant to nonspecific protein adsorption, while subsequent covalent conjugation with fibrinogen using EDC chemistry significantly assisted the adhesion and growth of MC3T3-E1 cell as compared to the bare polystyrene well plate.[112] Similarly, protein-resistant crosslinked POEGMA hydrogel based on complementary hydrazide and aldehyde reactive polymer precursors was conjugated with cell adhesive RGD peptide which assist the adhesion and growth of 3T3 mouse fibroblast,[105] while the POEGMA hydrogels (without RGD) with different side chain length combinations demonstrated temperature-switchable protein and cell adhesion properties (Figure 1.14).[113] Similar results were achieved by covalently immobilized RGD gradient on protein-resistant PEG hydrogel scaffold, which effectively supported the growth of NIH 3T3 cells.[114-115]

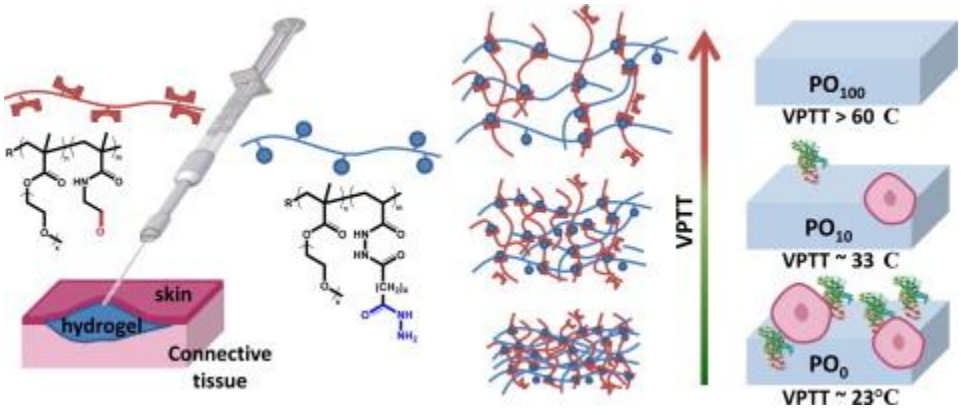

Figure 1.14 POEGMA hydrogels with a volume phase transition temperature (VPTT) below (PO_0, all short side chain), close to (PO_{10}, 10% long side chain and 90% short side chain) and well above (PO_{100}, all long side chain) physiological temperature have temperature-switchable protein and cell adhesion properties. (Figure reproduced from Ref.[113])

1.1.3 Applications of protein-resistant polymer and hydrogel coatings on biomaterials

1.1.3.1 Protein-resistant coatings for in vivo and in vitro biosensors

Biosensors are important tools for research in molecular biology, for medical diagnostics, environmental monitoring and food safety, allowing real-time observation and rapid detection of chemical and biological molecules and their interactions.[116] The success of a biosensor is based on sufficiently high and controlled binding capacity of target biomolecules, and also the activity of the immobilized biomolecules should be stable. One of the main problems with sensors, is loss of sensitivity due to biofouling, namely due to adhesion of proteins and other biological materials on the surface of the sensor. Biofouling (and its negative effects) has been observed in both *in vitro* (non-invasive) and *in vivo* (invasive) biosensors.[117-118] and it is widely regarded as the main cause of sensor failure.[119-120] Potential interference can be caused by nonspecific adsorption of biomolecules from the sample or the environment to the surface.[121] *In vitro* protein fouling studies have shown that biofouling on the membrane and the electrode would lead to decreased sensor signal.[119, 122]

To mitigate these problems, the sensor surface should have a low-fouling tendency, which is generally provided by using the bioinert polymers mentioned above.[25, 27, 123] Several approaches have been used to develop coatings that both enable a high degree of resistance to nonspecific adsorption and assist the immobilization of recognition molecules.[124-127] The immobilization of recognition molecules, which are often called bioreceptors, is usually done on carefully prepared low-fouling surfaces- the detailed methods and strategies of protein immobilization will be discussed in section 1.1.4 of this chapter.

A common strategy used in biosensing is the addition of inert proteins including BSA and casein, which can reduce the fouling rates by minimizing any hydrophobic and/or electrostatic attractions between the complex surface and the functionalized surface.[4, 11, 128] However, blocking with BSA sometimes leads to a substantial reduction of activity of the immobilized biomolecules/bioreceptor and decreased biorecognition activity thereby resulting in false negative results.[129-130] Instead, polymer coatings with active sites for binding active biomolecules have been developed for the application of highly sensitive biosensors.

PEG based polymers are most commonly used in passivation of biosensor surfaces. For example, a protein-resistant POEGMA brushes coated surface was functionalized with biotin and allowed further specific binding of streptavidin both on surface plasmon resonance (SPR) and quartz crystal microbalance (QCM) biosensors (Figure 1.15).[131] The resulting films showed enhanced signal-to-noise ratio (~10-fold enhancement) for the biospecific binding of streptavidin compared to biotinylated SAM without POEGMA, when fibrinogen and lysozyme were set as the interfering species. A similar approach is to use the activated end group of POEGMA on the surface to bond functionalized protein with Diels–Alder “click” reaction.[132]

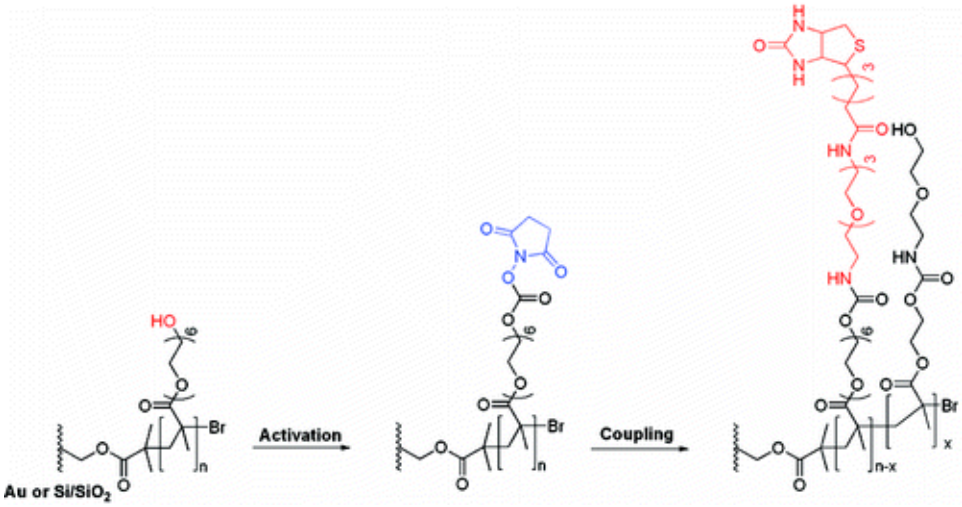

Figure 1.15 Schematic representation of the biotin conjugation reaction on POEGMA brushes on the sensor surface. (Figure reproduced from Ref.[131])

As a potential replacement of PEG based polymers, zwitterionic ultra-low-fouling pCBAA brushes were successfully used in immobilizing bioreceptors (in this case antibodies) on an SPR sensor (Figure 1.16).[133-134] This type of sensor was capable of detecting specific analytes in blood plasma without detectable signals of fouling molecules. Further studies from the same group used functionalized zwitterionic polymers to build up ω-dopamine-pCBAA grafted silicon resonator,[135] SiO_2-coated SPR sensor,[136] and catechol-pCBAA grafted gold SPR sensors.[137-138]

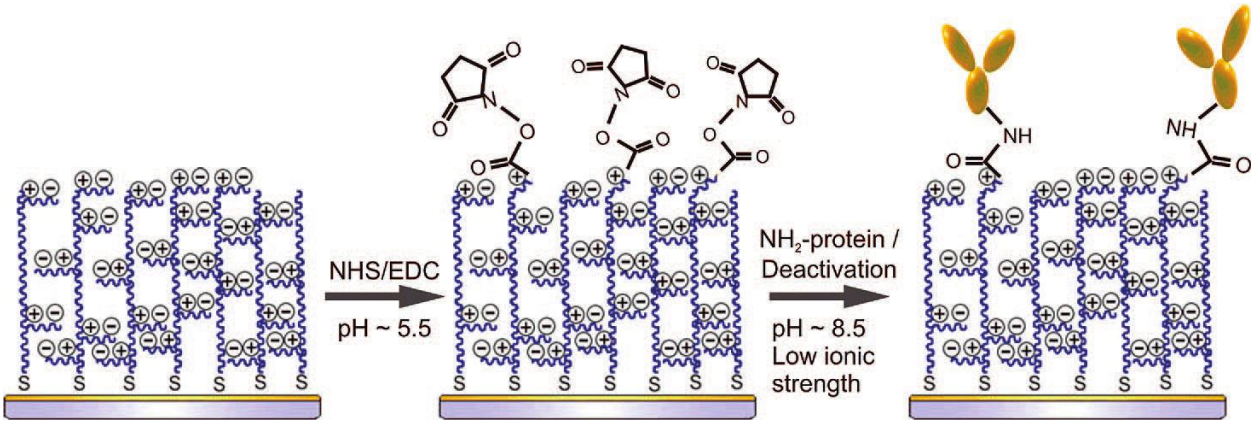

Figure 1.16 Schematic of the surface activation, protein immobilization, and surface deactivation of a pCBAA coated surface. (Figure reproduced from Ref.[133])

Unlike the flat basic materials used in aforementioned equipment-based biosensors, some point-of-care biosensors are built up on inexpensive porous materials such as paper and nitrocellulose membranes. Development of these types of paper-based devices for diagnostics and biosensing has attracted a great deal of interest as they provide portable, low-cost, low-volume, disposable, and simple analytical devices for bioassays and environmental analysis.[139] Recently, bioactive paper or lab-on-paper devices have been developed as a practical platform for assays in many different areas such as diagnostics, food and water testing, and military applications.[140-142] These paper-based sensing devices can be applied not only in point-of-care testing but also in field analysis. This technology is already having an impact in low-cost testing, and is expected to be used globally and in particular in resource-limited settings, in the near future.

While there are several proof-of-concept studies showing the potential of paper-based analytical devices, the adsorption and non-specific binding of proteins on paper surface is a serious problem for regular paper surfaces which may largely influence the accuracy of sensors.[143-144] The passivation of porous materials remains challenging as compared to the flat surfaces. As a basic requirement for the design and preparation of paper-based biosensor, anti-fouling properties must be built into the surface.[145] For this purpose, they are usually provided by modification with aforementioned hydrophilic polymers such as PEG analogues or zwitterionic polymers. For example, poly(carboxybetaine) (PCB) coated cellulose paper could significantly reduced the adsorption of human fibrinogen as compared with that of the unmodified control, and achieved rapid and sensitive glucose detection from undiluted human serum and specific antigen detection via covalently immobilized antibodies (Figure 1.17).[146]

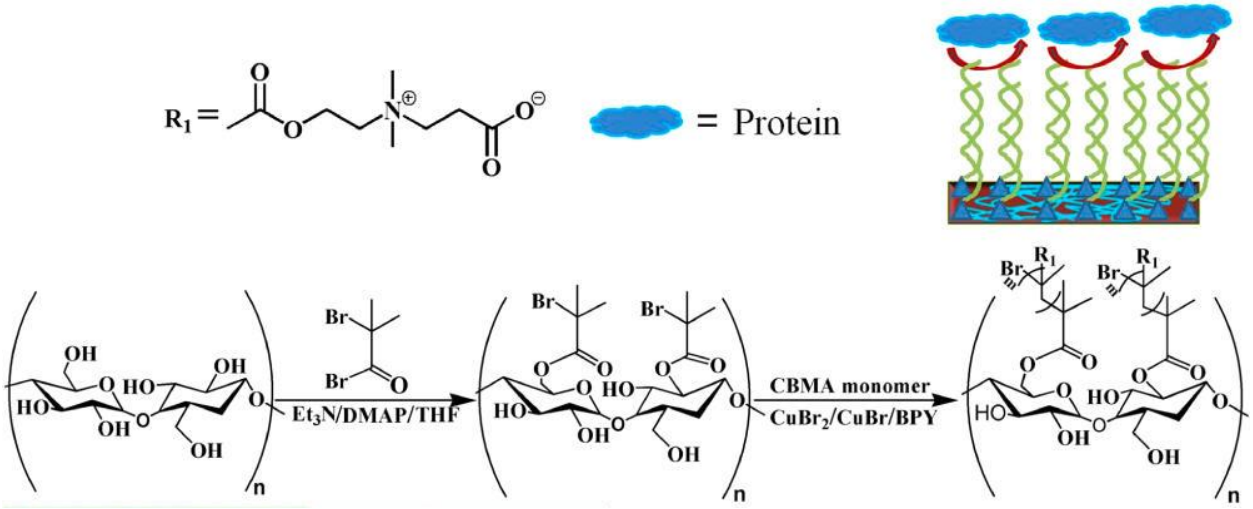

Figure 1.17 The reaction scheme of grafting protein-resistant poly(carboxybetaine) (PCB) onto cellulose substrates. (Figure reproduced from Ref.[146])

1.1.3.2 Protein-resistant coatings for contact lenses

Soft contact lenses made with hydrogels have been widely used for vision correction over more than 50 years.[147] These lenses always suffer from challenges related to the deposition of proteins from the tear fluid onto the lenses, such as lysozyme, human serum albumin and globulin,[148-152] and subsequent formation of a coating layer of protein on the surface will serve as a precursor for microbial colonization and will induce the formation of biofilms. Therefore, protein adsorption on contact lenses is correlated to microbial cell attachment and some severe issues for the wearer.[153-155] In addition, a strong correlation has been found between the deposited lysozyme from the tear film onto the lenses and discomfort experience by the wearer.[156]

Synthetic polymers associated with low protein adsorption, including poly(ethylene glycol) (PEG)[157] and 2-methacryloyloxyethyl phosphorylcholine (MPC),[158-159] and polymers with hydration improvement effects, such as poly(vinyl alcohol) (PVA),[160-161] have been entrapped within the bulk of the lens and improved the comfort of long term wear. Due to the protein-resistance-promoting properties of hyaluronic acid (HA),[162-164] a natural polysaccharide present in the tear film, various methods have been reported to incorporate HA into the bulk of the lens. Crosslinking is the most commonly used method to introduce HA into the bulk hydrogel network, with HA incorporation demonstrated directly with the main lens material(s) (e.g. via photopolymerization of methacrylated photocrosslinkable HA with HEMA[165]), within a secondary interpenetrating network (e.g. polyethyleneimine crosslinked HA within an independently crosslinked HEMA network[164]), or via physical entrapment of a higher molecular weight HA-based cluster or nanogel (e.g. conjugation of HA to polypropylenimine tetramine dendrimers that improve HA immobilization within the lens)[162-163, 166-167]. All of these approaches lowered the lysozyme and/or human serum albumin adsorption as compared to the native gels and have great potential to be developed into daily used contact lenses.

1.1.3.3 Protein-resistant hydrogel coatings on porous materials

As mentioned in the previous section, various types of hydrogels are protein repellent and the hydrogels coated on the cell culturing biointerfaces have great potential in reducing protein adsorption and controlling cell adhesion. Hydrogels have also been used in coating porous materials such as filtration membranes and tissue engineering implants in order to reduce fouling from the proteins and other components such as cells from the blood serum/plasma.

Membrane biofouling is a process that starts immediately upon contact of the surface with the fluid containing proteins, cells, particles and other components. They adhere to the surfaces in the pores of the membrane.[168] The most common method to improve membrane anti-fouling properties is by hydrophilic coating of the surfaces through physical adsorption, crosslinking, and sulfonation, or surface grafting through UV photo irradiation, plasma, high energy irradiation and "living"/controlled polymerisation.[169].

Anti-fouling hydrogel coating on porous solid substrates is a relative new technique in membrane surface modification. PEG-based hydrogel has been coated on polyamide nanofiltration membranes, and such modified membranes shows an improved fouling resistance compared to pristine membranes.[170] A bifunctional hydrogel-coated film exhibiting both protein fouling resistance and antimicrobial activities was prepared by the copolymerization of poly(ethylene glycol) diacrylate (PEGDA) and a functional monomer containing ammonium salt (RNH_3Cl) on polysulfones (PSF) membranes.[171] A hydrophilic hyperbranched poly(amido amine) (PAMAM) was successfully bonded onto the active polyamide reverse osmosis-membrane by chemical coupling.[172] Membranes modified with aqueous PAMAM solution showed very low protein adsorption compared to unmodified samples or samples modified with methanolic PAMAM solution. A poly(vinyl alcohol) (PVA) based polymer was synthesized and subsequently applied to modify a poly(vinylidene fluoride) (PVDF) membrane to both enhance the hydrophilicity and provide fouling resistance.

Free standing films containing hydrogel coating are prepared by a combination process of polymerization and crosslinking. For example, a polyhedral oligomeric silsesquioxane (POSS) derivative containing UV-curable methacrylate groups (methacryl-POSS) was used as a multifunctional cross-linker to form thin and durable hydrogel films with poly(ethylene glycol) methacrylate (PEGMA) as a hydrophilic comonomer.[173] Free standing films prepared by crosslinking PEG matrix on ultra-fine cellulose nanofibers exhibited excellent anti-fouling properties, which were confirmed by short-term and long-term fouling tests using a BSA solution.[174] Another free-standing membrane was synthesized through polymerization of acrylamide in the presence of sodium alginate using N,N'-methylene-bisacrylamide as the covalent crosslinker and $CaCl_2$ as the ionic crosslinker, and exhibited low fouling properties against yeast suspension and BSA solution.[175] Crosslinked PEGDA hydrogels as a free-standing ultrafiltration membrane film could absorb significant amounts of water, and the results from static protein adhesion experiments showed that more hydrophilic surfaces, obtained from higher prepolymerization water content or with longer PEGDA chains, generally exhibit less bovine serum albumin (BSA) accumulation.[176]

In addition, there are a few trials that used hydrogel coatings on tissue engineering implant materials to reduce the protein and cell fouling from the body fluid and tissue *in vivo*. Polyvinylpyrrolidone (PVP) hydrogel coating bonded to a polyurethane (PU) substrate improved the surface hemocompatibility of blood-contacting medical devices as shown by a reduced abruption of serum-derived fibrinogen and number of platelet aggregates formed during the contact of the material with blood over a long period (35 days).[177] In another approach, ECM hydrogel coated polypropylene mesh device was shown to decrease the long-term host tissue response to the device when compared to the uncoated mesh devices due to a decreased collagen deposition at day 180.[178]

1.1.4 Bioactive surfaces with protein immobilization

Creating surfaces that encourage specific protein binding has also been the focus of extensive research.[179-181] These type of bioactive surfaces have been used in biosensor and diagnostics,[182] tissue engineering,[183] and implant materials.[184] Proteins including antibodies, enzymes, extracellular matrix (ECM) proteins (including their active components) have been immobilized on surfaces, to promote specific interactions.

Selective immobilization of sensing biomolecules (enzymes, antibodies etc.) promotes specific interactions for electrodes, biosensors and microarray applications.[185-186] Antibody-antigen interaction is one of the most widely used specific interacting pairs for biorecognition. Antibodies, especially immunoglobulin G (IgG) binds with antigens with high affinity. IgG is a Y shaped protein with a molecular weight of approximately 150 kDa, including two antigen binding sites at the top of the Y and one stem site without antigen-binding activity. The active binding sites of the immobilized IgG used in biosensors should be exposed to the analytes containing antigens, which means that suitable orientation of the immobilized IgG on the surface is key to the efficiency of recognition and performance of the biosensor. [187-189]

The strategies of immobilizing antibodies can be categorized into three groups: covalent binding, physical adsorption, and specific biochemical interactions (bioaffinity).[182, 190] The most commonly used method is covalent binding. This method makes use of the amine groups on the antibody, which can be linked to an activated carboxy-functionalized surfaces.[130, 191] Since amine groups are distributed randomly on the antibody, the binding sites may be linked onto the surface. This can lead to an unfavorable orientation, thereby decreasing the availability of binding to the target antigen. Instead, thiol groups on the cysteine residues can be used for covalent binding.[192] The cysteine group can bind to maleimide-functionalized surfaces without destroying the binding sites. Methods based on physical adsorption of antibodies mainly employ ionic or hydrophobic interactions, which also suffer from the disadvantage of random antibody orientation.[190] In general, a randomly orientated immobilization is unfavorable for antigen binding, it may change the structure of active binding sites and sometimes leads to protein denaturation.

Specific biochemical interaction is an attractive strategy for antibody immobilization because of its high affinity and selectivity. The biotin/(strept)avidin system[193] is particularly attractive in regards to immobilizing proteins for making sensors, chips and arrays since many biotin or (strept)avidin-linked sensing molecules are commercially-available.[194] For instance, avidin or streptavidin coated surface can be used for anchoring biotinylated antibodies (Figure 1.18),[190, 195-197] or chemically bonded biotin on the polymer coated surface for subsequent binding of avidin derivatives.[198] Another specific biochemical interaction method is to use protein A and protein G to bind to the F_c region of antibodies without interfering the active F_{ab} region, which can also immobilize the antibody in a suitable oriented fashion.[199-201]

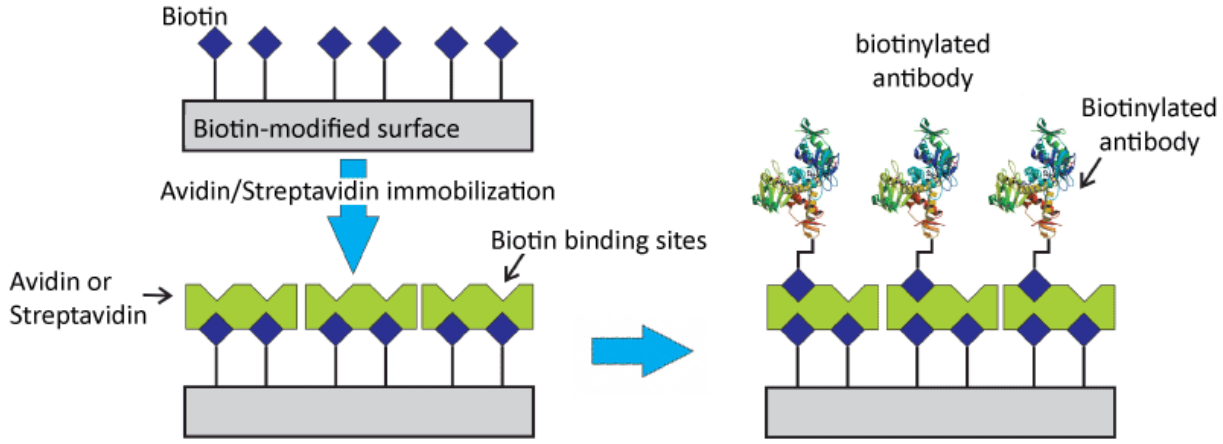

Figure 1.18 Depicting antibody attachment via biotin-avidin/streptavidin interactions. Initially, biotin is physically or covalently immobilized above an appropriate solid support and then further modified with multivalent avidin or streptavidin. A biotin labeled antibody is then attached. (Figure reproduced from Ref.[195])

Immobilization of ECM proteins (fibronectin, collagen etc.) and protein-based growth factors on surfaces can assist cell adhesion and promote cell growth in cell culture and tissue engineering.[202] The orientation of ECM proteins and growth factors on the surface are not as important as when using antibodies. Covalent conjugation of ECM proteins usually relies on the use of crosslinkers such as glutaraldehyde. For example, a poly(L-lactide-co-caprolactone) (PLLC) surface was first functionalized with 1,6-hexanediamine, and the amine group generated on the surface was crosslinked with the amine on the fibronectin and collagen by adding glutaraldehyde.[203] The surface containing immobilized fibronectin or collagen was able to support a long-term culture of epithelial cells. In another method, pyridyl disulphide was used to activate the PEG chains in Pluronic F108, and then conjugated with the thiolated fibronectin.[204] Epidermal growth factor (EGF) was covalently tethered to aminosilane-modified glass via a star shaped PEG, which elicited DNA synthesis and cell rounding responses of primary rat hepatocytes as compared to physically adsorbed EGF.[205]

1.2 Objectives

As reviewed and discussed in the previous sections of this Introduction chapter, nonspecific protein adsorption is a significant challenge in the development of biosensors and implantable biomaterials. On the opposite side to the spectrum, in some case it is necessary to attach proteins (and other biorecognition elements) to surfaces in highly specific manner- current protein immobilization methods can possibly interfere with the binding sites and thus reduce the activity

of biorecognition and specificity of binding. The objective of this thesis is try to solve these problems, as well as to develop biosensor and biomaterials with specific functions built-in. These sensors and materials should be easy to prepare, ready-to-use and capable of keeping their functionality for the long term.

This thesis focuses on the practical engineering aspects of applying various surface modification techniques to prepare functional biomaterials. All the work in this thesis targets on making functionalized materials and interfaces for the applications in biosensors and hydrogels. The specific goals for the various parts of this thesis were:

1. To develop a simple and scalable method to modify the surface of paper to minimize non-specific protein adsorption and to allow proteins to move with the water-front in lateral flow experiments. The coating should not alter the macroporosity of the paper, so that capillary flow in the paper is not slowed down. These objectives were achieved and proof-of-principle was obtained by performing highly selective paper-based enzyme-linked immunosorbent assays (ELISAs) that exhibit both lower limits of detection and higher dynamic ranges relative to papers blocked with the conventional blocking agents
2. To reduce protein adsorption on the surface of contact lenses from the tear film, by using a simple, yet effective polymer coating method. The physical and chemical properties of the contact lens material should not be greatly altered, while the hydrophilicity, water retention ability should be improved after the polymer coating.
3. To develop a fast and highly sensitive method to perform ELISAs on quartz crystal microbalances (QCM). The antibodies should be efficiently immobilized on the surface of a gold QCM biosensor, without affecting the bioactivity of the antibodies with respect of their specificity and ability to bind the antigens. The signal from the QCM should be large enough to allow specific detection of low concentrations of analyte in samples
4. To develop a biocompatible fast-self-healing hydrogel which is capable of healing at physiological pH as well as a wider range of conditions.

1.3 Thesis outline

Chapter 1. Introduction. This chapter presents a thorough background introduction of the project, as well as the relevant research reported in the literature. Controlling protein adsorption on biomaterials surfaces is extensively discussed, especially the methods for preparing protein-resistant polymer coating and methods for protein immobilization in surfaces. The objectives of the research project and the thesis outline are also listed in this chapter.

Chapter 2. Poly(oligoethylene glycol methacrylate) dip-coating: turning cellulose paper into a protein-repellent platform for biosensors. This chapter describes a passivation method to minimize non-specific protein adsorption onto paper by using hydrogel coatings. The *in situ* gelation of two POEGMA polymer precursors forms a thin layer of hydrogel coating on the cellulose surface, which does not affect the fiber morphology or macropore network of the paper. The hydrogel coating enables proteins to move in lateral flow tests, and also facilitates performing paper-based

ELISAs that exhibit both lower limits of detection and higher dynamic ranges relative to papers blocked with traditional methods. This work has been published in *Journal of the American Chemical Society*.[39]

Chapter 3. 'Click' chemistry-tethered hyaluronic acid-based contact lens coatings improve lens wettability and lower protein adsorption. This chapter reports a simple, mixing-based protocol for conjugating hyaluronic acid (HA) on the surface of a contact lens material using "click" hydrazone chemistry. This coating method only requires a one-step functionalization process for both the grafting of HA polymer and the oxidation of the PHEMA-based contact lens surface. Specially, the TEMPO/laccase-mediated oxidation method is reported here for the first time for oxidizing PHEMA. The lenses obtained from the one-step coating process are significantly more wettable, more water-retentive, and less prone to protein adsorption than the native lenses, without changing their transparency, refractive index, or key mechanical properties. This work has been published in *ACS Applied Materials & Interfaces*.[206]

Chapter 4. A highly sensitive immunosorbent assay based on biotinylated graphene oxide and the quartz crystal microbalance. This chapter describes a new approach for performing high sensitivity biomolecular assays by employing the high adsorption capacity of graphene oxide with the sensitivity of the quartz crystal microbalance (QCM). Antibodies were extensively immobilized onto the gold QCM sensor surface through the physical adsorption of graphene oxide and the specific biological interactions between biotin and avidin. This strategy allows complete functionalization of the QCM sensor within 5 hours, and gives quantitative detection of rabbit IgG concentrations ranging from 0.1 ng/mL to 10 μg/mL with high specificity. This work has been published in *ACS Applied Materials & Interfaces*.[207]

Chapter 5 Rapid self-healing of 2-amino phenylboronic acid-functionalized hyaluronic acid/poly(vinyl alcohol) hydrogels at both neutral and acidic pH. This chapter provides a novel method of synthesizing fast self-healing hydrogels through dynamic crosslinking using phenylboronic acid-modified hyaluronic acid and PVA. Once cut this hydrogel can "heal" and recover its mechanical integrity within 1 minute of cutting under both neutral and acidic pH conditions. The broad pH range under which the self-healing capability is maintained makes this biomaterial highly attractive for various applications. This chapter is in preparation for publication.

Chapter 6: Concluding remarks. This chapter summarizes the major contributions of this study.

References

1. Anderson, J. M., Biological responses to materials. *Annual Review of Materials Research* **2001,** *31* (1), 81-110.
2. Norde, W., My voyage of discovery to proteins in flatland… and beyond. *Colloids and Surfaces B: Biointerfaces* **2008,** *61* (1), 1-9.

3. Silva, R. A.; Urzúa, M. D.; Petri, D. F.; Dubin, P. L., Protein adsorption onto polyelectrolyte layers: effects of protein hydrophobicity and charge anisotropy. *Langmuir* **2010,** *26* (17), 14032-14038.
4. Jeyachandran, Y.; Mielczarski, J.; Mielczarski, E.; Rai, B., Efficiency of blocking of non-specific interaction of different proteins by BSA adsorbed on hydrophobic and hydrophilic surfaces. *Journal of colloid and interface science* **2010,** *341* (1), 136-142.
5. Wang, K.; Zhou, C.; Hong, Y.; Zhang, X., A review of protein adsorption on bioceramics. *Interface focus* **2012,** *2* (3), 259-277.
6. Meyers, S. R.; Grinstaff, M. W., Biocompatible and bioactive surface modifications for prolonged in vivo efficacy. *Chemical reviews* **2012,** *112* (3), 1615-1632.
7. Ratner, B. D., Replacing and renewing: synthetic materials, biomimetics, and tissue engineering in implant dentistry. *Journal of dental education* **2001,** *65* (12), 1340-1347.
8. Wei, Q.; Becherer, T.; Angioletti-Uberti, S.; Dzubiella, J.; Wischke, C.; Neffe, A. T.; Lendlein, A.; Ballauff, M.; Haag, R., Protein interactions with polymer coatings and biomaterials. *Angewandte Chemie International Edition* **2014,** *53* (31), 8004-8031.
9. Amiji, M.; Park, K., Surface modification of polymeric biomaterials with poly (ethylene oxide), albumin, and heparin for reduced thrombogenicity. *Journal of Biomaterials Science, Polymer Edition* **1993,** *4* (3), 217-234.
10. Oliva, A. G.; Cruz, H.; Rosa, C., Immunosensors for diagnostics. *Sensors Update* **2001,** *9*, 283-312.
11. Ogi, H.; Fukunishi, Y.; Nagai, H.; Okamoto, K.; Hirao, M.; Nishiyama, M., Nonspecific-adsorption behavior of polyethylenglycol and bovine serum albumin studied by 55-MHz wireless–electrodeless quartz crystal microbalance. *Biosensors and Bioelectronics* **2009,** *24* (10), 3148-3152.
12. Hucknall, A.; Rangarajan, S.; Chilkoti, A., In pursuit of zero: polymer brushes that resist the adsorption of proteins. *Advanced Materials* **2009,** *21* (23), 2441-2446.
13. Langer, R.; Tirrell, D. A., Designing materials for biology and medicine. *Nature* **2004,** *428* (6982), 487-492.
14. Schöttler, S.; Becker, G.; Winzen, S.; Steinbach, T.; Mohr, K.; Landfester, K.; Mailänder, V.; Wurm, F. R., Protein adsorption is required for stealth effect of poly (ethylene glycol)-and poly (phosphoester)-coated nanocarriers. *Nature nanotechnology* **2016,** *11* (4), 372-377.
15. Del Pino, P.; Pelaz, B.; Zhang, Q.; Maffre, P.; Nienhaus, G. U.; Parak, W. J., Protein corona formation around nanoparticles–from the past to the future. *Materials Horizons* **2014,** *1* (3), 301-313.
16. Pelegri-O'Day, E. M.; Lin, E.-W.; Maynard, H. D., Therapeutic protein–polymer conjugates: advancing beyond PEGylation. *Journal of the American Chemical Society* **2014,** *136* (41), 14323-14332.
17. Vogler, E. A., Structure and reactivity of water at biomaterial surfaces. *Advances in colloid and interface science* **1998,** *74* (1), 69-117.
18. Bolduc, O. R.; Clouthier, C. M.; Pelletier, J. N.; Masson, J.-F., Peptide self-assembled monolayers for label-free and unamplified surface plasmon resonance biosensing in crude cell lysate. *Analytical chemistry* **2009,** *81* (16), 6779-6788.
19. Prime, K. L.; Whitesides, G. M., Self-assembled organic monolayers: model systems for studying adsorption of proteins at surfaces. *Science (New York, NY)* **1991,** *252* (5009), 1164-1167.
20. Calderón, M.; Quadir, M. A.; Sharma, S. K.; Haag, R., Dendritic polyglycerols for biomedical applications. *Advanced Materials* **2010,** *22* (2), 190-218.

21. Holland, N. B.; Qiu, Y.; Ruegsegger, M.; Marchant, R. E., Biomimetic engineering of non-adhesive glycocalyx-like surfaces using oligosaccharide surfactant polymers. *Nature* **1998,** *392* (6678), 799-801.
22. Pidhatika, B.; Möller, J.; Benetti, E. M.; Konradi, R.; Rakhmatullina, E.; Mühlebach, A.; Zimmermann, R.; Werner, C.; Vogel, V.; Textor, M., The role of the interplay between polymer architecture and bacterial surface properties on the microbial adhesion to polyoxazoline-based ultrathin films. *Biomaterials* **2010,** *31* (36), 9462-9472.
23. Deng, L.; Mrksich, M.; Whitesides, G. M., Self-assembled monolayers of alkanethiolates presenting tri (propylene sulfoxide) groups resist the adsorption of protein. *Journal of the American Chemical Society* **1996,** *118* (21), 5136-5137.
24. Higuchi, A.; Shirano, K.; Harashima, M.; Yoon, B. O.; Hara, M.; Hattori, M.; Imamura, K., Chemically modified polysulfone hollow fibers with vinylpyrrolidone having improved blood compatibility. *Biomaterials* **2002,** *23* (13), 2659-2666.
25. Jiang, S.; Cao, Z., Ultralow-fouling, functionalizable, and hydrolyzable zwitterionic materials and their derivatives for biological applications. *Advanced Materials* **2010,** *22* (9), 920-932.
26. Amoozgar, Z.; Yeo, Y., Recent advances in stealth coating of nanoparticle drug delivery systems. *Wiley Interdisciplinary Reviews: Nanomedicine and Nanobiotechnology* **2012,** *4* (2), 219-233.
27. Chen, H.; Yuan, L.; Song, W.; Wu, Z.; Li, D., Biocompatible polymer materials: role of protein–surface interactions. *Progress in Polymer Science* **2008,** *33* (11), 1059-1087.
28. Kane, R. S.; Deschatelets, P.; Whitesides, G. M., Kosmotropes form the basis of protein-resistant surfaces. *Langmuir* **2003,** *19* (6), 2388-2391.
29. Groll, J.; Amirgoulova, E. V.; Ameringer, T.; Heyes, C. D.; Röcker, C.; Nienhaus, G. U.; Möller, M., Biofunctionalized, ultrathin coatings of cross-linked star-shaped poly (ethylene oxide) allow reversible folding of immobilized proteins. *Journal of the American Chemical Society* **2004,** *126* (13), 4234-4239.
30. Hynes, R. O., Integrins: bidirectional, allosteric signaling machines. *Cell* **2002,** *110* (6), 673-687.
31. Humphries, M., Integrin structure. *Biochemical Society Transactions* **2000,** *28* (4), 311-340.
32. Liu, L.; Qin, C.; Butler, W. T.; Ratner, B. D.; Jiang, S., Controlling the orientation of bone osteopontin via its specific binding with collagen I to modulate osteoblast adhesion. *Journal of Biomedical Materials Research Part A* **2007,** *80* (1), 102-110.
33. Petrie, T. A.; Capadona, J. R.; Reyes, C. D.; García, A. J., Integrin specificity and enhanced cellular activities associated with surfaces presenting a recombinant fibronectin fragment compared to RGD supports. *Biomaterials* **2006,** *27* (31), 5459-5470.
34. Keselowsky, B. G.; Collard, D. M.; García, A. J., Integrin binding specificity regulates biomaterial surface chemistry effects on cell differentiation. *Proceedings of the National Academy of Sciences* **2005,** *102* (17), 5953-5957.
35. Kim, K.; Kim, C.; Byun, Y., Preparation of a dipalmitoylphosphatidylcholine/cholesterol Langmuir-Blodgett monolayer that suppresses protein adsorption. *Langmuir* **2001,** *17* (16), 5066-5070.
36. Onclin, S.; Ravoo, B. J.; Reinhoudt, D. N., Engineering silicon oxide surfaces using Self-Assembled monolayers. *Angewandte Chemie International Edition* **2005,** *44* (39), 6282-6304.

37. Li, R.; Barbari, T., Performance of poly (vinyl alcohol) thin-gel composite ultrafiltration membranes. *Journal of membrane science* **1995,** *105* (1), 71-78.
38. Mizrahi, B.; Khoo, X.; Chiang, H. H.; Sher, K. J.; Feldman, R. G.; Lee, J.-J.; Irusta, S.; Kohane, D. S., Long-lasting antifouling coating from multi-armed polymer. *Langmuir* **2013,** *29* (32), 10087-10094.
39. Deng, X.; Smeets, N. M.; Sicard, C.; Wang, J.; Brennan, J. D.; Filipe, C. D.; Hoare, T., Poly (oligoethylene glycol methacrylate) dip-coating: turning cellulose paper into a protein-repellent platform for biosensors. *Journal of the American Chemical Society* **2014,** *136* (37), 12852–12855.
40. Heuberger, R.; Sukhorukov, G.; Vörös, J.; Textor, M.; Möhwald, H., Biofunctional polyelectrolyte multilayers and microcapsules: control of non-specific and bio-specific protein adsorption. *Advanced Functional Materials* **2005,** *15* (3), 357-366.
41. Harder, P.; Grunze, M.; Dahint, R.; Whitesides, G.; Laibinis, P., Molecular conformation in oligo (ethylene glycol)-terminated self-assembled monolayers on gold and silver surfaces determines their ability to resist protein adsorption. *The Journal of Physical Chemistry B* **1998,** *102* (2), 426-436.
42. Blaszykowski, C.; Sheikh, S.; Thompson, M., Surface chemistry to minimize fouling from blood-based fluids. *Chemical Society Reviews* **2012,** *41* (17), 5599-5612.
43. Jeon, S.; Lee, J.; Andrade, J.; De Gennes, P., Protein—surface interactions in the presence of polyethylene oxide: I. Simplified theory. *Journal of Colloid and Interface Science* **1991,** *142* (1), 149-158.
44. Feldman, K.; Hähner, G.; Spencer, N.; Harder, P.; Grunze, M., Probing resistance to protein adsorption of oligo (ethylene glycol)-terminated self-assembled monolayers by scanning force microscopy. *Journal of the American Chemical Society* **1999,** *121* (43), 10134-10141.
45. Zolk, M.; Eisert, F.; Pipper, J.; Herrwerth, S.; Eck, W.; Buck, M.; Grunze, M., Solvation of oligo (ethylene glycol)-terminated self-assembled monolayers studied by vibrational sum frequency spectroscopy. *Langmuir* **2000,** *16* (14), 5849-5852.
46. Wang, R.; Kreuzer, H.; Grunze, M., Molecular conformation and solvation of oligo (ethylene glycol)-terminated self-assembled monolayers and their resistance to protein adsorption. *The Journal of Physical Chemistry B* **1997,** *101* (47), 9767-9773.
47. Chen, S.; Li, L.; Zhao, C.; Zheng, J., Surface hydration: principles and applications toward low-fouling/nonfouling biomaterials. *Polymer* **2010,** *51* (23), 5283-5293.
48. Zheng, J.; Li, L.; Tsao, H.-K.; Sheng, Y.-J.; Chen, S.; Jiang, S., Strong repulsive forces between protein and oligo (ethylene glycol) self-assembled monolayers: a molecular simulation study. *Biophysical journal* **2005,** *89* (1), 158-166.
49. Chen, S.; Li, L.; Boozer, C. L.; Jiang, S., Controlled chemical and structural properties of mixed self-assembled monolayers of alkanethiols on Au (111). *Langmuir* **2000,** *16* (24), 9287-9293.
50. Jeon, S.; Andrade, J., Protein—surface interactions in the presence of polyethylene oxide: II. Effect of protein size. *Journal of Colloid and Interface Science* **1991,** *142* (1), 159-166.
51. Wu, J.; Zhao, C.; Hu, R.; Lin, W.; Wang, Q.; Zhao, J.; Bilinovich, S. M.; Leeper, T. C.; Li, L.; Cheung, H. M., Probing the weak interaction of proteins with neutral and zwitterionic antifouling polymers. *Acta biomaterialia* **2014,** *10* (2), 751-760.
52. Chang, Y.; Chu, W. L.; Chen, W. Y.; Zheng, J.; Liu, L.; Ruaan, R. C.; Higuchi, A., A systematic SPR study of human plasma protein adsorption behavior on the controlled surface

packing of self-assembled poly (ethylene oxide) triblock copolymer surfaces. *Journal of Biomedical Materials Research Part A* **2010,** *93* (1), 400-408.
53. Elbert, D. L.; Hubbell, J. A., Reduction of fibrous adhesion formation by a copolymer possessing an affinity for anionic surfaces. *Journal of biomedical materials research* **1998,** *42* (1), 55-65.
54. Huang, N.-P.; Michel, R.; Voros, J.; Textor, M.; Hofer, R.; Rossi, A.; Elbert, D. L.; Hubbell, J. A.; Spencer, N. D., Poly (L-lysine)-g-poly (ethylene glycol) layers on metal oxide surfaces: surface-analytical characterization and resistance to serum and fibrinogen adsorption. *Langmuir* **2001,** *17* (2), 489-498.
55. Dalsin, J. L.; Messersmith, P. B., Bioinspired antifouling polymers. *Materials today* **2005,** *8* (9), 38-46.
56. Hofer, R.; Textor, M.; Spencer, N., Alkyl phosphate monolayers, self-assembled from aqueous solution onto metal oxide surfaces. *Langmuir* **2001,** *17* (13), 4014-4020.
57. Pop-Georgievski, O.; Popelka, S. t. p. n.; Houska, M.; Chvostová, D.; Proks, V.; Rypáček, F. e., Poly (ethylene oxide) layers grafted to dopamine-melanin anchoring layer: stability and resistance to protein adsorption. *Biomacromolecules* **2011,** *12* (9), 3232-3242.
58. Sileika, T. S.; Kim, H.-D.; Maniak, P.; Messersmith, P. B., Antibacterial performance of polydopamine-modified polymer surfaces containing passive and active components. *ACS applied materials & interfaces* **2011,** *3* (12), 4602-4610.
59. Wei, Q.; Li, B.; Yi, N.; Su, B.; Yin, Z.; Zhang, F.; Li, J.; Zhao, C., Improving the blood compatibility of material surfaces via biomolecule-immobilized mussel-inspired coatings. *Journal of biomedical materials research Part A* **2011,** *96* (1), 38-45.
60. Rana, D.; Matsuura, T., Surface modifications for antifouling membranes. *Chemical reviews* **2010,** *110* (4), 2448-2471.
61. Zhou, Y.; Huang, W.; Liu, J.; Zhu, X.; Yan, D., Self-Assembly of Hyperbranched Polymers and Its Biomedical Applications. *Advanced Materials* **2010,** *22* (41), 4567-4590.
62. Siegers, C.; Biesalski, M.; Haag, R., Self-Assembled Monolayers of Dendritic Polyglycerol Derivatives on Gold That Resist the Adsorption of Proteins. *Chemistry–A European Journal* **2004,** *10* (11), 2831-2838.
63. Minko, S., Grafting on solid surfaces:"Grafting to" and "grafting from" methods. In *Polymer surfaces and interfaces*, Springer: **2008**, pp 215-234.
64. Ma, H.; Hyun, J.; Stiller, P.; Chilkoti, A., "Non-Fouling" Oligo (ethylene glycol)-Functionalized Polymer Brushes Synthesized by Surface-Initiated Atom Transfer Radical Polymerization. *Advanced Materials* **2004,** *16* (4), 338-341.
65. Yu, Q.; Zhang, Y.; Wang, H.; Brash, J.; Chen, H., Anti-fouling bioactive surfaces. *Acta biomaterialia* **2011,** *7* (4), 1550-1557.
66. Jiang, X.; Chen, H. Y.; Galvan, G.; Yoshida, M.; Lahann, J., Vapor-Based Initiator Coatings for Atom Transfer Radical Polymerization. *Advanced Functional Materials* **2008,** *18* (1), 27-35.
67. Ma, H.; Wells, M.; Beebe, T. P.; Chilkoti, A., Surface-Initiated Atom Transfer Radical Polymerization of Oligo (ethylene glycol) Methyl Methacrylate from a Mixed Self-Assembled Monolayer on Gold. *Advanced Functional Materials* **2006,** *16* (5), 640-648.
68. Yang, J.; Lv, J.; Behl, M.; Lendlein, A.; Yang, D.; Zhang, L.; Shi, C.; Guo, J.; Feng, Y., Functionalization of polycarbonate surfaces by grafting PEG and zwitterionic polymers with a multicomb structure. *Macromolecular bioscience* **2013,** *13* (12), 1681-1688.

69. Gunkel, G.; Weinhart, M.; Becherer, T.; Haag, R.; Huck, W. T., Effect of polymer brush architecture on antibiofouling properties. *Biomacromolecules* **2011,** *12* (11), 4169-4172.
70. Lutz, J. F., Polymerization of oligo(ethylene glycol) (meth)acrylates: Toward new generations of smart biocompatible materials. *J Polym Sci Pol Chem* **2008,** *46* (11), 3459-3470.
71. Hyun, J.; Ma, H.; Zhang, Z.; Beebe Jr, T. P.; Chilkoti, A., Universal route to cell micropatterning using an amphiphilic comb polymer. *Adv Mater* **2003,** *15* (7-8), 576-579.
72. Ma, H. W.; Hyun, J. H.; Stiller, P.; Chilkoti, A., "Non-fouling" oligo(ethylene glycol)-functionalized polymer brushes synthesized by surface-initiated atom transfer radical polymerization. *Adv Mater* **2004,** *16* (4), 338-+.
73. Tugulu, S.; Klok, H. A., Stability and nonfouling properties of poly (poly (ethylene glycol) methacrylate) brushes under cell culture conditions. *Biomacromolecules* **2008,** *9* (3), 906-912.
74. Gautrot, J. E.; Trappmann, B.; Oceguera-Yanez, F.; Connelly, J.; He, X.; Watt, F. M.; Huck, W. T. S., Exploiting the superior protein resistance of polymer brushes to control single cell adhesion and polarisation at the micron scale. *Biomaterials* **2010,** *31* (18), 5030-5041.
75. Fan, X. W.; Lin, L. J.; Dalsin, J. L.; Messersmith, P. B., Biomimetic anchor for surface-initiated polymerization from metal substrates. *J Am Chem Soc* **2005,** *127* (45), 15843-15847.
76. Fan, X. W.; Lin, L. J.; Messersmith, P. B., Cell fouling resistance of polymer brushes grafted from Ti substrates by surface-initiated polymerization: Effect of ethylene glycol side chain length. *Biomacromolecules* **2006,** *7* (8), 2443-2448.
77. Ma, H. W.; Li, D. J.; Sheng, X.; Zhao, B.; Chilkoti, A., Protein-resistant polymer coatings on silicon oxide by surface-initiated atom transfer radical polymerization. *Langmuir* **2006,** *22* (8), 3751-3756.
78. Zhang, Z.; Zhang, M.; Chen, S. F.; Horbetta, T. A.; Ratner, B. D.; Jiang, S. Y., Blood compatibility of surfaces with superlow protein adsorption. *Biomaterials* **2008,** *29* (32), 4285-4291.
79. Ladd, J.; Zhang, Z.; Chen, S.; Hower, J. C.; Jiang, S., Zwitterionic polymers exhibiting high resistance to nonspecific protein adsorption from human serum and plasma. *Biomacromolecules* **2008,** *9* (5), 1357-1361.
80. Raynor, J. E.; Capadona, J. R.; Collard, D. M.; Petrie, T. A.; García, A. J., Polymer brushes and self-assembled monolayers: Versatile platforms to control cell adhesion to biomaterials (Review). *Biointerphases* **2009,** *4* (2).
81. Trmcic-Cvitas, J.; Hasan, E.; Ramstedt, M.; Li, X.; Cooper, M. A.; Abell, C.; Huck, W. T. S.; Gautrot, J. E., Biofunctionalized protein resistant oligo (ethylene glycol)-derived polymer brushes as selective immobilization and sensing platforms. *Biomacromolecules* **2009,** *10* (10), 2885-2894.
82. Matyjaszewski, K.; Xia, J. H., Atom transfer radical polymerization. *Chem Rev* **2001,** *101* (9), 2921-2990.
83. Lutz, J.-F.; Andrieu, J.; Üzgün, S.; Rudolph, C.; Agarwal, S., Biocompatible, thermoresponsive, and biodegradable: simple preparation of “all-in-one” biorelevant polymers. *Macromolecules* **2007,** *40* (24), 8540-8543.
84. Mi, L.; Jiang, S., Integrated antimicrobial and nonfouling zwitterionic polymers. *Angewandte Chemie International Edition* **2014,** *53* (7), 1746-1754.
85. Ma, C.; Hou, Y.; Liu, S.; Zhang, G., Effect of microphase separation on the protein resistance of a polymeric surface. *Langmuir* **2009,** *25* (16), 9467-9472.
86. Tegoulia, V. A.; Rao, W.; Kalambur, A. T.; Rabolt, J. F.; Cooper, S. L., Surface properties, fibrinogen adsorption, and cellular interactions of a novel phosphorylcholine-containing self-assembled monolayer on gold. *Langmuir* **2001,** *17* (14), 4396-4404.

87. Yang, W.; Chen, S.; Cheng, G.; Vaisocherová, H.; Xue, H.; Li, W.; Zhang, J.; Jiang, S., Film thickness dependence of protein adsorption from blood serum and plasma onto poly (sulfobetaine)-grafted surfaces. *Langmuir* **2008,** *24* (17), 9211-9214.
88. Mi, L.; Bernards, M. T.; Cheng, G.; Yu, Q.; Jiang, S., pH responsive properties of non-fouling mixed-charge polymer brushes based on quaternary amine and carboxylic acid monomers. *Biomaterials* **2010,** *31* (10), 2919-2925.
89. Morra, M.; Cassineli, C., Non-fouling properties of polysaccharide-coated surfaces. *Journal of Biomaterials Science, Polymer Edition* **1999,** *10* (10), 1107-1124.
90. Fyrner, T.; Lee, H.-H.; Mangone, A.; Ekblad, T.; Pettitt, M. E.; Callow, M. E.; Callow, J. A.; Conlan, S. L.; Mutton, R.; Clare, A. S., Saccharide-functionalized alkanethiols for fouling-resistant self-assembled monolayers: synthesis, monolayer properties, and antifouling behavior. *Langmuir* **2011,** *27* (24), 15034-15047.
91. Martwiset, S.; Koh, A. E.; Chen, W., Nonfouling characteristics of dextran-containing surfaces. *Langmuir* **2006,** *22* (19), 8192-8196.
92. Suh, K. Y.; Yang, J. M.; Khademhosseini, A.; Berry, D.; Tran, T. N. T.; Park, H.; Langer, R., Characterization of chemisorbed hyaluronic acid directly immobilized on solid substrates. *Journal of Biomedical Materials Research Part B: Applied Biomaterials* **2005,** *72* (2), 292-298.
93. Liu, X.; Huang, R.; Su, R.; Qi, W.; Wang, L.; He, Z., Grafting hyaluronic acid onto gold surface to achieve low protein fouling in surface plasmon resonance biosensors. *ACS applied materials & interfaces* **2014,** *6* (15), 13034-13042.
94. Perrino, C.; Lee, S.; Choi, S. W.; Maruyama, A.; Spencer, N. D., A biomimetic alternative to poly (ethylene glycol) as an antifouling coating: resistance to nonspecific protein adsorption of poly (L-lysine)-graft-dextran. *Langmuir* **2008,** *24* (16), 8850-8856.
95. Yu, K.; Kizhakkedathu, J. N., Synthesis of functional polymer brushes containing carbohydrate residues in the pyranose form and their specific and nonspecific interactions with proteins. *Biomacromolecules* **2010,** *11* (11), 3073-3085.
96. Prucker, O.; Rühe, J., Polymer layers through self-assembled monolayers of initiators. *Langmuir* **1998,** *14* (24), 6893-6898.
97. Dalsin, J. L.; Hu, B.-H.; Lee, B. P.; Messersmith, P. B., Mussel adhesive protein mimetic polymers for the preparation of nonfouling surfaces. *Journal of the American Chemical Society* **2003,** *125* (14), 4253-4258.
98. Meyerbröker, N.; Kriesche, T.; Zharnikov, M., Novel Ultrathin Poly (ethylene glycol) Films as Flexible Platform for Biological Applications and Plasmonics. *ACS applied materials & interfaces* **2013,** *5* (7), 2641-2649.
99. Wei, Q.; Becherer, T.; Noeske, P. L. M.; Grunwald, I.; Haag, R., A universal approach to crosslinked hierarchical polymer multilayers as stable and highly effective antifouling coatings. *Advanced Materials* **2014,** *26* (17), 2688-2693.
100. Kuroki, H.; Tokarev, I.; Nykypanchuk, D.; Zhulina, E.; Minko, S., Stimuli-Responsive Materials with Self-Healing Antifouling Surface via 3D Polymer Grafting. *Advanced Functional Materials* **2013,** *23* (36), 4593-4600.
101. Ahmed, E. M., Hydrogel: Preparation, characterization, and applications. *Journal of Advanced Research* (0).
102. Peppas, N. A.; Hilt, J. Z.; Khademhosseini, A.; Langer, R., Hydrogels in biology and medicine: from molecular principles to bionanotechnology. *Advanced Materials* **2006,** *18* (11), 1345-1360.
103. Kopecek, J., Polymer chemistry: Swell gels. *Nature* **2002,** *417* (6887), 388-391.

104. Hahn, M. S.; Taite, L. J.; Moon, J. J.; Rowland, M. C.; Ruffino, K. A.; West, J. L., Photolithographic patterning of polyethylene glycol hydrogels. *Biomaterials* **2006,** *27* (12), 2519-2524.
105. Smeets, N. M.; Bakaic, E.; Patenaude, M.; Hoare, T., Injectable and tunable poly (ethylene glycol) analogue hydrogels based on poly (oligoethylene glycol methacrylate). *Chemical Communications* **2014,** *50* (25), 3306-3309.
106. Nuttelman, C. R.; Mortisen, D. J.; Henry, S. M.; Anseth, K. S., Attachment of fibronectin to poly (vinyl alcohol) hydrogels promotes NIH3T3 cell adhesion, proliferation, and migration. *Journal of biomedical materials research* **2001,** *57* (2), 217-223.
107. Massia, S. P.; Stark, J.; Letbetter, D. S., Surface-immobilized dextran limits cell adhesion and spreading. *Biomaterials* **2000,** *21* (22), 2253-2261.
108. Carr, L. R.; Zhou, Y.; Krause, J. E.; Xue, H.; Jiang, S., Uniform zwitterionic polymer hydrogels with a nonfouling and functionalizable crosslinker using photopolymerization. *Biomaterials* **2011,** *32* (29), 6893-6899.
109. Farrugia, B. L.; Kempe, K.; Schubert, U. S.; Hoogenboom, R.; Dargaville, T. R., Poly (2-oxazoline) hydrogels for controlled fibroblast attachment. *Biomacromolecules* **2013,** *14* (8), 2724-2732.
110. Abraham, S.; Brahim, S.; Ishihara, K.; Guiseppi-Elie, A., Molecularly engineered p (HEMA)-based hydrogels for implant biochip biocompatibility. *Biomaterials* **2005,** *26* (23), 4767-4778.
111. Kostina, N. Y.; Rodriguez-Emmenegger, C.; Houska, M.; Brynda, E.; Michálek, J. í., Non-fouling hydrogels of 2-hydroxyethyl methacrylate and zwitterionic carboxybetaine (meth) acrylamides. *Biomacromolecules* **2012,** *13* (12), 4164-4170.
112. Schroeder, M. E.; Zurick, K. M.; McGrath, D. E.; Bernards, M. T., Multifunctional polyampholyte hydrogels with fouling resistance and protein conjugation capacity. *Biomacromolecules* **2013,** *14* (9), 3112-3122.
113. Smeets, N. M.; Bakaic, E.; Patenaude, M.; Hoare, T., Injectable poly (oligoethylene glycol methacrylate)-based hydrogels with tunable phase transition behaviours: Physicochemical and biological responses. *Acta biomaterialia* **2014,** *10* (10), 4143-4155.
114. Zhang, C.; Hekmatfer, S.; Karuri, N. W., A comparative study of polyethylene glycol hydrogels derivatized with the RGD peptide and the cell-binding domain of fibronectin. *Journal of biomedical materials research Part A* **2014,** *102* (1), 170-179.
115. Guarnieri, D.; De Capua, A.; Ventre, M.; Borzacchiello, A.; Pedone, C.; Marasco, D.; Ruvo, M.; Netti, P., Covalently immobilized RGD gradient on PEG hydrogel scaffold influences cell migration parameters. *Acta biomaterialia* **2010,** *6* (7), 2532-2539.
116. Malmqvist, M., Biospecific interaction analysis using biosensor technology. *Nature* **1993,** *361* (6408), 186-187.
117. Kyrolainen, M.; Rigsby, P.; Eddy, S.; Vadgama, P., Bio-/haemocompatibility: implications and outcomes for sensors? *Acta Anaesthesiologica Scandinavica* **1995,** *39* (s104), 55-60.
118. Schlosser, M.; Ziegler, M.; Fraser, D., Biosensors in the Body. John Wiley & Sons, New York: **1997**.
119. Reddy, S. M.; Vagama, P. M., Surfactant-modified poly (vinyl chloride) membranes as biocompatible interfaces for amperometric enzyme electrodes. *Analytica chimica acta* **1997,** *350* (1), 77-89.

120. Eisele, S.; Ammon, H.; Kindervater, R.; Gröbe, A.; Göpel, W., Optimized biosensor for whole blood measurements using a new cellulose based membrane. *Biosensors and Bioelectronics* **1994,** *9* (2), 119-124.
121. Vaisocherová, H.; Brynda, E.; Homola, J., Functionalizable low-fouling coatings for label-free biosensing in complex biological media: advances and applications. *Analytical and bioanalytical chemistry* **2015,** *407* (14), 3927-3953.
122. Linke, B.; Kiwit, M.; Thomas, K.; Krahwinkel, M.; Kerner, W., Prevention of the decrease in sensitivity of an amperometric glucose sensor in undiluted human serum. *Clinical chemistry* **1999,** *45* (2), 283-285.
123. Elbert, D. L.; Hubbell, J. A., Surface treatments of polymers for biocompatibility. *Annual Review of Materials Science* **1996,** *26* (1), 365-394.
124. Banerjee, I.; Pangule, R. C.; Kane, R. S., Antifouling coatings: recent developments in the design of surfaces that prevent fouling by proteins, bacteria, and marine organisms. *Advanced Materials* **2011,** *23* (6), 690-718.
125. Rodriguez-Emmenegger, C.; Brynda, E.; Riedel, T.; Houska, M.; Šubr, V.; Alles, A. B.; Hasan, E.; Gautrot, J. E.; Huck, W. T., Polymer Brushes Showing Non-Fouling in Blood Plasma Challenge the Currently Accepted Design of Protein Resistant Surfaces. *Macromolecular rapid communications* **2011,** *32* (13), 952-957.
126. Rodriguez Emmenegger, C.; Brynda, E.; Riedel, T.; Sedlakova, Z.; Houska, M.; Alles, A. B., Interaction of blood plasma with antifouling surfaces. *Langmuir* **2009,** *25* (11), 6328-6333.
127. Barbey, R.; Lavanant, L.; Paripovic, D.; Schüwer, N.; Sugnaux, C.; Tugulu, S.; Klok, H.-A., Polymer brushes via surface-initiated controlled radical polymerization: synthesis, characterization, properties, and applications. *Chemical reviews* **2009,** *109* (11), 5437-5527.
128. Kenna, J.; Major, G.; Williams, R., Methods for reducing non-specific antibody binding in enzyme-linked immunosorbent assays. *Journal of immunological methods* **1985,** *85* (2), 409-419.
129. Bolduc, O. R.; Masson, J.-F., Monolayers of 3-mercaptopropyl-amino acid to reduce the nonspecific adsorption of serum proteins on the surface of biosensors. *Langmuir* **2008,** *24* (20), 12085-12091.
130. Vaisocherová, H.; Ševců, V.; Adam, P.; Špačková, B.; Hegnerová, K.; de los Santos Pereira, A.; Rodriguez-Emmenegger, C.; Riedel, T.; Houska, M.; Brynda, E., Functionalized ultra-low fouling carboxy-and hydroxy-functional surface platforms: functionalization capacity, biorecognition capability and resistance to fouling from undiluted biological media. *Biosensors and Bioelectronics* **2014,** *51*, 150-157.
131. Lee, B. S.; Chi, Y. S.; Lee, K.-B.; Kim, Y.-G.; Choi, I. S., Functionalization of poly (oligo (ethylene glycol) methacrylate) films on gold and Si/SiO2 for immobilization of proteins and cells: SPR and QCM studies. *Biomacromolecules* **2007,** *8* (12), 3922-3929.
132. Kuzmyn, A.; de los Santos Pereira, A.; Pop-Georgievski, O.; Bruns, M.; Brynda, E.; Rodriguez-Emmenegger, C., Exploiting end group functionalization for the design of antifouling bioactive brushes. *Polymer Chemistry* **2014,** *5* (13), 4124-4131.
133. Vaisocherova, H.; Yang, W.; Zhang, Z.; Cao, Z.; Cheng, G.; Piliarik, M.; Homola, J.; Jiang, S., Ultralow fouling and functionalizable surface chemistry based on a zwitterionic polymer enabling sensitive and specific protein detection in undiluted blood plasma. *Analytical chemistry* **2008,** *80* (20), 7894-7901.
134. Vaisocherová, H.; Zhang, Z.; Yang, W.; Cao, Z.; Cheng, G.; Taylor, A. D.; Piliarik, M.; Homola, J.; Jiang, S., Functionalizable surface platform with reduced nonspecific protein

adsorption from full blood plasma—Material selection and protein immobilization optimization. *Biosensors and Bioelectronics* **2009,** *24* (7), 1924-1930.
135. von Muhlen, M. G.; Brault, N. D.; Knudsen, S. M.; Jiang, S.; Manalis, S. R., Label-free biomarker sensing in undiluted serum with suspended microchannel resonators. *Analytical chemistry* **2010,** *82* (5), 1905-1910.
136. Brault, N. D.; Gao, C.; Xue, H.; Piliarik, M.; Homola, J.; Jiang, S.; Yu, Q., Ultra-low fouling and functionalizable zwitterionic coatings grafted onto SiO 2 via a biomimetic adhesive group for sensing and detection in complex media. *Biosensors and Bioelectronics* **2010,** *25* (10), 2276-2282.
137. Yang, W.; Xue, H.; Li, W.; Zhang, J.; Jiang, S., Pursuing "zero" protein adsorption of poly (carboxybetaine) from undiluted blood serum and plasma. *Langmuir* **2009,** *25* (19), 11911-11916.
138. Gao, C.; Li, G.; Xue, H.; Yang, W.; Zhang, F.; Jiang, S., Functionalizable and ultra-low fouling zwitterionic surfaces via adhesive mussel mimetic linkages. *Biomaterials* **2010,** *31* (7), 1486-1492.
139. Hossain, S. M. Z.; Luckham, R. E.; McFadden, M. J.; Brennan, J. D., Reagentless bidirectional lateral flow bioactive paper sensors for detection of pesticides in beverage and food samples. *Analytical chemistry* **2009,** *81* (21), 9055-9064.
140. Hossain, S. M. Z.; Brennan, J. D., β-Galactosidase-Based Colorimetric Paper Sensor for Determination of Heavy Metals. *Analytical chemistry* **2011,** *83* (22), 8772-8778.
141. Lewis, W.; Keshavarz-Moore, E.; Windust, J.; Bushell, D.; Parry, N., Construction and evaluation of novel fusion proteins for targeted delivery of micro particles to cellulose surfaces. *Biotechnology and bioengineering* **2006,** *94* (4), 625-632.
142. Su, S.; Nutiu, R.; Filipe, C. D. M.; Li, Y.; Pelton, R., Adsorption and covalent coupling of ATP-binding DNA aptamers onto cellulose. *Langmuir* **2007,** *23* (3), 1300-1302.
143. Pelton, R., Bioactive paper provides a low-cost platform for diagnostics. *TrAC Trends in Analytical Chemistry* **2009,** *28* (8), 925-942.
144. Jones, K. L.; O'Melia, C. R., Protein and humic acid adsorption onto hydrophilic membrane surfaces: effects of pH and ionic strength. *Journal of Membrane Science* **2000,** *165* (1), 31-46.
145. Brash, J. L., Exploiting the current paradigm of blood-material interactions for the rational design of blood-compatible materials. *J Biomat Sci-Polym E* **2000,** *11* (11), 1135-1146.
146. Zhu, Y.; Xu, X.; Brault, N. D.; Keefe, A. J.; Han, X.; Deng, Y.; Xu, J.; Yu, Q.; Jiang, S., Cellulose paper sensors modified with zwitterionic poly (carboxybetaine) for sensing and detection in complex media. *Analytical Chemistry* **2014,** *86* (6), 2871-2875.
147. Wichterle, O.; Lim, D., Hydrophilic gels for biological use. **1960,** *185*, 117-118.
148. Sindt, C. W.; Longmuir, R. A., Contact lens strategies for the patient with dry eye. *The ocular surface* **2007,** *5* (4), 294-307.
149. Luensmann, D.; Jones, L., Albumin adsorption to contact lens materials: a review. *Contact Lens and Anterior Eye* **2008,** *31* (4), 179-187.
150. Luensmann, D.; Jones, L., Protein deposition on contact lenses: the past, the present, and the future. *Contact Lens and Anterior Eye* **2012,** *35* (2), 53-64.
151. Lord, M. S.; Stenzel, M. H.; Simmons, A.; Milthorpe, B. K., The effect of charged groups on protein interactions with poly (HEMA) hydrogels. *Biomaterials* **2006,** *27* (4), 567-575.
152. Lord, M. S.; Stenzel, M. H.; Simmons, A.; Milthorpe, B. K., Lysozyme interaction with poly (HEMA)-based hydrogel. *Biomaterials* **2006,** *27* (8), 1341-1345.

153. Taylor, R. L.; Willcox, M. D.; Williams, T. J.; Verran, J., Modulation of bacterial adhesion to hydrogel contact lenses by albumin. *Optometry & Vision Science* **1998,** *75* (1), 23-29.
154. Miller, M. J.; Wilson, L. A.; Ahearn, D. G., Effects of protein, mucin, and human tears on adherence of Pseudomonas aeruginosa to hydrophilic contact lenses. *Journal of clinical microbiology* **1988,** *26* (3), 513-517.
155. Zhang, S.; Borazjani, R. N.; Salamone, J. C.; Ahearn, D. G.; Crow, S. A.; Pierce, G. E., In vitro deposition of lysozyme on etafilcon A and balafilcon A hydrogel contact lenses: effects on adhesion and survival of Pseudomonas aeruginosa and Staphylococcus aureus. *Contact Lens and Anterior Eye* **2005,** *28* (3), 113-119.
156. Subbaraman, L. N.; Glasier, M.-A.; Varikooty, J.; Srinivasan, S.; Jones, L., Protein deposition and clinical symptoms in daily wear of etafilcon lenses. *Optometry & Vision Science* **2012,** *89* (10), 1450-1459.
157. Thissen, H.; Gengenbach, T.; du Toit, R.; Sweeney, D. F.; Kingshott, P.; Griesser, H. J.; Meagher, L., Clinical observations of biofouling on PEO coated silicone hydrogel contact lenses. *Biomaterials* **2010,** *31* (21), 5510-5519.
158. Goda, T.; Matsuno, R.; Konno, T.; Takai, M.; Ishihara, K., Protein adsorption resistance and oxygen permeability of chemically crosslinked phospholipid polymer hydrogel for ophthalmologic biomaterials. *Journal of Biomedical Materials Research Part B: Applied Biomaterials* **2009,** *89* (1), 184-190.
159. Shimizu, T.; Goda, T.; Minoura, N.; Takai, M.; Ishihara, K., Super-hydrophilic silicone hydrogels with interpenetrating poly (2-methacryloyloxyethyl phosphorylcholine) networks. *Biomaterials* **2010,** *31* (12), 3274-3280.
160. Winterton, L. C.; Lally, J. M.; Sentell, K. B.; Chapoy, L. L., The elution of poly (vinyl alcohol) from a contact lens: the realization of a time release moisturizing agent/artificial tear. *Journal of Biomedical Materials Research Part B: Applied Biomaterials* **2007,** *80* (2), 424-432.
161. Peterson, R. C.; Wolffsohn, J. S.; Nick, J.; Winterton, L.; Lally, J., Clinical performance of daily disposable soft contact lenses using sustained release technology. *Contact lens and anterior eye* **2006,** *29* (3), 127-134.
162. Van Beek, M.; Jones, L.; Sheardown, H., Hyaluronic acid containing hydrogels for the reduction of protein adsorption. *Biomaterials* **2008,** *29* (7), 780-789.
163. Van Beek, M.; Weeks, A.; Jones, L.; Sheardown, H., Immobilized hyaluronic acid containing model silicone hydrogels reduce protein adsorption. *Journal of Biomaterials Science, Polymer Edition* **2008,** *19* (11), 1425-1436.
164. Kim, H.-J.; Ryu, G.-C.; Jeong, K.-S.; Jun, J., Hydrogel lenses functionalized with polysaccharide for reduction of protein adsorption. *Macromolecular Research* **2015,** *23* (1), 74-78.
165. Weeks, A.; Morrison, D.; Alauzun, J. G.; Brook, M. A.; Jones, L.; Sheardown, H., Photocrosslinkable hyaluronic acid as an internal wetting agent in model conventional and silicone hydrogel contact lenses. *Journal of Biomedical Materials Research Part A* **2012,** *100* (8), 1972-1982.
166. Weeks, A.; Boone, A.; Luensmann, D.; Jones, L.; Sheardown, H., The effects of hyaluronic acid incorporated as a wetting agent on lysozyme denaturation in model contact lens materials. *Journal of biomaterials applications* **2013,** *28* (3), 323-333.
167. Weeks, A.; Luensmann, D.; Boone, A.; Jones, L.; Sheardown, H., Hyaluronic acid as an internal wetting agent in model DMAA/TRIS contact lenses. *Journal of biomaterials applications* **2012,** *27* (4), 423-432.

168. Reuben, B. G.; Perl, O.; Morgan, N. L.; Stratford, P.; Dudley, L. Y.; Hawes, C., Phospholipid coatings for the prevention of membrane fouling. *Journal of Chemical Technology and Biotechnology* **1995,** *63* (1), 85-91.
169. Liu, F.; Hashim, N. A.; Liu, Y.; Abed, M. M.; Li, K., Progress in the production and modification of PVDF membranes. *Journal of Membrane Science* **2011,** *375* (1), 1-27.
170. Lei, J.; Ulbricht, M., Macroinitiator-mediated photoreactive coating of membrane surfaces with antifouling hydrogel layers. *Journal of Membrane Science* **2014,** *455*, 207-218.
171. La, Y.-H.; McCloskey, B. D.; Sooriyakumaran, R.; Vora, A.; Freeman, B.; Nassar, M.; Hedrick, J.; Nelson, A.; Allen, R., Bifunctional hydrogel coatings for water purification membranes: Improved fouling resistance and antimicrobial activity. *Journal of Membrane Science* **2011,** *372* (1), 285-291.
172. Nikolaeva, D.; Langner, C.; Ghanem, A.; Rehim, M. A.; Voit, B.; Meier-Haack, J., Hydrogel surface modification of reverse osmosis membranes. *Journal of Membrane Science* **2015,** *476*, 264-276.
173. La, Y.-H.; Sooriyakumaran, R.; McCloskey, B. D.; Allen, R. D.; Freeman, B. D.; Al-Rasheed, R., Enhancing water permeability of fouling-resistant POSS–PEGM hydrogels using 'addition–extraction'of sacrificial additives. *Journal of membrane science* **2012,** *401*, 306-312.
174. Wang, Z.; Ma, H.; Hsiao, B. S.; Chu, B., Nanofibrous ultrafiltration membranes containing cross-linked poly (ethylene glycol) and cellulose nanofiber composite barrier layer. *Polymer* **2014,** *55* (1), 366-372.
175. Zhang, X.; Lin, B.; Zhao, K.; Wei, J.; Guo, J.; Cui, W.; Jiang, S.; Liu, D.; Li, J., A free-standing calcium alginate/polyacrylamide hydrogel nanofiltration membrane with high anti-fouling performance: Preparation and characterization. *Desalination* **2015,** *365*, 234-241.
176. Ju, H.; McCloskey, B. D.; Sagle, A. C.; Kusuma, V. A.; Freeman, B. D., Preparation and characterization of crosslinked poly (ethylene glycol) diacrylate hydrogels as fouling-resistant membrane coating materials. *Journal of Membrane Science* **2009,** *330* (1), 180-188.
177. Butruk-Raszeja, B. A.; Łojszczyk, I.; Ciach, T.; Kościelniak-Ziemniak, M.; Janiczak, K.; Kustosz, R.; Gonsior, M., Athrombogenic hydrogel coatings for medical devices–Examination of biological properties. *Colloids and Surfaces B: Biointerfaces* **2015,** *130*, 192-198.
178. Faulk, D. M.; Londono, R.; Wolf, M. T.; Ranallo, C. A.; Carruthers, C. A.; Wildemann, J. D.; Dearth, C. L.; Badylak, S. F., ECM hydrogel coating mitigates the chronic inflammatory response to polypropylene mesh. *Biomaterials* **2014,** *35* (30), 8585-8595.
179. Xu, F.; Neoh, K.; Kang, E., Bioactive surfaces and biomaterials via atom transfer radical polymerization. *Progress in polymer science* **2009,** *34* (8), 719-761.
180. Wischerhoff, E.; Badi, N.; Lutz, J.-F.; Laschewsky, A., Smart bioactive surfaces. *Soft Matter* **2010,** *6* (4), 705-713.
181. Le Droumaguet, B.; Nicolas, J., Recent advances in the design of bioconjugates from controlled/living radical polymerization. *Polymer Chemistry* **2010,** *1* (5), 563-598.
182. Lin, P. C.; Weinrich, D.; Waldmann, H., Protein biochips: oriented surface immobilization of proteins. *Macromolecular Chemistry and Physics* **2010,** *211* (2), 136-144.
183. Ma, Z.; Mao, Z.; Gao, C., Surface modification and property analysis of biomedical polymers used for tissue engineering. *Colloids and Surfaces B: Biointerfaces* **2007,** *60* (2), 137-157.
184. Lloyd, A. W., Interfacial bioengineering to enhance surface biocompatibility. *Medical device technology* **2001,** *13* (1), 18-21.

185. Kim, D. C.; Kang, D. J., Molecular recognition and specific interactions for biosensing applications. *Sensors* **2008,** *8* (10), 6605-6641.
186. Cosnier, S., Biosensors based on immobilization of biomolecules by electrogenerated polymer films. *Applied biochemistry and biotechnology* **2000,** *89* (2-3), 127-138.
187. Lu, B.; Smyth, M. R.; O'Kennedy, R., Tutorial review. Oriented immobilization of antibodies and its applications in immunoassays and immunosensors. *Analyst* **1996,** *121* (3), 29R-32R.
188. Kausaite-Minkstimiene, A.; Ramanaviciene, A.; Kirlyte, J.; Ramanavicius, A., Comparative study of random and oriented antibody immobilization techniques on the binding capacity of immunosensor. *Analytical chemistry* **2010,** *82* (15), 6401-6408.
189. Song, H. Y.; Zhou, X.; Hobley, J.; Su, X., Comparative study of random and oriented antibody immobilization as measured by dual polarization interferometry and surface plasmon resonance spectroscopy. *Langmuir* **2011,** *28* (1), 997-1004.
190. Rusmini, F.; Zhong, Z.; Feijen, J., Protein immobilization strategies for protein biochips. *Biomacromolecules* **2007,** *8* (6), 1775-1789.
191. Diamanti, S.; Arifuzzaman, S.; Elsen, A.; Genzer, J.; Vaia, R. A., Reactive patterning via post-functionalization of polymer brushes utilizing disuccinimidyl carbonate activation to couple primary amines. *Polymer* **2008,** *49* (17), 3770-3779.
192. Kanno, S.; Yanagida, Y.; Haruyama, T.; Kobatake, E.; Aizawa, M., Assembling of engineered IgG-binding protein on gold surface for highly oriented antibody immobilization. *Journal of biotechnology* **2000,** *76* (2), 207-214.
193. Peluso, P.; Wilson, D. S.; Do, D.; Tran, H.; Venkatasubbaiah, M.; Quincy, D.; Heidecker, B.; Poindexter, K.; Tolani, N.; Phelan, M., Optimizing antibody immobilization strategies for the construction of protein microarrays. *Anal. Biochem.* **2003,** *312* (2), 113-124.
194. Diamandis, E. P.; Christopoulos, T. K., The biotin-(strept) avidin system: principles and applications in biotechnology. *Clin. Chem.* **1991,** *37* (5), 625-636.
195. Santos, A.; Davis, J. J.; Bueno, P. R., Fundamentals and Applications of Impedimetric and Redox Capacitive Biosensors. *Journal of Analytical & Bioanalytical Techniques* **2014,** *2015*.
196. Rao, S. V.; Anderson, K. W.; Bachas, L. G., Oriented immobilization of proteins. *Microchimica Acta* **1998,** *128* (3-4), 127-143.
197. Shumaker-Parry, J. S.; Zareie, M. H.; Aebersold, R.; Campbell, C. T., Microspotting streptavidin and double-stranded DNA arrays on gold for high-throughput studies of protein-DNA interactions by surface plasmon resonance microscopy. *Analytical chemistry* **2004,** *76* (4), 918-929.
198. Lee, B. S.; Lee, J. K.; Kim, W.-J.; Jung, Y. H.; Sim, S. J.; Lee, J.; Choi, I. S., Surface-initiated, atom transfer radical polymerization of oligo (ethylene glycol) methyl ether methacrylate and subsequent click chemistry for bioconjugation. *Biomacromolecules* **2007,** *8* (2), 744-749.
199. Wang, Z.; Jin, G., Feasibility of protein A for the oriented immobilization of immunoglobulin on silicon surface for a biosensor with imaging ellipsometry. *Journal of biochemical and biophysical methods* **2003,** *57* (3), 203-211.
200. Johnson, C. P.; Jensen, I. E.; Prakasam, A.; Vijayendran, R.; Leckband, D., Engineered protein A for the orientational control of immobilized proteins. *Bioconjugate chemistry* **2003,** *14* (5), 974-978.
201. Vijayendran, R. A.; Leckband, D. E., A quantitative assessment of heterogeneity for surface-immobilized proteins. *Analytical Chemistry* **2001,** *73* (3), 471-480.

202. Robertus, J.; Browne, W. R.; Feringa, B. L., Dynamic control over cell adhesive properties using molecular-based surface engineering strategies. *Chemical Society Reviews* **2010,** *39* (1), 354-378.
203. Zhu, Y.; Chian, K. S.; Chan-Park, M. B.; Mhaisalkar, P. S.; Ratner, B. D., Protein bonding on biodegradable poly (L-lactide-co-caprolactone) membrane for esophageal tissue engineering. *Biomaterials* **2006,** *27* (1), 68-78.
204. Webb, K.; Caldwell, K. D.; Tresco, P. A., A novel surfactant-based immobilization method for varying substrate-bound fibronectin. *Journal of biomedical materials research* **2001,** *54* (4), 509-518.
205. Kuhl, P. R.; Griffith-Cima, L. G., Tethered epidermal growth factor as a paradigm for growth factor-induced stimulation from the solid phase. *Nature medicine* **1996,** *2* (9), 1022-1027.
206. Deng, X.; Korogiannaki, M.; Rastegari, B.; Zhang, J.; Chen, M.; Fu, Q.; Sheardown, H.; Filipe, C.D.; Hoare, T., *ACS applied materials & interfaces* **2016,** DOI: 10.1021/acsami.6b07433.
207. Deng, X.; Chen, M.; Fu, Q.; Smeets, N. M.; Xu, F.; Zhang, Z.; Filipe, C. D.; Hoare, T., A highly-sensitive immunosorbent assay based on biotinylated graphene oxide and the quartz crystal microbalance. *ACS applied materials & interfaces* **2016,** *8* (3), 1893-1902.

Chapter 2 Poly(oligoethylene glycol methacrylate) dip-coating: turning cellulose paper into a protein-repellent platform for biosensors

In chapter 2, all experiments were conducted by myself with assistance from Dr. Niels M. B. Smeets, Dr. Clémence Sicard, and Dr. Jingyun Wang. The paper was initially drafted by myself, and edited later to final version by Dr. John D. Brennan, Dr. Carlos D. M. Filipe and Dr. Todd Hoare. This chapter has been published in *Journal of the American Chemical Society*, 2014, 136 (37), pp12852–12855.

JACS
JOURNAL OF THE AMERICAN CHEMICAL SOCIETY
Communication
pubs.acs.org/JACS

Poly(oligoethylene glycol methacrylate) Dip-Coating: Turning Cellulose Paper into a Protein-Repellent Platform for Biosensors

Xudong Deng,[†] Niels M. B. Smeets,[†] Clémence Sicard,[‡] Jingyun Wang,[†] John D. Brennan,[‡] Carlos D. M. Filipe,*[,†] and Todd Hoare*[,†]

[†]Department of Chemical Engineering, McMaster University, Hamilton, Ontario L8S 4L7, Canada
[‡]Department of Chemistry and Chemical Biology, McMaster University, Hamilton, Ontario L8S 4L7, Canada

Supporting Information

ABSTRACT: The passivation of nonspecific protein adsorption to paper is a major barrier to the use of paper as a platform for microfluidic bioassays. Herein we describe a simple, scalable protocol based on adsorption and cross-linking of poly(oligoethylene glycol methacrylate) (POEGMA) derivatives that reduces nonspecific adsorption of a range of proteins to filter paper by at least 1 order of magnitude without significantly changing the fiber morphology or paper macroporosity. A lateral-flow test strip coated with POEGMA facilitates effective protein transport while also confining the colorimetric reporting signal for easier detection, giving improved performance relative to bovine serum albumin (BSA)-blocked paper. Enzyme-linked immunosorbent assays based on POEGMA-coated paper also achieve lower blank values, higher sensitivities, and lower detection limits relative to ones based on paper blocked with BSA or skim milk. We anticipate that POEGMA-coated paper can function as a platform for the design of portable, disposable, and low-cost paper-based biosensors.

Paper-based devices have attracted widespread interest as portable, low-cost, low-volume, disposable, and simple analytical platforms for bioassays, point-of-care diagnostics, and environmental analysis.[1] Paper-based devices with direct reporting by changes in color,[2] fluorescence,[3] chemiluminescence,[4] or other easily identifiable signals offer particular benefits in resource-limited settings for diagnosis or screening without the need for complex analytical equipment.[2a,5] While several proof-of-concept studies have shown the potential of paper-based devices for meeting these challenges, nonspecific protein adsorption significantly limits both the accuracy and selectivity of such sensors.[1a,6] Typically, this problem is addressed by blocking the nonfunctionalized paper surface with bovine serum albumin (BSA)[2b] or other proteins immediately before use (see Table 1 in ref 1b for other methods used). However, protein blocking is an inconvenient and only partially effective additional step that limits the facile use of paper-based biosensors in the field.

Reducing protein adsorption at interfaces has long been a focus in the biomaterials literature[7] given the oft-cited link between protein adsorption and inflammation.[8] Typically, this is achieved by surface modification of the biomaterial with hydrophilic polymers,[9] with poly(ethylene glycol) (PEG) attracting particular interest.[10] Poly(oligoethylene glycol methacrylate) (POEGMA) exhibits similar non-cytotoxic and protein-repellent properties as PEG[11] while offering the advantage of facile copolymerization or grafting via free radical chemistry.[11c,12] However, the fragility of highly porous papers used for paper-based microfluidics at the typically elevated temperatures and high free radical concentrations required for grafting limits the practical utility of this approach.

Herein we demonstrate a mild and effective approach for passivating protein adsorption on cellulose paper via a simple, scalable sequential dipping method. Smeets and co-workers recently reported the formation of protein-repellent hydrogels based on POEGMA precursor polymers functionalized with hydrazide and aldehyde groups that form gels rapidly by simple mixing at ambient conditions (Figure 1a).[13] Here we apply this chemistry in a sequential dipping strategy to localize hydrogel formation on the fiber surface of filter paper (Figure 1b). Adsorption of aldehyde-functionalized POEGMA (POA) to the paper functionalizes the paper surface with aldehydes, while subsequent dipping into a hydrazide-functionalized POEGMA (POH) solution effectively assembles a thin POEGMA hydrogel layer directly on the fiber surface (Figure 1c).

The efficacy of POEGMA coating for modification of paper interfacial properties was first screened using a model cellulose surface. A cellulose-coated quartz crystal microbalance (QCM) chip was POEGMA-coated by sequentially flowing POA and POH over the chip (Figure 2a). The water contact angle slightly increased from 33 ± 1° (cellulose chip) to 52 ± 1° (with POA) and 53 ± 1° (with POA/POH) (Figure 2b), indicating that the hydrophilicity of the fiber interface was maintained while the potential for steric protein repulsion (characteristic of PEG coatings[10c]) was introduced. Four model proteins with different isoelectric points (pI) and molecular weights (MW) [see Table S1 in the Supporting Information (SI)] were then flowed over the POEGMA-coated chip to assess the capacity of the coating to inhibit protein adsorption (Figure S1 in the SI). A decrease in protein adsorption by at least 1 order of magnitude was observed for all proteins relative to an unmodified cellulose chip, independent of pI or MW (Figure 2c).

On the basis of this result, coatings were subsequently applied to cellulose filter paper (Whatman no. 40 ashless). The dipping procedure induced no significant changes in the fiber or pore morphology of the paper in either the dry state (scanning

Received: July 21, 2014
Published: August 29, 2014

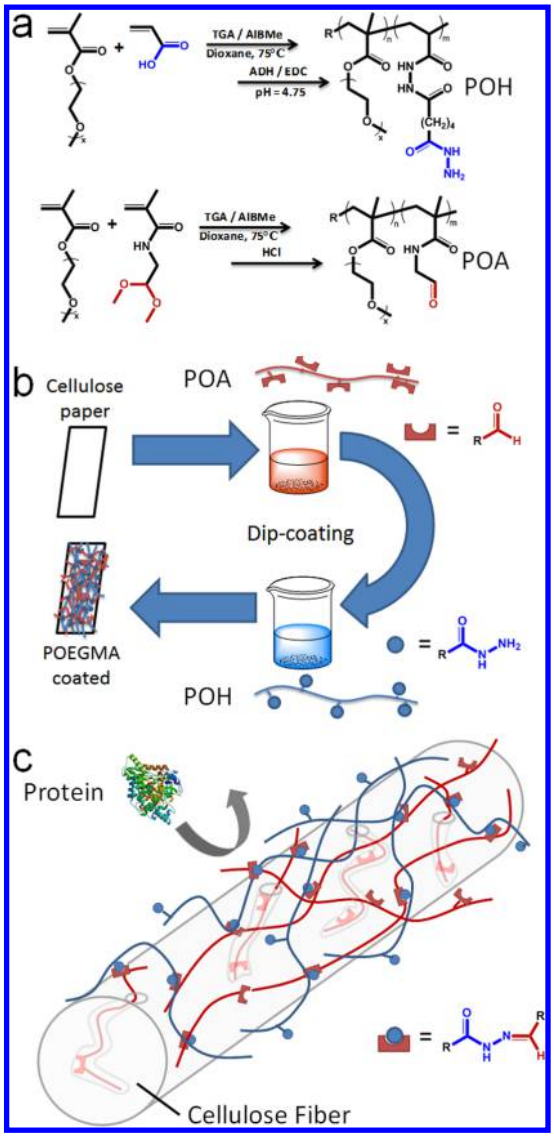

Figure 1. (a) Synthesis of hydrazide-functionalized POEGMA (POH) and aldehyde-functionalized POEGMA (POA). (b) Dip-coating procedure for modifying filter paper. (c) Hypothesized structure of surface-modified cellulose fibers and resulting mechanism of protein repellency.

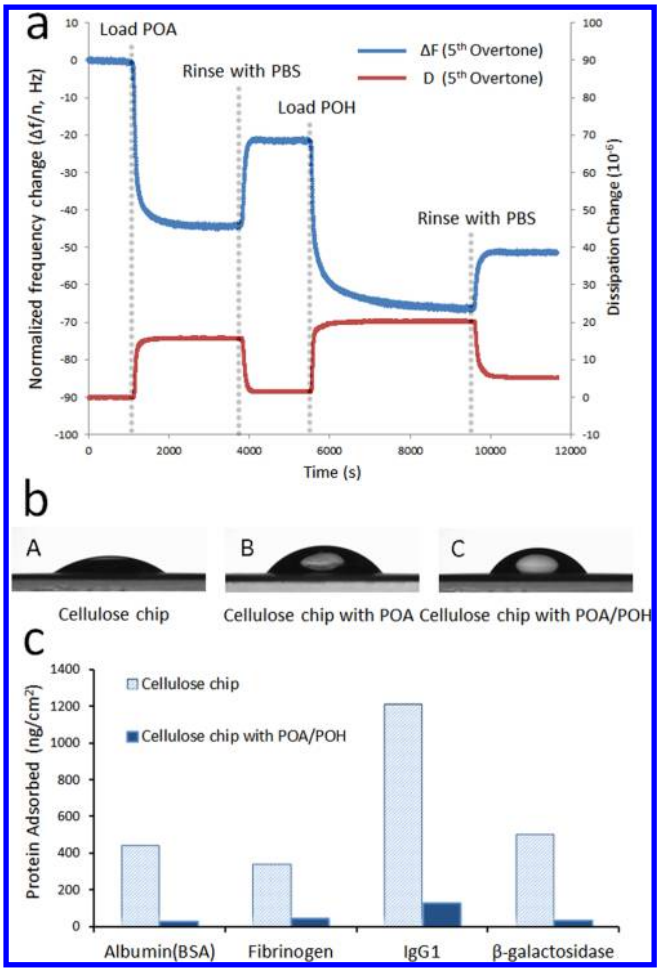

Figure 2. Interfacial properties of POA/POH-modified cellulose-coated QCM chips. (a) QCM-D monitoring of POA and POH adsorption (both 4% w/v) on a cellulose QCM chip. (b) Contact angle of water on a cellulose QCM chip before and after POA/POH coating. (c) QCM-D monitoring of protein adsorption on a cellulose QCM chip before and after POA/POH coating (100 μg/mL protein).

electron microscopy; Figure S2A–F) or the wet/swollen state (optical profilometry; Figure S2G–I), and no significant difference in surface roughness was observed for unmodified paper and POA or POA/POH dip-coated paper ($p > 0.05$). In addition, tensile testing of unmodified and POA/POH-modified paper strips indicated that the dipping procedure either maintained or slightly increased all of the key indicators of paper mechanics (Table S2). These results suggest that the dip modification procedure impacts neither the physical structure of the fiber nor the macroporous network morphology of the paper, unlike other techniques for polymer surface modification that cause significant fiber damage and/or clog the pore network and thus impact the paper's functionality as a microfluidic device.[14]

Confocal microscopy of dip-coated paper prepared by sequential dipping in rhodamine-labeled POA and fluorescein-labeled POH confirms adsorption of POA on the fiber surface throughout the paper cross section and suggests that dipping fills small pores inside the fibers (see Figure 3a-i). Subsequent colocalization and immobilization of POH on the fiber surface following the second dipping step are also confirmed (see Figure 3a-ii). Attenuated total reflectance FTIR spectroscopy shows an ester peak at 1727–1735 cm^{-1} (characteristic of POEGMA) that increases in intensity after each dipping step (Figures S3 and S4), and the dry weight of the treated papers increases significantly following each dipping step performed (Figure S5); both of these observations confirm deposition of the POEGMA polymers on the paper. Interestingly, following soaking of the papers over 24 h in phosphate-buffered saline (PBS), the POA/POH dip-modified paper shows a lower wet mass than unmodified paper (Figure S5). We hypothesize that this result is attributable to the filling of smaller pores inside and between cellulose fibers with polymers during the dipping procedure and restriction of the swelling of those polymers by the rigid cellulose network around those pores. This hypothesis is supported by the enhanced fluorescence observed at the edge and junction points between fibers (arrowheads in Figure S6A) and mercury porosimetery results that indicate a decrease in the total free pore volume upon POA/POH dipping accompanied by the effective disappearance of smaller pores (<0.1 μm) in the fiber network (Figure S7). Thus, while the dipping treatment does influence the fiber

dx.doi.org/10.1021/ja507372v | J. Am. Chem. Soc. 2014, 136, 12852–12855

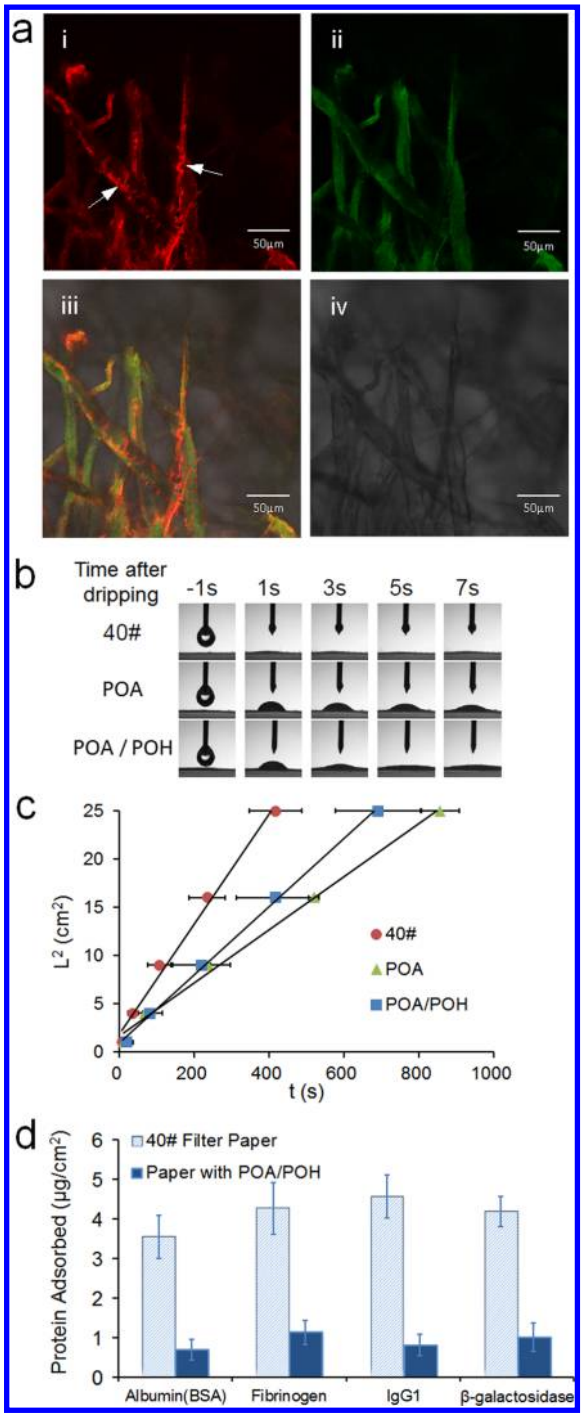

Figure 3. Interfacial and transport properties of POA/POH dip-coated Whatman no. 40 filter paper. (a) Filter paper fiber network following dip-coating of fluorescently labeled POA and POH viewed by confocal laser scanning microscopy (CLSM): (i) rhodamine 123-labeled POA; (ii) fluorescein-labeled POH; (iii) merged CLSM image; (iv) bright-field image. Arrowheads indicate the distribution of POA inside the cellulose fibers. (b, c) Hygroscopicity and surface properties of no. 40 filter paper before and after dip-coating with POA and POA/POH: (b) screenshots of sessile drop testing of the contact angle of filter paper samples; (c) plot of the square of the capillary rise distance (L^2) against capillary time (t) for a 0.8 cm × 8 cm paper strip ($n = 4$). (d) Adsorption of proteins on paper samples before and after POA/POH coating (protein concentration of 100 μg/mL, $n = 6$).

nanostructure, it does not significantly impact the paper macroporosity or topology.

To confirm that POA and POH chemically cross-link on the paper surface, residual aldehyde and hydrazide groups were reacted with fluorescein-5-thiosemicarbazide (5-FTSC) and 5-fluorescein isothiocyanate (5-FITC) respectively. POA-treated paper exhibits the same 5-FITC intensity but twice the 5-FTSC intensity compared with untreated paper, indicating adsorption of POA. POA/POH-treated paper exhibits the same 5-FTSC intensity of native paper (indicating consumption of POA aldehyde groups) but double the 5-FITC intensity, suggesting the presence of residual hydrazide groups (Figure S8). This result, coupled with the fluorescence result in Figure 3a, indicates that POA and POH chemically cross-link on the fiber surface to create a thin interfacial hydrogel layer.

The impact of POA/POH dip-coating on paper interfacial properties was assessed by measuring the penetration speed of water into and through the paper. Screenshots of sessile drop tests on filter paper samples before and after POA/POH dipping are shown in Figure 3b. The penetration speed of water into the paper varies as unmodified paper > POA/POH paper > POA paper. A similar result was observed via capillary rise experiments tracking the lateral flow of water through the filter paper before and after POEGMA dip-coating (Figure 3c). The speed of capillary rise obeys the Washburn equation, which in the case of zero applied pressure can be expressed as $L^2 = tD\gamma \cos\theta/4\eta$,[15] where L is the height of water penetration up the strip, t is the time, η is the viscosity, γ is the surface tension, θ is the contact angle, and D is the pore diameter. The slope of a plot L^2 versus t (representing differences in $D \cos\theta$ at constant fluid properties) varies as unmodified paper > POA/POH paper > POA paper, mirroring the sequence of water drop penetration speeds. Both results are consistent with the dipping procedure filling small pores inside cellulose fibers (lower D; Figure 3a-i) and slightly decreasing $\cos\theta$ (Figure 2b) while still preserving sufficiently fast water transport for microfluidic biosensor applications.

Consistent with the cellulose-coated QCM chip results, POA/POH coating on filter paper facilitated at least a 4-fold decrease in adsorption for all tested proteins (Figure 3d). No further reduction was noted following layer-by-layer deposition of additional POA/POH layers (Figure S9). On the basis of this result, the utility of POA/POH dip-coated paper as a platform for paper-based microfluidic or lateral flow devices was assessed. A model reaction in which β-galactosidase (β-GAL, enzyme) converts chlorophenol red β-galactopyranoside (CPRG, yellow, substrate) to chlorophenol red (red-magenta, product) was selected; capture of the chlorophenol red product by poly(L-arginine) in the sensing area generates a purple reporting signal indicative of capillary transport of the enzyme solution up the paper test strip (Figure 4a). Untreated paper cannot support the transport of β-GAL, and therefore, no purple band appeared (a1). BSA-blocked paper supported protein transport, but the signal was broadly dispersed up the test strip, suggesting that BSA blocking interferes with the activity of the color-capturing agent (a2). In contrast, POA/POH dip-coated paper successfully facilitated protein transport (signal generation) and confined the signal to the detection area (a3) at the cost of slightly increasing the test time due to the decreased rate of capillary rise through the POA/POH-coated paper (5.3 ± 0.7 min vs 3.7 ± 0.6 min for BSA-blocked paper, 4 cm transport length).

On the basis of this successful initial assay, POA/POH dip-coated papers were subsequently assessed as supports for paper-based enzyme-linked immunosorbent assays (ELISAs) (Figure 4b) using goat anti-rabbit IgG as the antigen and horseradish peroxidase (HRP)-conjugated rabbit IgG as the enzyme-linked

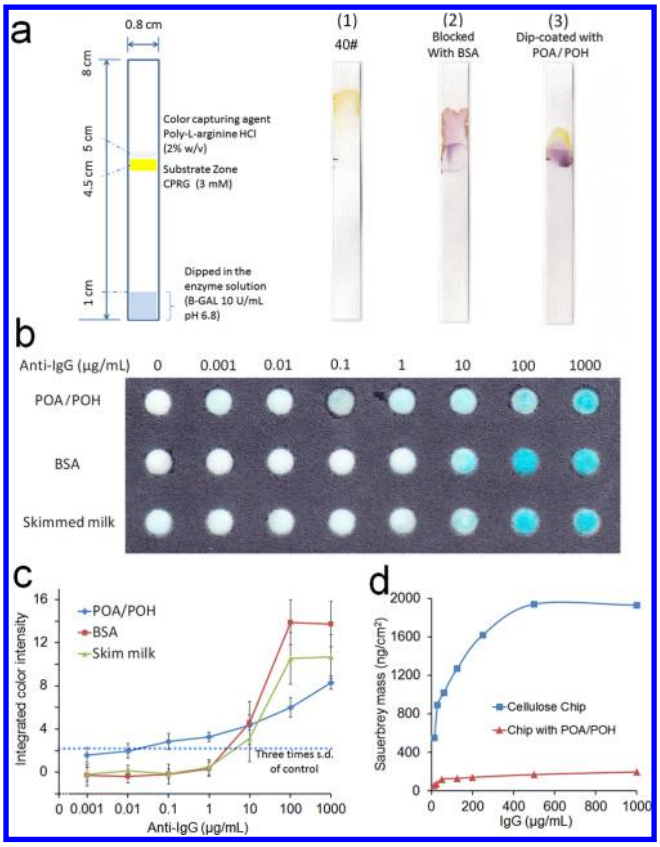

Figure 4. Model paper-based diagnostics using POA/POH dip-coated paper. (a) Schematic of β-galactosidase (β-GAL) test strip design and experimental mobility of β-GAL on 0.8 cm × 8 cm paper strips: (a1) pipetted control paper; (a2) BSA-blocked paper (0.1% w/v); (a3) POA/POH dip-coated paper. (b) Paper-based ELISA on a wax-printed microzone plate using dip-coated POA/POH as the blocking reagent, compared with BSA and skimmed milk. (c) Color intensity of paper-based ELISA using different blocking reagents (the blue dashed line represents the LOD, 3× the standard deviation of the nonblocked control). (d) Isothermal adsorption of rabbit immunoglobin (IgG) on a cellulose-coated QCM chip with or without POA/POH coating from QCM-D analysis.

antibody. The use of POA/POH dip-coating to block the filter paper resulted in a lower blank signal and a lower limit of detection (LOD) of between 0.1 and 1 μg/mL antigen relative to the use of BSA or skim milk, both of which result in significantly higher LODs (between 1 and 10 μg/mL) and lower dynamic ranges (Figure 4c). Given that POEGMA-coated cellulose can maintain nonspecific IgG adsorption at very low levels (<150 ng/cm^2), ~3-fold lower than for BSA-blocked paper (Figure S11), even at high concentrations (>1 mg/mL; Figure 4d), we hypothesize that POA/POH dip-coated papers are ideal platforms for performing ELISAs with a wide range of antibodies.

In summary, we have demonstrated the effective surface modification of paper via a simple, scalable, and mild dip-coating procedure that significantly suppresses nonspecific protein adsorption to paper without impacting the fiber morphology or paper macroporosity. We anticipate that POA/POH-coated paper has potential as a platform for the design and fabrication of complex biosensors, bioarrays, and other high-throughput tests in which protein transport is essential. Such modified papers may also have applications in the design of nonfouling filter papers for protein separation or protein chromatographic supports.

■ ASSOCIATED CONTENT

Supporting Information

Materials and methods, full polymer characterization, paper mechanical data, mercury intrusion results, surface topologies, dry and wet weights, FTIR data, and raw QCM results. This material is available free of charge via the Internet at http://pubs.acs.org.

■ AUTHOR INFORMATION

Corresponding Authors

hoaretr@mcmaster.ca

filipec@mcmaster.ca

Notes

The authors declare no competing financial interest.

■ ACKNOWLEDGMENTS

The authors thank the Natural Sciences and Engineering Research Council of Canada (CREATE Biointerfaces Training Program), the Sentinel Bioactive Paper Network, the Canada Foundation for Innovation, and the Ontario Innovation Trust for support. J.D.B. holds the Canada Research Chair in Bioanalytical Chemistry and Biointerfaces.

■ REFERENCES

(1) (a) Pelton, R. *TrAC, Trends Anal. Chem.* **2009**, *28*, 925. (b) Yetisen, A. K.; Akram, M. S.; Lowe, C. R. *Lab Chip* **2013**, *13*, 2210.

(2) (a) Martinez, A. W.; Phillips, S. T.; Butte, M. J.; Whitesides, G. M. *Angew. Chem., Int. Ed.* **2007**, *46*, 1318. (b) Abe, K.; Kotera, K.; Suzuki, K.; Citterio, D. *Anal. Bioanal. Chem.* **2010**, *398*, 885.

(3) Carrilho, E.; Phillips, S. T.; Vella, S. J.; Martinez, A. W.; Whitesides, G. M. *Anal. Chem.* **2009**, *81*, 5990.

(4) (a) Yu, J.; Ge, L.; Huang, J.; Wang, S.; Ge, S. *Lab Chip* **2011**, *11*, 1286. (b) Yu, J.; Wang, S.; Ge, L.; Ge, S. *Biosens. Bioelectron.* **2011**, *26*, 3284.

(5) Martinez, A. W.; Phillips, S. T.; Carrilho, E.; Thomas, S. W., III; Sindi, H.; Whitesides, G. M. *Anal. Chem.* **2008**, *80*, 3699.

(6) Jones, K. L.; O'Melia, C. R. *J. Membr. Sci.* **2000**, *165*, 31.

(7) Brash, J. L.; Horbett, T. A. *ACS Symp. Ser.* **1995**, *602*, 1.

(8) Bélanger, M. C.; Marois, Y. *J. Biomed. Mater. Res.* **2001**, *58*, 467.

(9) Brash, J. L. *J. Biomater. Sci., Polym. Ed.* **2000**, *11*, 1135.

(10) (a) Murthy, R.; Shell, C. E.; Grunlan, M. A. *Biomaterials* **2009**, *30*, 2433. (b) Sharma, S.; Popat, K. C.; Desai, T. A. *Langmuir* **2002**, *18*, 8728. (c) Yu, Q.; Zhang, Y.; Wang, H.; Brash, J.; Chen, H. *Acta Biomater.* **2011**, *7*, 1550.

(11) (a) Hyun, J.; Ma, H.; Zhang, Z.; Beebe, T. P., Jr.; Chilkoti, A. *Adv. Mater.* **2003**, *15*, 576. (b) Ma, H. W.; Hyun, J. H.; Stiller, P.; Chilkoti, A. *Adv. Mater.* **2004**, *16*, 338. (c) Lutz, J.-F.; Andrieu, J.; Üzgün, S.; Rudolph, C.; Agarwal, S. *Macromolecules* **2007**, *40*, 8540.

(12) (a) Xu, F. J.; Neoh, K. G.; Kang, E. T. *Prog. Polym. Sci.* **2009**, *34*, 719. (b) Fan, X.; Lin, L.; Dalsin, J. L.; Messersmith, P. B. *J. Am. Chem. Soc.* **2005**, *127*, 15843. (c) Fan, X. W.; Lin, L. J.; Messersmith, P. B. *Biomacromolecules* **2006**, *7*, 2443. (d) Ma, H.; Li, D.; Sheng, X.; Zhao, B.; Chilkoti, A. *Langmuir* **2006**, *22*, 3751. (e) Lutz, J. F. *J. Polym. Sci., Part A: Polym. Chem.* **2008**, *46*, 3459.

(13) (a) Smeets, N. M. B.; Bakaic, E.; Patenaude, M.; Hoare, T. *Chem. Commun.* **2014**, *50*, 3306. (b) Smeets, N. M. B.; Bakaic, E.; Patenaude, M.; Hoare, T. *Acta Biomater.* **2014**, DOI: 10.1016/j.actbio.2014.05.035.

(14) (a) Carlmark, A.; Malmström, E. E. *Biomacromolecules* **2003**, *4*, 1740. (b) Yu, D.; Chen, X.; Pelton, R.; Ghosh, R. *Biotechnol. Bioeng.* **2008**, *99*, 1434.

(15) Washburn, E. W. *Phys. Rev.* **1921**, *17*, 273.

Appendix: Supporting information for Chapter 2

1. Materials

Oligo (ethylene glycol) methyl ether methacrylate with an average number-average molecular weight of 475 g/mol ($OEGMA_{475}$, Sigma Aldrich, 95%) and (diethylene glycol) methyl ether methacrylate ($M(EO)_2MA$, Sigma Aldrich, 98%) were purified using a column of basic aluminum oxide (Sigma Aldrich, type CG-20) to remove the monomethyl ether hydroquinone (MEHQ) and butylated hydroxytoluene (BHT) inhibitors. Acrylic acid (AA, Sigma Aldrich, 99%), thioglycolic acid (TGA, Sigma Aldrich, 98%), 2,2-azobisisobutryic acid dimethyl ester (AIBMe, Wako Chemicals, 98.5%), adipic acid dihydrazyde (ADH, Alfa Aesar, 98%), N'-ethyl-N-(3-dimethylaminopropyl)-carbodiimide (EDC, Carbosynth, Compton CA, commercial grade), bovine serum albumin (BSA, Sigma Aldrich, 97%), fibrinogen from human plasma (Sigma Aldrich), IgG from rabbit serum (Sigma Aldrich, 95%), β-galactosidase from *Escherichia coli* (Grade VI, Sigma Aldrich), goat anti-rabbit IgG (whole molecule, Sigma), normal rabbit IgG-HRP (Santa Cruz Biotechnology), rhodamine 123 (Sigma Aldrich, 85%), fluorescein 5-isothiocyanate (5-FITC, Sigma Aldrich, 90%), and fluorescein-5-thiosemicarbazide (5-FTSC, Sigma Aldrich, 80%) were all used as received. TMB peroxidase substrate solution and peroxidase substrate solution B were purchased from KPL, Kirkegaard & Perry Laboratories, Inc. Hydrochloric acid (1M) was received from LabChem Inc. (Pittsburgh, PA). For all experiments, Milli-Q grade distilled deionized water (DIW) was used. Phosphate buffered saline (PBS) was diluted from a 10X liquid concentrate (Bioshop Canada Inc.). N-(2,2-dimethoxyethyl)methacrylamide (DMEMAm) monomer was synthesized according to a previously reported method.[1]

2. Polymer synthesis and characterization

Polymer characterization: Size exclusion chromatography (SEC) was performed using a Waters 2695 separations module equipped with a Waters 2996 photodiode array detector, a Waters 2414 refractive index detector, a Waters 2475 multi λ fluorescence detector and four Polymer Labs PLgel individual pore size columns maintained at 40 °C, with 5 μm bead size and pore sizes of 100, 500, 103 and 105 Å. THF was used as the eluent at a flow rate of 1.0 ml min^{-1}, and poly(methyl methacrylate) standards were used for calibration. ^{1}H-NMR and ^{13}C-NMR were performed on a Bruker AVANCE 600 MHz spectrometer using deuterated chloroform as the solvent (see section 20 of Supporting Information for full spectra)

Synthesis of aldehyde-functionalized poly(oligoethylene glycol methacrylate) (POA): POA precursors were prepared by adding AIBMe (38 mg, 0.16 mmol), $OEGMA_{475}$ (0.90 g, 1.9 mmol), $M(EO)_2MA$ (3.1g, 16 mmol), DMEMAm (0.60 g, 3.5 mmol) and TGA (7.5 μL, 0.15 mmol) to a 50 mL Schlenk flask. 1,4-Dioxane (20 mL) was added and the solution was purged with nitrogen

for at least 30 minutes. Subsequently, the flask was sealed and submerged in a pre-heated oil bath at 75°C for 4 hours under magnetic stirring. After polymerization, the solvent was removed and the poly($OEGMA_{475}$-co-$M(EO)_2MA$-co- DMEMAm) polymer was purified by dialysis against DIW over 6 cycles (6+ hours each time) and lyophilized to dryness. The acetal groups of POA precursors were subsequently converted to aldehydes by dissolving 4.0 g of the copolymer prepared above in 75 mL DIW and 25 mL 1.0 M HCl in a 250 mL round-bottom flask. The solution was left to stir for 24 hours, dialyzed for a minimum of 6 (6+ hour) cycles, and lyophilized to dryness. The polymers were dissolved in PBS and stored as 20 w/w% solutions at 4°C. The number-average molecular weight was determined to be $14 \cdot 10^3$ g/mol (Đ = 2.03) from size exclusion chromatography using THF as a solvent. The aldehyde content was determined to be 24 mol% (equivalent to 19 reactive aldehyde groups per chain) using ^{1}H-NMR based on the proton signals of the methoxy (O-CH_3, 3H, δ = 3.3 ppm) and aldehyde (CHO, 1H, δ = 9.2 ppm) groups.

Synthesis of the hydrazide-functionalized poly(oligoethylene glycol methacrylate) (POH): POH precursors were prepared by adding AIBMe (38 mg, 0.16 mmol), $OEGMA_{475}$ (0.95 g, 2.0 mmol), $M(EO)_2MA$ (3.1g, 16 mmol), AA (0.55 g, 7.6mmol), and TGA (7.5 μL, 0.15 mmol) to a 50 mL Schlenk flask. 1,4-Dioxane (20 mL) was added, and the solution was purged with nitrogen for at least 30 minutes. Subsequently, the flask was sealed and submerged in a pre-heated oil bath at 75°C for 4 hours under magnetic stirring. After the solvent was removed, the resulting poly($OEGMA_{475}$-co-$M(EO)_2MA$-co-AA) polymer was purified by dialysis against DIW over 6 cycles (6+ hours per cycle) and lyophilized to dryness. The carboxylic acid groups of POH precursor were subsequently converted to hydrazide groups via a carbodiimide-mediated conjugation of a large excess of adipic acid dihydrazide. The polymer (4.0 g) was dissolved in 100 mL DIW and added to a 250 mL round-bottom flask. ADH (4.33 g, 24.8 mmol, 8.16 mol eq.) was added and the pH of the solution was adjusted to pH = 4.75 using 0.1 M HCl. Subsequently, EDC (1.93 g, 12.4 mmol, 3.80 mol eq.) was added and the pH was maintained at pH = 4.75 by the dropwise addition of 0.1 M HCl over 4 hours. The solution was left to stir overnight, dialyzed against DIW over 6 cycles (6+ hours per cycle) and lyophilized to dryness. The polymers were dissolved in PBS and stored as 20 w/w% solutions at 4°C. The number-average molecular weight was determined to be $17 \cdot 10^3$ g/mol (Đ = 2.08) from size exclusion chromatography using THF as a solvent. The degree of hydrazide functionalization was determined to be 22 mol% (equivalent to 22 reactive hydrazide groups per chain) by conductometric base-into-acid titration by comparing the carboxylic acid content before and after ADH conjugation (0.1 M NaOH titrant, 50 mg polymer in 50 mg of 1 mM NaCl titration solution, ManTech automatic titrator).

Note that a 10mol% $OEGMA_{475}$ (n = 7-8 ethylene oxide repeat units on the side chain) and 90 mol% $M(EO)_2MA$ (n = 2 ethylene oxide repeat units on the side chain) copolymer was chosen for both the hydrazide and aldehyde-functionalized copolymers. This particular copolymer, in the

absence of hydrazide and aldehyde functionalization, has a thermal phase transition temperature just above room temperature (~32-33°C) and as such can more easily adsorb on to the cellulose paper in the first POA dipping step relative to a polymer prepared with 100% $OEGMA_{475}$. However, the hydrogel chosen still effectively repels proteins with near-equal efficacy to the 100% $OEGMA_{475}$ polymer (see reference 13b in the main manuscript for data on bulk hydrogels) due to the still significant presence of the longer side chain comonomer, and dip coating of 100% $OEGMA_{475}$ polymers onto the filter paper actually facilitated a lower protein repellency than the 10 mol% $OEGMA_{475}$ polymer used (~ 1.7-fold higher IgG adsorption) owing to the reduced surface coverage that can be achieved. Thus, the composition chosen represents an optimized chemistry for both promoting effective coverage of the paper and low non-specific protein adsorption.

3. Quartz crystal microbalance with dissipation monitoring (QCM-D)

The adsorption of POA and POH on cellulose and the ability of the resulting POEGMA interface to repel proteins were investigated using quartz crystal microbalance with dissipation (QCM-D, Q-Sense E4, Gothenburg, Sweden) equipped with QSX 334 cellulose sensors. The resonance frequency and dissipation shifts of the oscillating crystals were simultaneously monitored at the fundamental frequency (5 MHz) and its seven overtones (15, 25, 35, 45, 55, 65 and 75 MHz) at 25°C under constant fluid flow (0.1 mL/min). The cellulose chip surface was allowed to equilibrate for 3 hours in PBS buffer prior to measurements. All polymers (4%, w/v) and proteins (100 μg/mL) were dissolved in the same PBS solution and flowed over the pre-equilibrated chip until the measured frequency (and thus the adsorption of the polymer or protein added) reached a plateau characterized by a frequency change of less than 1 Hz/10 min. The adsorbed mass (Δm) was determined using Sauerbrey's equation under the assumptions that the adsorbed layer is rigid, uniformly distributed on the surface, and small compared to the crystal's mass (Equation 1)[2]:

$$\Delta m = -\frac{C \cdot \Delta f}{n} \qquad \text{(Equation 1)}$$

In this equation, C is the sensitivity constant (17.7 $ngHz^{-1}cm^{-2}$ for a 5 MHz crystal, as provided by the manufacturer), Δf is the measured change in frequency, and n is an overtone number. Only the changes in the normalized frequencies and dissipations of the fifth overtone are reported; analogous results were achieved with other overtones.

Figure 2a (main manuscript) shows the measured frequency changes upon sequential addition of POA and POH to the cellulose-coated QCM chip. Following rinsing to remove unbound polymer after each adsorption step, the bound masses of POA and POH (including bound water, assuming three moles of water is bound per mole of ethylene glycol repeat units in the POEGMA side chain[3]) were calculated to be 390 and 550 ng/cm^2, respectively. In addition, the significant increase in

dissipation following treatment of the surface with POH suggests an increase in the modulus of the surface consistent with covalent cross-linking of POA and POH to form a hydrogel.

The bound masses of the four proteins assayed (BSA, fibrinogen, rabbit IgG, and β-galactosidase, see Table S1 for representative properties) to the resulting POEGMA-coated surface defined in Figure 2a are shown in the main text (Figure 2c), with data calculated according to the raw normalized frequency changes measured in Figure S1.

Table S1. The molecular weight and isoelectric point of proteins with varying properties obtained from the NCBI protein database and ExPASy SIB Bioinformatics Resource Portal

Protein	Molecular Weight (kDa)	Isoelectric point
Albumin (BSA)	69.3	4.7 - 5.82
Fibrinogen	340	5.5
IgG1	150	8.6 ± 0.4
β-galactosidase	464	4.61

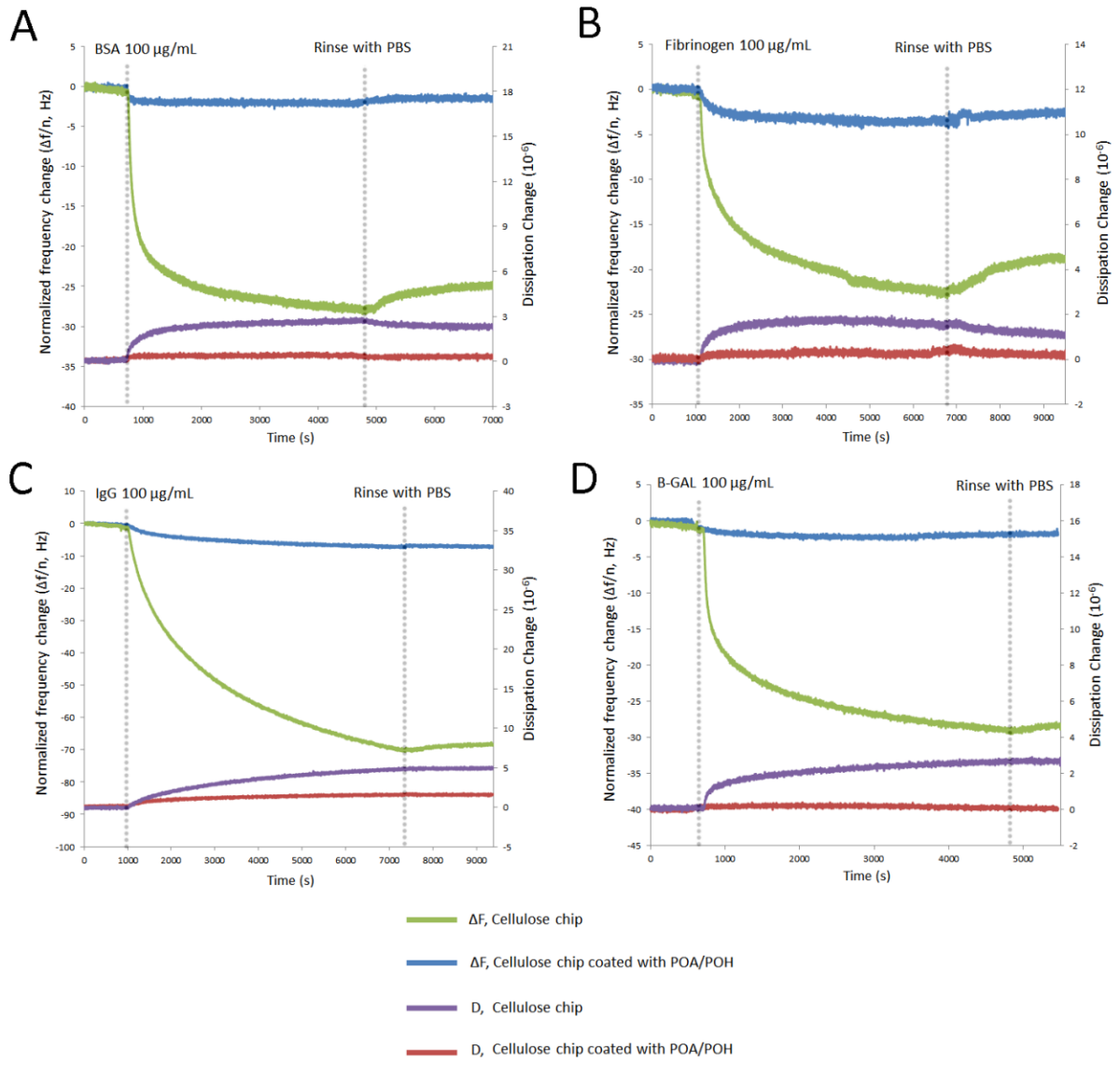

Figure S1. QCM-D results of the measured frequency change (ΔF) and dissipation (D) following adsorption of 100 µg/mL solutions of BSA (A), fibrinogen (B), rabbit IgG (C) and β-GAL (D) on a pre-equilibrated cellulose sensor with or without a POA/POH coating (as defined in Figure 2a)

4. Contact angle and droplet penetration assay

Water contact angle measurements were conducted using a Model 100-00-115 NRL contact angle goniometer (Ramé-Hart, Succasunna, NJ) equipped with a Sanyo VC8−3512T camera. Contact angles were measured by applying 5 µL droplets of distilled deionized water on the surface of both cellulose-coated QCM chips and Whatman 40# filter paper samples. For the QCM chips, the measurement of contact angle was conducted following rinsing with PBS until a stable frequency

plateau was achieved (see Fig. 2a) and subsequent drying of the chip under moderate nitrogen flow. For paper samples, the droplet evolution was tracked by video, and screen shots were taken 1 second before and 1, 3, 5, 7 seconds after the droplet was applied to the paper to track both the initial contact as well as the kinetics of the penetration of the droplet into the paper network.

5. Paper dipping method

The POEGMA polymers were dissolved in 4% (w/v) phosphate buffered saline (PBS) solutions. Samples of Whatman 40# ashless filter paper were cut into small pieces (1 cm × 2 cm) or strips (0.8 cm × 8 cm) and then dipped in the polymer solutions by completely submerging the paper in the solution. POA was used in the first dipping step for all reported experiments since initiating the sequential dipping with POA instead of POH was demonstrated in preliminary work to facilitate improved protein repellency; we attribute this result to the enhanced affinity between aldehyde-functionalized POA and paper, which can more effectively anchor the POEGMA polymer to the fiber network. After 4 h of gentle shaking (~30 rpm) at room temperature, the paper samples were removed from the solution and washed twice with PBS. Afterwards, all the samples were dried overnight at ambient conditions (~23°C and ~30% relative humidity). Subsequently, the dried paper was dipped in the 4% (w/v) POH solution for another 4 hours and then washed and dried using the same procedure outlined above. It should be noted that preliminary work was performed to investigate the utility of multiple dipping cycles on the ability of the dip-modified paper to suppress non-specific protein adsorption. While step-by-step mass gain (i.e. POEGMA adsorption or grafting) was achieved on sequential dipping cycles, no significant improvement in protein repellency was observed; as such, a single dipping cycle was used for all experiments discussed in this manuscript.

6. Surface topography

The filter paper samples were subjected to optical profilometry and scanning electron microscopy (SEM) imaging before and after dipping in the POA and POH solutions. Optical profilometry images were obtained using a WYKO Model NT 1100 optical profilometer operating under the VSI measurement mode at a magnification of 20x. For SEM analysis, samples were sputter-coated with platinum (layer thickness = 15 Å) to avoid charging effects and were imaged using a JEOL Model JSM-7000F SEM (Tokyo, Japan) operating at 2.8 kV and a probe distance of 5.9 mm.

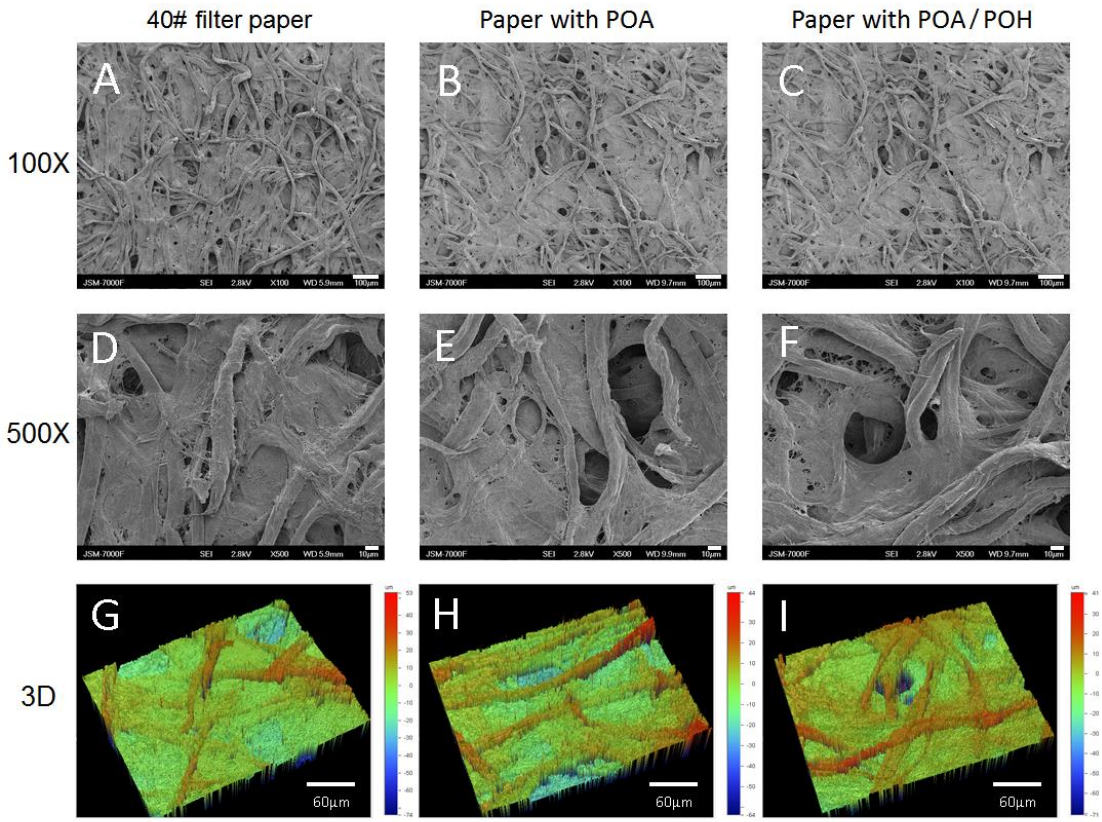

Figure S2. Scanning electron microscopy (SEM, A-F) and optical profilometry (G-I) images of 40# filter paper (A,D,G) and filter paper coated with POA (B,E,H) or with POA/POH (C,F,I) at 100x (A-C), 500x (D-F) and 400x (G-I) magnification.

As noted in the manuscript, no significant change in the morphology or roughness of the paper fiber network was observed upon POA or POA/POH dipping, as evidenced by the lack of change in both the SEM images as well as the optical profilometry results before and after both POA and POA/POH dipping.

7. Paper mechanics

The tensile strength of paper before and after dip modification was measured to assess the effect of dip coating on the paper mechanics. Prior to the test, paper samples were equilibrated overnight at 23°C and 50% relative humidity. Testing was conducted following TAPPI T494 (Tensile properties of paper and paperboard, using constant rate of elongation apparatus) using a 50 N load cell and operating at a deformation rate of 10 mm/min along the machine direction of paper. The rectangular sample width was 8.0 mm and the grip distance was 20.0 mm. The thickness of all

paper samples tested (including dipped papers) was 0.201 ± 0.006 mm (TMI digital micrometer), such that differences in modulus are not attributable to differences in thickness. Tensile strength, modulus, and elongation to break were calculated using Series IX standalone software (Version 1.1). Ten samples were tested in each group, with results expressed in terms of the mean ± standard deviation. Table S1 shows the tensile properties of unmodified filter paper, filter paper treated with POA, and filter paper treated with sequential dipping of POA/POH.

Table S2. Mechanical properties of 40# filter paper and paper coated with POA and POH obtained by tensile force measurements.

	Displacement at Peak (mm)	**Load at Peak (N)**	**Break Displacement (mm)**
40#	0.70±0.11	20.3±0.8	0.91±0.29
POA	0.94±0.06**	21.0±1.2	1.19±0.22*
POA/POH	0.94±0.08**	21.3±1.0*	1.18±0.25*

	0.2% Yield Strength (MPa)	**Modulus (MPa)**	**Energy at Break (mJ)**
40#	8.9±0.4	970±120	12.2±2.5
POA	7.3±0.7##	850±90#	16.8±2.0**
POA/POH	7.6±0.4##	910±70	17.3±2.5**

N=10; *p<0.05,**p<0.001, significantly higher than 40# filter paper; #p<0.05, ##p<0.001, significantly lower than 40# filter paper.

Following initial dipping of POA, the displacement at peak, break displacement, and energy at break all significantly increased while the load at peak and the modulus were not affected. Overall, this result suggests that the paper becomes more difficult to break as a result of POA adsorption. Subsequent dipping (and covalent bond formation) with POH maintains these same properties, although gel formation does not induce significant further strengthening of the paper. This demonstrated enhancement (or at least maintenance) of key paper mechanical properties is a point of significant contrast between this dipping method and other methods of paper modification (i.e. chemical grafting or paper oxidation), which typically significantly decrease the tensile strength

of the paper. Note that the "0.2% Yield Strength" reported is an offset yield point often reported in the literature in cases in which the true yield point is not easily defined based on the shape of the stress-strain curve and refers to the stress measured at 0.2% strain.[4]

8. FTIR of polymers

The infrared spectra of the reactive pre-gel polymers and the gel-coated paper samples were collected using a Nexus 6700 Fourier-transform infrared (FTIR) spectrometer (Thermo Fisher Scientific Inc.) equipped with an infrared microscope (Nicolet Continuμm). An attenuated total reflection (ATR) attachment was used for the measurement. The lyophilized samples of POA and POH were measured to obtain their individual spectra as shown in Figure S3.

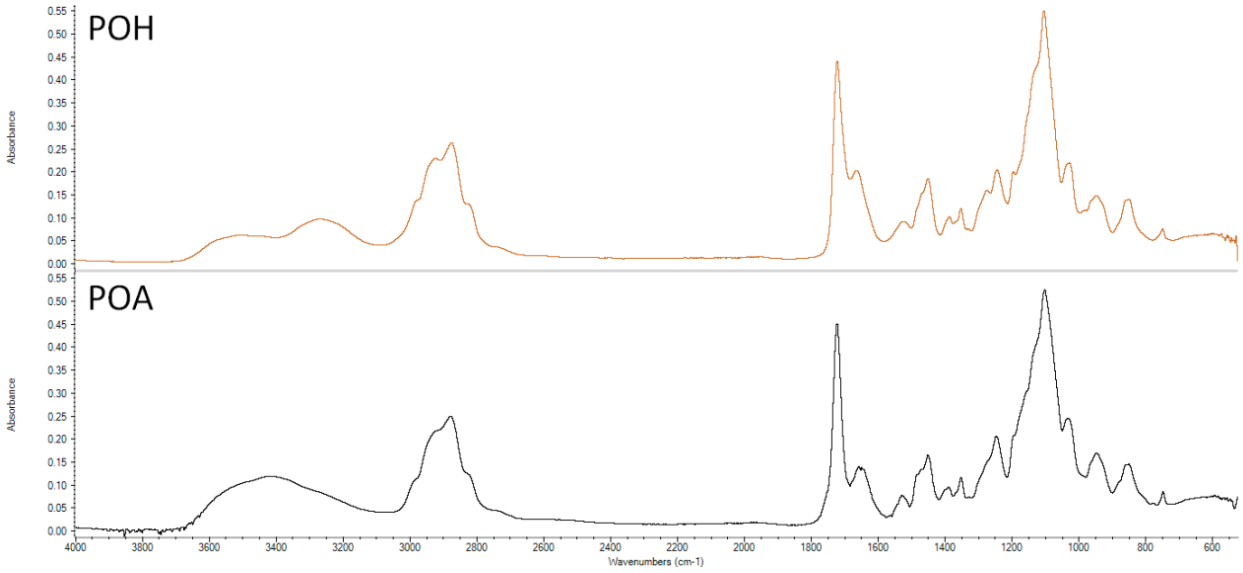

Figure S3. FTIR spectra of hydrazide-functionalized POEGMA (POH) and aldehyde-functionalized POEGMA (POA).

ATR-FTIR for POA (cm^{-1}): 3412m, 2877s, 1723s, 1657w, 1649w, 1529w, 1451m, 1389w, 1352w, 1246m, 1103s, 1033w, 947w, 850w, 748w.

ATR-FTIR for POH (cm^{-1}): 3265m, 2876s, 1722s, 1665w, 1524w, 1451m, 1388w, 1353w, 1245m, 1104s, 1029w, 947w, 850w, 749w.

The IR spectra of POA and POH are largely the same, with the strong peak at 1723 cm^{-1} and a

medium intensity peak at ~1245 cm^{-1} representing stretching vibrations indicative of the C=O ester groups that connect the backbone of the POEGMA polymers to the oligo(ethylene glycol) side chains and a very strong peak at 1103 cm^{-1} representing the antisymmetric stretching vibration of C-O-C in the oligo(ethylene glycol) in the side chain. Hydrazide and aldehyde groups both typically appear in the range of the ester signals and are thus convoluted with the higher intensity ester peaks.

9. FTIR of paper surface

The diffuse reflectance infrared Fourier transform spectroscopy (DRIFTS) method was employed to characterize the polymer-treated paper surface. DRIFTS was used in this case since it is well-documented to be useful for analyzing polymers (including foams, powders, fibers and composites) on rough and heterogeneous surfaces (like paper). The spectra of nascent 40# filter paper and the paper samples dipped with POA and sequential dipping of POA/POH are shown in Figure S4. The presence of the peaks at 1727-1735 cm^{-1} (corresponding to the ester groups in POEGMA, indicated by the dashed rectangle in each spectrum) confirms the deposition of POEGMA on to the paper surface as a result of the dipping procedure.

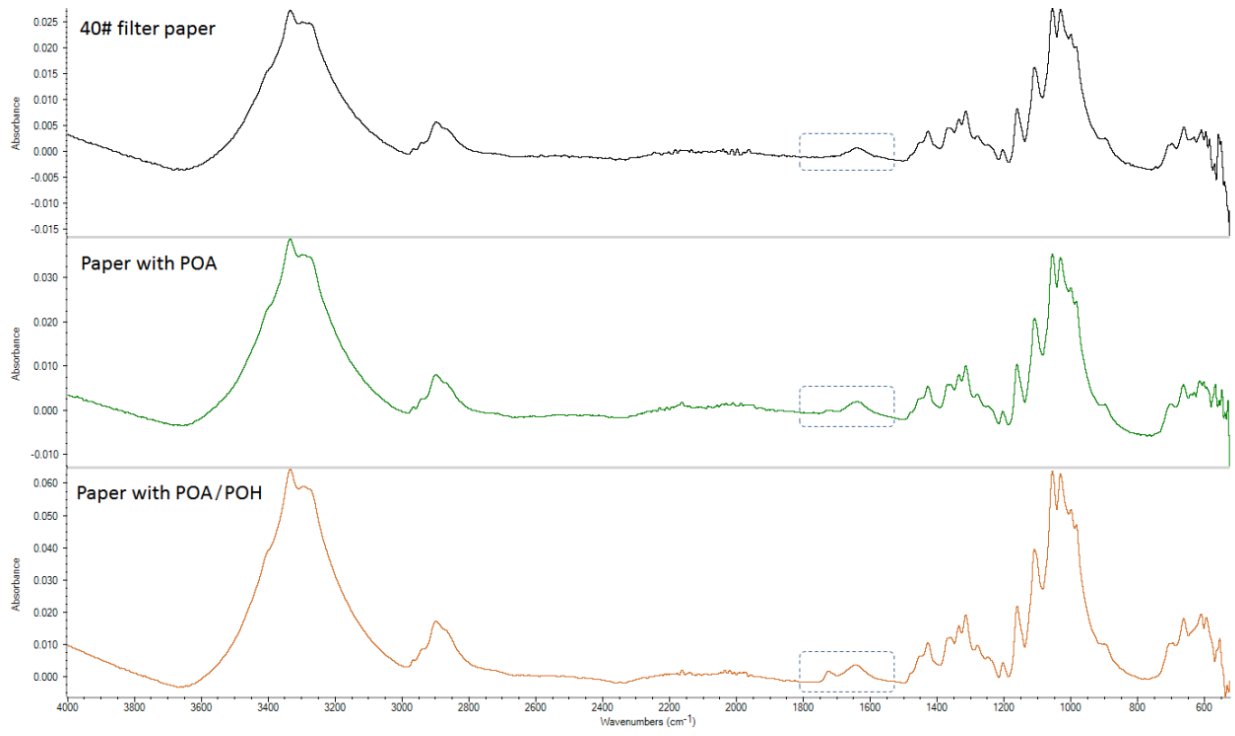

Figure S4. FTIR spectra of 40# filter paper, paper dipped with POA, and paper dipped with POA/POH.

10. Dry and wet weight of paper samples

Round pieces of unmodified and modified paper with diameters of ~6.6 mm were submerged in 250 µL of PBS for 24 hours inside a 96-well plate at room temperature. The dry and wet weight of the paper samples were measured before and after dipping. For dry weight measurements, the samples were dried in a 60°C oven and then equilibrated at 23°C and 50% relative humidity overnight prior to measurement to ensure consistency between samples. For wet weight measurements, the excess water on the surface of sample was removed by a rapid press (using 2.4 kg hand roller) between two Kimwipes to ensure that only absorbed/adsorbed water is considered in the swollen mass measurements. Results are shown in Figure S5.

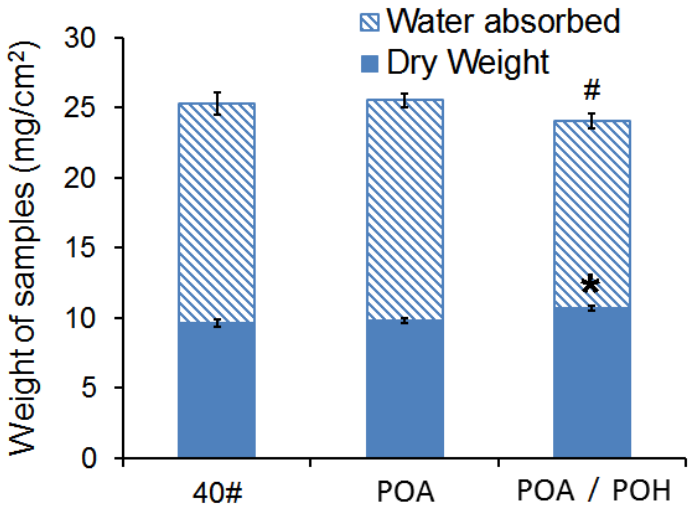

Figure S5. Dry and fully wetted weight of paper samples (n=12, *p<0.05 (dry), #p<0.05 (wet) relative to 40# filter paper).

As discussed in the manuscript, POEGMA dipping results in an increase in paper dry weight (associated with the immobilization of a POEGMA gel on the fiber surface) but a slight albeit significant decrease in wet weight. We hypothesize this result is related to the clogging of small pores in the fibers and/or between fibers by POEGMA gel formation.

11. Polymer distribution on paper

To confirm that the dipping method successfully modified the fiber surface, the sequential dipping procedure was repeated using rhodamine 123-labeled POA and fluorescein-labeled POH. For this purpose, POH was tethered with fluorescein isothiocyanate (FITC) via direct reaction between the isothiocyanate and hydrazide groups. Typically, 1 g of POH was reacted with 5 mg of FITC

overnight (at least 12 h) under gentle mechanical agitation at pH 8 and room temperature, targeting modification of only a small (~2 mol%) fraction of the available hydrazide groups so as not to disrupt the cross-linking capacity of the polymer. Analogously, POA (1 g) was labeled with rhodamine 123 (5 mg) via reductive amination between the amino group in rhodamine 123 and a small (~2 mol%) fraction of aldehyde groups in POA, with the resulting Schiff base reduced using sodium cyanoborohydride (8.25 mg, 10 fold molar excess to the rhodamine) to create a stable conjugate. All reactions were performed in a foil-covered reaction flask to prevent photobleaching during synthesis. The resulting labeled polymers were dialyzed exhaustively against deionized water (MWCO 3500 Da) for 6 cycles (6+ hours per cycle, all in the dark) to remove unbound FITC, lyophilized to dryness, dissolved in PBS as 4% w/v solution, and stored at 4°C in the dark. Fluorescently-labeled POA and POH solutions were subsequently used in place of non-labeled POA and POH in the dipping method outlined in section 4 to prepare a labeled POEGMA-coated paper. Following modification, the dried paper sample was exposed to blue (488 nm) and green (543 nm) light using a Zeiss 510 inverted confocal microscope to collect fluorescence images defining the localization of fluorescein-labeled (POH) and rhodamine-labeled (POA) polymers respectively on the paper surface. The images are shown in Figures 3a and S6, with the two figures presented representing images collected at two different z-planes within the sample. Each figure shows similar co-localization of POA and POH on the fiber surface, indicating that the bulk of the paper was successfully surface modified with POEGMA by dipping.

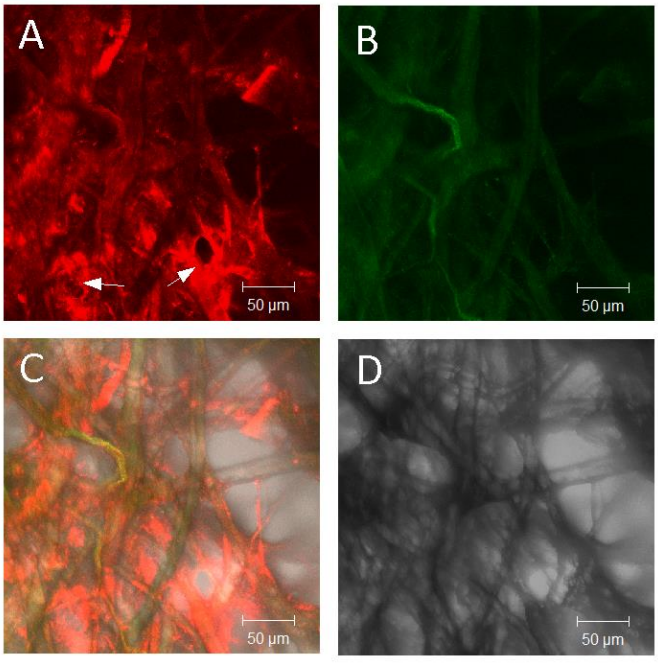

Figure S6. Cellulose fiber networks treated by fluorescently-labeled POA and POH as viewed by confocal laser scanning microscopy (CLSM) at a different z-plane from Figure 3a. A: rhodamine 123-labeled POA; B: fluorescein-labeled POH; C: merged CLSM image; D: bright field image.

Arrowheads in A indicate the concentration of POA at the edge and junction points between fibers.

12. Mercury intrusion porosimetry

Mercury intrusion porosimetry measurements were performed using a Quantachrome Poremaster GT mercury intrusion porosimeter (Boca Raton, USA) using high pressure mode and a fixed speed pressure gradient from 1.4 to 4195 kg·cm^{-1} (10.6 µm –3.57 nm pore diameter range). The average pore diameter, total porosity, and pore size distribution were determined as a function of intruded volume using the Poremaster (Version 5.00) software (Quantachrome). Figure S7 shows the number distribution of pores and the total pore volume of the paper before and after POEGMA dip coating treatment.

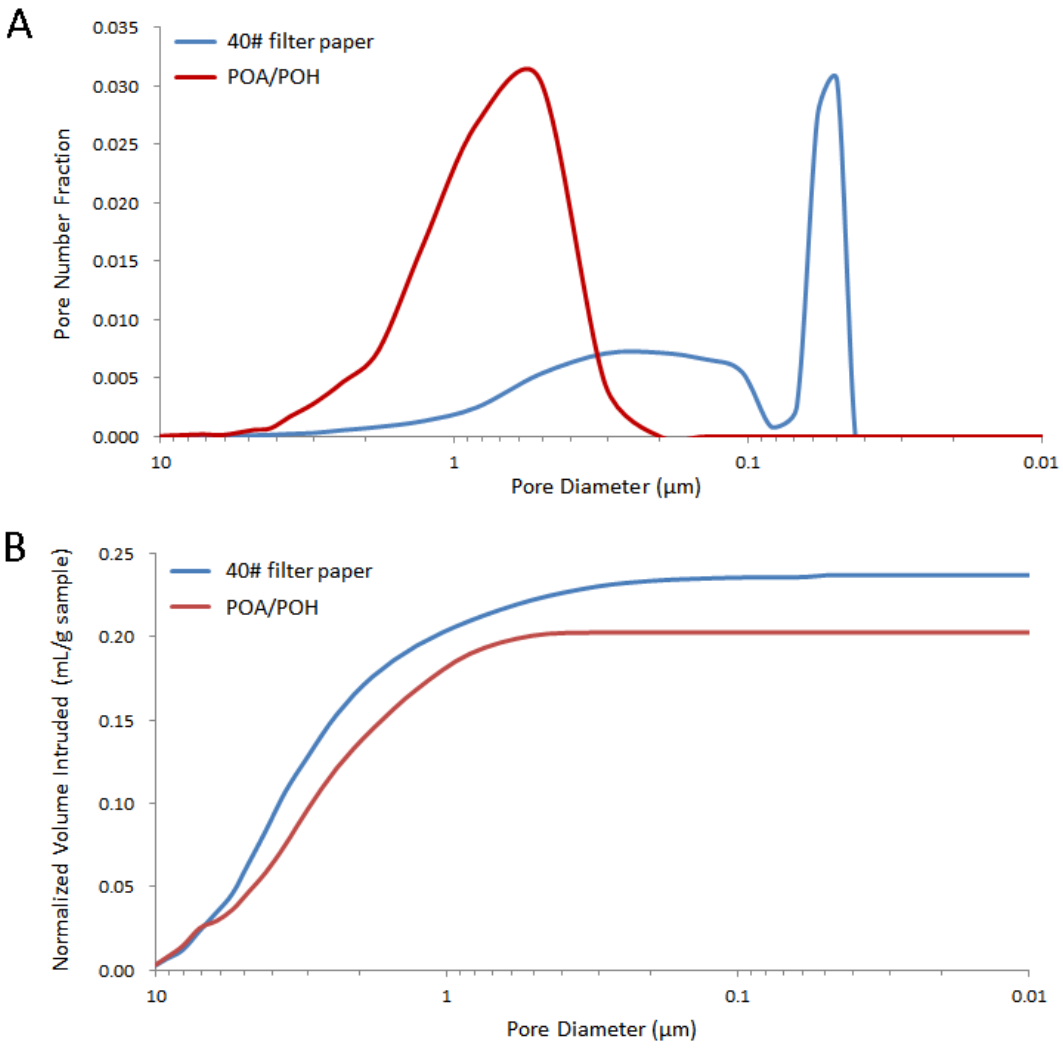

Figure S7. Number distribution of pore diameter (A) and normalized volume of mercury intrusion

(B) of 40# filter paper and filter paper coated with POA/POH operated at high pressure model.

This data indicates that the porosity measured by high pressure mercury porosimetry slightly decreased after coating with polymers, with the decrease in porosity attributable almost exclusively to the elimination of smaller pores (< 0.05 μm) while larger pores (~ 0.5 μm average size) remain relatively unaffected. This result further supports our hypothesis that POEGMA dipping results in the filling of nanopores/micropores within individual fibers but has little impact on the pores between fibers (i.e. the mesh size of the paper) relevant for defining transport properties. It should be noted that the high pressure operation of the porosimeter effectively collapses the macropore network of the paper, requiring the addition of the interparticle porosity data obtained under low pressure (~61% for both treated and untreated paper) to accurately estimate the total pore fraction inside the paper at ambient pressure. However, the high pressure data can more directly probe the fate of the smaller pores as a result of POEGMA treatment, of direct interest here in interpreting the role of POEGMA in regulating paper interfacial properties.

13. Residual aldehyde and hydrazide groups on paper surface

Fluorescent labeling was used to assess the presence of unreacted (free) aldehyde and hydrazide groups on POA and POA/POH treated paper. Following POEGMA modification of the paper surface using the dipping method described in section 4 (using non-fluorescent polymers), the dried POA and POA/POH dipped paper samples were soaked in solutions of 0.05 g/L fluorescein-5-thiosemicarbazide (5-FTSC, aldehyde-reactive) or 5-fluorescein isothiocyanate (5-FITC, hydrazide-reactive) overnight at pH 8 in a 96-well plate to detect the number of residual functional aldehyde or hydrazide functional groups respectively. Non-reacted probes were subsequently removed from the paper by soaking and rinsing the paper in pH 8 PBS buffer (15 wash cycles) to ensure that only covalently-tethered probe remained. The relative fluorescence intensity of the surface (directly correlated to the number of free aldehyde or hydrazide groups on the paper, depending on the probe used) was measured by a VICTOR 3 multi-label microplate reader using an excitation wavelength of 488 nm and an emission wavelength of 535 nm (Figure S8).

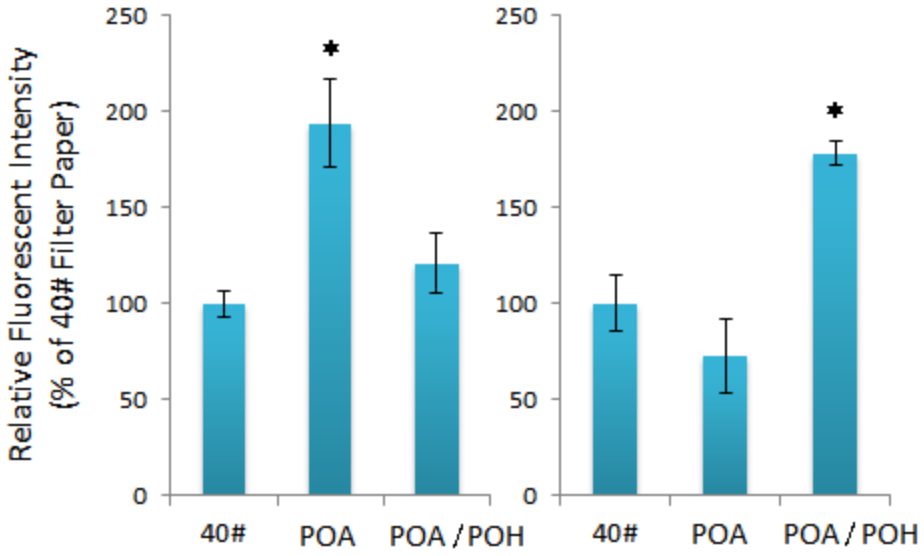

Figure S8. Relative density of aldehyde and hydrazide groups throughout the paper surface with or without POA and POH coating. The aldehyde and hydrazide groups were labeled by fluorescein-5-thiosemicarbazide (5-FTSC, left) and 5-fluorescein isothiocyanate (5-FITC, right) respectively. The fluorescence intensity of the paper samples was measured by fluorescent plate reader at the excitation wavelength of 488 nm and emission wavelength of 535 nm and normalized to the results obtained with unmodified 40# filter paper. *$p<0.05$ relative to 40# filter paper.

Addition of POA in the first dipping step results in a significant increase in the number of free aldehyde groups but no change in the number of hydrazide (nucleophilic) groups, as anticipated for POA adsorption to the paper. In the second dipping step, those excess aldehyde groups are consumed (returning to the concentration of aldehydes observed in unmodified 40# filter paper) while the number of free hydrazide (nucleophilic) groups significantly increases, indicating both the successful immobilization of POH and the occurrence of covalent cross-link formation between aldehyde groups in POA and hydrazide groups in POH. Thus, these results confirm that a thin interfacial hydrogel layer is formed on the fiber surface as a result of dipping.

14. Layer-by-layer dipping

Given the results above that suggest a large excess of hydrazide groups at the interface following a single POA/POH dipping cycle, we investigated the production of hydrogel films by sequential POA/POH dipping cycles in a process analogous to polyelectrolyte layer-by-layer assembly methods. Figure S9(a) shows the mass change measured over each cycle of POA/POH sequential

dipping, while Figure S9(b) shows the resulting protein adsorption to these multi-layer dipped filter papers.

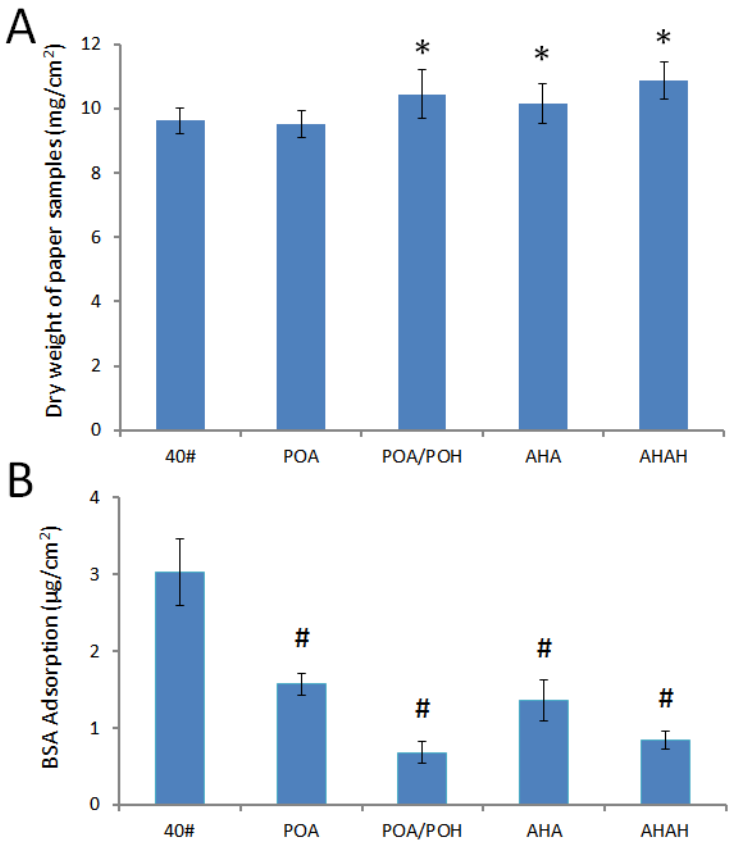

Figure S9. Dry mass change (n=6) (a) and the adsorption of BSA (100 µg/mL protein concentrations, n=6) (b) to layer-by-layer POA/POH dipped papers prepared by sequential dipping cycles. AHA and AHAH) indicate three or four dipping steps respectively using POA/POH sequentially. *p<0.05 higher, #p<0.05 lower relative to 40# filter paper.

A significant mass increase is observed upon each POA/POH dipping cycle (Fig. S9(a)), indicating the effectiveness of a layer-by-layer approach to build a hydrogel interface on the filter paper. However, no significant decrease in protein adsorption is observed as a result of this sequential hydrogel fabrication process; a single POA/POH dipping cycle is as effective as multiple cycles in terms of reducing non-specific adsorption ($p > 0.05$, Fig. S9(b)). Based on this result, coupled with the increased work associated with layer-by-layer approaches and the increased risk of macropore blockage as the hydrogel becomes thicker, a single POA/POH dipping cycle was used to produce all blocked filter papers discussed in the main manuscript. Note that regardless of the number of dipping cycles used, paper surfaces in which POA is used as the terminal dipping

polymer (i.e. the surface has excess aldehydes) consistently underperform paper surfaces in which POH is used as the terminal dipping polymer (i.e. the surface has excess hydrazides). We hypothesize this result is attributable to the lack of reactivity of hydrazide groups to proteins relative to aldehyde groups, which may form Schiff bases with terminal or pendant amines on proteins.

15. Capillary rise

Capillary rise experiments were performed on filter paper strips of width 0.8 cm, height 8 cm and thickness 0.2 mm prepared both with and without POEGMA coatings. One end of the strip was vertically submerged into a PBS bath at a depth of 1 cm, and the time required for the rising edge of the water to travel up the test strip was recorded at each centimeter of capillary rise to a total height of 5 cm from the point of submergence. At least three experiments were performed for each group of sample, with the reported capillary rise rates representing the mean ± standard deviation of these three experiments.

16. Protein adsorption on paper samples

Protein adsorption to unmodified and dipped paper samples was assessed by submerging two paper samples (1cm × 2cm) in PBS within a single well of a 12 well plate and allowing the paper samples to equilibrate over 24 hours. Afterwards, unabsorbed PBS was removed and 500 μL of 100 μg/mL protein solution (bovine serum albumin, fibrinogen, rabbit IgG, or β-galactosidase) was added to each well. The samples were incubated for 2 hours at 25°C under gentle shaking. After 2 hours, the paper samples were removed and the residual protein concentration in the solution was measured using a Bradford protein assay (1:1 sample to reagent ratio) according to the manufacturer's protocol.[5] Results were quantified by measuring the absorption of the residual (unadsorbed) protein solution at 595 nm using a Nanodrop 2000c spectrophotometer (Thermo Scientific). Each experiment (POA/POH coated paper as well as the controls) was done in triplicate, with reported errors representing the standard deviation of the replicates.

17. Benchmarking protein adsorption performance of POEGMA-blocked paper to BSA-blocked paper

To illustrate the performance of the POEGMA dip-coated paper relative to the current standard of BSA blocking in terms of resisting non-specific protein adsorption, IgG adsorption experiments were conducted on both a model cellulose surface using QCM and on Whatman 40# filter paper

using a fluorescence technique.

QCM on Cellulose-Modified Surface: BSA-blocked surfaces were first prepared by flowing BSA solution (1%, w/v in PBS) over cellulose-modified QCM chips until the QCM signal reached a plateau (i.e. adsorption equilibrium was achieved). The chips were subsequently washed with PBS until a plateau dissipation was observed (i.e. no further BSA desorption occurred). Next, rabbit IgG solution (25, 50, 100, 200, 500, or 1000 µg/mL in PBS) was flowed over the chip until steady state was achieved, after which the chip was subjected to a PBS wash (again until equilibrium was achieved). The adsorption of IgG was calculated by Sauerbrey equation, as described in section 3 of Supporting Information.

Figure S10 shows the Sauerbrey masses of rabbit IgG adsorbed to the QCM chip as a function of IgG concentration. Both POA/POH dip-coated paper as well as BSA-blocked paper performed similarly, with protein adsorption to either interface less than 1/10th of that observed for the bare cellulose chip.

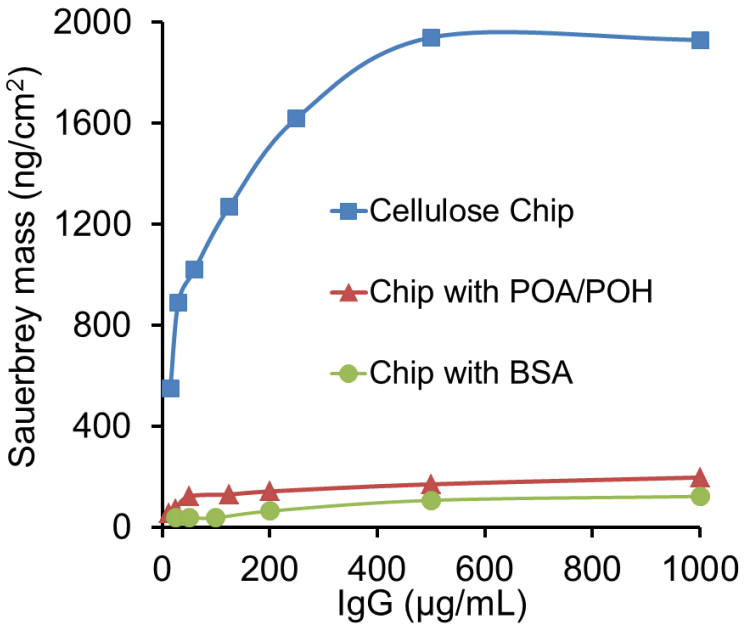

Figure S10. Sauerbrey mass (from QCM) as a function of time for rabbit IgG adsorption to a bare cellulose chip and cellulose QCM chips pre-treated with POA/POH and BSA

Filter paper: To assess the protein adsorption performance of Whatman 40# filter paper blocked with POA/POH relative to paper blocked with BSA, IgG was labeled with FITC according to the Thermo Scientific product protocol (# 53027). Briefly, 50 µg FITC (15- to 20-fold molar excess) was reacted with 1 mg IgG (500 µL, 2 mg/mL) at pH 8.5. Labeled protein was separated from free label via centrifugal filtration (10000 RPM, 10 min) using a membrane with a molecular-weight cutoff (MWCO) of 10 kDa (IgG=150 kDa, FITC=389 Da) instead of using resin in the protocol.

The filter paper was cut into a 1cm×2cm strip, submerged in BSA solution (1%, w/v) for 30 min, and then washed with PBS. The BSA-blocked paper (two pieces per well) was next submerged in the FITC-labeled IgG solution (100 µg/mL, 500 µL) for 2 hours and removed after a gentle shaking of the container. The fluorescent intensity of the solution before and after paper soaking (including the PBS rinse volumes) was measured using a VICTOR 3 multi-label microplate reader (excitation = 488 nm, emission = 535 nm). Fluorescence intensity values were converted to protein concentrations based on a calibration curve (R^2 = 0.997), with the amount of protein adsorbed to the paper calculated based on the difference between total protein content of the solution before and after paper exposure. Figure S11 shows the comparative adsorption result between unmodified (control), BSA-blocked, and POA/POH-blocked filter paper.

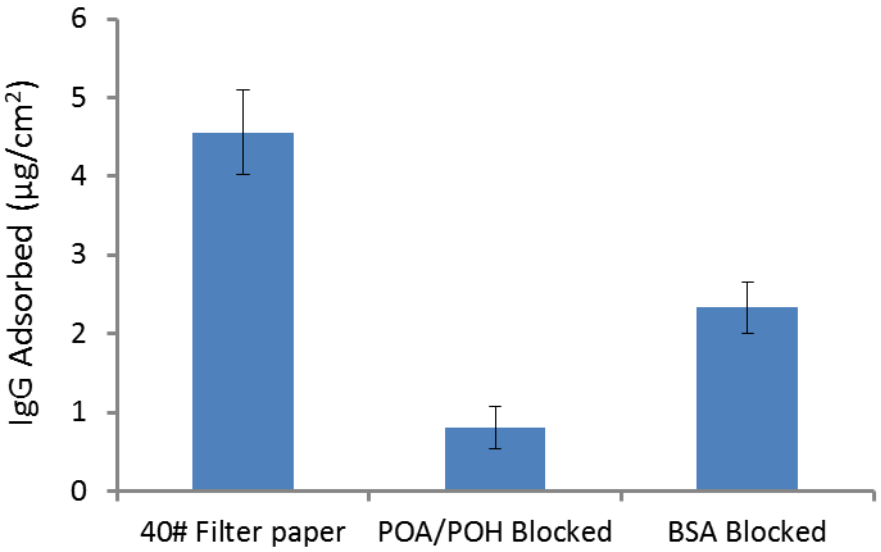

Figure S11. Amount of rabbit IgG adsorbed per unit cross-sectional area on BSA-blocked, POA/POH-blocked, and control (unmodified) paper.

BSA-blocked paper is significantly less effective at preventing protein adsorption relative to POA/POH-blocked filter paper, with approximately 3-fold less IgG adsorbed to the POA/POH-blocked paper. This result can be attributed to two factors: (1) POA/POH polymers are significantly smaller (~20 kDa compared to ~66 kDa) and significantly more flexible than BSA and thus can effectively block smaller pores in the paper that BSA cannot and (2) POA/POH forms a covalently cross-linked thin layer at the fiber interface that is fixed in place, while BSA can exchange with IgG dynamically via non-covalent interactions.

18. Construction of β-galactosidase (β-GAL) test strips

To assess the capacity of POEGMA-coated paper for selective lateral flow assays, a paper-based test strip was designed that utilized chlorophenol red β-galactopyranoside (CPRG) as a colorimetric sensor to confirm the mobility of β-galactosidase (β-GAL) within the paper matrix. CPRG (yellow color) is enzymatically converted by β-GAL into chlorophenol red (red-magenta color); capture of the chlorophenol red product by poly-L-arginine hydrochloride results in the red color changing to purple, allowing for site-specific colorimetric detection of the presence of β-GAL.

Test strips were constructed by dip-coating paper with POA/POH as described in section 4 and subsequently depositing CPRG (5μL, 3 mM) and poly-L-arginine hydrochloride (5 μL, 2% w/v) at a specific location on a 0.8 cm x 8 cm paper strip by pipetting to form a localized detection band (see Figure 4a, strips 1-3). The strips were air dried prior to use for testing. As compared, the BSA-blocked paper were prepared by submerging in BSA solution (1%, w/v) for 30 min, and then washed with PBS and air dried. Subsequently, the mobility of β-GAL was assayed by placing the test strips into the β-GAL solution (10U/mL in PBS, pH=6.8) at a depth of 1 cm and allowing the liquid to move up the strip until it crossed the poly-arginine band.

19. Indirect paper-based ELISA

Prior to the experiment, a paper microzone plate was fabricated using a wax printer (Xerox Phaser 6580). The patterned black wax on the 40# filter paper was melted in an oven at 120 °C for 2 minutes to form the hydrophobic barriers. Goat anti-rabbit IgG (the antigen) was subsequently transferred to the patterned paper at various concentrations in PBS solutions in 3 μL aliquots into different test zones on the microzone plate and allowed to dry for 10 minutes under ambient conditions (~23ºC, ~30% relative humidity). Each test zone was subsequently blocked by adding 3 μL total volume of various blocking agents: (1) POA and POH (both 4% (w/v) with 0.05% (v/v) Tween-20 in PBS), added in sequence and dried for 15 minutes each; (2) BSA (consisting of 1% (w/v) BSA and 0.05% (v/v) Tween-20 in PBS), dried for 30 minutes – “BSA-blocked paper” in the manuscript; (3) skimmed milk (5% in PBS), dried for 30 minutes – “skimmed milk-blocked

paper" in the manuscript. After blocking, a 3 µL solution containing horseradish peroxidase (HRP)-conjugated rabbit IgG (the antibody) in an incubation buffer (0.05% (v/v) Tween-20 in PBS) was added to each zone and allowed to incubate for 75 seconds. The whole paper was then washed three times by submerging into a PBS buffer with gentle shaking (3 x 1 minute cycles). Finally, a 3 µL solution of the colorimetric substrate for horseradish peroxidase (1:1 TMB peroxidase substrate solution and peroxidase substrate solution B, KPL) was added to each test zone immediately after the washing step and allowed to react for 5 minutes under ambient conditions. The paper microzone plate was scanned by a desktop scanner (CanoScan LiDE 700F, Canon), and the integrated intensity and mean gray value of the color were measured using ImageJ software. The detection limit was defined as three times the standard deviation of the control group.[6]

20. ^{1}H NMR and ^{13}C NMR spectra of POA and POH

^{1}H-NMR and ^{13}C-NMR were performed on a Bruker AVANCE 600 MHz spectrometer using deuterated chloroform as the solvent. Chemical shifts are reported relative to residual deuterated solvent peaks. Peak assignments are given on each spectrum based on the anticipated chemical structure of each polymer.

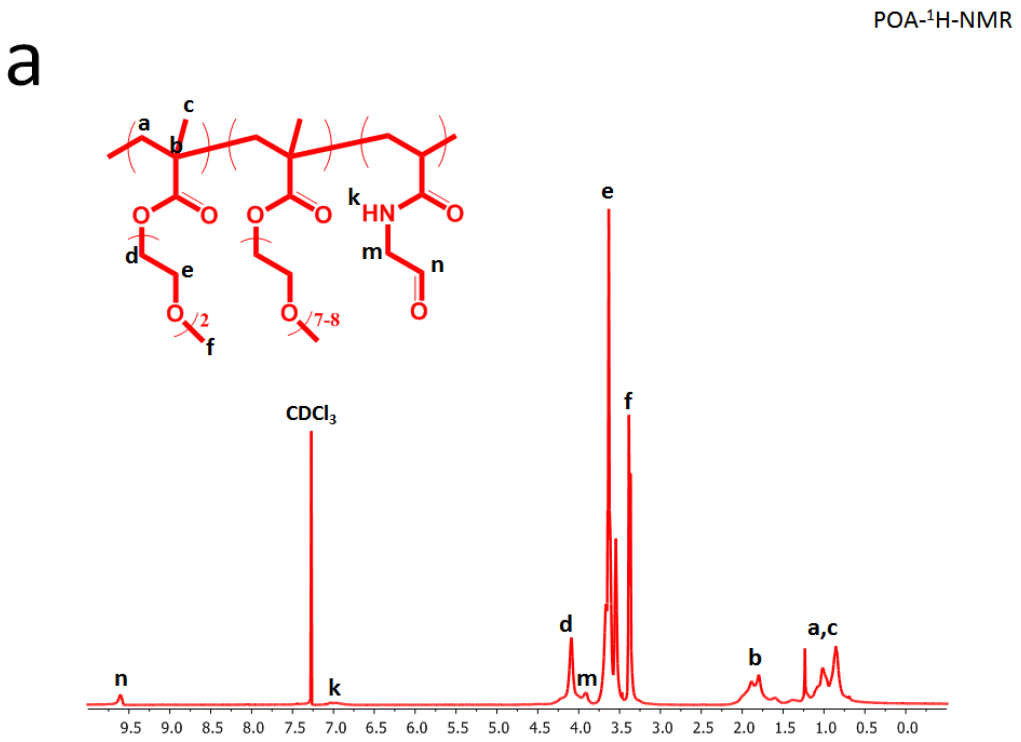

b

POA-^{13}C-NMR

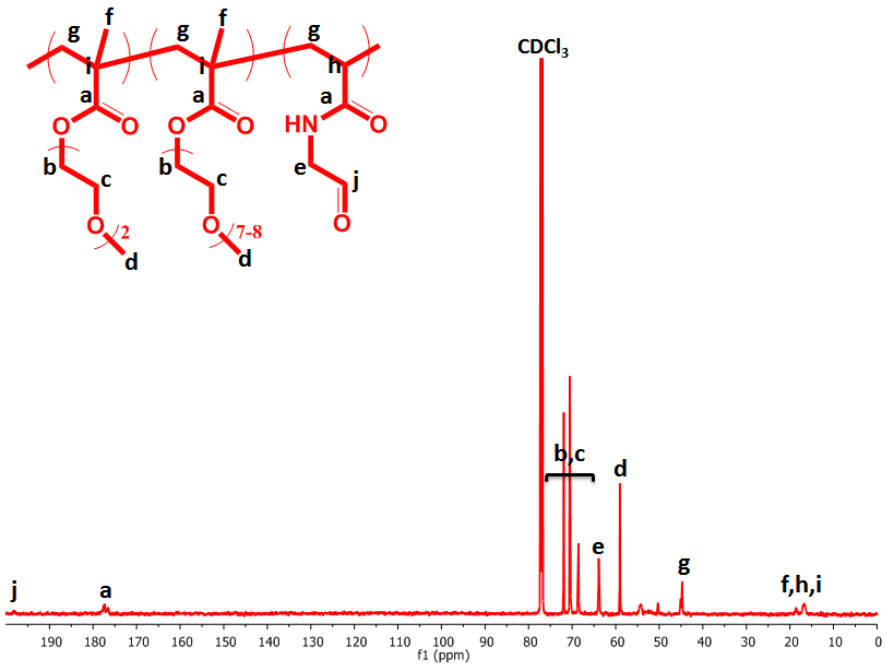

c

POH-^{1}H-NMR

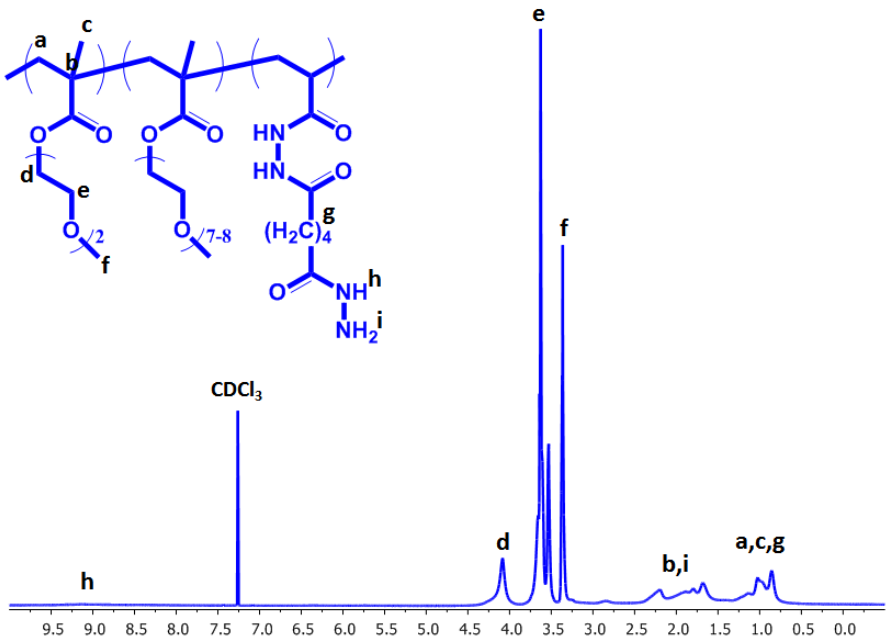

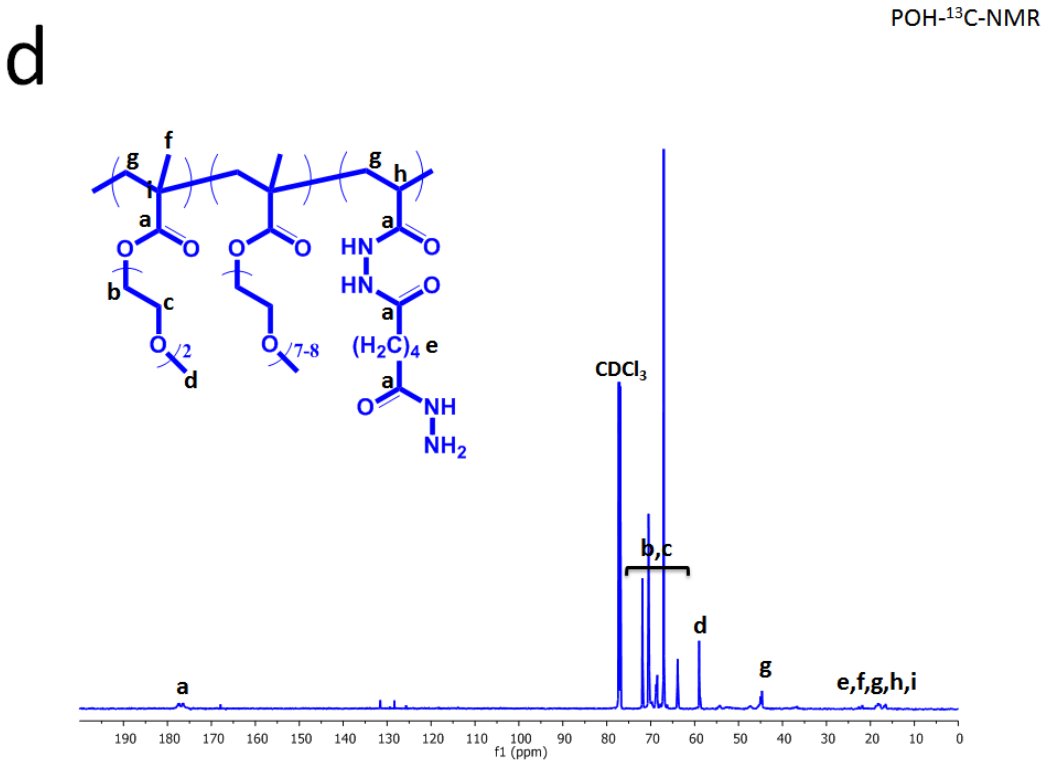

Figure S12. (a) ^{1}H NMR and (b) ^{13}C NMR spectra of POA; (c) ^{1}H NMR and (d) ^{13}C NMR spectra of POH.

21. Thermal analysis of POA and POH

Thermogravimetric analysis: Thermogravimetric analysis (TGA) was performed using a TA-Q50 instrument under an argon atmosphere. Samples were heated at 10 °C/min to 800 °C.

Figure S13 shows the TGA curves of POA and POH. Both polymers were thermally stable up to temperatures of >200 °C, facilitating storage stability. POH is more hydrophilic and hygroscopic than POA so absorbs water once removed from the drying oven, resulting in a small but significant water fraction that is removed at ~100 °C in the POH data.

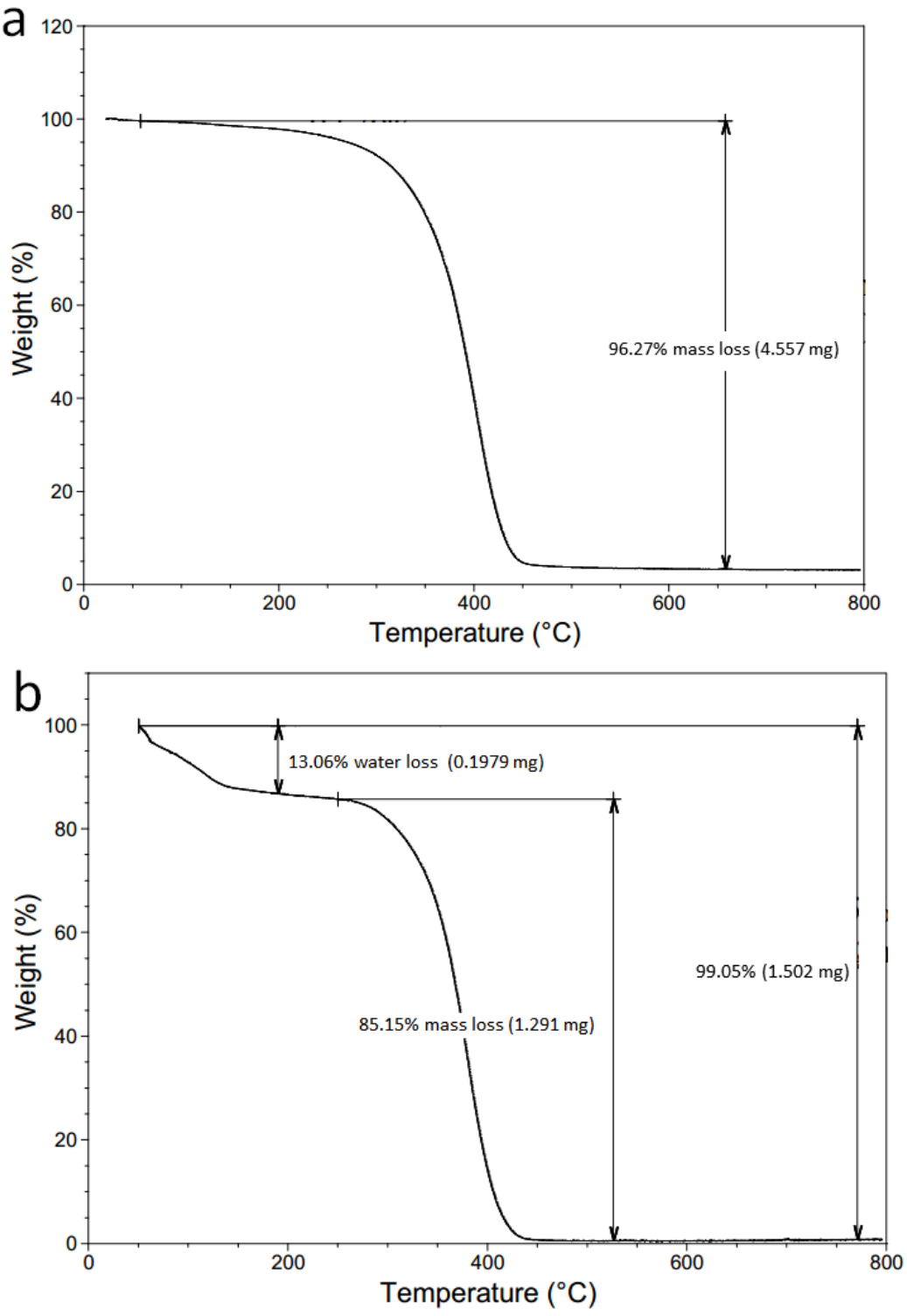

Figure S13. The weight loss of POA (a) and POH (b) as a function of temperature measured at a heating rate of 10 °C/min. using TGA

Differential Scanning Calorimetry: Differential scanning calorimetry (DSC) was performed using a TA Instruments Q200 DSC. 15 mg of a dried polymer sample was placed in a Tzero hermetic aluminum sample pan. An empty reference pan was used during testing. A modulated temperature ramp from -50°C to 100°C was performed on each sample using a 60 second modulation at an amplitude of ±1°C and a 3°C/min. heating rate. The glass transition temperature within this range was determined using the TA Instruments Analysis software.

Figure S14 shows the DSC results for POA and POH. Glass transitions were observed for both polymers, with both polymers exhibiting relatively low T_g values of ~11°C for POA and ~-14°C for POH. Note that the relevance of this result to the performance of the hydrogel in the present application is somewhat unclear, although the fact that the polymer is in the rubbery state at room temperature and dry should at least assist with maintaining paper flexibility even at very high polymer concentrations.

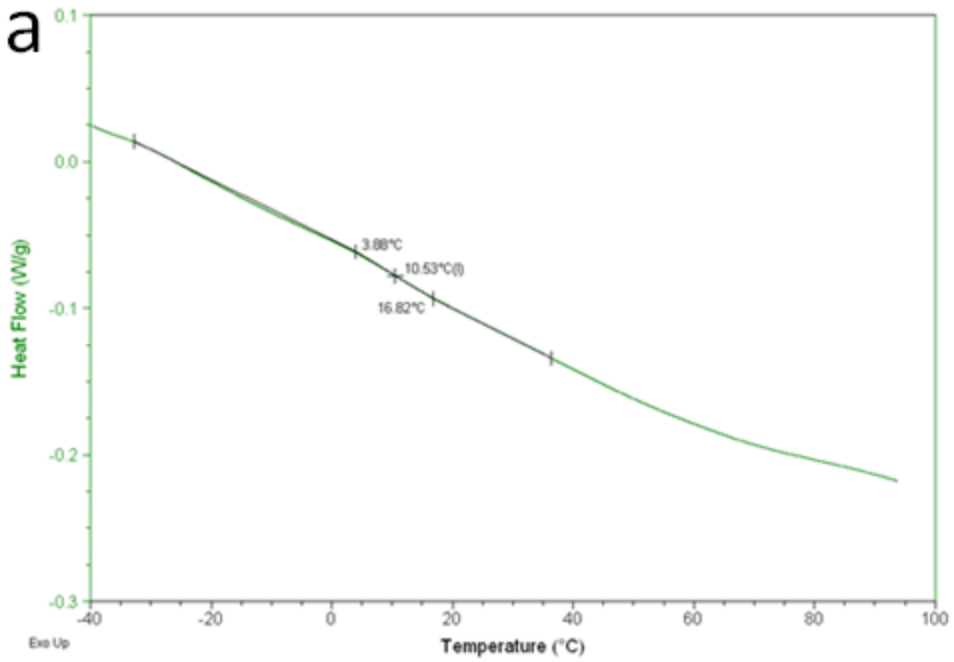

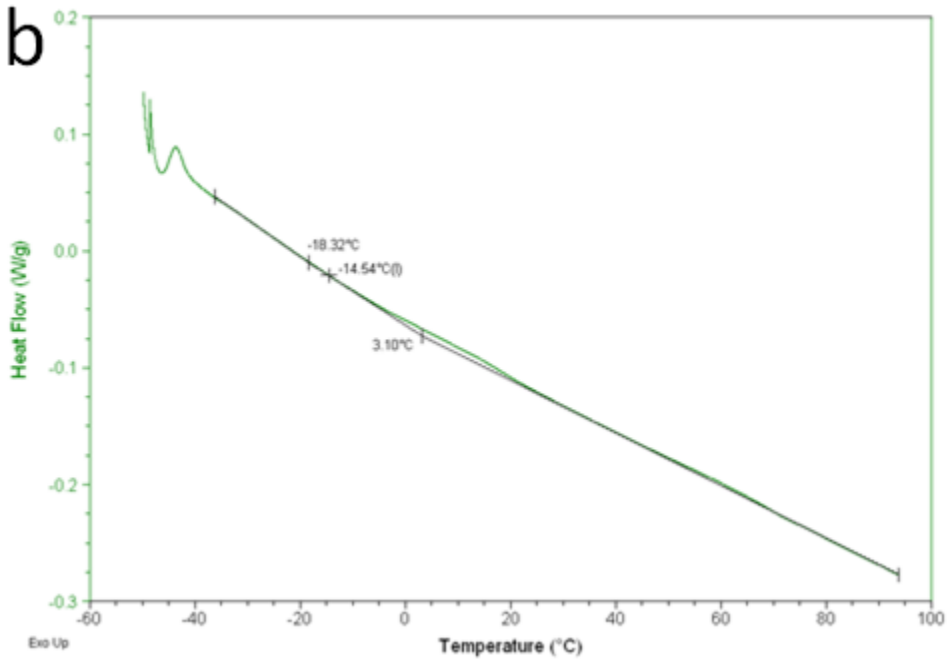

Figure S14. Differential scanning calorimetry results for POA (a) and POH (b).

22. Supplementary references

(1) N. M. B. Smeets, E. Bakaic, M. Patenaude, T. Hoare, *Chem. Comm.* **2014**, *50*, 3306-3309.

(2) (a) G. Sauerbrey, *Zeitschrift für Physik* **1959**, *155*, 206-222; (b) M. Rodahl, B. Kasemo, *Sensors Actuators A: Physical* **1996**, *54*, 448-456.

(3) K. Tasaki, *J. Am. Chem. Soc.* **1996**, *118*, 8459-8469.

(4) M. Henriksson, L. A. Berglund, P. Isaksson, T. Lindström, T. Nishino, *Biomacromolecules* **2008**, *9*, 1579-1585.

(5) Thermo Scientific, "Bradford Protein Assay". http://www.nanodrop.com/Library/T084-NanoDrop-2000-2000c-Bradford-Protocol.pdf.

(6) (a) C. M. Cheng, A. W. Martinez, J. Gong, C. R. Mace, S. T. Phillips, E. Carrilho, K. A. Mirica, G. M. Whitesides, *Angew. Chem. Int. Ed.* **2010**, *49*, 4771-4774; (b) X. Liu, C. Cheng, A. Martinez, K. Mirica, X. Li, S. Phillips, M. Mascarenas, G. Whitesides, in *Micro Electro Mechanical Systems (MEMS), 2011 IEEE 24th International Conference on*, IEEE, **2011**, 75-78.

Chapter 3 “Click” chemistry-tethered hyaluronic acid-based contact lens coatings improve lens wettability and lower protein adsorption

In chapter 3, all experiments were conducted by myself with assistance from Dr. Jianfeng Zhang, Banafsheh Rastegari, Mengsu Chen (undergraduate student), Qiang Fu, and Myrto Korogiannaki.. The chapter was initially drafted by myself, and edited later by Dr. Heather Sheardown, Dr. Carlos D. M. Filipe and Dr. Todd Hoare. This work has been published in *ACS applied materials & interfaces*, 2016, DOI: 10.1021/acsami.6b07433.

ACS APPLIED MATERIALS & INTERFACES

Research Article

www.acsami.org

"Click" Chemistry-Tethered Hyaluronic Acid-Based Contact Lens Coatings Improve Lens Wettability and Lower Protein Adsorption

Xudong Deng,[†] Myrto Korogiannaki,[†] Banafsheh Rastegari,[†,‡] Jianfeng Zhang,[†] Mengsu Chen,[§] Qiang Fu,[†] Heather Sheardown,[†] Carlos D. M. Filipe,[*,†] and Todd Hoare[*,†]

[†]Department of Chemical Engineering, McMaster University, Hamilton, Ontario L8S 4L7, Canada

[‡]Department of Biology, Faculty of Sciences, Shiraz University, Shiraz, Fars 71946-84636, Iran

[§]School of Nursing, McMaster University, Hamilton, Ontario L8S 4L8, Canada

Supporting Information

ABSTRACT: Improving the wettability of and reducing the protein adsorption to contact lenses may be beneficial for improving wearer comfort. Herein, we describe a simple "click" chemistry approach to surface functionalize poly(2-hydroxyethyl methacrylate) (pHEMA)-based contact lenses with hyaluronic acid (HA), a carbohydrate naturally contributing to the wettability of the native tear film. A two-step preparation technique consisting of laccase/TEMPO-mediated oxidation followed by covalent grafting of hydrazide-functionalized HA via simple immersion resulted in a model lens surface that is significantly more wettable, more water retentive, and less protein binding than unmodified pHEMA while maintaining the favorable transparency, refractive, and mechanical properties of a native lens. The dipping/coating method we developed to covalently tether the HA wetting agent is simple, readily scalable, and a highly efficient route for contact lens modification.

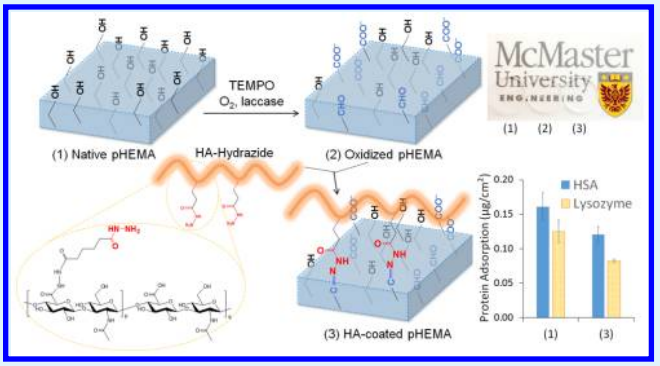

KEYWORDS: *hyaluronic acid, poly(2-hydroxyethyl methacrylate), TEMPO oxidation, surface wettability, protein adsorption*

1. INTRODUCTION

Soft contact lenses have been widely used for vision correction since their introduction by Wichterle in the 1960s.[1] The hydration and surface hydrophilicity of soft lenses significantly improve the oxygen permeability and wettability of the lens by the tear film, both of which are thought to enhance the overall comfort of the lens.[2,3] Hydroxyethyl methacrylate (HEMA) was the original hydrophilic monomer used for soft contact lens production and continues to be the most commonly used hydrophilic monomer in the production of both hydrogel-based and silicone hydrogel-based contact lenses.[4] However, poly(hydroxyethyl methacrylate) (pHEMA)-based contact lenses tend to dehydrate over time when applied on the eye, particularly over longer wear times;[5] this drying leads to user discomfort in the form of eye dryness and scratchiness, both of which lead to lens dropout.[6] In addition, both hydrogel and silicone hydrogel contact lenses suffer from challenges related to the deposition of proteins from the tear fluid onto the lenses,[7−9] correlated to a variety of adverse effects including microbial cell attachment[10,11] and inflammatory complications.[12]

In order to minimize the dehydration of and protein accumulation on soft contact lenses, a variety of chemical treatment methods have been employed to modify the lens surface and/or the lens as a whole before or after the polymerization process. Doping or tethering of highly hygroscopic polymeric wetting agents has been the most commonly pursued approach.[13,14] Synthetic polymers associated with high water binding capacity and low protein adsorption, including poly(vinyl alcohol) (PVA), poly(ethylene glycol) (PEG),[15] and 2-methacryloyloxyethyl phosphorylcholine (MPC),[16,17] have been either entrapped within the bulk of the lens (potentially enabling sustained release of the wetting agent over time)[18,19] or surface grafted to the lens (increasing the capacity for interfacial water retention).[20] However, these synthetic approaches have met with limited success in practice. For example, while PVA modification does increase lens wettability, PVA-containing lenses (FOCUS DAILIES with AquaComfort, nelfilcon A) have also performed worse than other daily disposable lenses such as 1-DAY ACUVUE (etafilcon A, Johnson & Johnson Vision Care, a copolymer of HEMA and methacrylic acid with a polyvinylpyrrolidone embedded wetting agent) in terms of comfort, maximum wear time, corneal staining, and lens fit.[21]

Recent work has focused on the use of hyaluronic acid (HA), a natural polysaccharide present in the eye and used in several

Received: June 20, 2016
Accepted: August 10, 2016

DOI: 10.1021/acsami.6b07433
ACS Appl. Mater. Interfaces XXXX, XXX, XXX−XXX

Scheme 1. Reaction Scheme Showing the Preparation of Hydrazide-Functionalized Hyaluronic Acid (HA-Hzd), Oxidation of pHEMA (Ox-pHEMA), and Coating HA-Hzd on Oxidized pHEMA (HA-pHEMA)

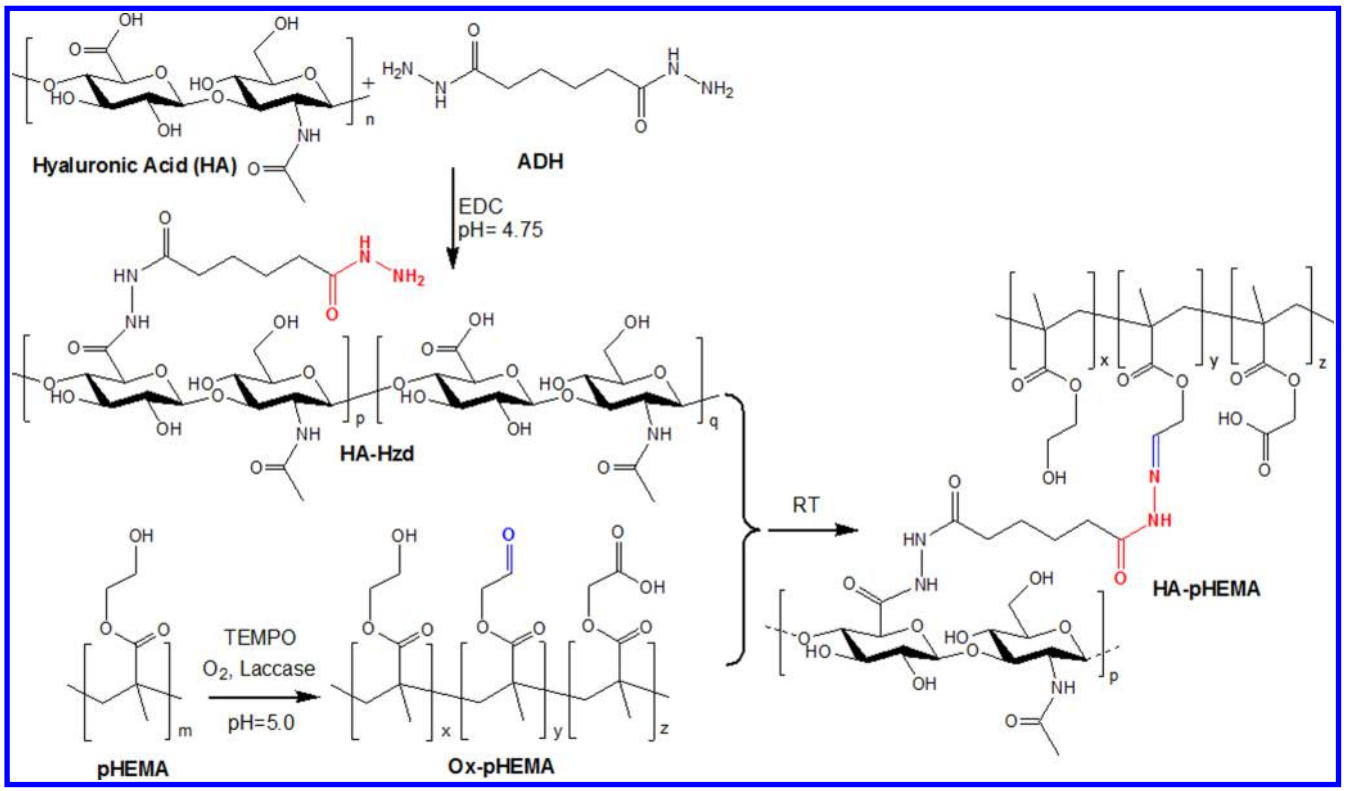

artificial tear formulations, as a preferred wetting agent. Coupled with its inherent wetting[22−24] and protein-resistance-promoting[25−27] properties, hyaluronic acid has also been associated with promoting corneal epithelial wound healing,[28] improving the integrity of superficial corneal cells,[29] reducing ultraviolet B (UVB) radiation-induced toxic effects,[30] protecting cells from oxidative damage,[31] and stabilizing the tear film.[32] Thus, it has the potential to provide multiple benefits in the context of contact lens coatings.

Various methods have been reported to incorporate HA into the bulk of the lens (facilitating wetting by either slow release of HA from the lens or self-assembly of HA at the lens−water interface) or immobilize HA on the lens surfaces (facilitating wetting directly at the interface). Cross-linking is the most commonly used method to introduce HA into the bulk hydrogel network, with HA incorporation having been demonstrated directly with the main lens material(s) (e.g., via photopolymerization of methacrylated photo-cross-linkable HA with HEMA[23]), within a secondary interpenetrating network (e.g., polyethylenimine cross-linked HA within an independently cross-linked HEMA network[27]), or via physical entrapment of a higher molecular weight HA-based cluster or nanogel (e.g., conjugation of HA to polypropylenimine tetramine dendrimers that improve HA immobilization within the lens).[22,25,26,33] In comparison, given the relatively low reactivity of HEMA for chemical modification, surface modification methods generally require the generation of a reactive functional group or interfacial binding site for HA immobilization. Again, HA attachment to the surface may be accomplished either directly or via another mediating chemistry. As an example of the former, thermal cross-linking has been used to conjugate thiolated HA to acrylated pHEMA surfaces via Michael addition chemistry during autoclaving;[34] as an example of the latter, covalent linkage of an HA-binding peptide (HABpep, with or without a PEG spacer) via EDC/NHS chemistry to a PureVision (balafilcon A, Bausch and Lomb) contact lens surface mediates ligand−receptor binding of HA at the lens interface.[24] However, each surface modification method reported to date is practically hampered by the multistep nature of the required protocols, including chemical modification of HA, HA uptake and cross-linking, and/or preparation of special linkers like HABpep. As a result, the development of a simple and fast surface modification strategy requiring fewer steps and/or using simpler reactions would be preferred to facilitate a scalable and thus commercially relevant method for preparing surface-wetted contact lenses.

To this end, we propose a click chemistry process[35] to facilitate more direct and high yield HA functionalization of a contact lens surface. We have extensively explored the click reaction between aldehyde and hydrazide groups to facilitate the rapid and high-yield formation of hydrazone bonds at physiological pH and have demonstrated the use of such chemistry to prepare a variety of bulk hydrogels,[36−39] electrospun hydrogel fibers,[40] and thin film hydrogels at the solid−liquid interface.[41] Hydrazide-functionalized HA (HA-Hzd) can be prepared at high yield via carbodiimide-mediated coupling of adipic acid hydrazide to the carboxylic acid on the glucuronic acid moieties of HA,[42,43] with such polymers already applied extensively in the preparation or modification of HA-based hydrogels for drug delivery and tissue engineering.[39,44−47] Correspondingly, pHEMA contains primary hydroxyl groups that can be oxidized into aldehyde groups, but very limited work has been reported on the oxidation of pHEMA hydrogels,[48] and relatively few oxidation methods have been demonstrated to reliably convert alcohols to aldehydes without continuing to carboxylic acids. Catalytic oxidation

DOI: 10.1021/acsami.6b07433
ACS Appl. Mater. Interfaces XXXX, XXX, XXX−XXX

using the stable nitroxyl radical 2,2′,6,6′-tetramethylpiperidinyl-1-oxy (TEMPO) as an electron transfer mediator is one of the most promising procedures to oxidize primary alcohol groups and has been widely used in the oxidation of natural polysaccharides.[49] While traditional TEMPO oxidation procedures have used bleach (NaClO) as the oxidizer together with NaBr,[50] the undesirable residual halide and requirement of high pH in such procedures have spurred the more recent use of oxidative enzymes such as laccase in combination with oxygen at neutral pH to promote oxidation.[51,52] To the best of our knowledge, TEMPO-mediated oxidation of primary alcohol groups in synthetic polymers like pHEMA has not previously been demonstrated.

In this work, we demonstrate the use of a simple click chemistry procedure involving the reaction of hydrazide-functionalized HA with TEMPO-oxidized pHEMA to covalently tether HA to the surface of a model contact lens via a simple two-step process (Scheme 1). Furthermore, we demonstrate the potential of this modification to significantly improve the surface wettability of the lens while also substantially decreasing nonspecific protein adsorption, both of which are linked to improved comfort and the potential for longer term wear of soft contact lenses.

2. EXPERIMENTAL SECTION

2.1. Chemicals and Materials. Sodium hyaluronate (Lot # 010600, M_n = 336.8 kDa, $Đ$ = 1.386 by GPC; see Supporting Information Figure S1) was obtained from Fidia Farmaceutici S.p.A. (Abano Terme, Italy). Adipic acid dihydrazyde (ADH, Sigma-Aldrich, 98%), *N*′-ethyl-*N*-(3-(dimethylamino)propyl)carbodiimide (EDC, Sigma-Aldrich, commercial grade), human serum albumin (HSA, Sigma-Aldrich, 97%), lysozyme from chicken egg white (Sigma-Aldrich, 41 800 units/mg solid), laccase from *Trametes versicolor* (EC 1.10.3.2, Sigma-Aldrich, ≥10 U/mg), TEMPO (Sigma-Aldrich, 99%), fluorescein isothiocyanate isomer I (FITC, Sigma-Aldrich, 97.5%), fluorescein-5-thiosemicarbazide (5-FTSC, Sigma-Aldrich, 80%), silver nitrate ($AgNO_3$, Sigma-Aldrich, ≥99.0%), and ammonium hydroxide (containing 28−30% NH_3, Caledon Laboratories) were all used as received. HEMA (2-hydroxyethyl methacrylate) and EGDMA (ethylene glycol dimethacrylate) were purchased from Sigma-Aldrich, with the 4-methoxyphenol inhibitor in both monomers removed prior to photopolymerization using an inhibitor removal column (Sigma-Aldrich, product number 306312). Photoinitiator Irgacure 184 was purchased from BASF Canada Inc. Hydrochloric acid (1 M, 0.1 M) and sodium hydroxide (1 M, 0.1 M) were received from LabChem Inc. (Pittsburgh, PA). Dulbecco's modified Eagle's medium (DMEM), fetal bovine serum (FBS), and penicillin−streptomycin solution (10 000 units penicillin; 10 000 μg streptomycin) were obtained from Gibco (Gaithersburg, MD). MTT ([3-4,5-dimethylthiazol-2-yl]-2,5-diphenyl-tetrazolium bromide) was obtained from Sigma-Aldrich. For all experiments, Milli-Q grade distilled deionized water (DIW) was used. Phosphate buffered saline (PBS) was diluted from a 10× liquid concentrate (Bioshop Canada Inc.).

2.2. pHEMA Hydrogel Synthesis. To prepare a pHEMA hydrogel mimicking a contact lens, 3 g of HEMA, 90 mg of EDGMA, and 7 mg of Irgacure 184 were first mixed and shaken for 5 min until the initiator was completely dissolved. The mixture was then transferred to a custom-made poly(methyl methacrylate) mold (dimensions 70 mm × 70 mm × 1 mm) and placed in a chamber equipped with a 400 W UV lamp (Cure Zone 2 CON-TROL-CURE, Chicago, IL) for 15 min. Before detaching from the mold, the cured HEMA plate was left at room temperature for 24 h to facilitate postcuring. After three cycles of extraction of this gel in Milli-Q water to remove unreacted monomer/cross-linker and initiator residues, the purified gel was immersed in Milli-Q water for 24 h to achieve an equilibrium swelling state prior to surface modification.

2.3. Laccase-Mediated TEMPO Oxidation of pHEMA Hydrogel (Ox-pHEMA). A combination of TEMPO, laccase, and oxygen was used to oxidize the pHEMA hydrogel, based on a previously reported method for cellulose oxidation.[53] In a typical experiment, 50 mg of TEMPO was dissolved in 200 mL of sodium acetate aqueous buffer (50 mM, pH 5.0), and one piece of pHEMA hydrogel (10 cm × 10 cm × ∼1 mm) was immersed in the solution for 30 min. Following, 50 mg of laccase was dissolved in the same sodium acetate buffer and added to the TEMPO/pHEMA mixture to create a 250 mL solution consisting of 250 mg/L TEMPO and 250 mg/L laccase. The oxidation solution was stirred under oxygen purging (1 bubble/s) for 24 h at room temperature. A polytetrafluoroethene (PTFE) grid was used to support the hydrogel and avoid direct contact between the magnetic stir bar and the hydrogel. After the oxidation procedure was complete, the oxidized pHEMA hydrogel was rinsed in the same sodium acetate buffer (3 × 5 min cycles) and then immersed in water for 8 h to remove the TEMPO and laccase.

The aldehyde content on the TEMPO-oxidized pHEMA hydrogel was assessed by both the silver mirror reaction and fluorescent labeling. For the silver mirror assay, Tollens' reaction was performed, exploiting the aldehyde-specific reduction of ammonia silver nitrate (a reaction that cannot be performed by either carboxylic acids or primary alcohols[54]). Tollens' reagent was first prepared from silver nitrate solution ($AgNO_3$, 0.02 M) and ammonia hydroxide (2.5 wt %),[55] after which one piece of unmodified pHEMA and one piece of TEMPO-oxidized pHEMA (1 cm × 2 cm × ∼1 mm) were immersed in ∼30 mL of the Tollens' reagent solution and warmed in a 50 °C water bath. After 3 min, the two samples were removed from the solution and rinsed three times with 50 mL of Milli-Q water. The relative aldehyde content was estimated based on visual observation of the silver mirror effect. For the fluorescent labeling technique, pHEMA hydrogels (1 cm × 2 cm × ∼1 mm) were immersed in a 0.05 g/L solution of fluorescein-5-thiosemicarbazide (5-FTSC) in carbonate buffer (pH = 9.0, 0.106 g of Na_2CO_3 and 0.966 g of $NaHCO_3$ in 500 mL of water) for 4 h. The hydrogels were then rinsed with 2 mL of buffer (15 × 5 min cycles) to remove nonreacted fluorescein probe, leaving only FTSC covalently bound to aldehyde groups in the pHEMA gel. Aldehyde content was then visualized with the BioRad ChemiDoc imaging system, using an excitation wavelength of 488 nm.

2.4. Hydrazide-Functionalized Hyaluronic Acid (HA-Hzd) Synthesis and Characterization. HA-Hzd was prepared according to a protocol reported by Luo et al.[47] Briefly, 60 mg of sodium hyaluronate was dissolved at a concentration of 5 mg/mL in DIW. Solid ADH (1.1 g) was first dissolved in 12 mL of water and then added into the HA solution following syringe filtration (5 μm pore size), followed by magnetic stirring for 30 min. The pH of the reaction mixture was adjusted to 4.75 by adding HCl, after which 0.1 g of EDC was dissolved in 1 mL of water and added dropwise. The pH of the reaction mixture was maintained at 4.75−4.80 by adding 0.1 M HCl over the full 4 h reaction time, after which the reaction was stopped by adding NaOH to raise the pH to 7.0. The reaction mixture was poured into a prewashed dialysis membrane tube (MWCO = 14 kDa) and dialyzed first against a large excess of 100 mM NaCl aqueous solution (3 cycles × 24 h) followed by a 1:3 (v/v) ethanol:water solution (1 cycles × 24 h) and then DIW (3 cycles × 24 h). The final solution was filtered through a 5 μm pore size syringe filter and then lyophilized to dryness. ^{1}H NMR was performed on a Bruker AVANCE 600 MHz spectrometer using D_2O (D, 99.96%, Cambridge Isotope Laboratories, Inc.) as the solvent. Results indicate that ∼53% of carboxyl groups on HA were successfully converted to hydrazide groups (Supporting Information, Figure S2). The degree of hydrazide group conversion was also confirmed by base-into-acid conductometric and potentiometric titration of both HA and HA-Hzd samples (Figure S3), with −COOH functionalization reduced from 2.23 ± 0.13 mM/g in HA to 1.07 ± 0.15 mM/g in HA-Hzd (52% substitution). Furthermore, FTIR spectroscopy using a KBr pellet technique (Nexus 6700 Fourier-transform infrared (FTIR) spectrometer, Thermo Fisher Scientific) indicated a slight shift of the peak around 1630 cm^{-1} (Figure S4), which could be attributed to the formation of a new amide bond between ADH and HA.

DOI: 10.1021/acsami.6b07433
ACS Appl. Mater. Interfaces XXXX, XXX, XXX−XXX

2.5. HA-Hzd Coating of Oxidized pHEMA Hydrogel (HA-pHEMA). HA-Hzd was dissolved overnight at 2 mg/mL in DIW under gentle shaking. The pHEMA hydrogel was cut or punched into the required shape, with most samples punched into disks with a diameter of 0.65 cm (1/4 in.) and thickness of ∼1 mm unless otherwise specified. For coating, the gel disk was then immersed into 25 mL of HA-Hzd solution. The reaction between aldehyde groups in the hydrogel and hydrazide groups in HA-Hzd was allowed to proceed at room temperatures for 8 h, after which the hydrogel was rinsed with DIW (3 × 5 min cycles). The resulting HA-grafted hydrogel was compared to a noncoated pHEMA hydrogel before and after oxidation using infrared spectroscopy (Nexus 6700 Fourier-transform infrared (FTIR) spectrometer with an attenuated total reflection (ATR) attachment, Thermo Fisher Scientific) and X-ray photoelectron spectroscopy (PHI Quantera II XPS scanning microprobe, Physical Electronics (Phi), Chanhassen, MN, 1486.7 eV monochromatic Al Kα X-ray source, beam diameter 200 μm, 280 eV pass energy) to confirm surface functionalization.

2.6. Fluorescent Visualization of HA Coating on HA-pHEMA Hydrogel. To confirm the successful surface modification, the coating procedure outlined in section 2.5 was repeated by substituting HA-Hzd with FITC-labeled HA-Hzd. HA-Hzd was prepared by reacting a small fraction (1.1 mol %) of Hzd groups in HA-Hzd with fluorescein isothiocyanate (FITC). Typically, 50 mg of HA-Hzd was reacted with 0.25 mg of FITC (1.1 mol % equivalent of the Hzd groups) overnight (at least 12 h) under gentile mechanical agitation in carbonate buffer at pH 9 and room temperature. The resulting labeled polymers were dialyzed exhaustively against deionized water (MWCO = 14 kDa, 6 × 6 h cycles) to remove unbound FITC, lyophilized to dryness, dissolved in water to form a 2 mg/mL solution, and stored at 4 °C in the dark. All reactions and purification steps were performed in aluminum foil-covered reaction flasks or containers to prevent photobleaching during synthesis. Following surface modification of the pHEMA hydrogel with FITC-HA-Hzd as per the protocol in section 2.5, the dried sample was cut in cross section and exposed to blue (488 nm) light using a Zeiss 510 inverted confocal microscope to collect fluorescence images and define the localization of FITC-labeled HA-Hzd throughout the hydrogel.

2.7. Contact Angle. To assess changes in the wettability of the contact lens mimic throughout the HA tethering process, water contact angle measurements were conducted using a Model 100-00-115 NRL contact angle goniometer (Ramé-Hart, Succasunna, NJ) equipped with a Sanyo VC8-3512T camera. Contact angles were measured by applying 25 μL droplets of DIW on the surface of the original and modified pHEMA hydrogel samples at 23 °C after gently wicking off the excess (i.e., nonbound/absorbed) water using a KimWipe. All the hydrogel samples were kept in OPTI-FREE Replenish contact lens solution for 14 days, changing the solution fresh every second day. Contact angles were tested following 1, 4, 7, and 14 days of soaking.

2.8. Dehydration Kinetics. Dried pHEMA samples were preweighed and then swollen in Milli-Q water for 24 h, a time point confirmed to reach the swelling equilibrium of the hydrogels in water. Following, the sample was removed from the water, wicked with a KimWipe to remove unbound water from the hydrogel surface, and weighed again to allow for calculation of the equilibrium water content. The samples were then incubated vertically on a holder in a constant temperature and humidity chamber to allow for evaporation from both sides (Platinous Sterling Series, ESL-2CA, ESPEC North America, 50% RH at 23 °C) and weighed again at time intervals of 0, 5, 10, 15, 20, 30, 60, 90, and 120 min to track the rate of evaporation as a function of pHEMA surface treatment.

2.9. Refractive Index and Light Transmittance Measurements. A digital hand-held pocket refractometer (Atago, Bellevue, WA) was used to measure the refractive index of the pHEMA hydrogel disks, with all measurements done in triplicate. The optical properties of the material were determined by measuring transmittance between 380 and 750 nm using a Beckman Coulter DU800 spectrophotometer (scan rate = 0.5 nm/s).

2.10. Mechanical Properties. The hardness and mechanical strength of samples before and after surface modification were measured to assess the effects of oxidation and HA coating on the hydrogel mechanics. Prior to the test, freshly prepared pHEMA hydrogel samples were soaked in Milli-Q water for 24 h. Shore A (MFG. Co. Inc., U.S. Patent 2453042) and Shore OO (Rex Gauge Company, Inc. U.S. Patent 2421449) durometers were used to characterize the hardness of pHEMA before and after oxidation and HA modification. The elastic modulus and elongation-at-break were characterized using a Universal Test System (INSTRON 3366, 50 N load cell) on dumbbell pHEMA samples (ASTM 638-14/95 Type V) mounted to the tester using grips and subsequently stretched at a crosshead speed of 20 mm/min. The thickness and width of the pHEMA specimens under tension (measured at the center of the dumbbell at three random positions) were analyzed using an electronic digital micrometer (Mitutoyo, Japan; 0.001 mm sensitivity).

2.11. Cell Culture and Viability Test. Cell toxicity was assessed with NIH 3T3 mouse fibroblasts. Cells were cultured in Dulbecco's Modified Eagle's Medium (DMEM) supplemented with 10% (v/v) heat-inactivated FBS and 1% (v/v) penicillin−streptomycin at 37 °C under a humidified atmosphere of 5% CO_2. For the cell toxicity assay, 5×10^4 cells/well were seeded in 24-well plates overnight, after which the cell medium was replaced by 500 μL of fresh culture medium. Disk samples of pHEMA, Ox-pHEMA, and HA-pHEMA were sterilized by immersing in ethanol solution (70% v/v) for 4 h and subsequently rinsed three times with sterile PBS prior to being inserted into the wells using tweezers. After 24 h of incubation, media was removed, 20 μL of the MTT solution (5.0 mg/mL in fresh culture medium) was added to each well, plates were wrapped with aluminum foil, and the plates were incubated for ∼4 h at 37 °C. Following, the culture medium was removed, and the resulting formazan crystals were dissolved in solubilization solution (40.0% (v/v) DMF, 16.0% (w/v) SDS, pH ∼ 4.7). The absorbance of the solubilized formazan was measured at 570 nm using a Tecan infinite-200M Pro colorimeter (Tecan Co, Switzerland). Cell viability relative to a cell-only control and a well containing only cell media was calculated via the equation

$$\text{viability (\%)} = \frac{A_{\text{sample}} - A_{\text{blank}}}{A_{\text{control}} - A_{\text{blank}}} \times 100$$

Six replicates were performed per sample, with the mean ± standard deviation reported for each.

2.12. Protein Adsorption. Proteins (human serum albumin and lysozyme from chicken egg white) were radiolabeled with $Na^{125}I$ using the iodine monochloride method (ICl).[56] Following, unbound ^{125}I was removed by passing the radiolabeled samples through two 3 mL syringes packed with AG 1-X4 resin (100−200 dry mesh in chloride form, Bio-Rad, Hercules, CA). Free iodide was measured by trichloroacetic acid precipitation of the protein. The free iodide in both radiolabeled HSA and lysozyme solutions was, in all cases, less than 1% of total radioactivity. To perform protein adsorption assays, pHEMA hydrogel disks were equilibrated in PBS for 24 h, blotted using a KimWipe to remove nonbound water, and subsequently placed in 96-well plates. HSA or lysozyme solution (1 mg/mL, contained 10% (w/w) radiolabeled protein, 250 mL) was added to the wells (n = 4), and the samples were incubated for 4 h at room temperature (23 °C). The samples were subsequently rinsed with fresh PBS buffer (3 × 5 min cycles) to remove any loosely bound protein. The surfaces were subsequently counted for radioactivity using a Wizard 3 1480 Automatic Gamma Counter (PerkinElmer), and the adsorbed amounts were calculated using background-corrected surface counts relative to the solution count for the individual protein solution.

RESULTS AND DISCUSSION

3.1. Oxidation of pHEMA Hydrogel. The oxidation of primary alcohols with laccase/TEMPO is generally reported to result in the generation of both aldehyde groups and some fraction of carboxyl groups.[52] Therefore, to first confirm the targeted conversion of alcohol to aldehyde, three methods were

DOI: 10.1021/acsami.6b07433
ACS Appl. Mater. Interfaces XXXX, XXX, XXX−XXX

applied to provide semiquantitative assessments of the aldehyde content. First, the silver mirror reaction is a classical method for identifying aldehyde groups,[57] tracking the reduction (precipitation) of $AgNO_3$ solution to silver nanoparticles by aldehydes to create a black or reflective film on the underlying substrate.[55] Figure 1A shows this characteristic dark black color on Ox-pHEMA, indicating the presence of aldehyde groups; in contrast, almost no color was observed on the native pHEMA hydrogel, indicating the presence of few if any aldehyde groups prior to oxidation. Second, the pHEMA hydrogels were reacted with 5-FTSC, an aldehyde-reactive fluorescent dye previously used to visualize the product of laccase/TEMPO oxidation of cellulose.[58] Figure 1B shows much stronger fluorescence on the Ox-pHEMA hydrogel compared to the native pHEMA hydrogel, again confirming the generation of aldehyde groups via the laccase/TEMPO reaction. Note that the native pHEMA samples still have some mild background emission, which could be attributed to physically adsorbed fluorescent dye. Third, the content of the aldehydes in Ox-pHEMA was determined by hydroxylamine hydrochloride titration (see Supporting Information, Figure S5).[59] The titration result yields an aldehyde content of 26.7 ± 3.3 μM aldehydes/g of Ox-pHEMA sample, comparable to the aldehyde content in TEMPO-oxidized native cellulose fibers (mechanically fibrillated pulp) reported in previous research.[60]

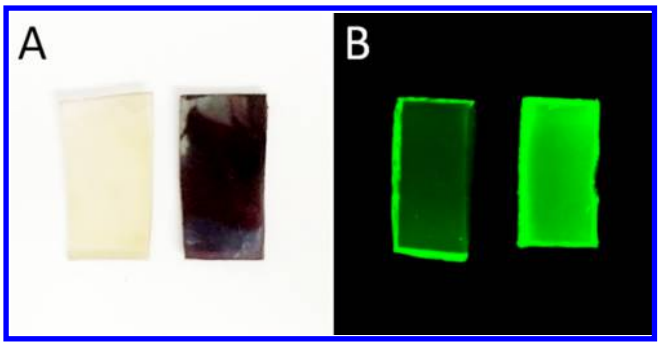

Figure 1. Visualizing the presence of aldehyde group on Ox-pHEMA by (A) silver mirror reaction on native pHEMA (left) and Ox-pHEMA (right); (B) fluorescein-5-thiosemicarbazide (5-FTSC) labeling on native pHEMA (left) and Ox-pHEMA (right).

The ATR-FTIR spectra of pHEMA and Ox-pHEMA (Figure 2A,B) further confirm oxidation based on the significant increase in intensity observed for the C═O carbonyl stretch at 1631 cm^{-1}, an observation consistent with previous TEMPO oxidation data.[61] While this peak may overlap with the ester signal, the appearance of additional peaks at 2750 cm^{-1} (Figure 2B,D) is consistent with the C−H stretch of aldehydes and offers further evidence of successful oxidation.[62,63] In addition, the change in the shape of the C−O−C peak at 1050−1200 cm^{-1} may suggest the formation of covalent bonds through hemiacetal and/or acetal linkages between aldehyde groups formed by the laccase/TEMPO oxidation and the hydroxyl groups in pHEMA;[60] while this reaction is not necessarily desirable in the context of contact lens modification, its occurrence would confirm the generation of aldehyde groups on Ox-pHEMA. Note that both spectra have a strong peak centered at 1705−1715 cm^{-1} primarily attributable to the ester group in HEMA;[64] the aldehyde group generated by oxidation is likely obscured by overlap with the ester signal. XPS (Figure 3), while unable to distinguish oxidation of C−OH to HC═O in terms of atom percent, does indicate no presence of nitrogen in the oxidized pHEMA sample (Figure 3), suggesting that all free TEMPO and laccase have been successfully removed by the washing steps.

3.2. Surface Conjugation of HA-Hzd to Ox-pHEMA Hydrogel. HA-coated pHEMA was prepared by simple immersion of the Ox-pHEMA hydrogel into a 2 mg/mL HA-Hzd solution. An amide band I peak at 1635 cm^{-1} is present in the ATR-FTIR spectra of HA-modified pHEMA sample (Figure 2), consistent with the spectrum of HA-Hzd prior to conjugation (Figure S4); however the overlap of this peak with the C═O stretching peak of the carboxyl group in Ox-pHEMA makes this result of limited utility for analysis. However, XPS shows an ∼1 atom % nitrogen content only after HA conjugation (Figure 3), suggesting the HA conjugation on Ox-pHEMA gel; furthermore, when FITC-labeled HA-Hzd is instead used for surface functionalization, confocal microscopy indicates that all bound HA-Hzd is localized at the surface of

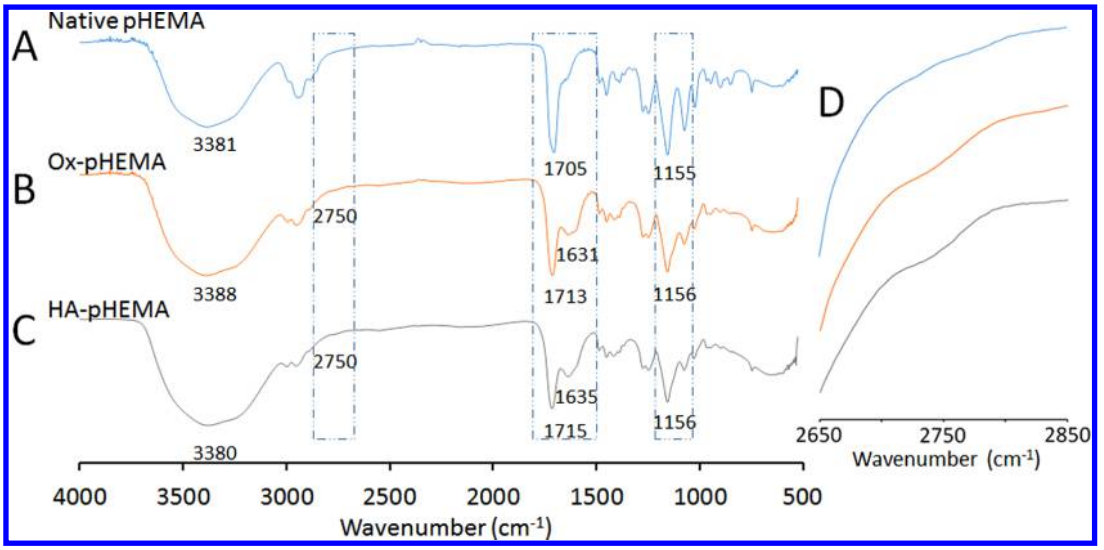

Figure 2. Attenuated total reflection (ATR)-FTIR spectra of (A) native pHEMA, (B) Ox-pHEMA, (C) HA-pHEMA, and (D) zoom of 2650−2850 cm^{-1} region showing evidence for aldehyde functionalization; key peaks discussed in the text are labeled by wavenumber.

DOI: 10.1021/acsami.6b07433
ACS Appl. Mater. Interfaces XXXX, XXX, XXX−XXX

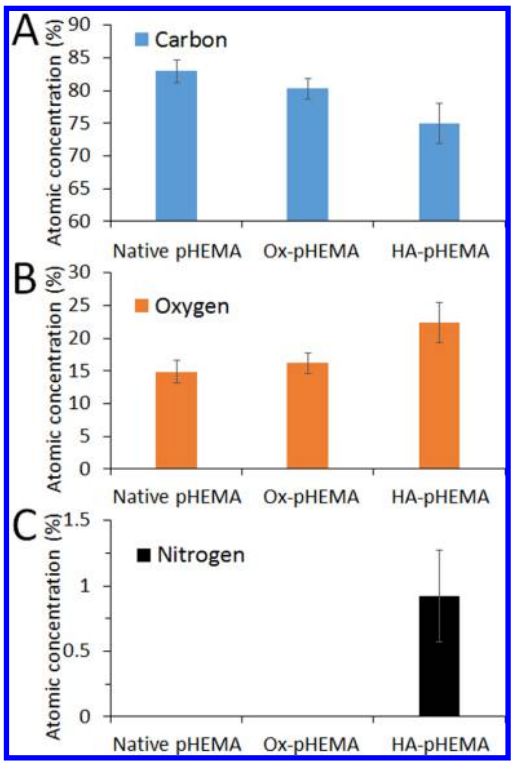

Figure 3. Elemental concentrations of native pHEMA, Ox-pHEMA, and HA-pHEMA from XPS analysis: (A) carbon; (B) oxygen; (C) nitrogen.

the model lens, with a continuous coating of FITC-HA-Hzd observed at both interfaces of the lens and no significant amount of HA detected in the bulk (Figure 4). We further confirmed that unfunctionalized HA could exhibits only weak physically adsorbance on either native pHEMA or Ox-pHEMA (Supporting Information, Figure S6), indicating that the chemical bond forming between aldehyde groups on Ox-pHEMA and hydrazide groups on HA-Hzd is primarily driving

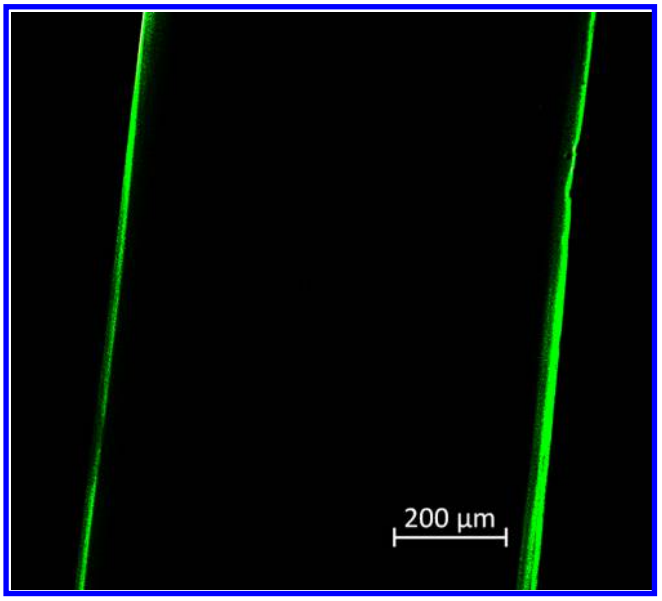

Figure 4. Cross section of pHEMA hydrogel coated with fluorescently labeled HA-Hzd as viewed by confocal laser scanning microscopy (CLSM).

the tethering of HA on the surface. Thus, by simple dipping of the Ox-pHEMA hydrogel into a HA-Hzd solution, effective surface functionalization of the lens can be achieved. Note that the molecular weight of HA was >300 kDa, making it unlikely that HA will penetrate into the bulk hydrogel (consistent with this result).

3.3. Optical and Mechanical Properties of Modified pHEMA Hydrogels. Optical properties including refractive index and transparency are critical for materials to be used as contact lenses. The refractive indices of Ox-pHEMA and HA-pHEMA are not significantly different than that of native pHEMA (p > 0.1 in both pairwise comparisons), with all samples yielding refractive index values between 1.332 and 1.334 that closely approximate the refractive index of human tears[65] (Figure 5A). Furthermore, UV−vis spectrophotometry

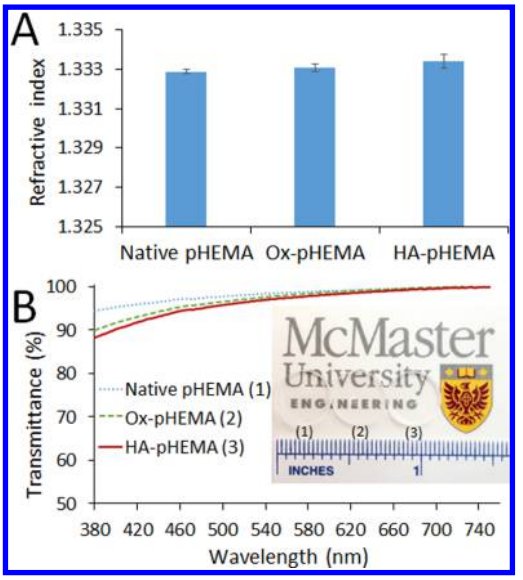

Figure 5. Optical properties of modified pHEMA hydrogels: (A) refractive index; (B) visible light transmittance and (B, inset) visual confirmation of the functional transparency (thickness = ∼1 mm) of native pHEMA, Ox-pHEMA, and HA-pHEMA hydrogels.

indicated that while a slight reduction in transparency was observed for Ox-pHEMA and HA-pHEMA hydrogels relative to native pHEMA, even the modified materials still transmitted more light (>88% transmittance over the full visible range) than the normal adult lens and appeared transparent to visual inspection (Figure 5B).[66] Both these results suggest the potential suitability of these materials for contact lens. From a chemical perspective, the lack of opacity or domain formation indicated by these results suggests that the modifications neither significantly change the bulk material morphology nor lead to the creation of phase-separated domains within the gels, supporting a surface grafting mechanism of modification.

The mechanics of the pHEMA hydrogel are also largely unaffected by the oxidation and HA tethering, with the compressive modulus, shear modulus, and tensile modulus all showing no significant increase after modification (p > 0.05 in all pairwise comparisons) and the softness (hardness) remaining in the same ranges (Table 1). However, the elasticity of the hydrogel (break elongation) did exhibit a significant decrease following laccase/TEMPO oxidation (p = 0.004 relative to native pHEMA). We attribute this result to a degree of depolymerization occurring during oxidation, caused by the

DOI: 10.1021/acsami.6b07433
ACS Appl. Mater. Interfaces XXXX, XXX, XXX−XXX

Table 1. Mechanical Properties of Native pHEMA, Ox-pHEMA, and HA-pHEMA[a]

	hardness		MicroSquisher		tensile test	
	shore A	shore OO	compression modulus (MPa)	shear modulus (MPa)	tensile modulus (MPa)	break elongation (%)
native pHEMA	55−60	85−90	1.76 ± 0.17	0.59 ± 0.06	11.2 ± 2.8	33.6 ± 5.3
Ox- pHEMA	55−60	85−90	2.15 ± 0.82	0.72 ± 0.27	12.2 ± 4.0	15.3 ± 4.5[a]
HA-pHEMA	45−50	85−90	2.65 ± 0.80	0.88 ± 0.26	14.2 ± 4.4	15.7 ± 4.6[a]

[a] $p \ll 0.01$, compared to native pHEMA gel.

in situ generation of active species such as hydroxyl radicals in side reactions of the hydroxylamine structure with oxygen during the oxidative treatment.[67] However, this degree of elongation is still similar to those of HEMA/MAA materials most commonly used in daily contact lens applications[68] and thus is not anticipated to be problematic in a practical application.

3.4. Surface Hydrophilicity and Water Retention. HA modification of pHEMA significantly improved both the surface hydrophilicity and the water retention of the model lens (Figure 6). Relative to unmodified pHEMA (water contact angle 69.7 ± 1.5°), oxidation reduced the contact angle to 41.5 ± 0.9° while subsequent HA grafting further reduced the contact angle to 35.0 ± 1.0° (Figure 6A). Of note, while the contact angle of unmodified pHEMA decreased from 69.7 ± 1.5° to 52.5 ± 0.3° over 14 days of storage in a contact lens care solution (likely attributable to the physical absorption of organic acids in the care solutions to surface hydroxyl groups), there was no significant change in the contact angles of Ox-pHEMA over this two week period in the same care solution ($p > 0.05$), while for HA-pHEMA, the contact angles show a small but significant decrease after 7 days of storage in the care solution to 31.3 ± 1.2° on day 7 and 31.6 ± 1.9° on day 14 (both $p < 0.05$ relative to the initial gel). Fundamentally, this result suggests the oxidized and HA-grafted interfaces have lower nonspecific adsorption and can maintain a higher degree of hydration at the surface. Practically, the more stable contact angles observed following soaking of the Ox-pHEMA and HA-pHEMA model lenses indicate that the products of the laccase/TEMPO oxidation and the HA coating step both remain intact and functional following 2 weeks of soaking in the care solution, suggesting the potential suitability of these materials as biweekly deposable lenses and/or for extended storage. This higher interfacial hydrophilicity in HA-pHEMA also acts to retard the evaporation of water from pHEMA hydrogels (50% RH in air, 23 °C), with HA-pHEMA in particular exhibiting a significantly lower rate of water evaporation relative to unmodified and base pHEMA hydrogels (Figure 6B). These observations, both strongly contributing to the comfort of the lens for the wearer, are all consistent with previous surface modifications of contact lenses with HA.[24]

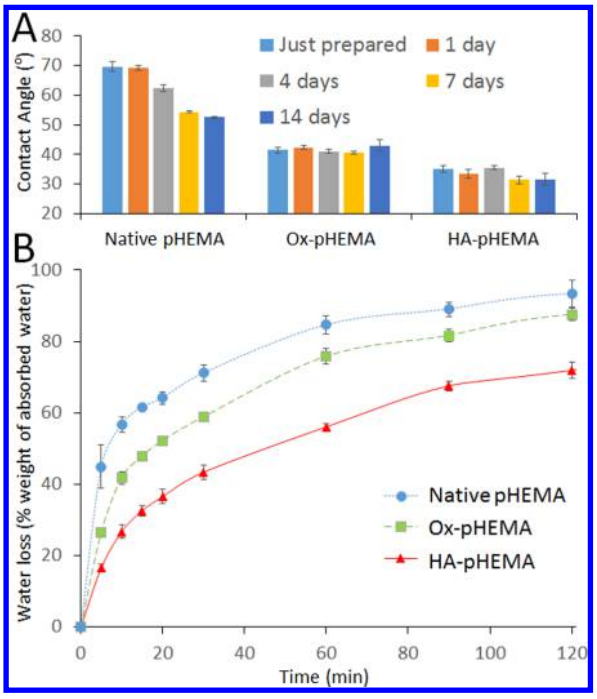

Figure 6. Hydrophilicity of pHEMA as a function of surface treatment: (A) water contact angle of native pHEMA, Ox-pHEMA, and HA-pHEMA; (B) water loss from native pHEMA relative to oxidized and HA-grafted pHEMA in a controlled temperature/humidity chamber (50% RH, 23 °C).

3.5. Cell Compatibility and Protein Adsorption. No significant cytotoxicity was observed for 3T3 fibroblasts (used as corneal feeder cells when cultured on contact lenses[69]) after 24 h of culturing in the presence of Ox-pHEMA and HA-pHEMA hydrogels (Figure 7). This result confirms the effective removal of free TEMPO and laccase via the rinsing process used and, in the case of HA-pHEMA, is consistent with the noted compatibility of HA in culturing ocular cells.[30] Furthermore, protein adsorption to HA-pHEMA lenses (key to reducing fouling and optimizing wear times) was reduced by ~25% for HSA and ~35% for lysozyme compared to the native pHEMA hydrogel following 4 h of adsorption time (Figure 8). We have further tested HSA adsorption over both 12 and 24 h periods using fluorescently labeled protein to assess the potential longer term impact of any residual aldehydes in the Ox-pHEMA gel on protein adsorption (Supporting Information, Figure S7). While protein adsorption increases with time for both native pHEMA and oxidized pHEMA (the latter of which presents aldehyde groups directly at the interface), HA-pHEMA shows no significant change in protein adsorption (p =

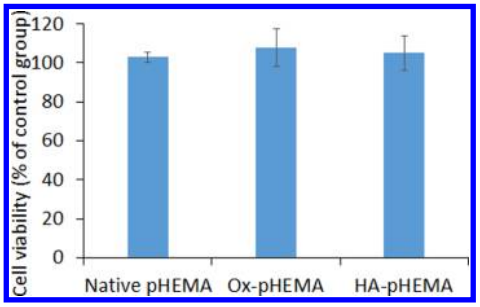

Figure 7. Cell viability (relative to cell-only control) of 3T3 fibroblasts in the presence of native pHEMA, Ox-pHEMA, and HA-pHEMA hydrogel disks via the MTT assay.

DOI: 10.1021/acsami.6b07433
ACS Appl. Mater. Interfaces XXXX, XXX, XXX−XXX

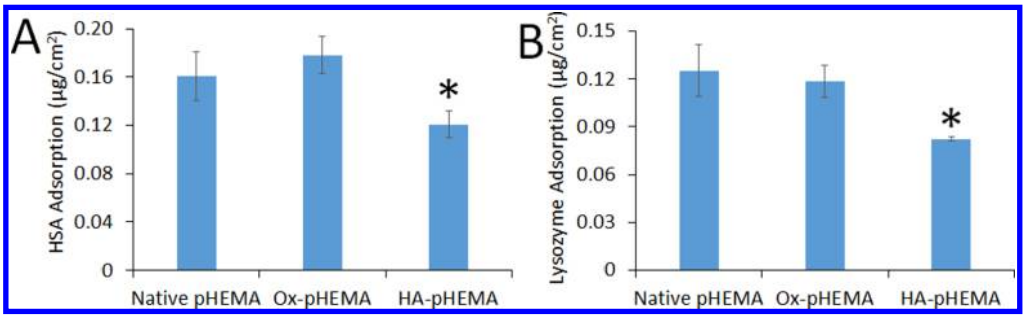

Figure 8. Protein adsorption on the surface of native pHEMA, Ox-pHEMA, and HA-pHEMA in 4 h at 23 °C: (A) human serum albumin (HSA, 1.0 mg/mL); (B) lysozyme (1.0 mg/mL). *p < 0.01, compared to the native pHEMA group.

0.08) as a function of time, maintaining its low HSA adsorption over even the longer test periods. This result suggests that HA effectively screens any residual aldehyde groups on Ox-pHEMA to avoid any potential issues with imine-promoted protein deposition over time and is consistent with previous research indicating that HA modification reduces protein adsorption on various types of biomaterials.[22,23,25−27] Thus, HA modification of the model lens surface through our click chemistry technique significantly reduces protein adsorption while increasing wetting without inducing any significant cytotoxicity, suggesting the potential translatability of this coating to practical applications.

4. CONCLUSIONS

In this study, we demonstrate a facile click chemistry-based strategy for covalently tethering an HA layer on the surface of pHEMA hydrogel that mimics a daily wear contact lens. Only two steps are required in our coating method: laccase/TEMPO oxidation and subsequent dipping in a hydrazide-functionalized HA solution. The resulting modified surfaces exhibit significantly improved wettability and water retention and reduced protein adsorption while largely maintaining the favorable transparency, refractive, mechanical, and storage stability properties of pHEMA. Given the capacity for efficient surface modification provided by this simple dipping or coating process, we anticipate that our method has potential for translation to industrial contact lens manufacturing.

■ ASSOCIATED CONTENT

Supporting Information

The Supporting Information is available free of charge on the ACS Publications website at DOI: 10.1021/acsami.6b07433.

GPC curve of HA, ^{1}H NMR and FTIR spectra of HA and HA-Hzd, titration curves of HA and HA-Hzd, hydroxylamine hydrochloride titration of native pHEMA and Ox-pHEMA, adsorption of fluorescently labeled HA/HA-Hzd on native pHEMA and Ox-pHEMA, and adsorption of fluorescently labeled HSA on native pHEMA, Ox-pHEMA, and HA-pHEMA (PDF)

■ AUTHOR INFORMATION

Corresponding Authors

*E-mail filipec@mcmaster.ca (C.D.M.F.).
*E-mail hoaretr@mcmaster.ca (T.H.).

Notes

The authors declare no competing financial interest.

■ ACKNOWLEDGMENTS

The authors thank Ms. Fei Xu and Ms. Maryam Badv for their generous help with the mechanical and NMR tests. The authors thank the Natural Sciences and Engineering Research Council of Canada (CREATE Biointerfaces Training Program-10532261, and Discovery Grants RGPIN-356609-12 and RGPIN-261686-13), the Sentinel Bioactive Paper Network (NSERC NETGP 398408), the Canada Foundation for Innovation (Leaders Opportunity Fund Grant # 29131), and the Ontario Innovation Trust for financial support.

■ REFERENCES

(1) Wichterle, O.; Lim, D. Hydrophilic Gels for Biological Use. *Nature* **1960**, *185*, 117−118.
(2) Lai, Y. C.; Friends, G. D. Surface Wettability Enhancement of Silicone Hydrogel Lenses by Processing with Polar Plastic Molds. *J. Biomed. Mater. Res.* **1997**, *35*, 349−356.
(3) López-Alemany, A.; Compañ, V.; Refojo, M. F. Porous Structure of Purevision Versus Focus® Night&Day and Conventional Hydrogel Contact Lenses. *J. Biomed. Mater. Res.* **2002**, *63*, 319−325.
(4) Nicolson, P. C.; Vogt, J. Soft Contact Lens Polymers: An Evolution. *Biomaterials* **2001**, *22*, 3273−3283.
(5) Pritchard, N.; Fonn, D. Dehydration, Lens Movement and Dryness Ratings of Hydrogel Contact Lenses. *Ophthal. Physiol. Opt.* **1995**, *15*, 281−286.
(6) Brennan, N. A.; Efron, N. Symptomatology of Hema Contact Lens Wear. *Optom. Vision Sci.* **1989**, *66*, 834−838.
(7) Luensmann, D.; Jones, L. Albumin Adsorption to Contact Lens Materials: A Review. *Cont. Lens. Anterior. Eye* **2008**, *31*, 179−187.
(8) Luensmann, D.; Jones, L. Protein Deposition on Contact Lenses: The Past, the Present, and the Future. *Cont. Lens. Anterior. Eye* **2012**, *35*, 53−64.
(9) Lord, M. S.; Stenzel, M. H.; Simmons, A.; Milthorpe, B. K. The Effect of Charged Groups on Protein Interactions with Poly (Hema) Hydrogels. *Biomaterials* **2006**, *27*, 567−575.
(10) Taylor, R. L.; Willcox, M. D.; Williams, T. J.; Verran, J. Modulation of Bacterial Adhesion to Hydrogel Contact Lenses by Albumin. *Optom. Vis. Sci.* **1998**, *75*, 23−29.
(11) Miller, M. J.; Wilson, L. A.; Ahearn, D. G. Effects of Protein, Mucin, and Human Tears on Adherence of Pseudomonas Aeruginosa to Hydrophilic Contact Lenses. *J. Clin. Microbiol.* **1988**, *26*, 513−517.
(12) Tan, M. E.; Demirci, G.; Pearce, D.; Jalbert, I.; Sankaridurg, P.; Willcox, M. D. Contact Lens-Induced Papillary Conjunctivitis Is Associated with Increased Albumin Deposits on Extended Wear Hydrogel Lenses. In *Lacrimal Gland, Tear Film, and Dry Eye Syndromes 3*; Springer: 2002; pp 951−955.
(13) Fonn, D. Targeting Contact Lens Induced Dryness and Discomfort: What Properties Will Make Lenses More Comfortable. *Optom. Vis. Sci.* **2007**, *84*, 279−285.
(14) Papas, E. B.; Ciolino, J. B.; Jacobs, D.; Miller, W. L.; Pult, H.; Sahin, A.; Srinivasan, S.; Tauber, J.; Wolffsohn, J. S.; Nelson, J. D. The Tfos International Workshop on Contact Lens Discomfort: Report of

DOI: 10.1021/acsami.6b07433
ACS Appl. Mater. Interfaces XXXX, XXX, XXX−XXX

the Management and Therapy Subcommitteemanagement and Treatment of Cld. *Invest. Ophthalmol. Visual Sci.* **2013**, *54*, TFOS183−TFOS203.
(15) Thissen, H.; Gengenbach, T.; du Toit, R.; Sweeney, D. F.; Kingshott, P.; Griesser, H. J.; Meagher, L. Clinical Observations of Biofouling on Peo Coated Silicone Hydrogel Contact Lenses. *Biomaterials* **2010**, *31*, 5510−5519.
(16) Goda, T.; Matsuno, R.; Konno, T.; Takai, M.; Ishihara, K. Protein Adsorption Resistance and Oxygen Permeability of Chemically Crosslinked Phospholipid Polymer Hydrogel for Ophthalmologic Biomaterials. *J. Biomed. Mater. Res., Part B* **2009**, *89*, 184−190.
(17) Shimizu, T.; Goda, T.; Minoura, N.; Takai, M.; Ishihara, K. Super-Hydrophilic Silicone Hydrogels with Interpenetrating Poly (2-Methacryloyloxyethyl Phosphorylcholine) Networks. *Biomaterials* **2010**, *31*, 3274−3280.
(18) Winterton, L. C.; Lally, J. M.; Sentell, K. B.; Chapoy, L. L. The Elution of Poly (Vinyl Alcohol) from a Contact Lens: The Realization of a Time Release Moisturizing Agent/Artificial Tear. *J. Biomed. Mater. Res., Part B* **2007**, *80*, 424−432.
(19) Peterson, R. C.; Wolffsohn, J. S.; Nick, J.; Winterton, L.; Lally, J. Clinical Performance of Daily Disposable Soft Contact Lenses Using Sustained Release Technology. *Cont. Lens. Anterior. Eye* **2006**, *29*, 127−134.
(20) Xu, L.; Ma, P.; Yuan, B.; Chen, Q.; Lin, S.; Chen, X.; Hua, Z.; Shen, J. Anti-Biofouling Contact Lenses Bearing Surface-Immobilized Layers of Zwitterionic Polymer by One-Step Modification. *RSC Adv.* **2014**, *4*, 15030−15035.
(21) Walker, J.; Young, G.; Hunt, C.; Henderson, T. Multi-Centre Evaluation of Two Daily Disposable Contact Lenses. *Cont. Lens. Anterior. Eye* **2007**, *30*, 125−133.
(22) Weeks, A.; Luensmann, D.; Boone, A.; Jones, L.; Sheardown, H. Hyaluronic Acid as an Internal Wetting Agent in Model Dmaa/Tris Contact Lenses. *J. Biomater. Appl.* **2012**, *27*, 423−432.
(23) Weeks, A.; Morrison, D.; Alauzun, J. G.; Brook, M. A.; Jones, L.; Sheardown, H. Photocrosslinkable Hyaluronic Acid as an Internal Wetting Agent in Model Conventional and Silicone Hydrogel Contact Lenses. *J. Biomed. Mater. Res., Part A* **2012**, *100*, 1972−1982.
(24) Singh, A.; Li, P.; Beachley, V.; McDonnell, P.; Elisseeff, J. H. A Hyaluronic Acid-Binding Contact Lens with Enhanced Water Retention. *Cont. Lens. Anterior. Eye* **2015**, *38*, 79−84.
(25) Van Beek, M.; Jones, L.; Sheardown, H. Hyaluronic Acid Containing Hydrogels for the Reduction of Protein Adsorption. *Biomaterials* **2008**, *29*, 780−789.
(26) Van Beek, M.; Weeks, A.; Jones, L.; Sheardown, H. Immobilized Hyaluronic Acid Containing Model Silicone Hydrogels Reduce Protein Adsorption. *J. Biomater. Sci., Polym. Ed.* **2008**, *19*, 1425−1436.
(27) Kim, H.-J.; Ryu, G.-C.; Jeong, K.-S.; Jun, J. Hydrogel Lenses Functionalized with Polysaccharide for Reduction of Protein Adsorption. *Macromol. Res.* **2015**, *23*, 74−78.
(28) Nishida, T.; Nakamura, M.; Mishima, H.; Otori, T. Hyaluronan Stimulates Corneal Epithelial Migration. *Exp. Eye Res.* **1991**, *53*, 753−758.
(29) Yokoi, N.; Komuro, A.; Nishida, K.; Kinoshita, S. Effectiveness of Hyaluronan on Corneal Epithelial Barrier Function in Dry Eye. *Br. J. Ophthalmol.* **1997**, *81*, 533−536.
(30) Pauloin, T.; Dutot, M.; Joly, F.; Warnet, J.-M.; Rat, P. High Molecular Weight Hyaluronan Decreases Uvb-Induced Apoptosis and Inflammation in Human Epithelial Corneal Cells. *Mol. Vis.* **2009**, *15*, 577−583.
(31) Presti, D.; Scott, J. E. Hyaluronan-Mediated Protective Effect against Cell Damage Caused by Enzymatically Produced Hydroxyl (Oh·) Radicals Is Dependent on Hyaluronan Molecular Mass. *Cell Biochem. Funct.* **1994**, *12*, 281−288.
(32) Aragona, P.; Papa, V.; Micali, A.; Santocono, M.; Milazzo, G. Long Term Treatment with Sodium Hyaluronate-Containing Artificial Tears Reduces Ocular Surface Damage in Patients with Dry Eye. *Br. J. Ophthalmol.* **2002**, *86*, 181−184.
(33) Weeks, A.; Boone, A.; Luensmann, D.; Jones, L.; Sheardown, H. The Effects of Hyaluronic Acid Incorporated as a Wetting Agent on Lysozyme Denaturation in Model Contact Lens Materials. *J. Biomater. Appl.* **2013**, *28*, 323−333.
(34) Korogiannaki, M.; Sheardown, H. Surface Modified Contact Lenses with a Wetting Agent for Improved Comfort. *Invest. Ophthalmol. Visual Sci.* **2014**, *55*, 4658−4658.
(35) Kolb, H. C.; Finn, M.; Sharpless, K. B. Click Chemistry: Diverse Chemical Function from a Few Good Reactions. *Angew. Chem., Int. Ed.* **2001**, *40*, 2004−2021.
(36) Smeets, N. M.; Bakaic, E.; Patenaude, M.; Hoare, T. Injectable and Tunable Poly (Ethylene Glycol) Analogue Hydrogels Based on Poly (Oligoethylene Glycol Methacrylate). *Chem. Commun.* **2014**, *50*, 3306−3309.
(37) Smeets, N. M.; Bakaic, E.; Patenaude, M.; Hoare, T. Injectable Poly (Oligoethylene Glycol Methacrylate)-Based Hydrogels with Tunable Phase Transition Behaviours: Physicochemical and Biological Responses. *Acta Biomater.* **2014**, *10*, 4143−4155.
(38) Patenaude, M.; Hoare, T. Injectable, Degradable Thermoresponsive Poly (N-Isopropylacrylamide) Hydrogels. *ACS Macro Lett.* **2012**, *1*, 409−413.
(39) Patenaude, M.; Hoare, T. Injectable, Mixed Natural-Synthetic Polymer Hydrogels with Modular Properties. *Biomacromolecules* **2012**, *13*, 369−378.
(40) Xu, F.; Sheardown, H.; Hoare, T. Reactive Electrospinning of Degradable Poly (Oligoethylene Glycol Methacrylate)-Based Nanofibrous Hydrogel Networks. *Chem. Commun.* **2016**, *52*, 1451−1454.
(41) Deng, X.; Smeets, N. M.; Sicard, C.; Wang, J.; Brennan, J. D.; Filipe, C. D.; Hoare, T. Poly (Oligoethylene Glycol Methacrylate) Dip-Coating: Turning Cellulose Paper into a Protein-Repellent Platform for Biosensors. *J. Am. Chem. Soc.* **2014**, *136*, 12852−12855.
(42) Pouyani, T.; Prestwich, G. D. Functionalized Derivatives of Hyaluronic Acid Oligosaccharides: Drug Carriers and Novel Biomaterials. *Bioconjugate Chem.* **1994**, *5*, 339−347.
(43) Pouyani, T.; Harbison, G. S.; Prestwich, G. D. Novel Hydrogels of Hyaluronic Acid: Synthesis, Surface Morphology, and Solid-State Nmr. *J. Am. Chem. Soc.* **1994**, *116*, 7515−7522.
(44) Bajaj, G.; Kim, M. R.; Mohammed, S. I.; Yeo, Y. Hyaluronic Acid-Based Hydrogel for Regional Delivery of Paclitaxel to Intraperitoneal Tumors. *J. Controlled Release* **2012**, *158*, 386−392.
(45) Oh, E. J.; Kang, S. W.; Kim, B. S.; Jiang, G.; Cho, I. H.; Hahn, S. K. Control of the Molecular Degradation of Hyaluronic Acid Hydrogels for Tissue Augmentation. *J. Biomed. Mater. Res., Part A* **2008**, *86*, 685−693.
(46) Prestwich, G. D.; Marecak, D. M.; Marecek, J. F.; Vercruysse, K. P.; Ziebell, M. R. Controlled Chemical Modification of Hyaluronic Acid: Synthesis, Applications, and Biodegradation of Hydrazide Derivatives. *J. Controlled Release* **1998**, *53*, 93−103.
(47) Luo, Y.; Kirker, K. R.; Prestwich, G. D. Cross-Linked Hyaluronic Acid Hydrogel Films: New Biomaterials for Drug Delivery. *J. Controlled Release* **2000**, *69*, 169−184.
(48) Noolandi, J.; Ta, C.; Huie, Jr., P.; Smith, A. J.; Waymouth, R.; Blumenkranz, M. Artificial Cornea. U.S. Patent No. 6976997B2, 2005.
(49) Bragd, P.; Van Bekkum, H.; Besemer, A. Tempo-Mediated Oxidation of Polysaccharides: Survey of Methods and Applications. *Top. Catal.* **2004**, *27*, 49−66.
(50) Kitaoka, T.; Isogai, A.; Onabe, F. Chemical Modification of Pulp Fibers by Tempo-Mediated Oxidation. *Nord. Pulp Pap. Res. J.* **1999**, *14*, 279−284.
(51) Fabbrini, M.; Galli, C.; Gentili, P.; Macchitella, D. An Oxidation of Alcohols by Oxygen with the Enzyme Laccase and Mediation by Tempo. *Tetrahedron Lett.* **2001**, *42*, 7551−7553.
(52) Aracri, E.; Valls, C.; Vidal, T. Paper Strength Improvement by Oxidative Modification of Sisal Cellulose Fibers with Laccase−Tempo System: Influence of the Process Variables. *Carbohydr. Polym.* **2012**, *88*, 830−837.
(53) Shi, S.; Pelton, R.; Fu, Q.; Yang, S. Comparing Polymer-Supported Tempo Mediators for Cellulose Oxidation and Subsequent Polyvinylamine Grafting. *Ind. Eng. Chem. Res.* **2014**, *53*, 4748−4754.

DOI: 10.1021/acsami.6b07433
ACS Appl. Mater. Interfaces XXXX, XXX, XXX−XXX

(54) Benet, W. E.; Lewis, G. S.; Yang, L. Z.; Hughes, P. D. The Mechanism of the Reaction of the Tollens Reagent. *J. Chem. Res.* **2011**, *35*, 675−677.
(55) Shi, Y.; Li, Y.; Zhang, J.; Yu, Z.; Yang, D. Electrospun Polyacrylonitrile Nanofibers Loaded with Silver Nanoparticles by Silver Mirror Reaction. *Mater. Sci. Eng., C* **2015**, *51*, 346−355.
(56) Ceska, M.; Sjödin, A.; Grossmüller, F. Some Quantitative Aspects of the Labelling of Proteins with 125i by the Iodine Monochloride Method. *Biochem. J.* **1971**, *121*, 139−143.
(57) Siggia, S.; Segal, E. Determination of Aldehydes in Presence of Acids, Ketones, Acetals, and Vinyl Ethers. *Anal. Chem.* **1953**, *25*, 640−642.
(58) Liu, J.; Pelton, R.; Obermeyer, J. M.; Esser, A. Laccase Complex with Polyvinylamine Bearing Grafted Tempo Is a Cellulose Adhesion Primer. *Biomacromolecules* **2013**, *14*, 2953−2960.
(59) Zhao, H.; Heindel, N. D. Determination of Degree of Substitution of Formyl Groups in Polyaldehyde Dextran by the Hydroxylamine Hydrochloride Method. *Pharm. Res.* **1991**, *8*, 400−402.
(60) Saito, T.; Isogai, A. Introduction of Aldehyde Groups on Surfaces of Native Cellulose Fibers by Tempo-Mediated Oxidation. *Colloids Surf., A* **2006**, *289*, 219−225.
(61) Gomez-Bujedo, S.; Fleury, E.; Vignon, M. R. Preparation of Cellouronic Acids and Partially Acetylated Cellouronic Acids by Tempo/Naclo Oxidation of Water-Soluble Cellulose Acetate. *Biomacromolecules* **2004**, *5*, 565−571.
(62) Mansur, H. S.; Oréfice, R. L.; Mansur, A. A. Characterization of Poly (Vinyl Alcohol)/Poly (Ethylene Glycol) Hydrogels and Pva-Derived Hybrids by Small-Angle X-Ray Scattering and Ftir Spectroscopy. *Polymer* **2004**, *45*, 7193−7202.
(63) Mansur, H. S.; Sadahira, C. M.; Souza, A. N.; Mansur, A. A. Ftir Spectroscopy Characterization of Poly (Vinyl Alcohol) Hydrogel with Different Hydrolysis Degree and Chemically Crosslinked with Glutaraldehyde. *Mater. Sci. Eng., C* **2008**, *28*, 539−548.
(64) Castillo, E.; Koenig, J.; Anderson, J.; Kliment, C.; Lo, J. Surface Analysis of Biomedical Polymers by Attenuated Total Reflectance-Fourier Transform Infra-Red. *Biomaterials* **1984**, *5*, 186−193.
(65) Craig, J.; Simmons, P.; Patel, S.; Tomlinson, A. Refractive Index and Osmolality of Human Tears. *Optom. Vis. Sci.* **1995**, *72*, 718−724.
(66) van den Berg, T. J.; Spekreijse, H. Near Infrared Light Absorption in the Human Eye Media. *Vision Res.* **1997**, *37*, 249−253.
(67) Shibata, I.; Isogai, A. Depolymerization of Cellouronic Acid During Tempo-Mediated Oxidation. *Cellulose* **2003**, *10*, 151−158.
(68) Tranoudis, I.; Efron, N. Tensile Properties of Soft Contact Lens Materials. *Cont. Lens. Anterior. Eye* **2004**, *27*, 177−191.
(69) Gore, A.; Horwitz, V.; Gutman, H.; Tveria, L.; Cohen, L.; Cohen-Jacob, O.; Turetz, J.; McNutt, P. M.; Dachir, S.; Kadar, T. Cultivation and Characterization of Limbal Epithelial Stem Cells on Contact Lenses with a Feeder Layer: Toward the Treatment of Limbal Stem Cell Deficiency. *Cornea* **2014**, *33*, 65−71.

DOI: 10.1021/acsami.6b07433
ACS Appl. Mater. Interfaces XXXX, XXX, XXX−XXX

Appendix: Supporting information for Chapter 3

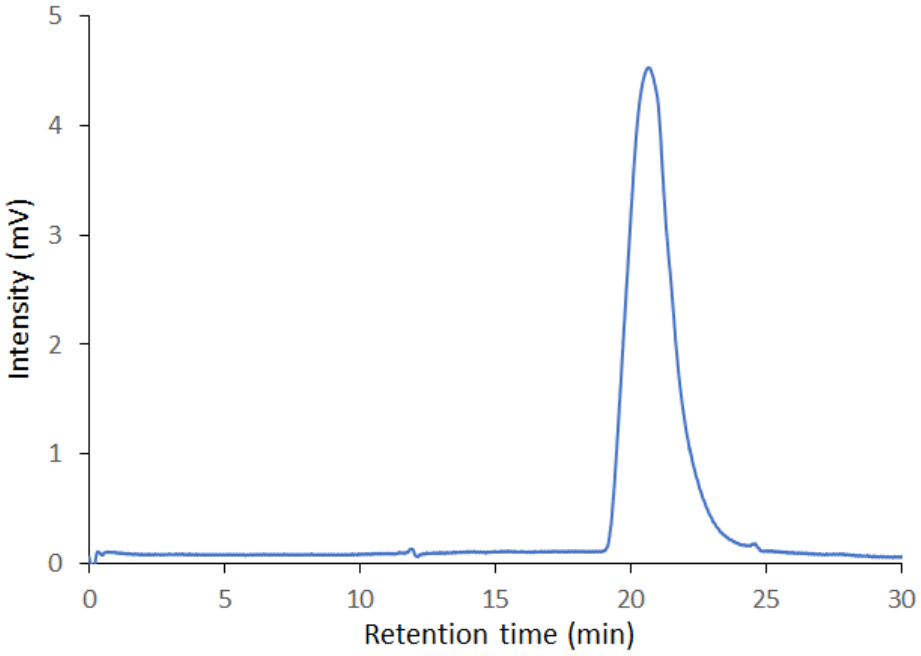

	Retention time (min)	M_n (kg/mol)	M_w (kg/mol)	M_P (kg/mol)	M_z (kg/mol)	Polydispersity
HA	20.646	336.8	466.8	706.4	538.8	1.386

Figure S1. Gel permeation chromatography (GPC) trace of HA. Calculations of molecular weight are based on comparing the retention time against linear polyethylene glycol (PEG) standards.

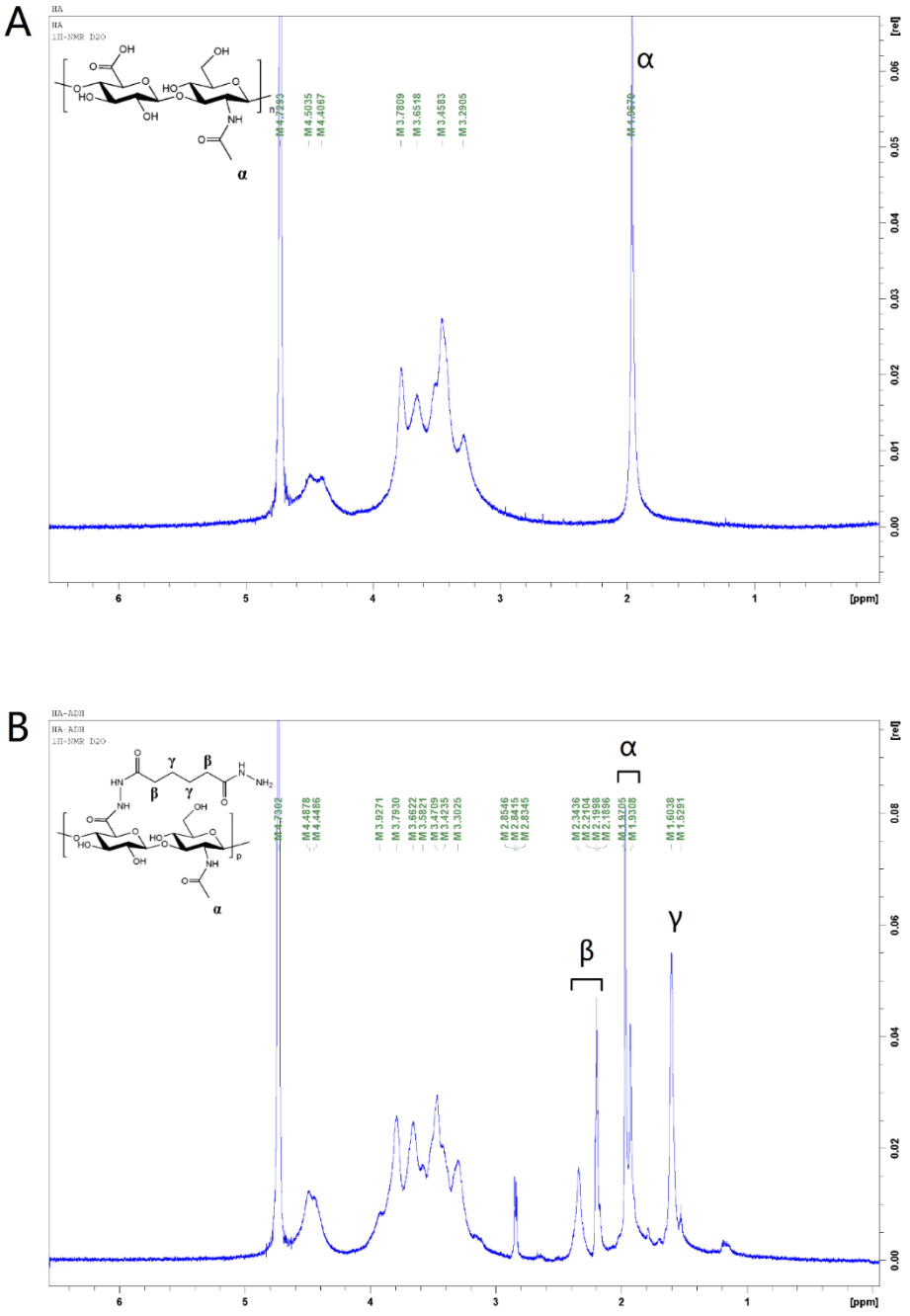

Figure S2. ^{1}H NMR spectra of HA (A) and HA-Hzd (B).

The peak assignment and determination of the degree of ADH modification were carried out according to the method of Kuo et al.[1] The methyl resonance (δ = 1.85–1.95 ppm) of the acetamido moiety of the N-acetyl-D-glucosamine was used as an internal standard. The degree of ADH

modification of HA at the carboxyl group is ~53%, as determined by the peak area of methylene protons of ADH at δ = 1.7 and 2.4 ppm.

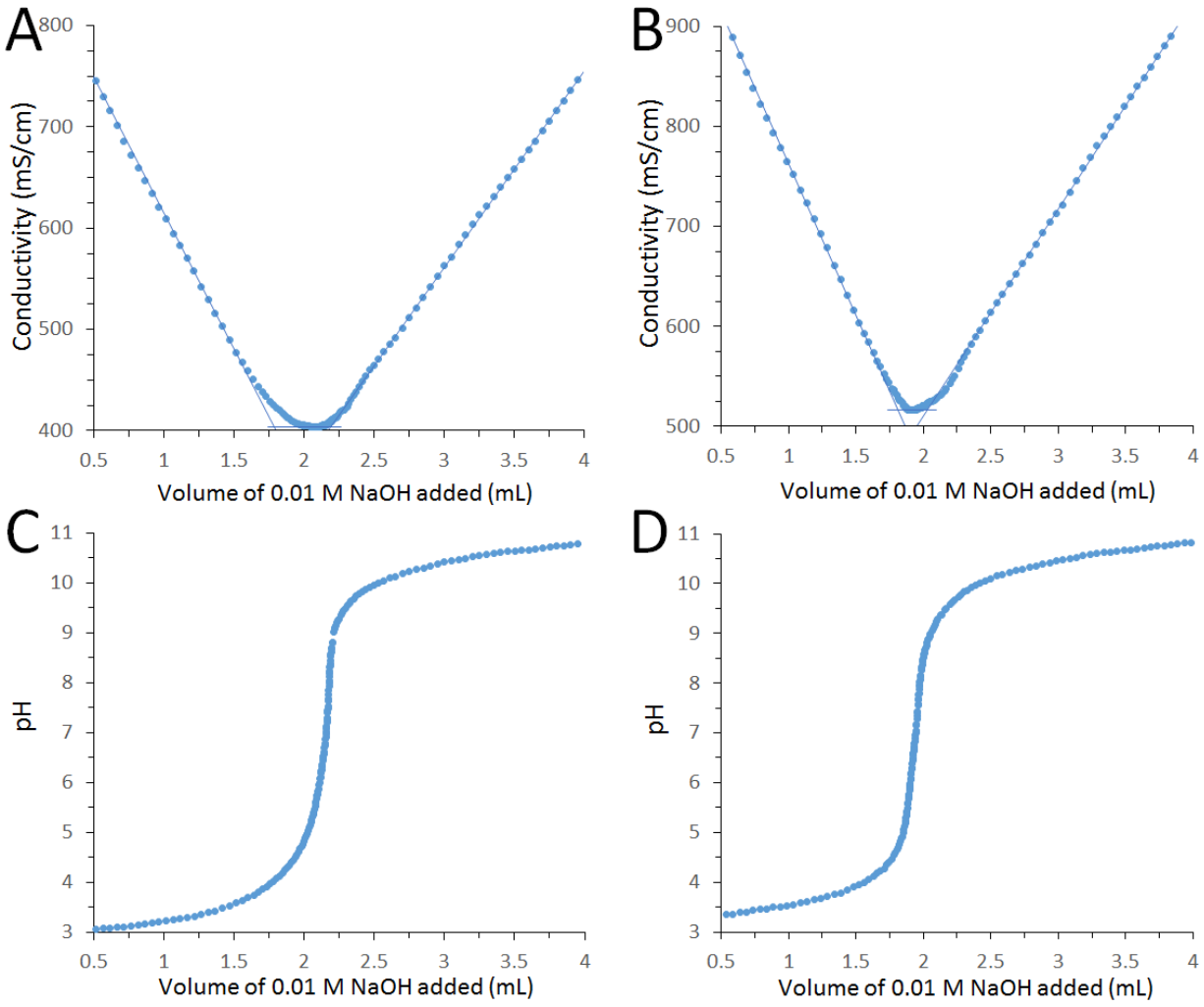

Figure S3. Conductometric and potentiometric titration curves of (A and C) HA and (B and D) HA-Hzd.

Conductometric and potentiometric base-into-acid titration for analysis of reactive carboxyl groups on HA and HA-Hzd was performed with a ManTech automatic titrator using 0.01 M NaOH as the titrant and 19.6 mg HA or 18.4 mg HA-Hzd suspended in 50 mL of 1 mM KCl as the sample.

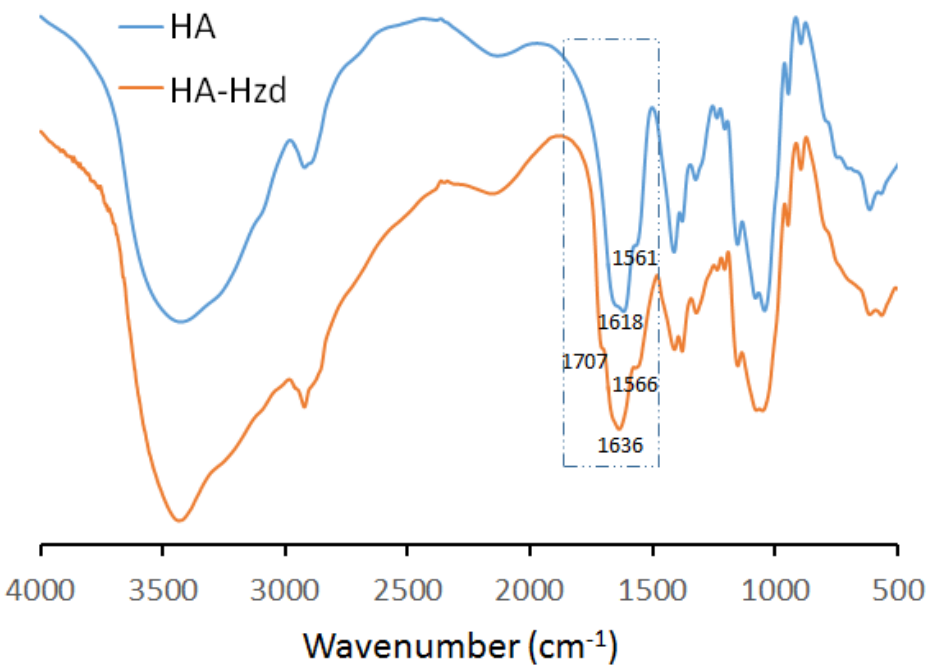

Figure S4. FTIR spectra of HA (blue) and HA-Hzd (orange).

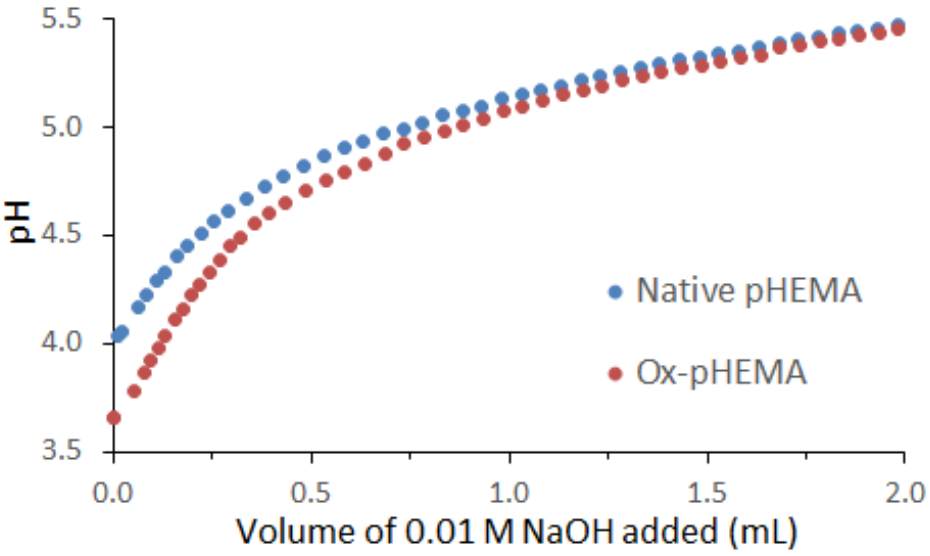

Figure S5. Hydroxylamine hydrochloride potentiometric titration of native pHEMA and Ox-pHEMA.

The degree of oxidation (aldehyde content) of pHEMA was determined by pH titration, as described by Zhao et al.[2] The Ox-pHEMA samples (8 discs with a total weight of 200 mg) were soaked in 0.1 M hydroxylamine hydrochloride solution, sealed in container, and stirred for 24 h in dark, while untreated pHEMA samples were used as a blank. Aldehydes on the pHEMA gel surface and hydroxylamine hydrychloride will react at a 1:1 ratio, releasing one mole of HCl per mole of aldehyde present that can then be titrated for quantification. The pH titration was carried out following removal of the pHEMA samples from the hydroxylamine hydrochloride solution using 0.01 M NaOH as the titrant and a Burivar-I2 automatic buret (Man Tech Associates). The titration was repeated at least twice for both the pHEMA samples and blanks. The aldehyde content was calculated based on the sample weights (mmol aldehyde per gram samples, mM/g), according to aforementioned method.

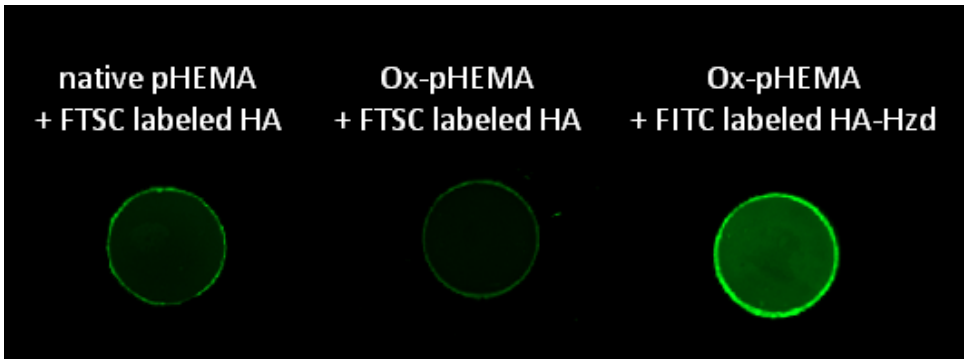

Figure S6. Comparison of the adsorption of fluorescently labeled HA/HA-Hzd on native pHEMA and Ox-pHEMA.

FTSC labeled HA was prepared by reacting a small fraction (~0.5 mol%) of carboxylic groups in HA with fluorescein-5-thiosemicarbazide (5-FTSC). Typically, 50 mg of HA was reacted with 0.30 mg of 5-FTSC (0.54 mol% equivalent of carboxylic acid groups) and 0.14 mg of EDC (0.54 mol% equivalent of carboxylic acid groups) overnight (at least 12 h) under gentle mechanical agitation in PBS at pH 7 and room temperature. The resulting labeled HA was dialyzed exhaustively against deionized water (MWCO = 14 kDa, 6 x 6 hour cycles) to remove unbound FTSC and EDC, lyophilized to dryness, dissolved in water to form a 2 mg/mL solution, and stored at 4°C in the dark. All reactions and purification steps were performed in aluminum foil-covered reaction flasks or containers to prevent photobleaching during synthesis. Following coating procedure analogous to that described in sections 2.5 and 2.6, the samples coated with FTSC labeled HA or FITC-HA-Hzd were visualized under the BioRad ChemiDoc Imaging System using an excitation wavelength of 488 nm. The results indicate significantly higher fluorescence in oxidized pHEMA/FTSC-HA-Hzd combination that would facilitate hydrazone bond formation, indicating that it is primarily the covalent conjugation chemistry and not simple physical adsorption driving the contact lens modification.

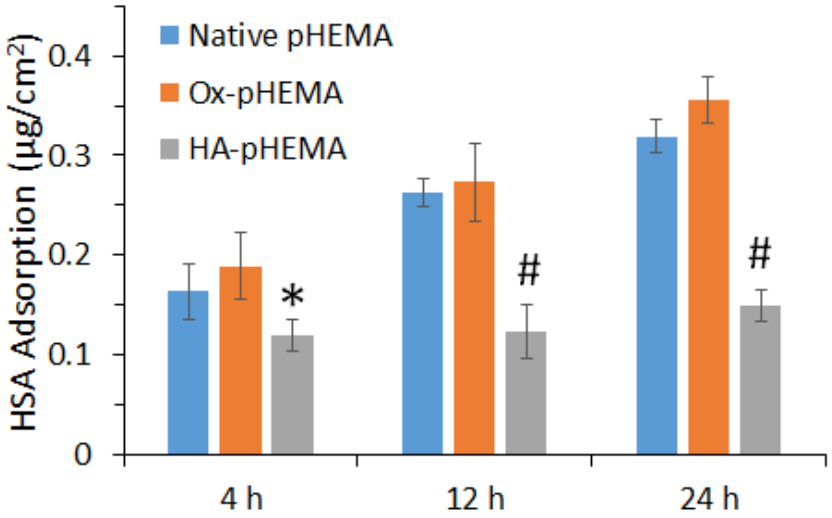

Figure S7. FITC-labeled human serum albumin (HSA, 1.0 mg/mL) adsorption on the surface of native pHEMA, Ox-pHEMA, and HA-pHEMA over a 24 hour period at 23 ºC. *p<0.05, #p<0.01, compared to the native pHEMA group at the same time period.

Human serum albumin (HSA) adsorption over both 12 and 24 h periods was determined using fluorescently-labeled protein[3] to assess the potential longer-term impact of any residual aldehydes in the Ox-pHEMA gel on protein adsorption. Fluorescein-isothiocyanate (FITC)-labelled HSA (FITC-HSA) was prepared according to a previously reported method.[4] Briefly, 100 mg of the protein was first dissolved in a 200 mL carbonate buffer at pH = 9.0. FITC (2 mg) was added, and the solution was incubated at room temperature for at least 12 h under gentle mechanical agitation. The FITC-labelled protein was subsequently dialyzed against distilled deionized water for 6 cycles (6+ hours each) and lyophilized to dryness. The FITC labeled protein was stored at 4 °C in the dark.

The pHEMA samples before and after modification were punched into circular pieces by a puncher with a diameter of 1/4 inch (0.653 cm). 200 µL of 1 mg/mL FITC-HSA in PBS was added into the 96-well plate together with one piece of sample. After an incubation over 4, 12, 24 h at room temperature (23 ºC), the samples was washed four times with PBS and then visualized under the BioRad ChemiDoc Imaging System using an excitation wavelength of 488 nm. A series of standard solution (50 µL, at 5, 10, 15, 20, 25, 30 µg/mL) was prepared to prepare a calibration curve relating protein adsorption to adsorption.

References

(1) Kuo, J. W.; Swann, D. A.; Prestwich, G. D. Chemical Modification of Hyaluronic Acid by Carbodiimides. Bioconjugate Chem. 1991, 2, 232-241.

(2) Zhao, H.; Heindel, N. D. Determination of Degree of Substitution of Formyl Groups in Polyaldehyde Dextran by the Hydroxylamine Hydrochloride Method. Pharm. Res. 1991, 8, 400-402.

(3) Xiao, X.; Nie, G.; Zhang, X.; Tian, D.; Li, H. Protein Adsorption Switch Constructed by a Pillar [5] Arene‐Based Host–Guest Interaction. Chem. - Eur. J. 2016, 22, 941-945.

(4) Smeets, N. M.; Bakaic, E.; Patenaude, M.; Hoare, T. Injectable and Tunable Poly (Ethylene Glycol) Analogue Hydrogels Based on Poly (Oligoethylene Glycol Methacrylate). Chem. Commun. 2014, 50, 3306-3309.

Chapter 4 A highly sensitive immunosorbent assay based on biotinylated graphene oxide and the quartz crystal microbalance

In chapter 4, all experiments were conducted by myself with assistance from Mengsu Chen (undergraduate student), Qiang Fu, Dr. Niels M. B. Smeets, Fei Xu and Dr. Zhuyuan Zhang. The paper was initially drafted by myself, and edited later to final version by Dr. Carlos D. M. Filipe and Dr. Todd Hoare. This work has been published in *ACS applied materials & interfaces*, 2016, 8 (3), pp1893−1902.

ACS APPLIED MATERIALS & INTERFACES

Research Article

www.acsami.org

A Highly Sensitive Immunosorbent Assay Based on Biotinylated Graphene Oxide and the Quartz Crystal Microbalance

Xudong Deng,[†] Mengsu Chen,[‡] Qiang Fu,[†] Niels M. B. Smeets,[†] Fei Xu,[†] Zhuyuan Zhang,[†] Carlos D. M. Filipe,*[,†] and Todd Hoare*[,†]

[†]Department of Chemical Engineering, McMaster University, Hamilton, Ontario L8S 4L7, Canada

[‡]Department of Biochemistry and Biomedical Sciences, McMaster University, Hamilton, Ontario L8S 4L8, Canada

Supporting Information

ABSTRACT: A high-sensitivity flow-based immunoassay is reported based on a gold-coated quartz crystal microbalance (QCM) chip functionalized directly in the QCM without requiring covalent conjugation steps. Specifically, the irreversible adsorption of a biotinylated graphene oxide-avidin complex followed by loading of a biotinylated capture antibody is applied to avoid more complex conventional surface modification chemistries and enable chip functionalization and sensing all within the QCM instrument. The resulting immunosensors exhibit significantly lower nonspecific protein adsorption and stronger signal for antigen sensing relative to simple avidin-coated sensors. Reproducible quantification of rabbit IgG concentrations ranging from 0.1 ng/mL to 10 μg/mL (6 orders of magnitude) can be achieved depending on the approach used to quantify the binding with simple mass changes used to detect higher concentrations and a horseradish peroxidase-linked detection antibody that converts its substrate to a measurable precipitate used to detect very low analyte concentrations. Sensor fabrication and assay performance take ~5 h in total, which is on par with or faster than other techniques. Quantitative sensing is possible in the presence of complex protein mixtures, such as human plasma. Given the broad availability of biotinylated capture antibodies, this method offers both an easy and flexible platform for the quantitative sensing of a variety of biomolecule targets.

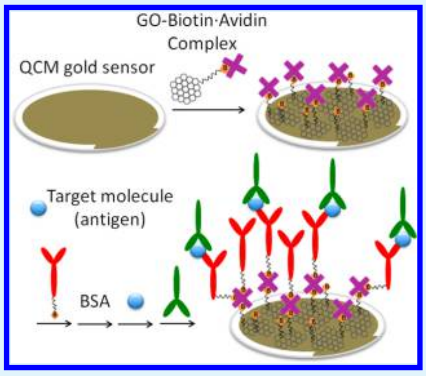

KEYWORDS: *quartz crystal microbalance, graphene oxide, biotinylation, immunoassay*

1. INTRODUCTION

Solid-phase sandwich immunoassays are widely used for antigen detection in clinical diagnosis and laboratory research because of their sensitivity and comparative low cost relative to other assay types.[1−3] However, existing immunoassay approaches are limited by three main factors. First, the sensitivity of most conventional immunoassays is in the microgram or submicrogram range, which is insufficient for detecting less concentrated proteins relevant to many disease diagnosis or biochemical pathway studies.[4] Second, for any coupling strategy to be successful, nonspecific protein binding must be suppressed to achieve quantitative detection.[5] Minimizing such effects typically requires a precoating step (e.g., bovine serum albumin adsorption[6]) to block nonconjugated surfaces on the solid support immediately before use, a step that typically requires several hours and thus prolongs the required time for any bioassay. Third, the various strategies used to attach antibodies to the solid phase often at least in part compromise the activity of the sensing molecule. Covalent conjugation strategies based on carbodiimide chemistry,[7] glutaraldehyde,[8] *N*-succinimidyl 4-maleimidobutyrate (GMBS),[9] and self-assembled monolayer (SAM) formation using 11-mercaptoundecanoic acid (MUA)[10] are time-consuming and pose risks of altering the biological activity of the antigen binding site of the antibodies;[5] similarly, thiol-directed self-assembly of antibody fragments onto a gold surface requires that intact antibody is first split into two fragments by reducing intramolecular disulfide bonds.[11] Noncovalent functionalization via physical adsorption can result in unstable interfaces and/or can lead to significant antibody denaturation via support surface-mediated protein unfolding.[12] Even more specific noncovalent attachment techniques, such as interactions between immobilized protein-G or protein-A and the Fc-part of immunoglobulin G (IgG),[13−15] are limited in terms of their flexibility (i.e., they cannot bind other types of immunoglobulins, such as IgA, IgD, or IgM[16]) and consistency (i.e., their binding capacity for IgG varies with the species[17]).

In the past decade, graphene and graphene oxide (GO) have been widely explored as support materials relevant in diagnosis, environmental and safety monitoring, and drug screening.[18] The changes observed in the electronic and electrochemical properties of graphene as a function of surface chemistry have attracted the most interest in the context of sensing.[18−20] The conjugated π-bonded structure of graphene provides a platform

Received: October 20, 2015
Accepted: January 3, 2016
Published: January 3, 2016

DOI: 10.1021/acsami.5b10026
ACS Appl. Mater. Interfaces 2016, 8, 1893−1902

to stably and irreversibly adsorb biomolecules containing aromatic rings (via $\pi-\pi$ stacking interactions)[21] as well as a range of solid surfaces commonly used as sensor supports, such as silica,[22] amino-modified glass,[23] and gold[24,25] (mainly via van der Waal interactions[26]). GO-facilitated adsorption is non-specific, so GO needs to be functionalized for use in immunoassays to provide binding specificity. The biotin/(strept)avidin system[27] is particularly attractive in this regard because many biotin or (strept)avidin-linked antibodies and other types of sensing molecules are commercially available.[28] The combination of these approaches has been previously applied to prepare functional GO/streptavidin conjugates[29] or a streptavidin layer on a GO-coated surface,[30] suggesting the potential to prepare GO-antibody conjugates for immunosensing.

Although GO is typically used in electrochemical sensors,[31] our interest lies in applying GO-antibody conjugates together with the quartz crystal microbalance (QCM) to create a novel sensing platform. QCM biosensors offer several advantages over other available sensing technologies, including direct gravimetry-based measurements of binding, relatively high sensitivity, and the capacity for real-time measurements.[32,33] However, QCM is inherently limited in the detection of antigen targets with low concentrations because the very small mass change observed upon binding of that target often lies below the detection threshold of the technique.[34] For addressing this challenge, various mass amplification strategies have been reported to increase the mass loaded on the surface as a function of a single specific binding event.[35−40] One such strategy consists of sandwiching the detection antibody with a horseradish peroxidase (HRP) enzyme-labeled antibody followed by the addition of H_2O_2 and the 4-chloro-1-naphthol (4C1N) substrate to generate large masses of insoluble precipitate (benzo-4-chlorocyclohexadienone, B4C)[37,39] that accumulates on the QCM surface; longer reaction times result in further enhanced mass amplification of the presence of an antigen binding event.[39] Gold nanoparticles have also been employed for mass amplification in both sandwich[35] or competitive-type[36] immunoassays but must be modified with targeted antibodies for effective function.

In this work, we aim to address the challenges of facile QCM biosensor functionalization and low-threshold detection of biomolecule targets using a GO-biotin-based sandwich immunoassay approach (Figure 1). Specifically, by exploiting the high-yield and irreversible adsorption of GO to a variety of substrates (including standard gold-coated QCM chips used here), we demonstrate effective functionalization of a QCM chip in real time by simple flow-based strategies, avoiding the conventional time-consuming chemical prefunctionalization approaches typically employed for this purpose.[41] In addition, by coupling this functionalization strategy with the HRP-induced precipitation strategy previously reported,[37,39] we demonstrate the use of such GO-modified QCM chips for fast, online, and highly sensitive detection of an antigen target. We anticipate the simple, flow-based, on-chip nature of both the functionalization and detection strategies employed will facilitate the use of QCM-based strategies in a broader range of biosensing applications.

2. EXPERIMENTAL SECTION

2.1. Chemicals and Materials. Graphene oxide (GO, Sigma-Aldrich, Product No. 777676, 4 mg/mL, dispersion in H_2O), (+)-biotin hydrazide (Sigma-Aldrich, 97%), bovine serum albumin

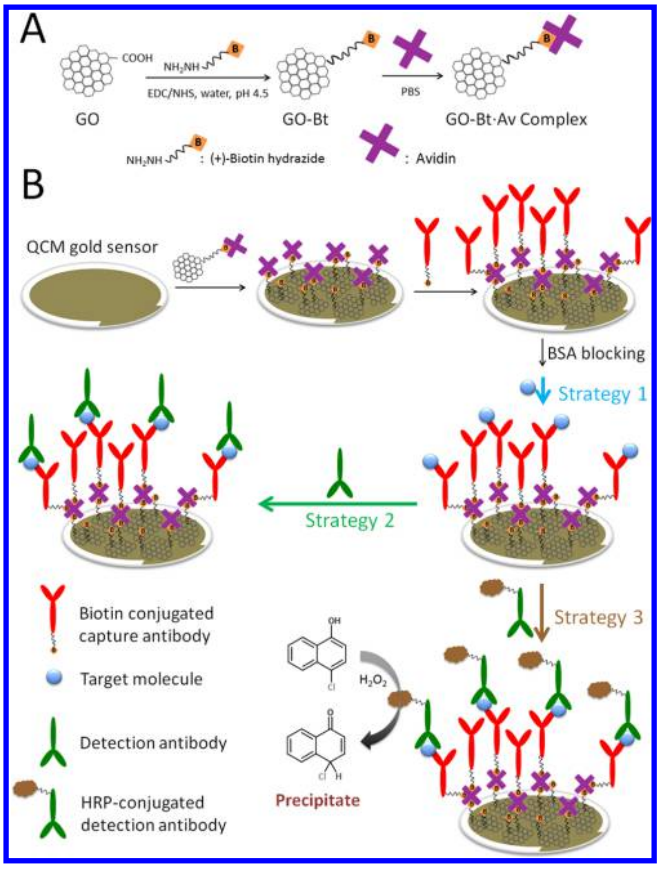

Figure 1. Design of proposed immunosensor. (A) Reaction scheme to form biotinylated graphene oxide (GO-Bt) and graphene oxide·avidin (GO-Bt·Av) complex. (B) Schematic diagram of the flow-based fabrication of QCM-based immunosensor and the three tested strategies for antigen quantification.

(BSA, Sigma-Aldrich, 98%), avidin from egg white (BioUltra, lyophilized power, 98%, Sigma-Aldrich), IgG from rabbit serum (Sigma-Aldrich, 95%), IgG from sheep serum (Sigma-Aldrich, 95%), IgG from goat serum (Sigma-Aldrich, 95%), antirabbit IgG (whole molecule) antibody produced in goat (affinity isolated antibody, lyophilized powder, Sigma-Aldrich), antirabbit IgG (whole molecule)-peroxidase antibody produced in goat (affinity isolated antibody, Sigma-Aldrich), antirabbit IgG (Fc specific)-biotin antibody produced in goat (affinity isolated antibody, buffered aqueous solution, Sigma-Aldrich), *N*′-ethyl-*N*-(3-(dimethylamino)propyl)-carbodiimide (EDC, Carbosynth, Compton CA, commercial grade), *N*-hydroxysuccinimide (NHS, Sigma-Aldrich, 98%), HABA/avidin reagent (lyophilized powder, Sigma-Aldrich), and 4-chloro-1-naphthol (4C1N) solution (0.48 mM, Sigma-Aldrich) were all used as received. Hydrochloric acid (1 M, 0.1 M) and sodium hydroxide (1 M, 0.1 M) were received from LabChem Incorporated (Pittsburgh, PA). For all experiments, Milli-Q grade distilled deionized water (DIW) was used. Phosphate buffered saline (PBS) was diluted from a 10× liquid concentrate (Bioshop Canada Incorporated).

2.2. Synthesis of Biotinylated Graphene Oxide (GO-Bt) and Graphene Oxide·Avidin Complex (GO-Bt·Av). Biotinylated graphene oxide (GO-Bt) was synthesized using EDC-NHS carbodiimide chemistry in water. In brief, 2 mL of GO suspension (8 mg GO) was diluted in 40 mL of water, after which the EDC solution (1.5 mg dissolved in 20 mL of water) was added dropwise over 14 min under 60 rpm magnetic stirring. Then, NHS solution (0.46 mg in 10 mL of water) was added dropwise over 7 min, and the flask contents were stirred for an additional 30 min. The pH was then adjusted to 4.5 using 0.1 M NaOH, and (+)-biotin hydrazide solution (12 mg in 10 mL of water) was added dropwise over 7 min. The reaction was allowed to continue for 4 h, after which the modified GO suspension was

DOI: 10.1021/acsami.5b10026
ACS Appl. Mater. Interfaces 2016, 8, 1893−1902

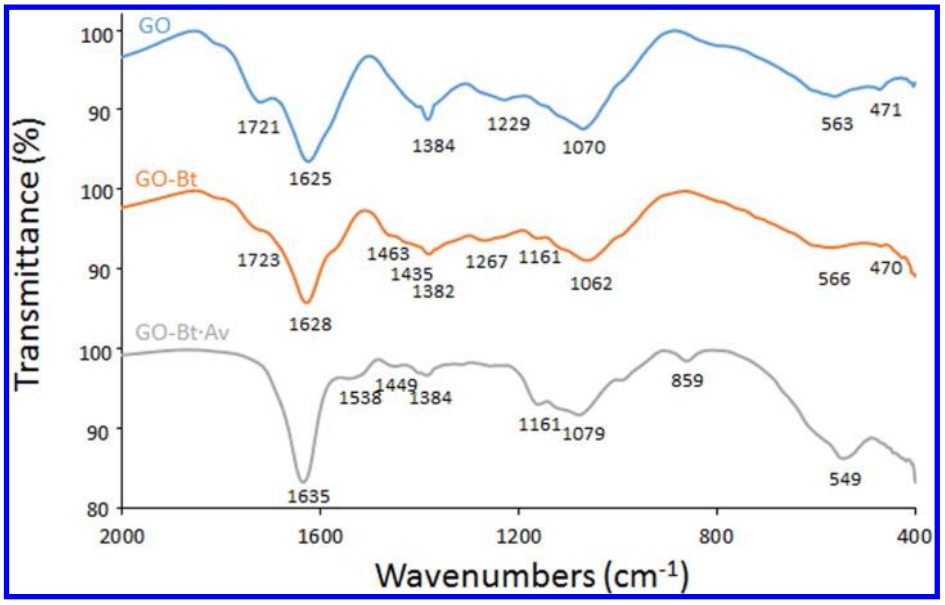

Figure 2. FTIR spectra of GO, GO-Bt, and GO-Bt·Av complex.

centrifuged at 10,000 rpm for 10 min over two centrifugation cycles (completely replacing the supernatant each cycle). All the pellets following the second centrifugation cycle were collected and either resuspended in 4 mL of water (for further functionalization) or dried on a glass slide at 40 °C overnight (for characterization).

The GO-Bt·Av was prepared by adding a diluted GO-Bt solution (10 μg/mL in 5 mL water) dropwise into an avidin solution (1 mg/mL in 10 mL PBS) over ∼3 min. The mixture was gently shaken (∼30 rpm) for 1 h at room temperature, followed by purification via centrifugation and resuspension using the same process outlined above for GO-Bt.

2.3. Characterization of Modified GO. Infrared spectroscopy was performed using a KBr pellet technique with a Nexus 6700 Fourier-transform infrared (FTIR) spectrometer (Thermo Fisher Scientific Inc.). X-ray photoelectron spectroscopy (XPS) was performed using a PHI Quantera II XPS scanning microprobe (Physical Electronics (Phi), Chanhassen, MN) equipped with a 1486.7 eV monochromatic Al Kα X-ray source operating with a beam diameter of 200 μm and a 280 eV pass energy. Conductometric base-into-acid titration for analysis of reactive carboxyl groups on GO was performed with a ManTech automatic titrator using 0.1 M NaOH as the titrant and 5 mg of GO suspended in 50 mL of 1 mM KCl as the sample. UV−vis spectrophotometry for estimating the concentration of GO was performed using a Beckman Coulter DU800 spectrophotometer; the standard curve used to estimate the concentration of GO is shown in Figure S1. Electrophoretic mobility of GO samples was measured using a ZetaPlus zeta potential analyzer (Brookhaven Instruments Corporation) operating in phase analysis light scattering (PALS) mode using samples dispersed in 1 mM KCl and adjusted to pH 7.4 using NaOH or HCl. A total of ten runs (15 cycles each) were carried out for each sample; the experimental uncertainties represented the standard error of the mean of the replicate runs.

2.4. Quartz Crystal Microbalance with Dissipation Monitoring (QCM-D). GO-Bt-based immunoassays were performed using a quartz crystal microbalance with dissipation (QCM-D, Q-Sense E4, Gothenburg, Sweden) equipped with QSX 301 gold sensors (AT-cut piezoelectric quartz crystals, diameter ∼14 mm, 100 nm thick gold coating). The resonance frequency and dissipation shifts of the oscillating crystals were simultaneously monitored at the fundamental frequency (5 MHz), and its six harmonics (15, 25, 35, 45, 55, and 65 MHz) at 25 °C under constant fluid flow (0.1 mL/min) provided by a digital peristaltic pump (IsmaTec, IDEX) operating in suction mode. The gold chip surface was allowed to equilibrate for 30 min in PBS buffer prior to all measurements. All samples (dissolved in PBS) were flowed over the pre-equilibrated chip until the measured frequency (and thus the adsorption of the samples added) reached a plateau characterized by a frequency change of less than 1 Hz/10 min. The adsorbed mass (Δm) was then determined using Sauerbrey's equation under the assumptions that the adsorbed layer was rigid, uniformly distributed on the surface, and small compared to the crystal's mass (eq 1).[42,43]

$$\Delta m = -\frac{C \cdot \Delta f}{n} \quad (1)$$

In this equation, C is the sensitivity constant (17.7 ng Hz^{-1} cm^{-2} for a 5 MHz crystal, as provided by the manufacturer), Δf is the measured change in frequency, and n is a harmonic number. The average value of Δf over the period at which the absorption reached steady states was used for calculations. Only the changes in the normalized frequencies and dissipations of the fifth harmonic were reported; analogous results were achieved with other harmonics. We note that more accurate models recently reported for converting frequency changes to mass were considered for use herein;[44−46] however, these were deemed too complex to apply to our multicomponent system containing both grafted and adsorbed species due to their requirement for inputting chemical-specific coefficients.

2.5. Scanning Electron Microscopy (SEM). The morphology of the gold sensor surface was studied by scanning electron microscopy (SEM) imaging before and after coating GO-Bt and GO-Bt·Av as well as adsorbing avidin directly. The full sensor surfaces were first sputter-coated with gold (layer thickness = 15 Å) to avoid charging effects; the resulting samples were then imaged using a Tescan VEGA II LSU SEM (Tescan USA, PA) operating at 20.0 kV and a probe distance of 6.0 mm.

2.6. Cyclic Voltammetry in QCM-D. Cyclic voltammetry was used to determine the residual amount of 4-chloro-1-naphthol (4C1N) inside the QCM sensor chamber (Q-Sense Electrochemistry Module, QEM 401). In the sensor chamber, a gold-coated crystal (Q-sense QSX 301) served as the working electrode, and a platinum plate parallel to the Au crystal surface served as the counter electrode. The two electrodes were separated by a Viton O-ring (Biolin Scientific), forming a flow cell with a volume of approximately 0.1 mL. Both electrodes had a surface area of 0.79 cm^2 exposed to the studied solution. A 2 mm diameter Ag|AgCl electrode (Dri-REFTM, WPI) served as the reference. A potentiostat (CH Instruments, model 420B) was connected to the QCM system for the cyclic voltammetry experiment. A potential was then applied between the working electrode and the reference electrode, and the resulting current was measured. The potential was swept back and forth between two set

DOI: 10.1021/acsami.5b10026
ACS Appl. Mater. Interfaces 2016, 8, 1893−1902

Table 1. Elemental Concentrations (via XPS) and Electrophoretic Mobilities of Native GO, GO-Bt, and GO-Bt·Av

	elemental composition (mol %)					
	C 1s	N 1s	O 1s	S 2p	Na 1s	electrophoretic mobility ($\times 10^{-8}$ m^2 V^{-1} s^{-1})
GO	76.43		23.57			−1.87 ± 0.06
GO-Bt	79.98	1.30	18.39	0.34		−1.00 ± 0.06
GO-Bt·Av	65.40	9.71	23.72		1.16	−0.76 ± 0.07

values (0.3−0.8 V) at a specific scan rate (0.05 V/s), leading to oxidation and/or reduction of analyte on the working electrode, and thus a change in the measured current if the scan window was suitable.

3. RESULTS AND DISCUSSION

3.1. Synthesis and Characterization of GO-Bt. Although previous efforts to functionalize GO with biotin used organic solvent (DMF) in conjunction with two coupling reagents,[29] herein, GO was biotinylated in aqueous suspension using carbodiimide chemistry (EDC/NHS) to couple the -COOH of GO to the -NH-NH$_2$ of (+)-biotin hydrazide (Figure 1A). This alternate chemistry facilitates both easier purification and easier translation to larger-scale synthesis if required. Key to this reaction is keeping the concentration of EDC < 0.1 mM in the aqueous phase;[47] higher concentrations of EDC have been shown to induce the aggregation of GO by enhancing the van der Waals force between GO surfaces.[48] The final concentrations of GO, EDC, and NHS were kept low at 0.1 mg/mL, 0.1 mM, and 0.05 mM, respectively, for this purpose. Conductometric titration (Figure S2-A) indicated that the content of reactive carboxyl groups in the purchased GO was 3.02 ± 0.03 mM/g; thus, a 2-fold excess concentration of (+)-biotin hydrazide (0.6 μM) was used in the grafting reaction.

FTIR analysis of GO (Figure 2) showed the presence of carboxy/carbonyl C═O (ν = 1721 cm^{-1}), aromatic C═C (ν = 1625 cm^{-1}), carboxy C−O (ν = 1384 cm^{-1}), epoxy/ether C−O (ν = 1229 cm^{-1}), and alkoxy C−O (ν = 1070 cm^{-1}) stretches, as reported previously.[49] For the GO-Bt, the peaks at 1435 cm^{-1} (corresponding to C−N stretch) and 1267 cm^{-1} (corresponding to amide II band in the biotin ureido ring, interaction between the N−H bending and C−N stretching)[50,51] confirmed the presence of (+)-biotin hydrazide (see Figure S3-A for the FTIR spectrum of (+)-biotin hydrazide). The UV−vis spectrum of GO-Bt did not show any significant changes as compared to the GO (Figure S4) because the (+)-biotin hydrazide does not absorb UV/visible light within the scanned wavelength range. XPS data (Table 1 and Figure S5) indicated that the native GO contained 76% C and 24% O (no other elements present), whereas GO-Bt exhibited a nitrogen content of 1.3%; on the basis of the % nitrogen in (+)-biotin hydrazide, this elemental percentage corresponds to a biotin content in GO-Bt of 65 mg of biotin/g of GO-Bt. Conductometric titration of the remaining carboxyl groups on GO after biotinylation yielded a COOH density of 2.73 ± 0.11 mM COOH/g of GO-Bt (Figure S2-B); comparing this result to the initial COOH density on GO and assuming that the consumption of one COOH group corresponds to the grafting of one NH$_2$−NH-biotin,[52] this result corresponds to a biotin content of 70 ± 7 mg of biotin/g of GO-Bt, which matches the XPS result. Measurement of residual (+)-biotin hydrazide in the supernatant following centrifugation yields an identical biotin content of 70 ± 7 mg of biotin/g of GO-Bt. Thus, on the basis of three independent measurements, ∼9% of the COOH groups on the original GO were biotinylated. Electrophoretic mobility results (Table 1) also confirmed consumption of the COOH groups via biotin grafting with the absolute mobility value decreasing as (neutral) biotin is grafted to (anionic) COOH residues.

3.2. Synthesis and Characterization of GO-Bt·Av. Biotinylated GO (GO-Bt) in water was subsequently suspended in an avidin solution to form a GO·avidin complex (GO-Bt·Av). Because biotin binds to avidin in a 4:1 stoichiochemistry,[53] a large molar excess of avidin relative to the biotin content of GO-Bt (biotin/avidin ≈ 1:11) was used to minimize the potential for avidin-mediated cross-linking of GO-Bt,[54] corresponding to concentrations of GO-Bt and avidin of 3.3 μg/mL and 0.67 mg/mL, respectively. FTIR (Figure 2) confirms complexation of avidin with GO-Bt via the appearance of characteristic avidin peaks at 1637 cm^{-1} (corresponding to amide I) and 1525 cm^{-1} (corresponding to amide II) (see Figure S3-B for the FTIR spectrum of avidin itself for reference). Correspondingly, the %N measured via XPS (Table 1, Figure S5) increases from 1.3% in GO-Bt to 9.7% in GO-Bt·Av, suggesting the complexation of ∼570 mg of avidin/g of GO-Bt·Av. Note that the additional presence of sodium in GO-Bt·Av sample is attributable to the PBS buffer used for diluting avidin (1.37 M NaCl, 27 mM KCl, 100 mM Na_2HPO_4, 18 mM KH_2PO_4). Furthermore, the absolute electrophoretic mobility decreases upon avidin complexation (Table 1), consistent with the high isoelectric point of avidin (10.5[55]) that would result in it exhibiting a net cationic charge under the pH 7.4 measurement conditions.

3.3. Adsorption of GO, GO-Bt, GO-Bt·Av, and biotinylated antibody on gold surface. Two methods were used to assemble the GO-Bt·Av complex on the gold QCM chip: (1) GO or GO-Bt was first adsorbed followed by flowing avidin over the chip to create the complex on-chip (Figure 3A) or (2) precomplexed GO-Bt·Av was flowed over the QCM chip (Figure 3B). Each of GO, GO-Bt, and GO-Bt·Av could stably adsorb on the gold surface (Figure 3A and B). Scanning electron microscope (SEM) images confirmed that GO-Bt and GO-Bt·Av adsorption effectively covered most of the area of the gold sensor surface (Figure 4B and D); in comparison, simple avidin adsorption covered a much smaller fraction of the bare gold surface (Figure 4C), consistent with the lower total adsorption amount observed via QCM (Figure 3A).

Modifying GO with biotin groups reduces the adsorbed mass from 142 to 100 ng/cm^2 (according to Sauerbrey's equation, Figure 3A), consistent with previous research showing that defects in the carbon π-π network induced by oxygen containing groups on GO increased the distance between the GO sheet and the gold surface and thus weakens the interaction[56] (an effect likely to be further exacerbated by subsequent biotinylation). However, because carboxyl groups are mainly distributed at the edge of the GO sheet,[57] the biotinylated GO still retained a strong capacity for adsorption onto the gold surface. Furthermore, once the GO-modified QCM biosensors were exposed to avidin, GO-Bt adsorbed

DOI: 10.1021/acsami.5b10026
ACS Appl. Mater. Interfaces 2016, 8, 1893−1902

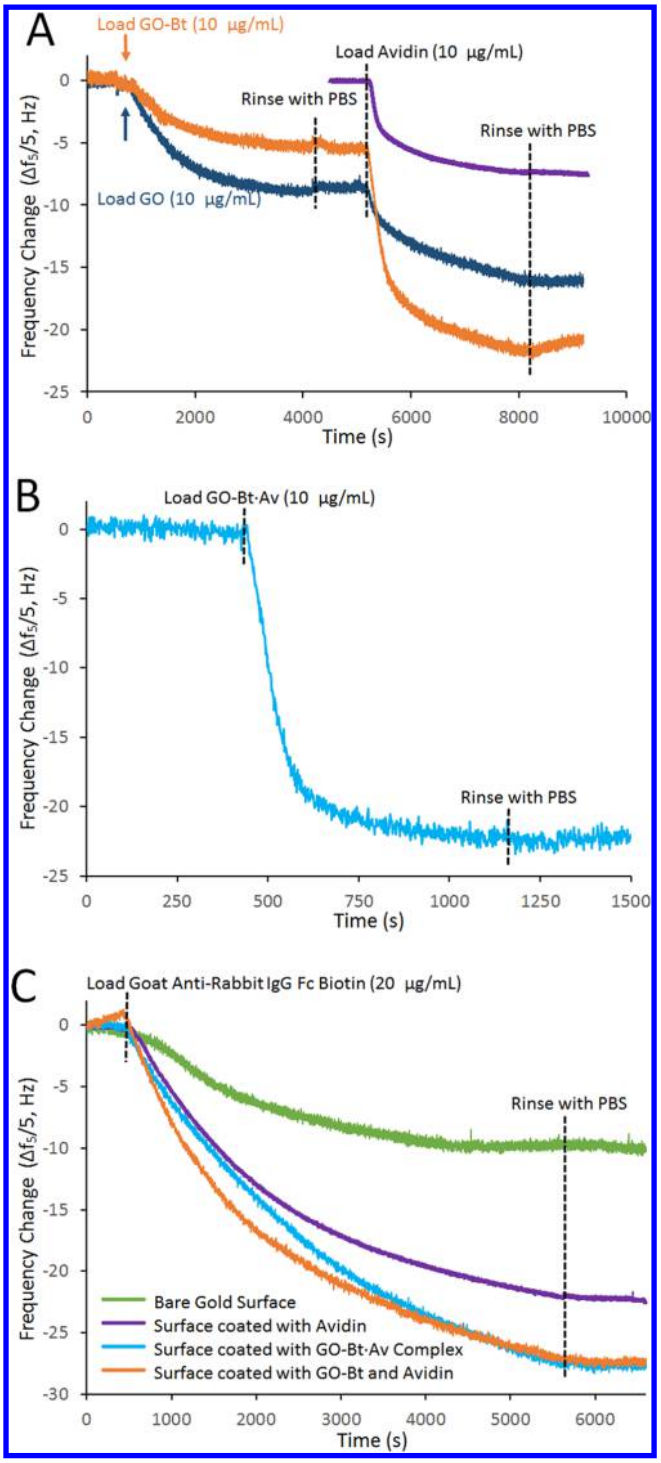

Figure 3. Time-dependent frequency changes associated with (A) loading GO/avidin, GO-Bt/avidin, and avidin alone on a bare gold surface; (B) loading precomplexed GO-Bt·Av complex on a bare gold surface; (C) loading of biotinylated capture antibody on a bare gold surface, an avidin-coated surface, a GO-Bt + avidin-coated surface, and a precomplexed GO-Bt·Av-coated surface.

significantly more avidin (277 ng/cm^2) compared to unmodified GO (129 ng/cm^2), consistent with biotin−avidin complexation. Note that the amount of avidin adsorbed on a bare QCM chip (Figure 3A, purple curve) was similar to the amount of avidin adsorbed by the unmodified GO surface (Figure 3A, dark blue curve), suggesting that GO itself has no significant specificity for avidin binding without biotinylation. In comparison, direct adsorption of preformed GO-Bt·Av complex on the bare sensor surface (Figure 3B) resulted in similar total adsorption to the two-step method described above (395 ng/cm^2 relative to 377 ng/cm^2 for sequential GO-Bt and avidin adsorption/complexation) while facilitating significantly faster construction of a functional QCM immunosensor (reaching steady state within ∼1000 s as opposed to ∼9000 s for the sequential approach). Moreover, the adsorbed GO-Bt·Av exhibited no significant change in dissipation following adsorption (see Figure S6), suggesting that the adsorbed layer was relatively rigid and constricted (indicative of strong adsorption).

A biotinylated capture antibody (Fc-specific antirabbit IgG-biotin, 20 μg/mL) was subsequently flowed over the avidin-functionalized QCM chips to facilitate complexation-driven QCM chip functionalization (Figure 3C). Both one-step adsorption of GO-Bt·Av and sequential adsorption of GO-Bt followed by avidin resulted in similar high quantities of antibody immobilized to the QCM chip (489 and 483 ng/cm^2, respectively); in comparison, a bare gold surface (172 ng/cm^2) and a simple avidin-coated surface (393 ng/cm^2) both immobilize significantly less antibody. Thus, on the basis of the sequential adsorption of GO-Bt·Av followed by a biotin-labeled antibody, a functionalized QCM surface can be made directly inside the QCM instrument in ∼2 h with sufficient antibody density to allow for sensitive detection of analytes. Note that given the time savings associated with adsorption of precomplexed GO-Bt·Av instead of the two-step GO-Bt/Av complexation, GO-Bt·Av was used for all subsequent experiments. In addition, it should be noted that the conventional method of biotinylating a gold surface via self-assembled monolayer formation based on alkylthiolated biotin and subsequent blocking of bare surface with a hydroxylated alkylthiol requires multiple steps and typically overnight or 24 h preparation times,[58,59] making the method reported herein significantly more convenient and enabling of faster assays.

3.4. Surface Blocking. Bovine serum albumin (BSA, 1% w/v) was used to block nonoccupied sites on the sensor surface (Figure 5). Large quantities of BSA adsorption were observed on a capture antibody-loaded bare gold sensor (249 ng/cm^2), a GO-Bt-coated gold sensor (195 ng/cm^2), and an avidin-coated gold sensor (185 ng/cm^2). However, after coating with GO-Bt·Av complex and loading of the capture antibody, BSA adsorption decreased approximately 3-fold to 62.0 ng/cm^2. This result suggests that the preloaded GO-Bt·Av and capture antibodies together covered the majority of the gold surface (as further suggested by the SEM result, Figure 4D) whereas other functionalization strategies do not. Note that the very high BSA adsorption to the avidin-coated gold sensor confirms the likelihood of some nonspecific binding of capture antibody onto the gold surface (as opposed to complexation with avidin) in Figure 3C, again consistent with the relatively low surface coverage of avidin observed in the SEM image in Figure 4C; this observation makes the enhanced specific antibody capture by GO-Bt·Av more significant relative to the avidin-only control. In addition, no significant adsorption of detecting antibody (whole molecule antirabbit IgG) was observed following BSA blocking of the GO-Bt·Av/capture antibody complex-modified biosensor (Figure S7), confirming that nonspecific detecting antibody adsorption to the blocked immunosensor is insignificant and will not affect sensor performance.

DOI: 10.1021/acsami.5b10026
ACS Appl. Mater. Interfaces 2016, 8, 1893−1902

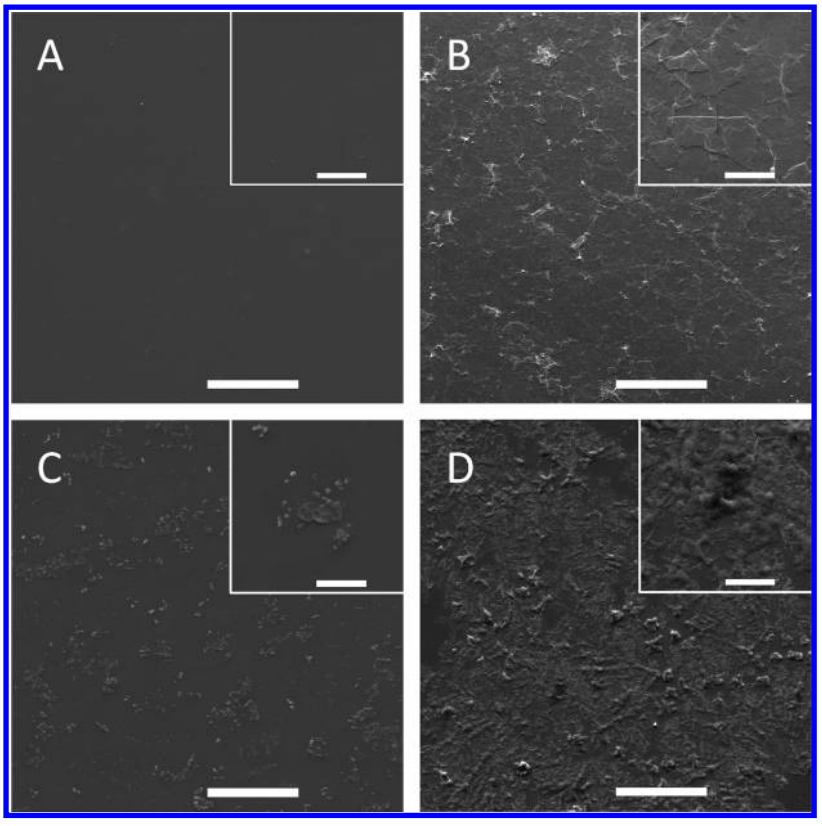

Figure 4. Scanning electron microscope (SEM) images of (A) a bare gold surface, (B) a GO-Bt-coated surface, (C) an avidin-coated surface, and (D) a precomplexed GO-Bt·Av complex-coated surface. Scale bar = 100 μm in the lower magnification images; scale bar = 20 μm in the higher magnification images in the top right corner of each panel.

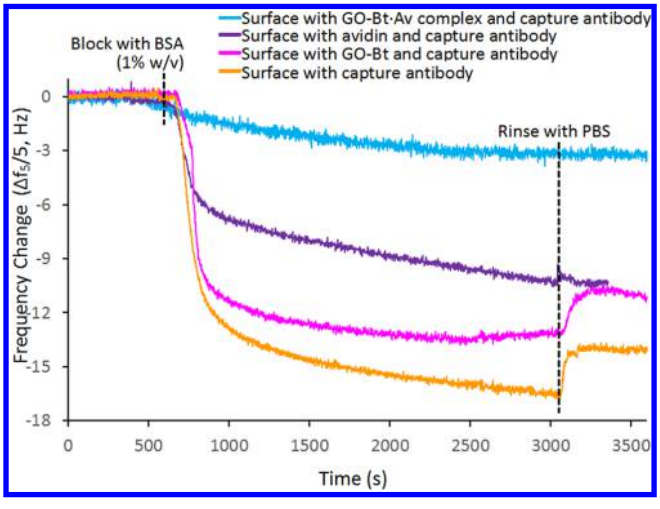

Figure 5. Time-dependent frequency changes associated with BSA blocking on gold surface pretreated with capture antibody alone (orange), GO-Bt and capture antibody (no avidin, pink), avidin/capture antibody complex (blue), and GO-Bt·Av/capture antibody complex (purple).

3.5. Sensor Performance. A conventional mass-based QCM detection strategy was first used to assess the capacity of the BSA-blocked GO-Bt·Av/capture antibody sensors for detecting a target antigen (rabbit IgG), first by tracking the binding of the target antigen itself (strategy 1 in Figure 1) and then by performing a sandwich assay with a detecting antibody (whole-molecule antirabbit IgG, strategy 2 in Figure 1) (Figure 6A). The minimum equilibrium loading times for the antigen and detecting antibody were 40 and 60 min, respectively, requiring only small (~4 mL) samples of each for effective quantification. Tracking the mass change associated with antigen binding alone (strategy 1) allowed for detection of rabbit IgG concentrations of >100 ng/mL, whereas subsequent complexation with the detection antibody (strategy 2) enables the quantification of rabbit IgG concentrations within the range of 10 ng/mL to 10 μg/mL; samples containing less than 10 ng/mL of rabbit IgG could not be quantified using either technique (i.e., the signal-to-noise ratio was less than 3). Comparing the performance of the GO-Bt·Av-based sensor to a simple avidin-coated sensor (Figure 6B), roughly 4-fold higher signals were achieved with the GO-Bt·Av sensor at the same antigen concentration. Interestingly, although the avidin-coated surface binds roughly 2/3 of the capture antibodies as the GO-Bt·Av surface (Figure 3C), it offers only 1/4 the antigen binding capacity; this result is likely related to the observed role of GO-Bt·Av in minimizing nonspecific protein adsorption (Figure 5A) and suggests an added benefit of using GO-Bt·Av for avidin surface modification. Note also that the sensor yields highly reproducible results, both between different sensors tested at the same storage time as well as sensors prepared at the same time but stored over different periods (Figure S8), suggesting the stability of this sensor design.

For lowering the detection limit further, an alternative strategy was used in which the detecting antibody was substituted with a horseradish peroxidase (HRP)-linked antibody (whole molecule antirabbit IgG, 1:10000 dilution according to the manufacturer's protocol) that converts 4C1N to B4C precipitate that can be detected by QCM (strategy 3 in Figure 1). After the 4C1N solution had filled the inner volume

DOI: 10.1021/acsami.5b10026
ACS Appl. Mater. Interfaces 2016, 8, 1893−1902

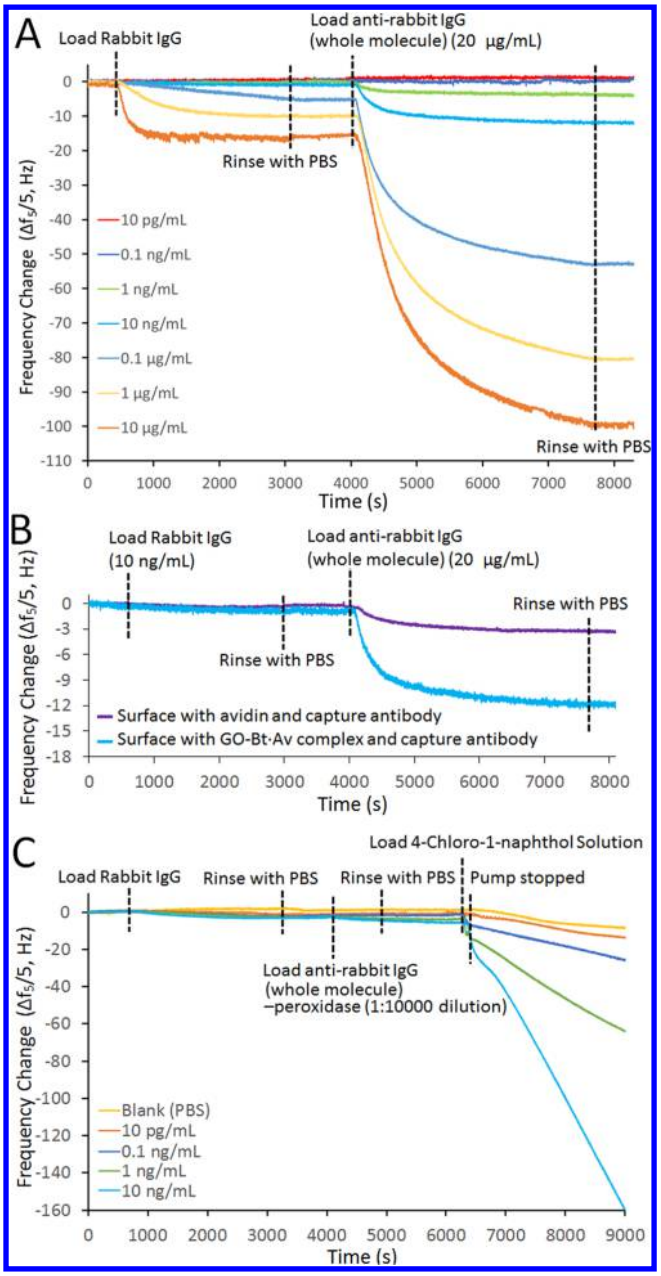

Figure 6. Performance of GO-Bt·Av-coated QCM immunosensor. (A) Time-dependent frequency changes associated with loading different concentrations of rabbit IgG followed by antirabbit IgG on the QCM immunosensor. (B) Comparison of time-dependent frequency changes associated with loading 10 ng/mL of rabbit IgG on an avidin-functionalized gold surface relative to a GO-Bt·Av-coated gold surface. (C) Time-dependent frequency changes associated with loading different concentrations of rabbit IgG followed by HRP-linked antirabbit IgG and exposure of the detecting antibody to 4-chloro-1-naphthol solution.

of the QCM sensor chamber, the pump was stopped, allowing the in situ generation of B4C by HRP. At a fixed substrate (4C1N) concentration, the rate of mass change associated with B4C precipitation is directly related to the density of HRP bonded on the sensor surface and thus the target antigen concentration.[40] Rabbit IgG concentrations in the range of 0.1−10 ng/mL can be accurately measured using this strategy (Figure 6C); however, 10 pg/mL of rabbit IgG could not be distinguished from the blank sample, which also exhibited a slight precipitation signal likely attributable to limited nonspecific adsorption of HRP-linked antibody within the QCM chamber. It should be noted that the composition of the surface does not itself affect the signal (see Figure S9), confirming the signal is dependent only on specific antibody interactions rather than nonspecific effects. Measurement of the residual 4C1N concentration inside the sensor chamber by cyclic voltammetry (CV) 1 h after the pump was stopped shows only one current peak per curve (i.e., 4C1N can only be irreversibly oxidized) with the height of the oxidation peak (relating to the residual amount of 4C1N remaining in the chamber, Figure S10) correlating inversely with the mass gain signal measured via QCM (Figure 6C).

Figure 7 summarizes the correlation between frequency change signals and concentrations of target molecule (rabbit IgG) using each of the three described strategies (Go-Bt·Av used as the sensor coating in each). Use of the detection antibody lowers the threshold detection limit by ∼1 order of magnitude, whereas use of the HRP-linked antibody in conjunction with 4C1N further reduces the detection limit by another 1−2 orders of magnitude. Specifically, rabbit IgG levels as low as 0.1 ng/mL can be detected using this QCM-based technique accompanied by CV measurement. In comparison, the observed detection limits of IgG using QCM-based methods in papers published within the past decade are 0.05 mg/mL,[60] 5 μg/mL,[61] 62 ng/mL,[62] 46 ng/mL,[63] 15 ng/mL,[64] 10 ng/mL,[65] 3.5 ng/mL,[66] 1 ng/mL,[67] and 5 pg/mL;[37] our method is more sensitive than all but the last report, which employed synthetic magnetic beads and a more complex bienzyme reporting system.

3.6. Sensor Specificity. The specificity of the GO-Bt·Av immunosensor was examined using IgG from sheep serum (sheep IgG, 0.1 μg/mL), IgG from goat serum (goat IgG, 0.1 μg/mL), and a mixture of rabbit IgG (10 ng/mL) and sheep IgG (0.1 μg/mL) using strategy 2 (the detecting antibody approach) for quantification (Figures 8). Neither sheep IgG (Figure 8A) nor goat IgG (Figure 8B) showed any signal when loaded on the antirabbit IgG complexed immunosensor or following incubation with the antirabbit IgG detecting antibody; furthermore, the mixture of rabbit IgG and a 10-fold excess of sheep IgG resulted in a similar frequency change to that associated with 10 ng/mL of rabbit IgG alone (Figure 8C). Thus, the sensor is highly specific for the target rabbit IgG antigen even in the presence of similarly structured competing antigens.

The selectivity of the GO-Bt·Av-based sensor in complex mixtures of proteins was also characterized using human plasma as the background. Rabbit IgG (10 ng/mL) was dissolved in 4 mL of human plasma, and strategy 3 (4C1N precipitation by HRP-anti rabbit IgG detection antibodies) was used to determine the rabbit IgG concentration in the sample (Figure 9). The detected rabbit IgG-related signal was similar to that measured using the same concentration of rabbit IgG in the absence of human plasma, confirming the robustness of this assay against a broad spectrum of competing species. Although a slight binding event is noted following plasma loading that is not observed in the PBS blank (attributable to limited plasma protein adsorption to the surface via competitive adsorption with the BSA blocking protein), the majority of such binding could be washed out in the following step, and no precipitate was observed to form over time after 4C1N was added, maintaining high signal-to-noise for measuring rabbit IgG concentration. Thus, the sensors are both highly selective to the

DOI: 10.1021/acsami.5b10026
ACS Appl. Mater. Interfaces 2016, 8, 1893−1902

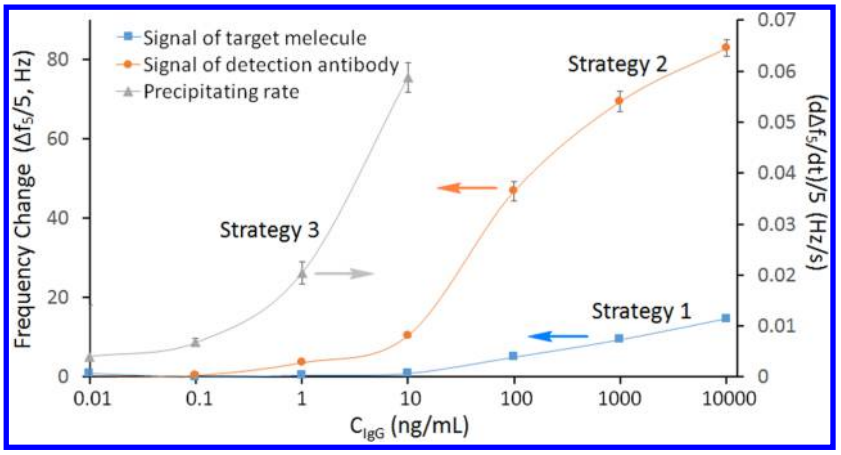

Figure 7. Calibration curve relating the frequency change (left axis, strategies 1 and 2) and the slope of frequency change versus time (right axis, strategy 3) measured via QCM using each of the three detection strategies tested to the concentration of rabbit IgG loaded into the sensor. Error bars indicate the standard deviation of frequency changes obtained simultaneously from two different channels (different sensors) of the Q-Sense E4 QCM; smooth lines connecting data points are guides to the eye.

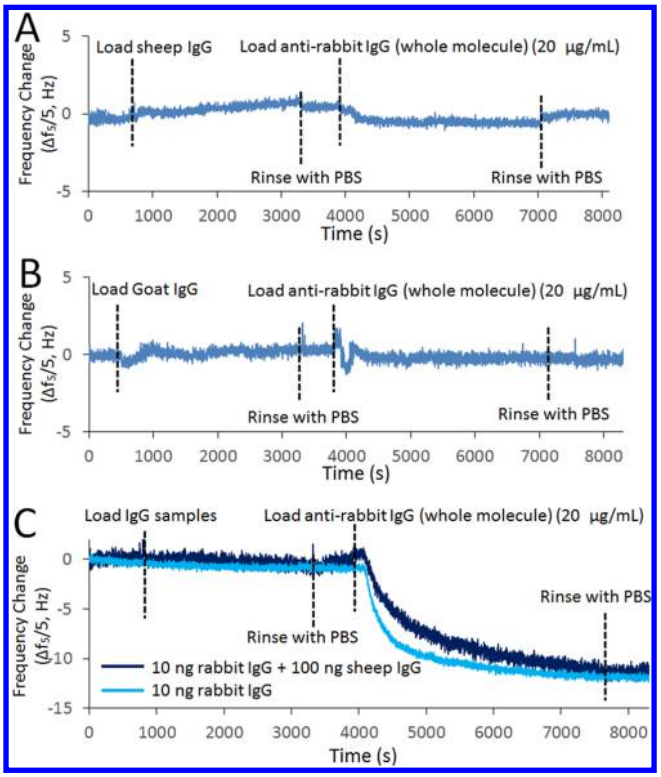

Figure 8. Selectivity of GO-Bt·Av/capture antibody complex-modified gold QCM immunosensor measured via time-dependent frequency changes associated with loading (A) sheep IgG (10 ng/mL), (B) goat IgG (10 ng/mL), and (C) a mixture of rabbit IgG (10 ng/mL) and sheep IgG (100 ng/mL) compared to rabbit IgG (10 ng/mL) alone.

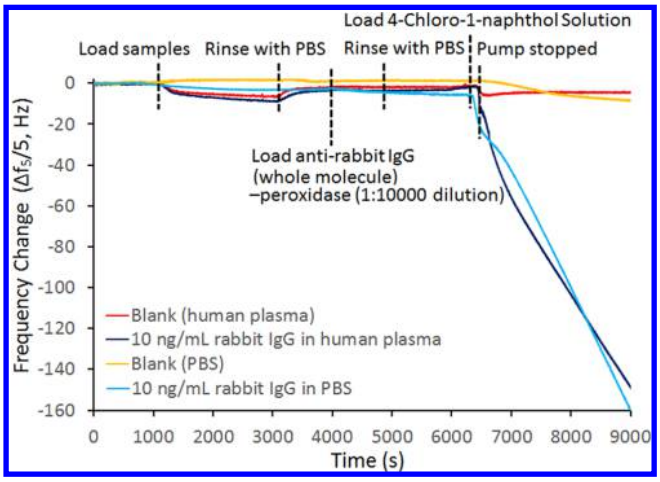

Figure 9. Time-dependent frequency changes associated with loading human plasma, rabbit IgG (10 ng/mL) in human plasma, or rabbit IgG (10 ng/mL) in PBS on a QCM immunosensor using the GO-Bt·Av complex as a support for the antirabbit IgG capture antibody and the HRP-detection antibody catalyzed precipitation of 4-chloro-1-naphthol as the detection strategy. The PBS-only blank is included for reference.

target antigen (even in complex mixtures) and highly sensitive to detect low antigen concentrations.

CONCLUSIONS

We have demonstrated a simple, highly sensitive, and selective flow-based immunosensor based on the functionalization of a gold QCM chip with a graphene oxide-biotin–avidin complex followed by the capture of a biotinylated antibody. Quantification of rabbit IgG at concentrations ranging from 0.1 ng/mL to 10 μg/mL (a 6 orders of magnitude dynamic range) is possible depending on the method used for detection with direct sensing of antigen binding possible at higher concentration ranges and precipitation-based detection antigen strategies used to amplify the measured mass change associated with a single antibody–antigen binding event at lower concentration ranges. The sensor can specifically quantify rabbit IgG in the presence of other types of IgGs as well as complex backgrounds, such as plasma. The fully online strategy to both prepare the functional QCM chip and to perform the immunoassays requires only ~5 h; this time is competitive with most current methods while also avoiding complex chemical functionalization strategies for sensor preparation. In addition, this method is modular in that the same principle may be used to bind any type of biotinylated capture antibody (and thus quantify the corresponding target antigen), allowing broad use of this method for highly sensitive detection of a range of biological targets of interest.

DOI: 10.1021/acsami.5b10026
ACS Appl. Mater. Interfaces 2016, 8, 1893–1902

■ ASSOCIATED CONTENT

Supporting Information

The Supporting Information is available free of charge on the ACS Publications website at DOI: 10.1021/acsami.5b10026.

Standard curve of GO, titration curves of GO and GO-Bt, UV−vis spectrum of GO, GO-Bt and biotin hydrazide, FTIR spectra of biotin hydrazide and avidin, XPS data, additional QCM data, and cyclic voltammograms (PDF)

■ AUTHOR INFORMATION

Corresponding Authors

*E-mail: filipec@mcmaster.ca.

*E-mail: hoaretr@mcmaster.ca.

Notes

The authors declare no competing financial interest.

■ ACKNOWLEDGMENTS

The authors thank the Natural Sciences and Engineering Research Council of Canada (CREATE Biointerfaces Training Program 10532261 and Discovery Grant RGPIN-356609), the Sentinel Bioactive Paper Network (NSERC NETGP 398408), the Canada Foundation for Innovation (Leaders Opportunity Fund Grant #29131), and the Ontario Innovation Trust for financial support.

■ REFERENCES

(1) Butler, J. E. Solid Supports in Enzyme-Linked Immunosorbent Assay and Other Solid-Phase Immunoassays. *Methods* **2000**, *22*, 4−23.

(2) Vandermeeren, M.; Mercken, M.; Vanmechelen, E.; Six, J.; Voorde, A.; Martin, J. J.; Cras, P. Detection of Proteins in Normal and Alzheimer's Disease Cerebrospinal Fluid with a Sensitive Sandwich Enzyme-Linked Immunosorbent Assay. *J. Neurochem.* **1993**, *61*, 1828−1834.

(3) Wide, L. Radioimmunoassays Employing Immunosorbents. *Eur. J. Endocrinol.* **1969**, *62*, S207−S221.

(4) Katus, H. A.; Looser, S.; Hallermayer, K.; Remppis, A.; Scheffold, T.; Borgya, A.; Essig, U.; Geuss, U. Development and in Vitro Characterization of a New Immunoassay of Cardiac Troponin T. *Clin. Chem.* **1992**, *38*, 386−393.

(5) Jung, Y.; Jeong, J. Y.; Chung, B. H. Recent Advances in Immobilization Methods of Antibodies on Solid Supports. *Analyst* **2008**, *133*, 697−701.

(6) Steinitz, M. Quantitation of the Blocking Effect of Tween 20 and Bovine Serum Albumin in ELISA Microwells. *Anal. Biochem.* **2000**, *282*, 232−238.

(7) Löfås, S.; Johnsson, B. A Novel Hydrogel Matrix on Gold Surfaces in Surface Plasmon Resonance Sensors for Fast and Efficient Covalent Immobilization of Ligands. *J. Chem. Soc., Chem. Commun.* **1990**, 1526−1528.

(8) Babacan, S.; Pivarnik, P.; Letcher, S.; Rand, A. Evaluation of Antibody Immobilization Methods for Piezoelectric Biosensor Application. *Biosens. Bioelectron.* **2000**, *15*, 615−621.

(9) Shriver-Lake, L. C.; Donner, B.; Edelstein, R.; Breslin, K.; Bhatia, S. K.; Ligler, F. S. Antibody Immobilization Using Heterobifunctional Crosslinkers. *Biosens. Bioelectron.* **1997**, *12*, 1101−1106.

(10) Kausaite-Minkstimiene, A.; Ramanaviciene, A.; Kirlyte, J.; Ramanavicius, A. Comparative Study of Random and Oriented Antibody Immobilization Techniques on the Binding Capacity of Immunosensor. *Anal. Chem.* **2010**, *82*, 6401−6408.

(11) Karyakin, A. A.; Presnova, G. V.; Rubtsova, M. Y.; Egorov, A. M. Oriented Immobilization of Antibodies onto the Gold Surfaces Via Their Native Thiol Groups. *Anal. Chem.* **2000**, *72*, 3805−3811.

(12) Butler, J.; Ni, L.; Brown, W.; Joshi, K.; Chang, J.; Rosenberg, B.; Voss, E. The Immunochemistry of Sandwich ELISA—Vi. Greater Than 90% of Monoclonal and 75% of Polyclonal Anti-Fluorescyl Capture Antibodies (Cabs) Are Denatured by Passive Adsorption. *Mol. Immunol.* **1993**, *30*, 1165−1175.

(13) Bae, Y. M.; Oh, B.-K.; Lee, W.; Lee, W. H.; Choi, J.-W. Study on Orientation of Immunoglobulin G on Protein G Layer. *Biosens. Bioelectron.* **2005**, *21*, 103−110.

(14) Oh, B.-K.; Chun, B. S.; Park, K.-W.; Lee, W.; Lee, W. H.; Choi, J.-W. Fabrication of Protein G Lb Film for Immunoglobulin G Immobilization. *Mater. Sci. Eng., C* **2004**, *24*, 65−69.

(15) Ngai, P. K.; Ackermann, F.; Wendt, H.; Savoca, R.; Bosshard, H. R. Protein a Antibody-Capture Elisa (Pace): An ELISA Format to Avoid Denaturation of Surface-Adsorbed Antigens. *J. Immunol. Methods* **1993**, *158*, 267−276.

(16) Björck, L.; Kronvall, G. Purification and Some Properties of Streptococcal Protein G, a Novel Igg-Binding Reagent. *J. Immunol.* **1984**, *133*, 969−974.

(17) Eliasson, M.; Andersson, R.; Olsson, A.; Wigzell, H.; Uhlén, M. Differential Igg-Binding Characteristics of Staphylococcal Protein a, Streptococcal Protein G, and a Chimeric Protein Ag. *J. Immunol.* **1989**, *142*, 575−581.

(18) Liu, Y.; Dong, X.; Chen, P. Biological and Chemical Sensors Based on Graphene Materials. *Chem. Soc. Rev.* **2012**, *41*, 2283−2307.

(19) Shao, Y.; Wang, J.; Wu, H.; Liu, J.; Aksay, I. A.; Lin, Y. Graphene Based Electrochemical Sensors and Biosensors: A Review. *Electroanalysis* **2010**, *22*, 1027−1036.

(20) Pumera, M.; Ambrosi, A.; Bonanni, A.; Chng, E. L. K.; Poh, H. L. Graphene for Electrochemical Sensing and Biosensing. *TrAC, Trends Anal. Chem.* **2010**, *29*, 954−965.

(21) Varghese, N.; Mogera, U.; Govindaraj, A.; Das, A.; Maiti, P. K.; Sood, A. K.; Rao, C. Binding of DNA Nucleobases and Nucleosides with Graphene. *ChemPhysChem* **2009**, *10*, 206−210.

(22) Wang, X.; Ouyang, Y.; Li, X.; Wang, H.; Guo, J.; Dai, H. Room-Temperature All-Semiconducting Sub-10-nm Graphene Nanoribbon Field-Effect Transistors. *Phys. Rev. Lett.* **2008**, *100*, 206803.

(23) Jung, J. H.; Cheon, D. S.; Liu, F.; Lee, K. B.; Seo, T. S. A Graphene Oxide Based Immuno-Biosensor for Pathogen Detection. *Angew. Chem., Int. Ed.* **2010**, *49*, 5708−5711.

(24) Song, B.; Li, D.; Qi, W.; Elstner, M.; Fan, C.; Fang, H. Graphene on Au (111): A Highly Conductive Material with Excellent Adsorption Properties for High-Resolution Bio/Nanodetection and Identification. *ChemPhysChem* **2010**, *11*, 585−589.

(25) Abdelhafiz, A.; Vitale, A.; Joiner, C.; Vogel, E.; Alamgir, F. M. Layer-by-Layer Evolution of Structure, Strain, and Activity for the Oxygen Evolution Reaction in Graphene-Templated Pt Monolayers. *ACS Appl. Mater. Interfaces* **2015**, *7*, 6180−6188.

(26) Jalkanen, J.-P.; Halonen, M.; Fernández-Torre, D.; Laasonen, K.; Halonen, L. A Computational Study of the Adsorption of Small Ag and Au Nanoclusters on Graphite. *J. Phys. Chem. A* **2007**, *111*, 12317−12326.

(27) Peluso, P.; Wilson, D. S.; Do, D.; Tran, H.; Venkatasubbaiah, M.; Quincy, D.; Heidecker, B.; Poindexter, K.; Tolani, N.; Phelan, M. Optimizing Antibody Immobilization Strategies for the Construction of Protein Microarrays. *Anal. Biochem.* **2003**, *312*, 113−124.

(28) Diamandis, E. P.; Christopoulos, T. K. The Biotin-(Strept) Avidin System: Principles and Applications in Biotechnology. *Clin. Chem.* **1991**, *37*, 625−636.

(29) Liu, Z.; Jiang, L.; Galli, F.; Nederlof, I.; Olsthoorn, R. C.; Lamers, G. E.; Oosterkamp, T.; Abrahams, J. P. A Graphene Oxide Streptavidin Complex for Biorecognition−Towards Affinity Purification. *Adv. Funct. Mater.* **2010**, *20*, 2857−2865.

(30) Stebunov, Y. V.; Aftenieva, O.; Arsenin, A. V.; Volkov, V. Highly Sensitive and Selective Sensor Chips with Graphene-Oxide Linking Layer. *ACS Appl. Mater. Interfaces* **2015**, *7*, 21727−21734.

(31) Chen, D.; Feng, H.; Li, J. Graphene Oxide: Preparation, Functionalization, and Electrochemical Applications. *Chem. Rev.* **2012**, *112*, 6027−6053.

(32) Ebersole, R. C.; Ward, M. D. Amplified Mass Immunosorbent Assay with a Quartz Crystal Microbalance. *J. Am. Chem. Soc.* **1988**, *110*, 8623−8628.

(33) Cooper, M. A.; Singleton, V. T. A Survey of the 2001 to 2005 Quartz Crystal Microbalance Biosensor Literature: Applications of Acoustic Physics to the Analysis of Biomolecular Interactions. *J. Mol. Recognit.* **2007**, *20*, 154−184.
(34) Mutlu, S. In *Biosensors in Food Processing, Safety, and Quality Control*; Mutlu, M., Ed.; CRC Press: Boca Raton, FL, 2010; Chapter 3, pp 71−88.
(35) Uludag, Y.; Tothill, I. E. Cancer Biomarker Detection in Serum Samples Using Surface Plasmon Resonance and Quartz Crystal Microbalance Sensors with Nanoparticle Signal Amplification. *Anal. Chem.* **2012**, *84*, 5898−5904.
(36) Tang, D.; Zhang, B.; Tang, J.; Hou, L.; Chen, G. Displacement-Type Quartz Crystal Microbalance Immunosensing Platform for Ultrasensitive Monitoring of Small Molecular Toxins. *Anal. Chem.* **2013**, *85*, 6958−6966.
(37) Akter, R.; Rhee, C. K.; Rahman, M. A. A Highly Sensitive Quartz Crystal Microbalance Immunosensor Based on Magnetic Bead-Supported Bienzymes Catalyzed Mass Enhancement Strategy. *Biosens. Bioelectron.* **2015**, *66*, 539−546.
(38) Zhang, X.; Chen, J.; Liu, H.; Zhang, S. Quartz Crystal Microbalance Detection of Protein Amplified by Nicked Circling, Rolling Circle Amplification and Biocatalytic Precipitation. *Biosens. Bioelectron.* **2015**, *65*, 341−345.
(39) Bardea, A.; Katz, E.; Willner, I. Probing Antigen−Antibody Interactions on Electrode Supports by the Biocatalyzed Precipitation of an Insoluble Product. *Electroanalysis* **2000**, *12*, 1097−1106.
(40) Patolsky, F.; Zayats, M.; Katz, E.; Willner, I. Precipitation of an Insoluble Product on Enzyme Monolayer Electrodes for Biosensor Applications: Characterization by Faradaic Impedance Spectroscopy, Cyclic Voltammetry, and Microgravimetric Quartz Crystal Microbalance Analyses. *Anal. Chem.* **1999**, *71*, 3171−3180.
(41) Cheng, C. I.; Chang, Y.-P.; Chu, Y.-H. Biomolecular Interactions and Tools for Their Recognition: Focus on the Quartz Crystal Microbalance and Its Diverse Surface Chemistries and Applications. *Chem. Soc. Rev.* **2012**, *41*, 1947−1971.
(42) Rodahl, M.; Kasemo, B. On the Measurement of Thin Liquid Overlayers with the Quartz-Crystal Microbalance. *Sens. Actuators, A* **1996**, *54*, 448−456.
(43) Sauerbrey, G. Verwendung Von Schwingquarzen Zur Wägung Dünner Schichten Und Zur Mikrowägung. *Eur. Phys. J. A* **1959**, *155*, 206−222.
(44) Huang, M.; He, J. a.; Gan, J.; Ma, H. Solidified Liquid Layer Model Makes Quartz Crystal Microbalance a Convenient Molecular Ruler. *Colloids Surf., B* **2011**, *85*, 92−96.
(45) Bingen, P.; Wang, G.; Steinmetz, N. F.; Rodahl, M.; Richter, R. P. Solvation Effects in the Quartz Crystal Microbalance with Dissipation Monitoring Response to Biomolecular Adsorption. A Phenomenological Approach. *Anal. Chem.* **2008**, *80*, 8880−8890.
(46) Tellechea, E.; Johannsmann, D.; Steinmetz, N. F.; Richter, R. P.; Reviakine, I. Model-Independent Analysis of QCM Data on Colloidal Particle Adsorption. *Langmuir* **2009**, *25*, 5177−5184.
(47) Liu, Q.; Shi, J.; Sun, J.; Wang, T.; Zeng, L.; Jiang, G. Graphene and Graphene Oxide Sheets Supported on Silica as Versatile and High-Performance Adsorbents for Solid-Phase Extraction. *Angew. Chem.* **2011**, *123*, 6035−6039.
(48) Whitby, R. L.; Korobeinyk, A.; Glevatska, K. V. Morphological Changes and Covalent Reactivity Assessment of Single-Layer Graphene Oxides under Carboxylic Group-Targeted Chemistry. *Carbon* **2011**, *49*, 722−725.
(49) Park, S.; Lee, K.-S.; Bozoklu, G.; Cai, W.; Nguyen, S. T.; Ruoff, R. S. Graphene Oxide Papers Modified by Divalent Ions—Enhancing Mechanical Properties Via Chemical Cross-Linking. *ACS Nano* **2008**, *2*, 572−578.
(50) Lapin, N. A.; Chabal, Y. J. Infrared Characterization of Biotinylated Silicon Oxide Surfaces, Surface Stability, and Specific Attachment of Streptavidin. *J. Phys. Chem. B* **2009**, *113*, 8776−8783.
(51) Polyak, B.; Geresh, S.; Marks, R. S. Synthesis and Characterization of a Biotin-Alginate Conjugate and Its Application in a Biosensor Construction. *Biomacromolecules* **2004**, *5*, 389−396.
(52) Xu, Y.; Pharand, L.; Wen, Q.; Gonzaga, F.; Li, Y.; Ali, M. M.; Filipe, C. D.; Pelton, R. Controlling Biotinylation of Microgels and Modeling Streptavidin Uptake. *Colloid Polym. Sci.* **2011**, *289*, 659−666.
(53) Wilchek, M.; Bayer, E. A. The Avidin-Biotin Complex in Bioanalytical Applications. *Anal. Biochem.* **1988**, *171*, 1−32.
(54) Sastry, M.; Lala, N.; Patil, V.; Chavan, S.; Chittiboyina, A. Optical Absorption Study of the Biotin-Avidin Interaction on Colloidal Silver and Gold Particles. *Langmuir* **1998**, *14*, 4138−4142.
(55) Zocchi, A.; Jobé, A. M.; Neuhaus, J.-M.; Ward, T. R. Expression and Purification of a Recombinant Avidin with a Lowered Isoelectric Point in Pichia Pastoris. *Protein Expression Purif.* **2003**, *32*, 167−174.
(56) Xue, T.; Cui, X.; Chen, J.; Liu, C.; Wang, Q.; Wang, H.; Zheng, W. A Switch of the Oxidation State of Graphene Oxide on a Surface Plasmon Resonance Chip. *ACS Appl. Mater. Interfaces* **2013**, *5*, 2096−2103.
(57) Pei, S.; Cheng, H.-M. The Reduction of Graphene Oxide. *Carbon* **2012**, *50*, 3210−3228.
(58) Azzaroni, O.; Mir, M.; Knoll, W. Supramolecular Architectures of Streptavidin on Biotinylated Self-Assembled Monolayers. Tracking Biomolecular Reorganization after Bioconjugation. *J. Phys. Chem. B* **2007**, *111*, 13499−13503.
(59) Seifert, M.; Rinke, M. T.; Galla, H.-J. Characterization of Streptavidin Binding to Biotinylated, Binary Self-Assembled Thiol Monolayers - Influence of Component Ratio and Solvent. *Langmuir* **2010**, *26*, 6386−6393.
(60) Zhang, Y.; Islam, N.; Carbonell, R. G.; Rojas, O. J. Specific Binding of Immunoglobulin G with Bioactive Short Peptides Supported on Antifouling Copolymer Layers for Detection in Quartz Crystal Microgravimetry and Surface Plasmon Resonance. *Anal. Chem.* **2013**, *85*, 1106−1113.
(61) Jaruwongrungsee, K.; Waiwijit, U.; Wisitsoraat, A.; Sangworasil, M.; Pintavirooj, C.; Tuantranont, A. Real-Time Multianalyte Biosensors Based on Interference-Free Multichannel Monolithic Quartz Crystal Microbalance. *Biosens. Bioelectron.* **2015**, *67*, 576−581.
(62) Mizutani, N.; Korposh, S.; Selyanchyn, R.; Wakamatsu, S.; Lee, S.-W. Application of a Quartz Crystal Microbalance (QCM) Twin Sensor for Selective Label-Free Immunoassay to Simultaneous Antigen-Antibody Reactions. *Sens. Transducers J.* **2012**, *137*, 1−9.
(63) Crosson, C.; Rossi, C. Quartz Crystal Microbalance Immunosensor for the Quantification of Immunoglobulin G in Bovinemilk. *Biosens. Bioelectron.* **2013**, *42*, 453−459.
(64) Zhang, Y.; Wang, H.; Yan, B.; Zhang, Y.; Li, J.; Shen, G.; Yu, R. A Reusable Piezoelectric Immunosensor Using Antibody-Adsorbed Magnetic Nanocomposite. *J. Immunol. Methods* **2008**, *332*, 103−111.
(65) Nelson, J. T.; Kim, S.; Reuel, N. F.; Salem, D. P.; Bisker, G.; Landry, M. P.; Kruss, S.; Barone, P. W.; Kwak, S.; Strano, M. S. Mechanism of Immobilized Protein a Binding to Immunoglobulin G on Nanosensor Array Surfaces. *Anal. Chem.* **2015**, *87*, 8186−8193.
(66) Chu, X.; Zhao, Z.-L.; Shen, G.-L.; Yu, R.-Q. Quartz Crystal Microbalance Immunoassay with Dendritic Amplification Using Colloidal Gold Immunocomplex. *Sens. Actuators, B* **2006**, *114*, 696−704.
(67) Ogi, H.; Motohisa, K.; Hatanaka, K.; Ohmori, T.; Hirao, M.; Nishiyama, M. Concentration Dependence of IgG−Protein a Affinity Studied by Wireless-Electrodeless QCM. *Biosens. Bioelectron.* **2007**, *22*, 3238−3242.

DOI: 10.1021/acsami.5b10026
ACS Appl. Mater. Interfaces 2016, 8, 1893−1902

Appendix: Supporting information for Chapter 4

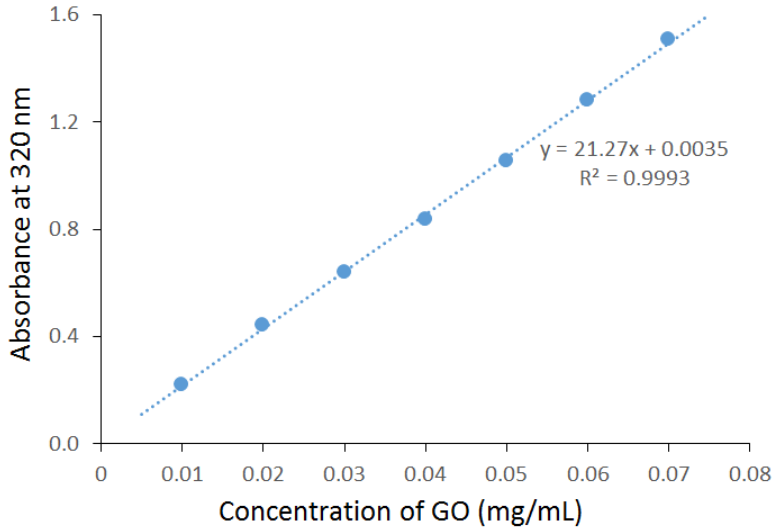

Figure S1. Standard curve of absorbance as a function of GO concentration at the wavelength of 320 nm.

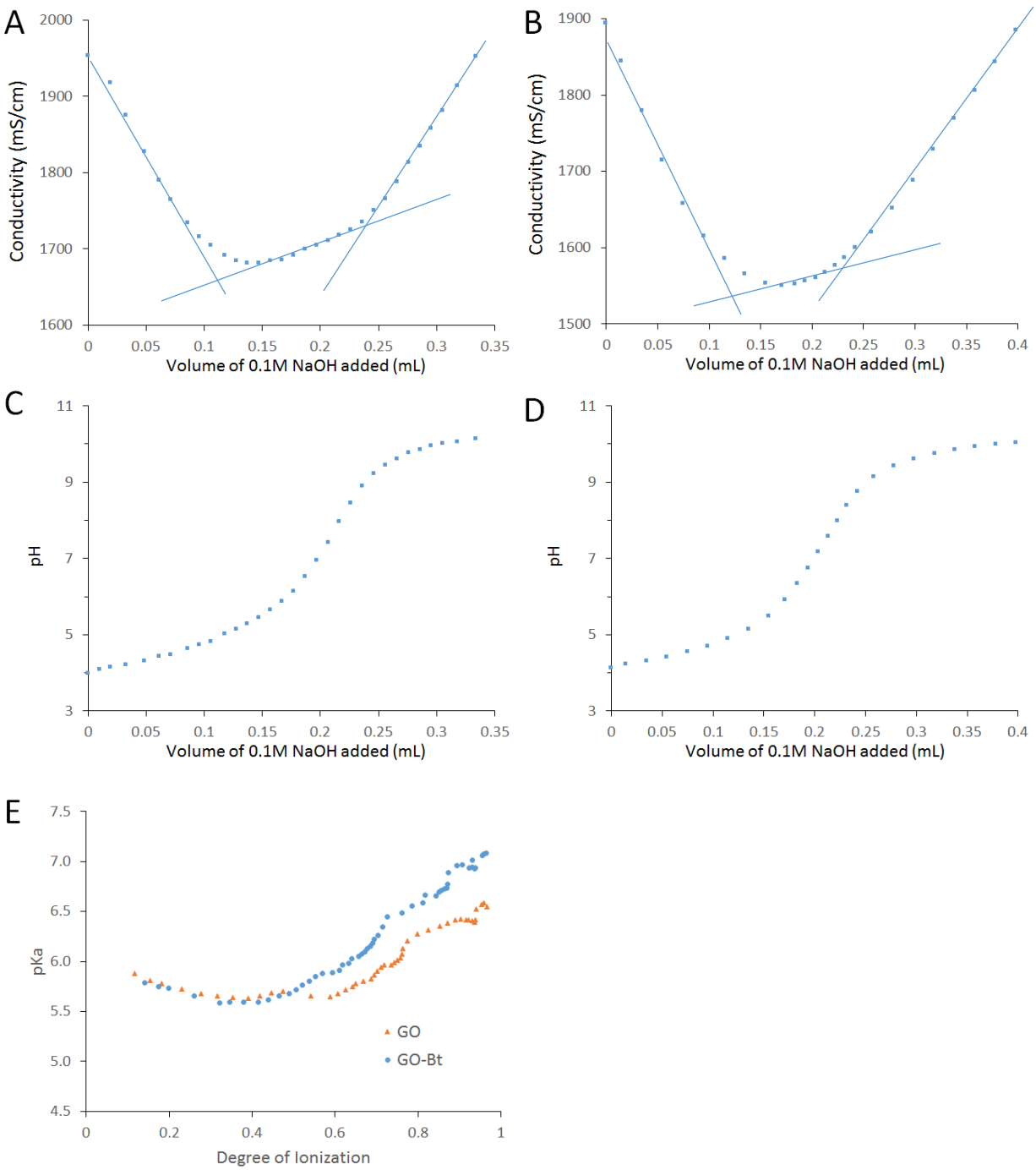

Figure S2. Conductometric and potentiometric titration curves of (A and C) GO and (B and D) GO-Bt and (E) pK_a as a function of degree of ionization for GO and GO-Bt

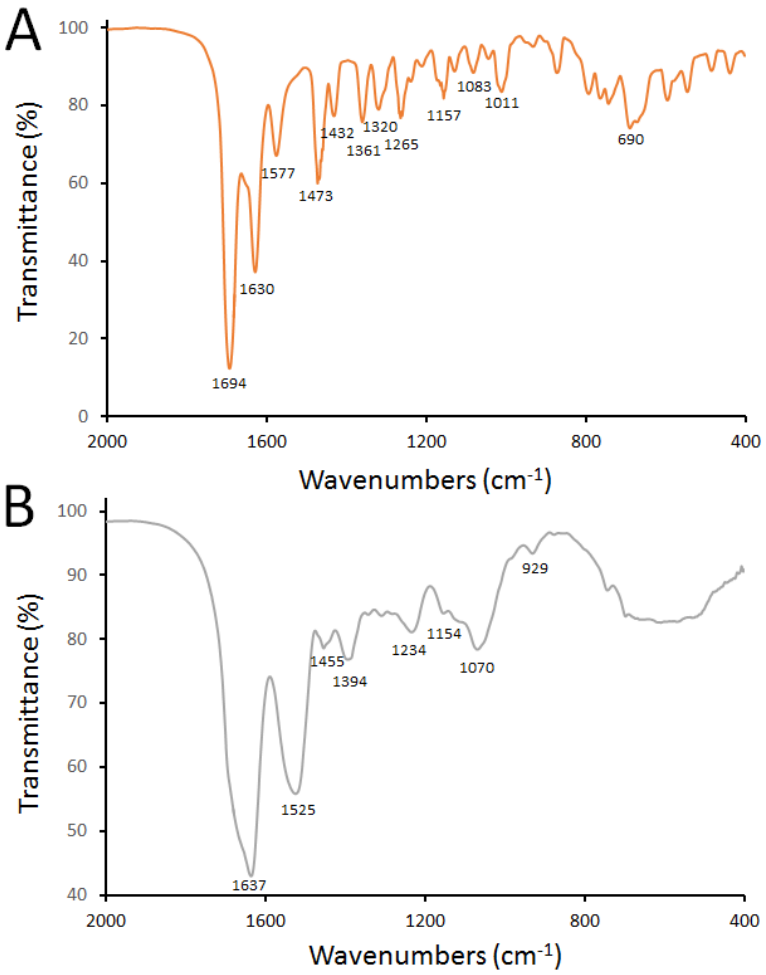

Figure S3. FTIR spectra of (A) (+)-biotin hydrazide alone and (B) avidin alone showing characteristic peaks of each.

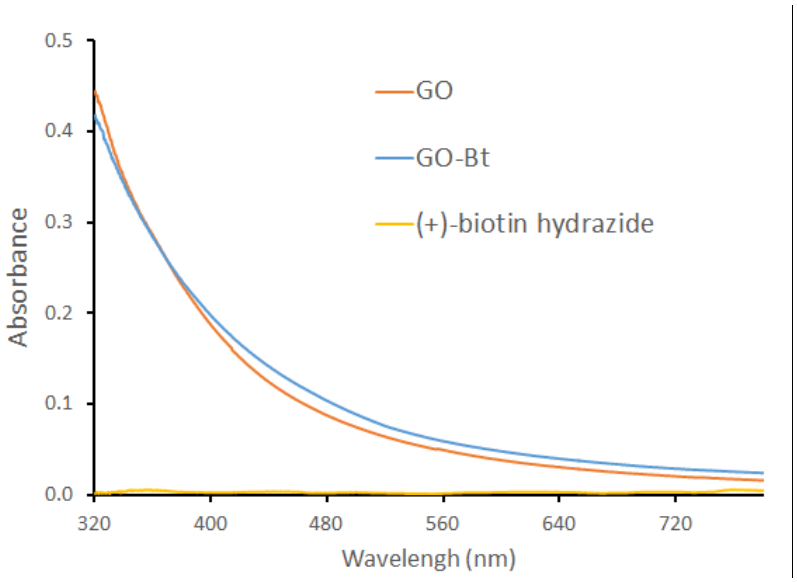

Figure S4. UV-VIS spectrum of GO (0.02 mg/mL), GO-Bt (0.02 mg/mL) and (+)-biotin hydrazide (0.1 mg/mL).

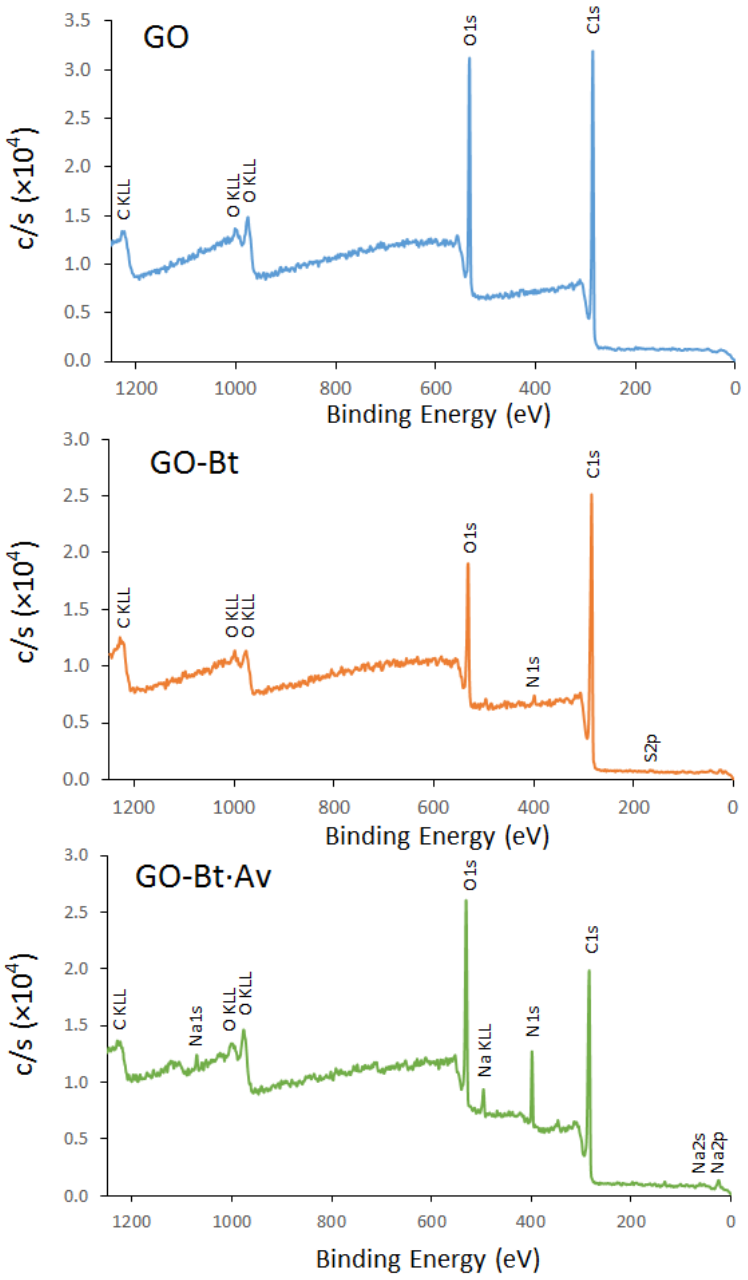

Figure S5. XPS spectra of GO, GO-Bt and the GO-Bt·Av complex.

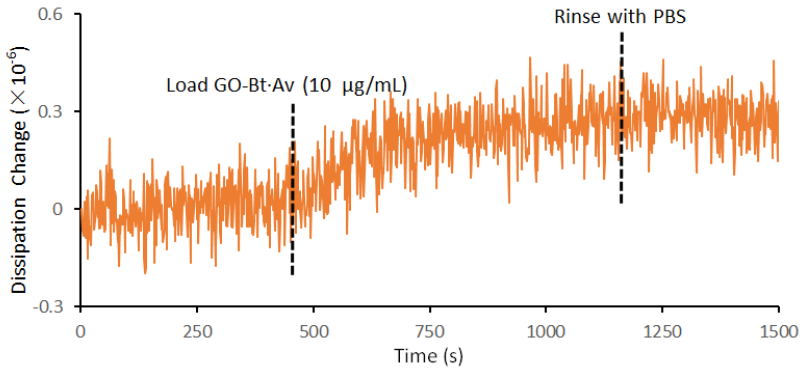

Figure S6. Time-dependent dissipation change associated with loading the GO-Bt·Av complex on a bare gold surface.

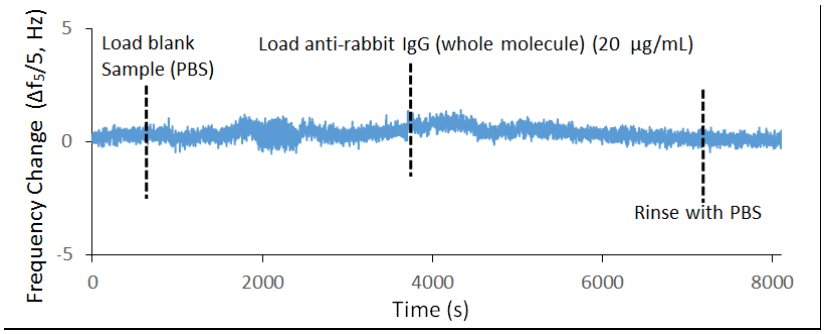

Figure S7. Adsorption of detecting antibody (anti-rabbit IgG, whole molecule) on a BSA-blocked GO-Bt·Av/capture antibody surface confirming no significant non-specific adsorption of detection antibody on the modified surface.

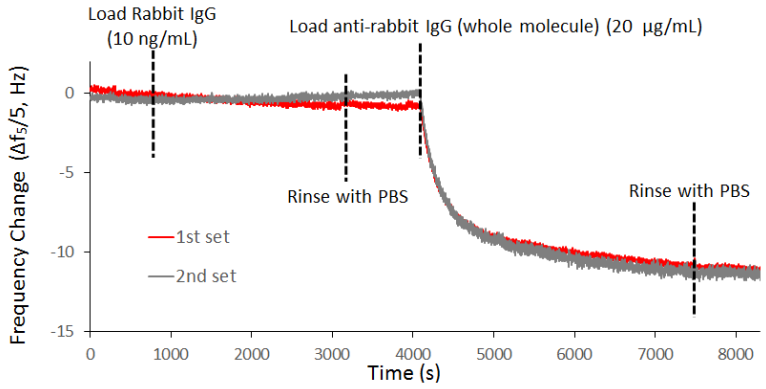

Figure S8. Time-dependent frequency changes associated with sensor performance in detecting 10 ng/mL of rabbit IgG using (set 1) a freshly-prepared GO-Bt·Av and (set 2) a GO-Bt·Av prepared two days prior to the experiment.

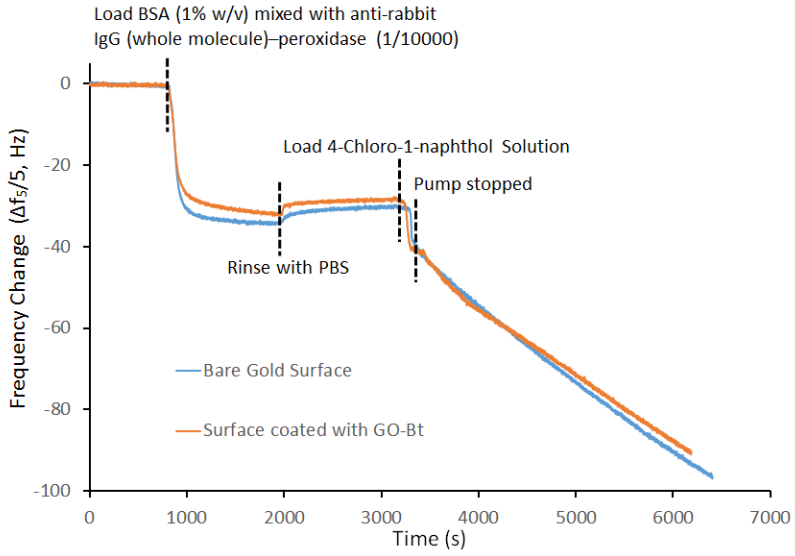

Figure S9. Time-dependent frequency change associated with loading BSA mixed with HRP-linked detecting antibody on a bare gold surface and a GO-Bt surface followed by exposure of the HRP-linked antibody to its substrate, 4-chloro-1-naphthol.

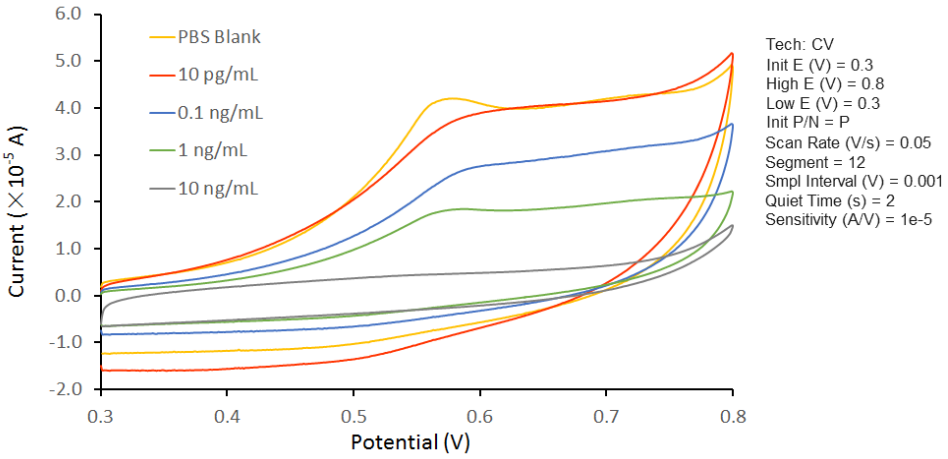

Figure S10. Cyclic voltammograms obtained one hour after loading 4-chloro-1-naphthol on the QCM immunosensor.

Chapter 5 Rapid self-healing of 2-amino phenylboronic acid-functionalized hyaluronic acid/poly(vinyl alcohol) hydrogels at both neutral and acidic pH

In chapter 5, all experiments were conducted by myself with assistance from Ms. Mengsu Chen (undergraduate student). The chapter was initially drafted by myself, and revised later by Dr. Todd Hoare and Dr. Carlos D. M. Filipe.

Abstract: A self-healing hydrogel prepared by mixing 2-aminophenylboronic acid functionalized hyaluronic acid (HA-2APBA) with poly(vinyl alcohol) (PVA) is described. Substantive macroscopic (weight-bearing) and microscopic (rheological) self-healing was observed just one minute following fracture at both neutral and acidic pH, facilitated by both the reversible boronate ester crosslinks as well as the chemical properties of the 2APBA graft.

Key words: self-healing hydrogel, 2-amino phenylboronic acid, hyaluronic acid.

While the general biological compatibility,[1] responsiveness to external stimuli,[2-4] anti-fouling behavior,[5] and degradability[6] of hydrogels have led to their utility in a wide range of applications, the unsatisfactory mechanics of most hydrogels still remains a challenge in many applications.[7] By optimizing the network structure, the mechanical properties of hydrogels have been tuned through using double networks,[8-9] slide-ring connection,[10] ideally homogeneous networks,[11] and dynamic crosslinking approaches.[12-15] Among these approaches, dynamic crosslinking strategy allows breaking and reforming of crosslinking, which contributes to the stretchable and self-healable properties of hydrogels. A particularly interesting type of dynamic covalent bond for the fabrication of hydrogels is the boronic ester bond formed by the reaction of phenylboronic acid (PBA), or its derivatives, with diols.[16-18] An intrinsic disadvantage of this system, however, is that it can only be used at pH values above 8-9 for the boronate esterification, near the pK_a of PBA.[19]

Hyaluronic acid (HA) is a nonsulfated glycosaminoglycan that is distributed widely throughout connective, epithelial, and neural tissues and plays important structural and biological roles in the human body.[20] As such, it is frequently used as a backbone polymer for self-healing polymer structures.[21-24] A recent example reported that HA-3APBA demonstrated gelation with maltose-functionalized HA at physiological pH through boronate-diol interactions.[25] Physiological activity in this case was attributed to the coordination occurring between the carboxylate anion of HA and phenylboronic acid, resulting in reorientation of the boron center from its trigonal to the tetrahedral form and thereby decreasing the effective pK_a of the boronic acid groups. This mechanism of effective pK_a lowering was also observed with a poly(ethylene glycol)(PEG)-block-poly(acrylic acid)(PAA) copolymer modified with PBA (PEG-b-(PAA-*co*-PAAPBA))[26].

Several approaches have been pursued to improve the activity of PBA groups at physiological conditions, primarily aiming to inductively lower the pKa of the PBA group by grafting PBA via electron-donating functional groups (i.e. secondary or tertiary amines)[27] or through using a *p*-amido-substituted boronic acid.[28-29] While *para*-functionalized phenylboronic acids have conventionally been used for grafting, *ortho*-functionalized phenylboronic acids have recently attracted more interest. In particular, if 2-amino phenylboronic acid (2APBA) is conjugated to a carboxylic acid group on a polymer backbone via an amide linkage, intramolecular coordination

is observed between the carbonyl oxygen and the boron of the boronic acid group (Scheme 1).[30-31] This intramolecular B-O coordination maintains the boron center in a favorable tetrahedral form for boronate-*cis* diol interactions at neutral and even acidic pH values, facilitating dynamic covalent crosslinking at physiologically-relevant conditions without the need for additional functionalization.[30]

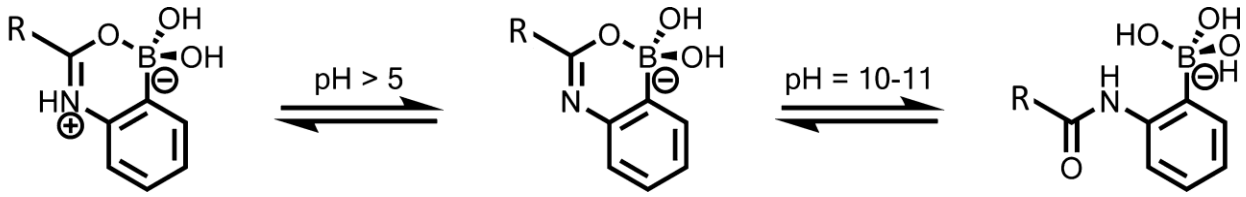

Scheme 1. Equilibrium of amidated 2-amino phenylboronic acid (2APBA) in water. Intramolecular B−O bond formation leads to the formation of tetrahedral geometry at the boron center that promotes boronate ester formation. (Scheme reproduced from Ref.[30-31])

Taking advantage of this potential for intramolecular coordination with 2APBA, we herein report the preparation and self-healing properties of a hydrogel prepared by simple mixing of 2APBA-conjugated HA and poly(vinyl alcohol) (PVA), a polymer in which every repeat unit has a pendant alcohol group and thus can bind strongly with *cis*-diol binding PBA groups.[18] 2APBA-modified HA (HA-2APBA) was obtained via a conjugation reaction performed in aqueous buffer between HA (M_w = 330 kDa) and 2-amino phenylboronic acid mediated by 1-ethyl-3-(3-dimethylaminopropyl)carbodiimide hydrochloride (EDC) (Scheme 2). The degree of substitution (DS) of the HA-2APBA conjugate was determined to be 15% from ^{1}H NMR analysis (Figure S1), leaving ~85% of $–COO^-$ groups on HA free to also complex with grafted PBA groups.

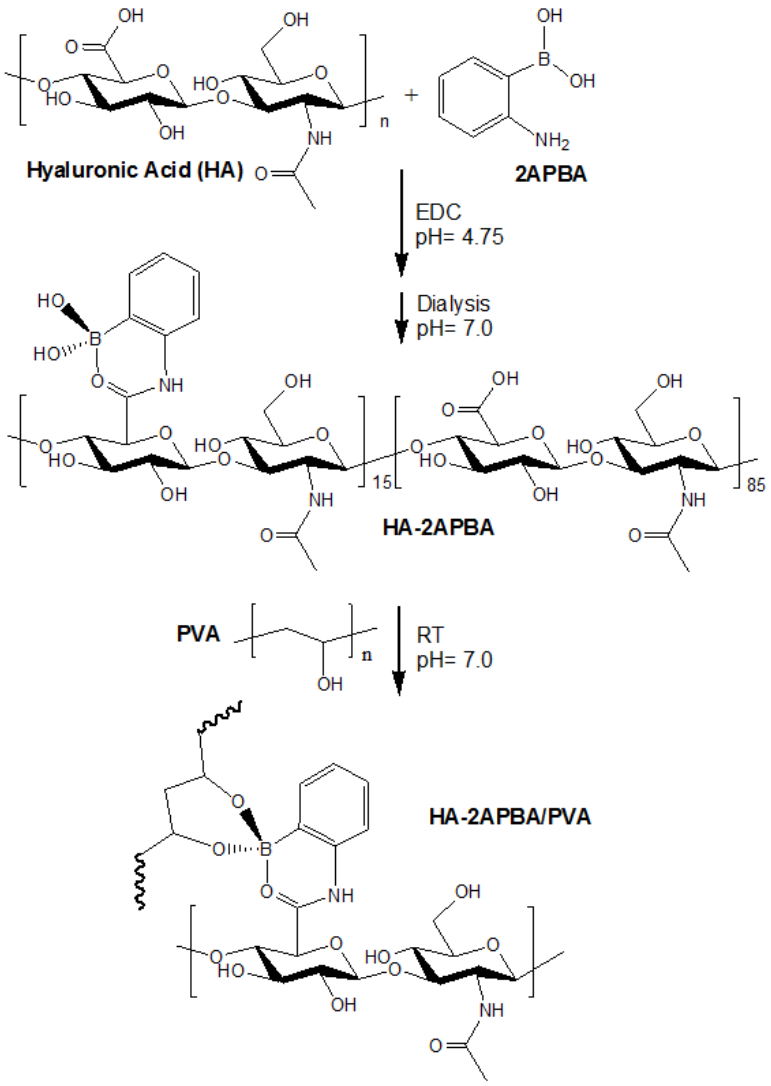

Scheme 2. Synthesis of HA-2APBA and hypothesized mechanism of hydrogel formation between HA-2APBA with PVA at neutral pH.

Hydrogels were subsequently formed by simple mixing of 1 wt% solutions of HA-2APBA with PVA in buffers with pH 4.0 (acetate buffer 0.2M), 5.5 (acetate buffer 0.2M), and 7.0 (Tris buffer 0.1 M). Hydrogel formation was qualitatively confirmed through a vial inversion test (Figure 1). At pH 4.0, 5.5 and 7.0, gelation occurred immediately after mixing, suggesting effective boronate ester formation under both acidic and neutral conditions facilitated by the combined effects of intramolecular 2APBA coordination (likely prelevalent) and carboxylate coordination to the boronic acid center (Scheme 2)

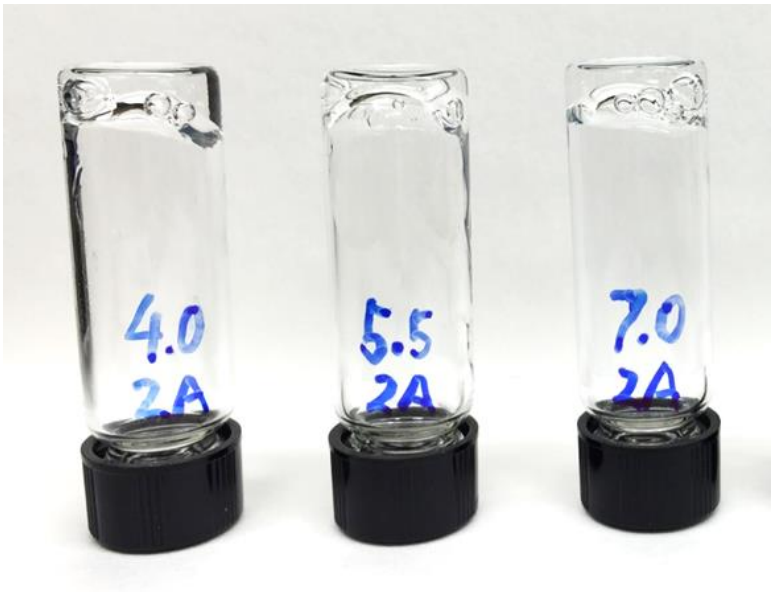

Figure 1. HA-2APBA/PVA hydrogel formation (1 wt% solutions) in pH 4.0, 5.5, and 7.0 buffer.

Given that cross-linking within the hydrogel was expected to be dynamic-covalent as a result of the rapid exchange between boronate ester formation and hydrolysis,[32-33] the self-healing characteristics of the gels were subsequently investigated using a more rigid gel that can more rigorously maintain its macroscopic dimensions and be handled with tweezers (3 wt% of both polymer) in the context of a qualitative recovery test. In this test, a hydrogel disk that was cut in half using a scalpel and then moved back into contact showed rapid healing (within one minute) at both pH 4.0 (Figure 2) and 7.0 (Figure 3), as evidenced by the rapid disappearance of the scar at the damage site. Throughout the healing process, the remainder of the gels retained their macroscopic dimensions (indicating that healing is not simply a result of flow); furthermore, the healed gels were strong enough to support their own weight when suspended just one minute following being moved back into contact (Figures 2D and 3D). The lower rigidity of the pH 4 gel relative to the pH 7 gel (as evidenced by the deformation observed in the pH 4 gels following cutting, Figs 2A and 2B) results in faster dynamic bond exchange during self-healing, leading to the improved visual healing of the cut at the 1 minute time point analyzed.

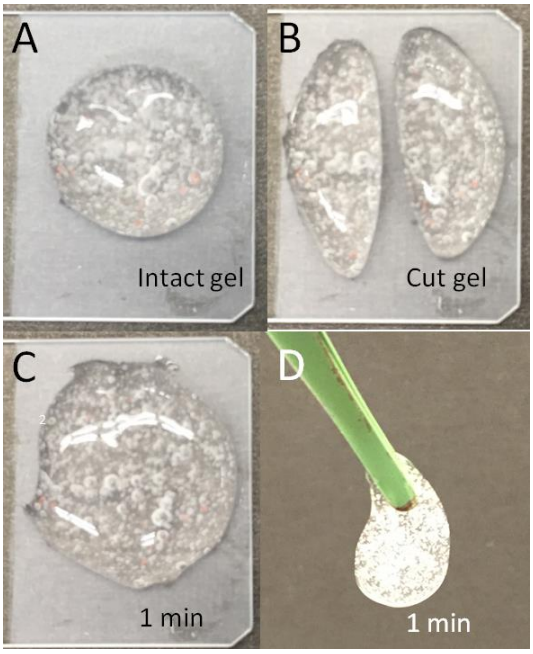

Figure 2. Self-healing of hydrogels formed by cross-linking HA-2APBA with PVA (both 30 mg/mL) at pH 4.0 (acetate buffer 0.2M): (A) intact gel; (B) cut gel; (C) gel halves placed in contact for one minute after cutting; (D) healed gel suspended under its own weight.

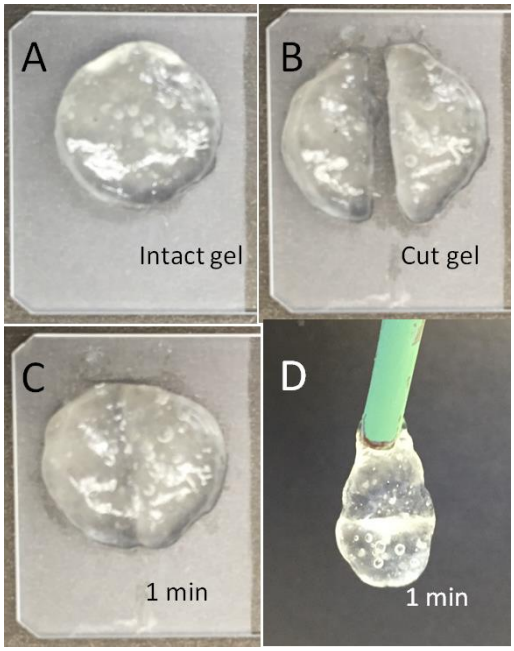

Figure 3. Self-healing of hydrogels formed by cross-linking HA-2APBA with PVA (both 30 mg/mL) at pH 7.0 (Tris buffer 0.1 M): (A) intact gel; (B) cut gel; (C) gel halves placed in contact for one minute after cutting; (D) healed gel suspended under its own weight.

The mechanics and self-healing capacity of the HA-2APBA/PVA system were further analyzed by a series of dynamic rheological experiments tracking the shear storage modulus (G') of HA-2APBA/PVA hydrogel as a function of frequency (Figure S2). A strain sweep healing test was conducted by switching the applied strain from being relatively small (1.468° rotation, 1.468 Hz) to large (to disrupt the gel structure: 29.36° rotation, 1.468 Hz, 10 cycles), back to small (to track self-healing: 1.468° @ 1.468 Hz), the results of which for the pH 7 hydrogel are shown in Figure 4. Introduction of the larger shear coincides with a decrease in the measured G' value from ~800 Pa to ~350 Pa, indicating disruption of cross-links within the hydrogel. However, following a return to a low-shear condition, the gel exhibited nearly complete self-healing behavior within one minute, consistent with macroscopic observations in Figure 3 for the same hydrogels. Collectively, these results suggest the potential of boronate ester formation across the damaged interface to rapidly heal both small and large defects in HA-2APBA/PVA hydrogels.

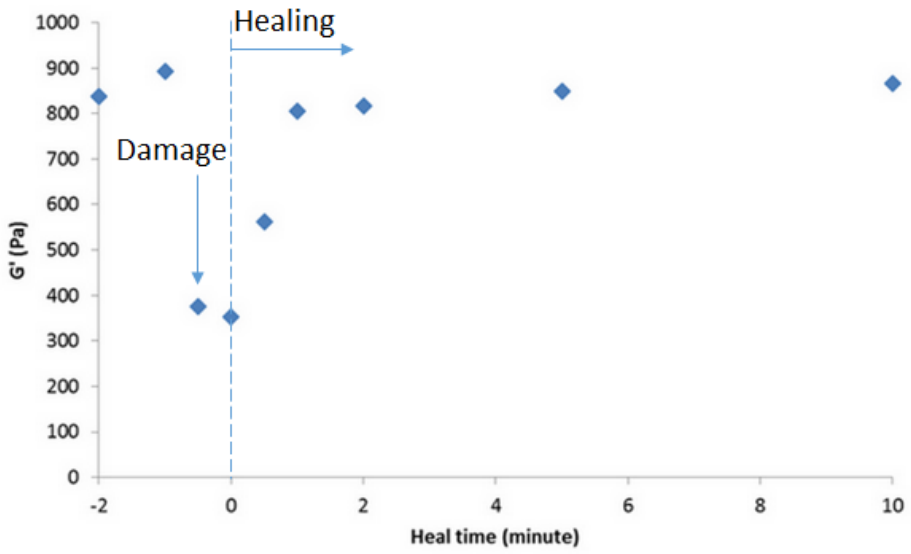

Figure 4. Rheological properties of HA-2APBA/PVA hydrogels (3 wt% of both polymers, pH 7.0) when response to a strain sweep initiated at low shear (1.468° rotation, 1.468 Hz) followed by the application of high shear (29.36° rotation, 1.468 Hz, 10 cycles - indicated as Damage in the figure), and then return to low shear (1.468° rotation, 1.468 Hz - indicated as Healing in the figure).

In conclusion, this study provides a convenient method to prepare dynamic covalent hydrogels based on simple mixing of HA-2APBA and PVA that can both form and rapidly self-heal in physiologically-relevant conditions. The hydrogel's ability to form a transient network at both

neutral and acidic pH values is attributed to the intramolecular coordination within 2APBA grafts, which act to stabilize the high-binding affinity tetrahedral geometry at the boron center. Self-healing was both rapid (<1 minute) and effective in terms of resulting in the hydrogel's ability to support its own weight following macroscopic breaks and recover its storage modulus following microscale fractures in this very short time frame. Such fast and complete self-healing achievable over a broad pH suggests additional possible applications of boronate ester hydrogels as biological materials, with the stability of the gel at both low and neutral pH values suggesting possible applications in the gastrointestinal tract or as intestinal mucoadhesives that can be easily delivered by flow-based techniques. The conjugation and gel formation method could also be applied to various carboxylate-containing polysaccharides, giving access to new classes of self-healing and biologically-relevant gel materials.

ASSOCIATED CONTENT

*S Supporting Information

A list of materials and chemicals used, a detailed synthesis protocol for HA-2APBA, a ^{1}H NMR spectrum of HA-2APBA, and full methodology for rheological testing as well as additional frequency-dependent mechanical tests on the described gels are all provided.

References

(1) Cushing, M. C.; Anseth, K. S. Hydrogel Cell Cultures. *Science* **2007,** *316*, 1133-1134.
(2) Hu, J.; Zhang, G.; Liu, S. Enzyme-Responsive Polymeric Assemblies, Nanoparticles and Hydrogels. *Chemical Society Reviews* **2012,** *41*, 5933-5949.
(3) Tokarev, I.; Minko, S. Stimuli-Responsive Hydrogel Thin Films. *Soft Matter* **2009,** *5*, 511-524.
(4) Tokarev, I.; Minko, S. Stimuli-Responsive Porous Hydrogels at Interfaces for Molecular Filtration, Separation, Controlled Release, and Gating in Capsules and Membranes. *Advanced materials* **2010,** *22*, 3446-3462.
(5) Kostina, N. Y.; Rodriguez-Emmenegger, C.; Houska, M.; Brynda, E.; Michálek, J. í. Non-Fouling Hydrogels of 2-Hydroxyethyl Methacrylate and Zwitterionic Carboxybetaine (Meth) Acrylamides. *Biomacromolecules* **2012,** *13*, 4164-4170.
(6) Park, M. H.; Joo, M. K.; Choi, B. G.; Jeong, B. Biodegradable Thermogels. *Acc. Chem. Res.* **2011,** *45*, 424-433.
(7) Tanaka, Y.; Gong, J. P.; Osada, Y. Novel Hydrogels with Excellent Mechanical Performance. *Progress in Polymer Science* **2005,** *30*, 1-9.
(8) Gong, J. P. Why Are Double Network Hydrogels So Tough? *Soft Matter* **2010,** *6*, 2583-2590.

(9) Gong, J. P.; Katsuyama, Y.; Kurokawa, T.; Osada, Y. Double-Network Hydrogels with Extremely High Mechanical Strength. *Advanced Materials* **2003,** *15*, 1155-1158.
(10) Mayumi, K.; Ito, K. Structure and Dynamics of Polyrotaxane and Slide-Ring Materials. *Polymer* **2010,** *51*, 959-967.
(11) Sakai, T.; Matsunaga, T.; Yamamoto, Y.; Ito, C.; Yoshida, R.; Suzuki, S.; Sasaki, N.; Shibayama, M.; Chung, U.-i. Design and Fabrication of a High-Strength Hydrogel with Ideally Homogeneous Network Structure from Tetrahedron-Like Macromonomers. *Macromolecules* **2008,** *41*, 5379-5384.
(12) Cui, J.; del Campo, A. Multivalent H-Bonds for Self-Healing Hydrogels. *Chemical Communications* **2012,** *48*, 9302-9304.
(13) Lin, P.; Ma, S.; Wang, X.; Zhou, F. Molecularly Engineered Dual-Crosslinked Hydrogel with Ultrahigh Mechanical Strength, Toughness, and Good Self-Recovery. *Advanced Materials* **2015,** *27*, 2054-2059.
(14) Nakahata, M.; Takashima, Y.; Yamaguchi, H.; Harada, A. Redox-Responsive Self-Healing Materials Formed from Host–Guest Polymers. *Nature communications* **2011,** *2*, 511.
(15) Tuncaboylu, D. C.; Sari, M.; Oppermann, W.; Okay, O. Tough and Self-Healing Hydrogels Formed Via Hydrophobic Interactions. *Macromolecules* **2011,** *44*, 4997-5005.
(16) Cambre, J. N.; Sumerlin, B. S. Biomedical Applications of Boronic Acid Polymers. *Polymer* **2011,** *52*, 4631-4643.
(17) Cheng, F.; Jäkle, F. Boron-Containing Polymers as Versatile Building Blocks for Functional Nanostructured Materials. *Polymer Chemistry* **2011,** *2*, 2122-2132.
(18) Guan, Y.; Zhang, Y. Boronic Acid-Containing Hydrogels: Synthesis and Their Applications. *Chemical Society Reviews* **2013,** *42*, 8106-8121.
(19) Ivanov, A.; Larsson, H.; Galaev, I. Y.; Mattiasson, B. Synthesis of Boronate-Containing Copolymers of N, N-Dimethylacrylamide, Their Interaction with Poly (Vinyl Alcohol) and Rheological Behaviour of the Gels. *Polymer* **2004,** *45*, 2495-2505.
(20) Dicker, K. T.; Gurski, L. A.; Pradhan-Bhatt, S.; Witt, R. L.; Farach-Carson, M. C.; Jia, X. Hyaluronan: A Simple Polysaccharide with Diverse Biological Functions. *Acta biomaterialia* **2014,** *10*, 1558-1570.
(21) Highley, C. B.; Rodell, C. B.; Burdick, J. A. Direct 3d Printing of Shear-Thinning Hydrogels into Self-Healing Hydrogels. *Advanced Materials* **2015,** *27*, 5075-5079.
(22) Nejadnik, M. R.; Yang, X.; Bongio, M.; Alghamdi, H. S.; Van den Beucken, J. J.; Huysmans, M. C.; Jansen, J. A.; Hilborn, J.; Ossipov, D.; Leeuwenburgh, S. C. Self-Healing Hybrid Nanocomposites Consisting of Bisphosphonated Hyaluronan and Calcium Phosphate Nanoparticles. *Biomaterials* **2014,** *35*, 6918-6929.
(23) Rodell, C. B.; MacArthur, J. W.; Dorsey, S. M.; Wade, R. J.; Wang, L. L.; Woo, Y. J.; Burdick, J. A. Shear-Thinning Supramolecular Hydrogels with Secondary Autonomous Covalent Crosslinking to Modulate Viscoelastic Properties in Vivo. *Advanced functional materials* **2015,** *25*, 636-644.

(24) Rodell, C. B.; Kaminski, A. L.; Burdick, J. A. Rational Design of Network Properties in Guest–Host Assembled and Shear-Thinning Hyaluronic Acid Hydrogels. *Biomacromolecules* **2013,** *14*, 4125-4134.
(25) Tarus, D.; Hachet, E.; Messager, L.; Catargi, B.; Ravaine, V.; Auzély-Velty, R. Readily Prepared Dynamic Hydrogels by Combining Phenyl Boronic Acid-and Maltose-Modified Anionic Polysaccharides at Neutral Ph. *Macromolecular rapid communications* **2014,** *35*, 2089-2095.
(26) Wang, B.; Ma, R.; Liu, G.; Liu, X.; Gao, Y.; Shen, J.; An, Y.; Shi, L. Effect of Coordination on the Glucose-Responsiveness of Peg-B-(Paa-Co-Paapba) Micelles. *Macromolecular rapid communications* **2010,** *31*, 1628-1634.
(27) Kim, K. T.; Cornelissen, J. J.; Nolte, R. J.; Hest, J. C. v. Polymeric Monosaccharide Receptors Responsive at Neutral Ph. *Journal of the American Chemical Society* **2009,** *131*, 13908-13909.
(28) Matsumoto, A.; Ikeda, S.; Harada, A.; Kataoka, K. Glucose-Responsive Polymer Bearing a Novel Phenylborate Derivative as a Glucose-Sensing Moiety Operating at Physiological Ph Conditions. *Biomacromolecules* **2003,** *4*, 1410-1416.
(29) Roy, D.; Sumerlin, B. S. Glucose-Sensitivity of Boronic Acid Block Copolymers at Physiological Ph. *ACS Macro Letters* **2012,** *1*, 529-532.
(30) Deng, C. C.; Brooks, W. L.; Abboud, K. A.; Sumerlin, B. S. Boronic Acid-Based Hydrogels Undergo Self-Healing at Neutral and Acidic Ph. *ACS Macro Letters* **2015,** *4*, 220-224.
(31) Yang, X.; Lee, M. C.; Sartain, F.; Pan, X.; Lowe, C. R. Designed Boronate Ligands for Glucose-Selective Holographic Sensors. *Chemistry–A European Journal* **2006,** *12*, 8491-8497.
(32) Cash, J. J.; Kubo, T.; Bapat, A. P.; Sumerlin, B. S. Room-Temperature Self-Healing Polymers Based on Dynamic-Covalent Boronic Esters. *Macromolecules* **2015,** *48*, 2098-2106.
(33) Bapat, A. P.; Roy, D.; Ray, J. G.; Savin, D. A.; Sumerlin, B. S. Dynamic-Covalent Macromolecular Stars with Boronic Ester Linkages. *Journal of the American Chemical Society* **2011,** *133*, 19832-19838.

Appendix: Supporting information for Chapter 5

Chemicals

Sodium hyaluronate (Lot# 010600, M_n = 336.8 kDa, Đ = 1.386 by GPC, see Appendix of Chapter 3) was obtained from Fidia Farmaceutici S.p.A. (Abano Terme, Italy). N-ethyl-N'-(3-dimethylaminopropyl) carbodiimide hydrochloride (EDC, 98%), 2-amino phenylboronic acid hydrochloride (2APBA, 95%), poly(vinyl alcohol) (PVA) (M_w 85,000-124,000, 99+% hydrolyzed), 2-(N-morpholino)ethanesulfonic acid (MES) hydrate (99.5%) were all purchased from Sigma-Aldrich and were used without further purification. The water used in all experiments was purified by a MilliQ purification system, with a resistivity of at least 18.2 MΩ cm.

Buffer preparation

Acetate buffer 0.2 M at pH 4.0: mix 18 mL of 0.2 M sodium acetate solution with 82 mL of 0.2 M acetic acid solution.

Acetate buffer 0.2 M at pH 5.5: mix 89 mL of 0.2 M sodium acetate solution with 11 mL of 0.2 M acetic acid solution.

Tris buffer 0.1 M at pH 7.0: dissolve 1.2114 g of Tris into 100 mL MilliQ water and adjust pH to 7.0 by adding 0.1M HCl or 0.1M NaOH.

Synthesis and characterization of HA-2APBA

HA (100 mg) was dissolved in 100 mL of 10 mM MES buffer. An aqueous solution of EDC (95.8 mg) was added into the solution, and the pH was adjusted to 4.75 by the addition of 1 M NaOH. After waiting for 10 min, 2APBA (258.8 mg) was then added into the mixture, and the pH of the reaction mixture was maintained at 4.75 by addition of 0.1 M NaOH or HCl. The reaction was allowed to proceed at room temperature until no further change in pH was observed (~4 hours). The reaction was stopped by addition of 0.1 M NaOH in order to adjust the pH of the mixture to 7.0. The modified HA was then purified by dialysis against a large excess of water using a prewashed dialysis membrane tube (MWCO = 14 kDa). The dialysis was stopped when the conductivity of the dialysate was less than 5 μS cm^{-1}, after which the HA-2APBA product was recovered by freeze-drying. ^{1}H-NMR of HA-2APBA was performed on a Bruker AVANCE 600 MHz spectrometer using D_2O (D, 99.96%, Cambridge Isotope Laboratories, Inc.) as the solvent. Digital integration of the NMR signals arising from the anomeric protons of HA and protons of the PBA group indicated a substitution degree of 0.15 ± 0.01 per disaccharide repeat unit.

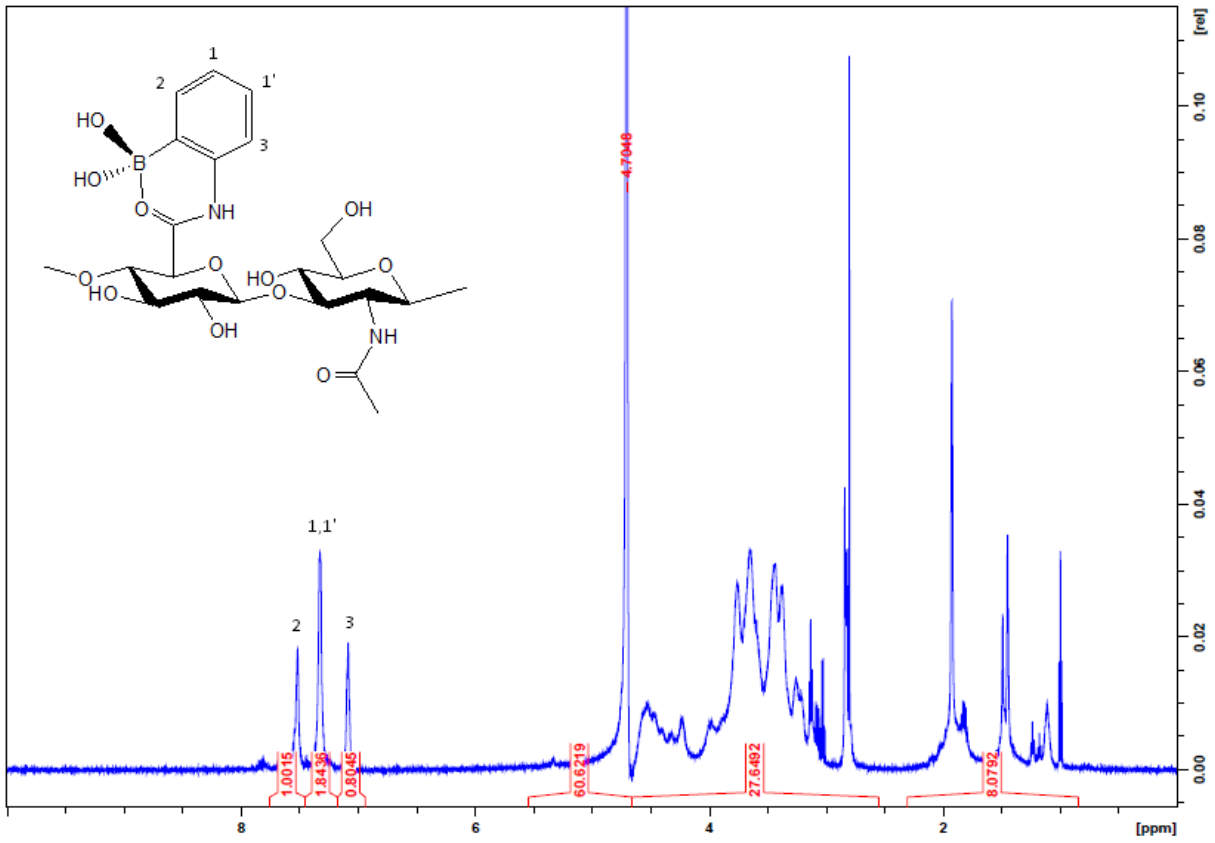

Figure S1. ^{1}H NMR spectrum (600 MHz) of 2APBA-modified hyaluronic acid (HA-2APBA, DS = 0.15, 6 mg mL^{-1} in D_2O).

Rheological testing

The rheological properties of the hydrogel were characterized using a Mach-1 Mechanical Tester (Biomomentum Inc., Laval, QC) operating under parallel plate geometry at room temperature. Hydrogel disks (diameter = 11.5 mm, height = 3.5 mm) were allowed to gel overnight and then transferred from the silicone mold to the mechanical tester. Shear testing was performed by pre-compressing the gels to 75% of the sample height and subsequently subjecting them to a strain sweep test using amplitudes ranging from 0.1 to 2.2° at 0.5 Hz to determine the linear viscoelastic region (LVE) of the gel. The gel were subsequently subjected to a dynamic frequency sweep (0.1 to 2.2 Hz) within the linear viscoelastic range (LVE) to determine their shear storage modulus (G'), see Figure S2. All experiments were repeated in triplicate; reported results represent the average of these replicates, with error bars representing one standard deviation from the mean.

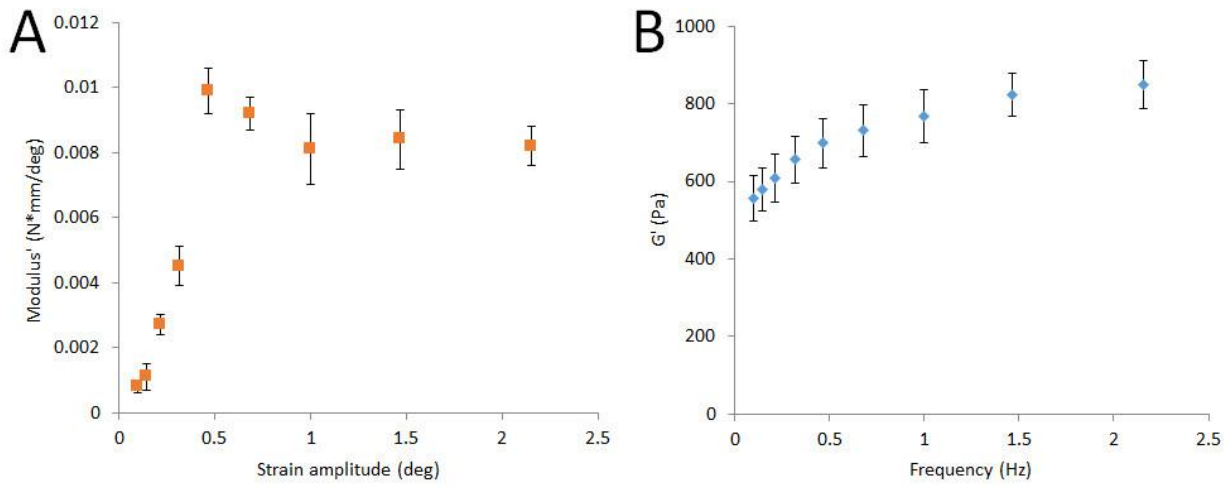

Figure S2. Rheological properties of HA-2APBA/PVA hydrogels (3 wt% of both polymers, pH 7.0) (A) modulus as a function of strain amplitude (0.1-2.1 degrees) to find the linear viscoelastic region; (B) shear storage modulus (G') over a frequency sweep (0.1 – 2.1 Hz) within the gel's linear viscoelastic region (1.5 degree strain amplitude).

Chapter 6 Concluding remarks

6.1 Summary of work

This work focuses on the engineering of biological interfaces to promote non-specific protein adsorption, functional grafting of active proteins, and/or dynamic crosslinking responsive to environmental stimuli. The detailed major contributions of this work are given as follows:

1. An effective surface modification of paper via a simple, scalable, and mild dip-coating procedure has been demonstrated. A POEGMA hydrogel coating layer, generated from sequentially dipping in solutions of aldehyde and hydrazide functionalized POEGMA precursor polymers, was successfully formed around cellulose fibers *in situ* and has been demonstrated to significantly suppress nonspecific protein adsorption to paper without impacting the fiber morphology or paper macroporosity. The dip-coated paper was subsequently used as a platform for the construction of lateral flow enzyme assays and enzyme-linked immunoassays with lower non-specific protein adsorption and thus higher sensitivity. Based on this proof-of-concept, this same approach has potential to be employed in the design and fabrication of complex biosensors, bio-arrays, and other high-throughput tests where protein transport is essential.

2. A simple "click" chemistry-based approach was developed to surface functionalize poly(2-hydroxyethyl methacrylate) (PHEMA)-based contact lenses with hyaluronic acid (HA). A two-step preparation technique consisting of laccase/TEMPO-mediated oxidation of PHEMA followed by covalent grafting of hydrazide-functionalized HA via simple immersion resulted in a model lens surface that is significantly more wettable, more water-retentive, and less protein binding than unmodified PHEMA while maintaining the favorable transparency, refractive, and mechanical properties of a native lens. The coating method we developed to covalently tether the HA wetting agent is a simple, readily scalable, and highly efficient route for contact lens modification.

3. A high-sensitivity flow-based immunoassay was developed on a gold-coated quartz crystal microbalance (QCM) chip functionalized directly via the irreversible adsorption of a biotinylated graphene oxide-avidin complex followed by loading of a biotinylated capture antibody. The whole process, which takes only 5 hours in total, does not need conventional complex surface modification chemistries. The resulting immunosensors exhibit significantly lower non-specific protein adsorption and stronger signal for antigen sensing relative to simple avidin-coated sensors. Quantification of rabbit IgG concentrations ranging from 0.1 ng/mL to 10 μg/mL can be achieved by tracking mass changes, either directly as a result of protein binding at higher concentrations or via a signal amplification method to detect very low analyte concentrations. Quantitative detection can be achieved

even in the presence of complex protein mixtures such as human plasma. The broad availability of biotinylated capture antibodies enables the application of this method as an easy and flexible platform for the quantitative detection of a variety of biomolecule targets.

4. A novel method for synthesizing fast self-healing hydrogels through dynamic crosslinking has been developed. This method employs two precursors, namely 2-aminophenylboronic acid-modified hyaluronic acid and poly(vinyl alcohol), to form a gel following simple mixing. The hydrogel is able to heal both macroscopic and microscopic fractures and largely recover the mechanical strength after an injury event at both neutral (7.0) and acidic pH (4.0) within 1 minute upon breaking. This demonstrated self-healing capacity over a broad and physiologically-relevant pH range suggests the potential of using boronate ester-based hydrogels as biomaterials in acidic-neutral environments.

6.2 Limitations and future work

All the work in this thesis targets on making functionalized materials and interfaces for the applications in biosensors and hydrogels. Even though the proof-of-concept tests have been done in most cases in this thesis, these methods still require additional studies in order for their practical usage. The detailed limitations and proposed future work are listed below:

1. In Chapter 2, although the dip-coating process for functionalizing the paper with a POEGMA hydrogel layer is simple and easy, drawbacks persist in terms of the time required for the coating/drying steps (much longer than the timescale of conventional papermaking) as well as potentially irreproducible polymer deposition, limiting the large scale application of this method. Printing technologies are therefore introduced to overcome these problems. In response, I and my colleagues are now exploring methods to efficiently print these polymers onto cellulose paper and other types of porous materials, such as nitrocellulose membranes, for applications in biosensing.

2. As mentioned in Chapter 3, the TEMPO-mediated oxidation of PHEMA hydrogel could efficiently generate aldehyde and carboxylic groups both on the surface and within the bulk gel. Such oxidation process will inevitably lead to a certain loss of the elongation ability of the materials, as shown in the data presented, and is likely avoidable since bulk modification of the lens is not expected to lead to significant improvements in practical performance. In addition, the aldehyde groups in the bulk gel are not chemically linked with the hydrazide groups tethered on HA chain, which leaves potential active sites for interaction with the components in the tear fluid and other environmental factors. Therefore, it is important to develop a surface oxidation technology that does not interfere the bulk properties of the hydrogel. One possible route is to tether the TEMPO molecule onto a polymer chain, which will confine the oxidation to take place only on the surface by

restricting the diffusion of the oxidant into the gel bulk. Such polymer-grafted TEMPO has been synthesized recently and provides a possible tool for the proposed surface oxidation.

3. In Chapter 4, the immobilization of antibodies on the gold QCM sensor is realized by physical adsorption of a GO-biotin·avidin complex, enabling quantitative detection of rabbit IgG at low concentrations. However, the method demonstrated is strictly proof-of-concept, with no applications to-date in the detection of clinical or practically important biological targets. Furthermore, the assembly of the detecting system based on QCM is still somewhat complicated and instrument-dependent, and the cost of gold sensor is relative high even though the gold sensor is reusable. To address the cost challenge, the immobilization strategy used here will be applied on other types of cheap substrates that can further be developed into point-of-care or high-throughput testing platforms for some practical applications. However, given the dependence on QCM measurements, it is recognized that this method is likely only useful for advanced target detection in cases where other sensors do not give adequate sensitivity to inform clinical decision-making.

4. In Chapter 5, the development of fast self-healing hydrogel is at an early stage. For anticipated applications, the mechanical properties of the hydrogel must be tuned through changing the chain length, grafting density and the concentration of the polymer, in this case HA. In particular, self-healing performance on different samples (to show repeatability) *and* self-healing over multiple disruption cycles on a single cycle (to show reversibility) will be assessed both using the rheological measurements described already in Chapter 5 as well as tensile measurements on the healed hydrogels. Furthermore, additional insight into the mechanism of self-healing will be sought by performing control mechanical, self-healing, and isothermal titration calorimetry measurements with 3APBA (which cannot form the projected cyclic structures possible with 2APBA and rely only on carboxylic acid induction for promoting physiological activity). This work is now ongoing and is anticipated to more clearly identify both the mechanism by which these gels self-heal as well as the best possible applications for such hydrogels moving forward.